Analogue, Numerical And Field Site Studies Of EM Induction In The China-Korea-Japan Region

Zhiwei Meng
B.Sc., University of Science & Technology of China 1982
M.S., Institute of Geophysics, The State Seismological Bureau of China, 1984

A THESIS SUBMITTED IN PARTIAL FULFILLMENT

OF THE REQUIREMENTS FOR THE DEGREE OF

DOCTOR OF PHILOSOPHY

in the Department

of

Physics and Astronomy

We accept this thesis as conforming to the required standard

ACCEPTED
FACULTY OF GRADUATE STUDIES

DEAN

DATE 91/10/07

Dr. H.W. Dosso

Dr. J.T. Weaver

Dr. R.M. Clements

Dr. T.W. Dingle

Dr. D.E. Hewgill

Dr. M.E. Best

Supervisor: Dr. H.W. Dosso

ABSTRACT

Electromagnetic induction in the continental Bohai Bay coastal region of China and the island region of Japan is studied with the aid of laboratory analogue models. Detailed model measurements of the electric (E_x, E_y) and magnetic (B_x, B_y, B_z) field components are presented for an approximately uniform overhead horizontal source field for E- and B-polarizations. With the aid of 2D numerical models, criteria are developed for permitting approximate removal of the coast effect responses in field site measurements in coastal regions.

For the Bohai Bay laboratory analogue model, large anomalous in-phase and quadrature model magnetic fields are observed over the Korea-Japan strait for E-polarization, and over the Bohai strait for B-polarization, due to current channelling through the straits. Large responses over the peninsulas in the shallow coastal areas occur at short periods but decrease abruptly with increasing period. The model induction arrows show that the induction in the local Bohai Bay is important primarily at short periods. At long periods, induction in the distant deeper Yellow Sea must be considered in any interpretation of field site measurements. In general, the analogue model results indicate that the effects of peninsulas, straits, bays and the irregularities in the coastlines play an important role in determining the electric and magnetic field responses both on-shore and off-shore for this complex coastal Bohai Bay region.

For the Japan laboratory analogue model, electromagnetic field measurements are examined in detail for a series of traverses over Japan, the Korean peninsula, and the coastal region of China and the U.S.S.R. Large anomalous in-phase model magnetic fields are observed over the Korea-Japan strait for E-polarization and over Bohai strait, Tsugaru strait, and La Perouse strait for B-polarization due to off-shore current channelling. The significant responses observed at short periods over the peninsulas in the shallow coastal areas decrease with increasing period. Large gradients in the in-phase B_z are observed over all regions of Japan for E-polarization for both short and long periods due to the effects of induced currents in the surrounding oceans. Thus, induction arrow responses over all regions of Japan show the dominant effects of the ocean.

The 2D numerical calculations of EM induction in continental and island coastal regions for an anomalous conductor in the form of an upwelling or a depression in the conductive substratum, show that if the anomalous conductor - ocean separation distance is at least as great as the coast effect response range Y_R (defined in the present work to be the range where the coast effect $|B_z/B_{yn}|$ has decreased to a value of 0.2), then the coast effect can be removed by vector subtraction to yield a response, approximately that of the anomalous conductor alone. For a given period (in the range 5 - 120 min), Y_R is found to increase with increasing ocean depth, conductive substratum depth, and island width. Further, the dependance on period is found to vary from model to model, but the general trend is for Y_R to decrease with increasing period, on account of the increasing importance of the underlying conductive substratum through the skin depth effect in the host. Empirical curves are presented showing how the response

range depends on the ocean depth, the conductive substratum depth, the island width and the period.

Coast effect response values for 3D laboratory analogue models are employed to approximately remove the geomagnetic coast effects in field measurements for some coastal sites in the Bohai Bay continental region of China and the island regions of Japan. The validity of the subtraction is examined for several models of conductive anomalies at sufficiently large anomalous conductor - ocean ranges to satisfy the response range criteria developed for 2D numerical models. The resulting interpretation of field site measurements in complex coastal regions is discussed.

With the coast effect removed though subtraction of the model arrows from field site results available in the Bohai Bay region, the resulting difference arrows indicate a N-S striking conductor to the west of Bohai Bay. These difference arrows, as well as the 2D numerical calculations, support the premise of such a conductor, in the form of an upwelling in the conductive substratum (with conductivity 0.5 Sm^{-1} at 80 km depth), situated at about 150 km from the Bohai Bay coastline to account for the field site observations. A comparison of laboratory analogue model and field site MT results at two sites west of Bohai Bay shows that the analogue model apparent resistivities are about an order of magnitude greater than the field site apparent resistivities. This result also supports the model of a conductive anomaly, in addition to the conductive substratum at 80 km depth.

Laboratory analogue model measurements are employed to subtract the ocean effect in field measurements to yield difference arrow for these complex island regions of Japan (the Kii Peninsula region, the central Honshu region and the

regions of northern Honshu, Hokkaido and Tsugaru strait). These difference arrows as well as the 2-D numerical model result for the Kii Peninsula region, the central Honshu region, and the northern Honshu region support the premise of two conductive anomalies (with conductivity $0.5Sm^{-1}$), one beneath the Pacific Ocean and one beneath the Japan Sea at a depth of 30 km. Further, the difference arrows over the entire Japan region suggest that the two conductors roughly follow the general trend of the island arc, and eventually may be connected by an E-W striking conductor beneath Tsugaru strait to the north.

Examiners:

Dr. H.W. Dosso

Dr. J.T. Weaver

Dr. R.M. Clements

Dr. T.W. Dingle

Dr. D.E. Hewgill

Dr. M.E. Best

CONTENTS

FIGURES

ACKNOWLEDGEMENTS

I am deeply grateful to my supervisor, Dr. H.W. Dosso, for encouraging me in my studies and for the direction and advice in carrying out this research. His ideas, insights and suggestions have not only helped make this work stimulating for me, but have also made a large contribution towards the success of this research.

The friendship and comradeship I have found within the Geophysics group at Uvic has meant a great deal to me. Here, I would like to thank my fellow graduate students J. Chen , S. Kang and X. Pu for their support and useful discussions in the various stages of my research.

I also wish to thank Dr. J. T. Weaver for the use of the Brewitt-Taylor and Weaver 2D computer program, and Dr. A. Agarwal for useful discussions.

The financial support in the form of a University of Victoria Fellowship, and a research assistantship provided by my supervisor Dr. H. W. Dosso is gratefully acknowledged.

Chapter I

INTRODUCTION

1.1 Magnetotelluric and Geomagnetic Depth Sounding Studies

The distribution of electrical conductivity in the earth can be studied by using the phenomenon of electromagnetic induction. According to Maxwell's electromagnetic theory, a transient magnetic field induces an electric current in a conducting earth. The varying electromagnetic field observed on the earth's surface thus consists of an external field (generated by oscillating currents in the ionosphere and magnetospere) and an internal field (arising from electric currents induced by the external field) which contains information on the conductivity structure within the earth. An external field originating in the ionosphere and magnetosphere can approximately be treated as being spatially uniform within a certain area of local extent. As early as the 1950's (Rikitake and Yokoyama, 1953) it was noticed that in some regions of the earth the vertical components of geomagnetic variations (having periods shorter than a few hours) are considerably different in behavior from one station to another within a distance of some tens of kilometers. Such a geomagnetic variation anomaly can be accounted for neither by an external field nor by induction in a layered laterally uniform earth. However, it could be reasonably interpreted as indicating the existence of a lateral heterogeneity in conductivity, denoted by a conductivity anomaly. Investigation of a conductivity anomaly may be carried out by means of geomagnetic depth

sounding (GDS), based on geomagnetic variations characterized by anomalous vertical fields, or by magnetotelluric (MT) sounding, based on ratios of horizontal electric and magnetic fields.

As a general feature in GDS studies, the vertical magnetic field is much smaller than the horizontal field in mid-latitudes (Uyeda and Rikitake, 1970), and the vertical field is usually well correlated with one of the two horizontal components, or both. Such good correlations between the vertical and horizontal magnetic fields were first noted by Parkinson (1959). He studied local induction at coastal sites in Australia and found that the magnetic variations at a given frequency (though in the time domain) tend to be confined to a "preferred plane". The projection of the normal of this plane onto the horizontal plane has come to be defined as the Parkinson arrow. Wiese (1962) introduced a somewhat different approach in order to investigate the relationships of the horizontal (H, D) and the vertical (Z) magnetic components. He chose the magnetic components (H, D, Z) at the point where Z reached a maximum value for a given frequency and plotted (in two dimensions) the ratio D/Z as a function of H/Z. He found that the results lay approximately along a straight line, which has become known as the "Wiese line". The Wiese line should exist because of the existence of the Parkinson plane. The "Wiese" line can be expressed as

$$\gamma(H/Z)-\lambda(D/Z)+1 =0, \qquad (1.1)$$

where γ and λ are defined (Wiese, 1962) as the components of the "Wiese vector" along the positive H and D directions respectively. In a related analysis, Schmucker (1964, 1970) introduced the transfer function technique of geomagnetic depth sounding gi- en by

$$B_z = aB_x + bB_y, \qquad (1.2)$$

where B_z, B_x and B_y are the Fourier transformations of the vertical and two horizontal components,and a and b are transfer functions at a frequency ω. The induction arrow is then defined as

$$V = (-a, -b), \qquad (1.3)$$

which is now a complex vector. Its real and imaginary components are called the in-phase (real) and quadrature (imaginary) induction arrows. It has been shown (Honkura, 1978) that the in-phase induction arrow has a feature similar to that of the Parkinson arrow in that it usually points towards current concentration in a conductive body, and has an amplitude (length) that is qualitatively indicative of the current strength. The properties of the quadrature induction arrow have been more of a puzzle. Sign reversal of the quadrature induction arrow at some frequency has been reported for field measurements (e.g. Lilley and Arora, 1982; Parkinson et al., 1988), analogue modelling results (e.g. Nienaber et al. 1983; Dosso et al., 1985; Hu et al., 1989) and numerical calculations (e.g. Weaver et al., 1987; Chen and Fung, 1988; and Agarwal and Dosso, 1990). It has been shown by Agarwal and Dosso (1990) that for a 2D model, the quadrature arrows at sufficiently short periods point away from current concentrations, then at the characteristic period reverse to point towards current concentrations (The characteristic period is defined as the period at which the quadrature arrow amplitude is minimum and the in-phase arrow amplitude is maximum). This has been observed in various analogue model studies. For the time variation of $\exp(-i\omega t)$. It should be noted that with the time variation of the field described by $\exp(i\omega t)$, the signs of both in-phase and quadrature transfer functions should be reversed in order that

both components of the induction arrows point towards current concentrations. However, the sign of the in-phase transfer function should be reversed while the sign of the quadrature part should not. This convention is in keeping with the work of other authors (Edwards et al., 1971; Bailey and Edwards, 1976; Lilley and Arora, 1982; Wolf, 1982; Agarwal and Dosso, 1990).

The relationships between the Parkinson arrow, the Wiese vector and the induction arrow (from transfer function analysis) have been discussed by Gregori and Lanzerotti (1980), Jones (1981), Wolf (1982), and Gregori et al. (1982). It seems that a unifying picture of the representations of the arrows may not be obtained in general due to the original definitions. However their equivalences under certain assumptions are still quite useful. According to Gregori et al. (1982), if the phase shifts could be disregarded, a relationship between the Parkinson arrow (V_p) and the Wiese vector (V_w) could be expressed as

$$|V_p| = |V_w|/(1+|V_w|^2)^{1/2}. \qquad (1.4)$$

The Wiese vector, on the other hand, is simply related to the in-phase induction arrow, expressed as

$$V_{real}=V_w. \qquad (1.5)$$

Another somewhat different approach, used to study regional conductivity distribution in the crust and upper mantle, employs the magnetotelluric(MT) method. This method utilizes mutually perpendicular horizontal electric (E) and magnetic (B) natural source fields generated by ionospheric and magnetospheric currents. The large horizontal spatial extent of the MT source field over a broad frequency band allows examination of the conductivity structure within the earth via surface measurements of the resulting electric and magnetic fields. Although

earlier workers (e.g. Tikhonov, 1950) investigated the potential of using natural electromagnetic fields, the MT method was essentially established by Cagniard (1953). Under the assumption that the earth is horizontally stratified and excited by uniform, monochromatic electromagnetic plane waves, he showed that the apparent resistivity can be expressed as

$$\rho_a = 0.2\ T\ [E/B]^2, \tag{1.6}$$

where ρ_a is the apparent resistivity in Ωm, T is the period in seconds, E and B are mutually perpendicular horizontal components of the electric and magnetic fields in mV/km and nanoteslas (nT) respectively. The apparent resistivity is a function only of the conductivity structure and the frequency of the source field, and is not dependent on the strength of the source field. However, the actual conductivity distribution in the earth's crust is much more complex than the one-dimensional model originally investigated. In general, it is essential to understand the effects on the EM fields of both two- and three-dimensional features. Since the strength and polarization of the MT source field varies randomly as a function of time, it is customary to express the earth's electromagnetic response in terms of a frequency dependent linear transfer function, or impedance tensor. The impedance tensor expresses the linear relation between the horizontal components of the electric and magnetic fields, and satisfies

$$E_x = Z_{xx}B_x + Z_{xy}B_y, \tag{1.7}$$

$$E_y = Z_{yx}B_x + Z_{yy}B_y, \tag{1.8}$$

where Z_{ij} are the elements of the impedance tensor.

It is important to note that the elements of the impedance tensor are dependent on the choice of the orientation of the measuring axes. For the purposes of interpretation, a principal (or intrinsic) coordinate system can be found in which the impedance tensor reduces to a particularly simple form that is more readily amenable to interpretation and insight. For two-dimensional (2D) structures, the impedance tensor contains the information required to determine the horizontal rotation angle to this intrinsic coordinates system. The rotation of the impedance tensor results in an off-diagonal form when the orientation of one of the coordinate axes is along the strike direction of the structure. In this case the impedance tensor consists of two intrinsic complex impedances. Each impedance is associated with one of the two-dimensional polarizations (i.e. E-polarization where the electric source field is parallel to the strike of the structure, or B-polarization where the magnetic source field is parallel to the strike of the structure). However, for a general three-dimensional (3D) conductivity distribution, the corresponding impedance tensor cannot be off-diagonalized for any real rotation angle. Swift (1967) has shown how to retrieve the two impedances and strike direction. He defined the principal axes as those which maximize the quantity $|Zxy(\theta)+Zyx(\theta)|$, where θ is angle of the rotation. Various other measures of the impedance tensor are also used in characterizing the impedance, such as "skewness" (S) which, according to Vozoff(1972) is defined as

$$S = |Z_{xx}+Z_{yy}|/|Z_{xy}-Z_{yx}|, \tag{1.9}$$

$$\phi = \arctan(S). \tag{1.10}$$

The skewness ratio is useful in estimating the earth structure being dealt with. If S is large (larger than unity), the structure of the earth appears to be three-dimensional at that frequency. Recently a number of attempts to extend Swift's work to the more general case of an arbitrary 3D conductivity structure have been made by several scientists (e.g. Eggers, 1982; LaTorraca et al., 1986). Yee and Paulson (1987) have developed a canonical decomposition technique in which the impedance tensor is represented in terms of eight physically relevant structural parameters which specify the transfer characteristics of the earth system and intrinsic coordinate system for the impedance tensor. However, the properties of the canonical parameters require further study (by numerical and/or analogue modelling) before wide acceptance by the magnetotelluric community can be expected. Groom and Baley (1988) developed a decomposition technique for the impedance tensor that incorporates a superposition of local 3D and regional 2D structure. Bahr (1990) proposed a MT tensor interpretation algorithm which can deal with the case that the regional conductivity model is more complicated than 2D.

1.2 Numerical and Analogue Modelling of Electromagnetic Induction

Lateral variations in conductivity are also studied using analytical, numerical and laboratory analogue model techniques. The analytic solutions, though somewhat limited to problems with simplified geometry, are very useful as accuracy checks on the various numerical techniques in use. An early analytic solution of electromagnetic induction in the earth with lateral conductivity variations was obtained by D'Erceville and Kunetz(1962) who considered the effect of a vertical contact

between two homogeneous media with contrasting conductivity. Rankin (1962) extended their solution to treat a vertical dike embedded in a homogeneous structure. Weaver (1963) obtained the analytic solution for the vertical contact to an infinite depth. Geyer (1972) studied the effect of a dipping contact of two homogeneous regions. More recently, models with more than one vertical contact have been investigated by other scientist (e.g. Wait,1982; Weaver et al., 1985).

Numerical methods at present play an important role in analysing problems of more complex structures. Various techniques have been used -- difference equation (finite difference and finite element), integral equation, thin sheet approximation, and hybrid methods. Since the introduction of the finite difference method by Jones and Pascoe (1971), a number of successful 2D computer programs based on difference equations have been developed, for example, the finite difference program of Brewitt-Taylor and Weaver (1976) and the finite element programs of Lee and Morrison (1982) and Wannamaker et al. (1987).

The three-dimensional numerical method, employing the difference equation (Lines and Jones, 1973; Dey and Morrison, 1979; Pridmore et al., 1981; and Chen and Fung, 1985), on the other hand, is still in its infancy due in part to the lack of large computer storage and computing speed. However, some progress has been made in developing 3D integral equation algorithms. Hohmann (1975) has improved the general 3D integral equation solution by utilizing a vector-scalar potential approach and incorporating symmetry through group theory. Wannamker er al. (1984) developed on algorithm for 3D anomalies in a multi-layered medium. Very recently, Lee et al. (1989) have shown that the integral transform can be extended to include vector fields. The integral equation method is most suitable for solving problems of isolated anomalies embedded in a simpler substrate (Hohmann, 1983).

The inhomogeneous thin sheet approximation technique, employing a uniformly conducting half space overlain by a surface layer of variable conductance, has been developed by Vasseur and Weidelt (1977) and treated further by Dawson and Weaver (1979), Ranganayaki and Madden (1980), Dawson et al. (1982), and Dawson (1983). McKirdy and Weaver (1984) developed the 2D thin sheet layered medium model, and McKirdy et al. (1985) generalized this for the 3D case. The thin sheet method has been used to study the distortion effects in the EM field due to near surface inhomogenities (Weaver, 1982; Agarwal and Weaver, 1988, Weaver and Agarwal, 1989) and the effects of current channelling between two oceans (McKirdy and Weaver, 1983).

The hybrid methods, which attempt to combine the advantages of the difference equation and the integral equation solutions, were developed by Scheen (1978) and studied further by Lee et al. (1981) and Best et al. (1985). Based on the hybrid theory of Lee et al.(1981), Gupta et al. (1987, 1989) developed the compact finite element method, a condensed version of the hybrid method.

Since analytical and numerical methods are difficult to apply in solving certain complex 3D structures, laboratory analogue modelling methods can be particularly useful in studying actual geophysical cases. The theory of analogue scale modelling has been treated in considerable detail by Sinclair (1948), Strangway (1966), Ward (1967), and Frischknecht (1971). Dosso (1966a) constructed an analogue modelling facility in which earth conductivity structures are simulated by graphite and salt (Nacl) solution that has been used to study a wide range of induction problems. These include the studies of (i) idealized conductivity structures such as vertical faults and dikes (Dosso, 1966b; Charters et al., 1989), conducting

spheres and cylinders (Ogunade et al., 1974; Ogunade and Dosso, 1977, 1980, 1981; Ramaswamy and Dosso, 1977), bay, capes, channels and islands (Nienaber et al., 1976, 1977; Chan et al., 1981a; Dosso et al., 1986) and more recently, the seamount (Hu et al., 1984, 1986; Hu and Dosso, 1989), (ii) the effect of various inducing source fields, such as a uniform plane wave field (Dosso, 1966c), an oscillating line current field (Dosso, 1966d; Dosso and Jacobs, 1968; Ogunade and Dosso, 1981), magnetic dipole fields (Ramaswamy et al., 1972; Thomson et al., 1972; Ramaswamy and Dosso, 1973, 1975), a vertical line current source to simulate lightning induced Schumann Resonances (Heard et al., 1985), (iii) magnetic variations induced by ocean waves (Miles et al., 1977; Miles and Dosso, 1979, 1980), and (iv) coast-island regions (for a uniform source field), such as Vancouver Island (Nienaber et al., 1977, 1979a, b), the British Isles (Dosso et al., 1980; Nienaber et al., 1981), the Queen Charlottle islands (Chan et al., 1981b, 1983), an arctic bay (Heard et al., 1983), Newfoundland (Dosso et al., 1980; Hebert et al., 1983a, b), the Tasmania region of Australia (Dosso et al., 1985; Parkinson et al., 1988), the Hainan Island region of China (Hu et al., 1983, 1984, 1986), the Bohai Bay region of China (Meng, et al., 1990) and the Japan-Korea -China region (Meng and Dosso, 1990). The analogue model facility has also been used to study regions of active tectonic plate subduction such as the West coast of Canada and the U.S.A. by including in the laboratory model a simulation of postulated conductivity structure associated with the subducting Juan de Fuca plate (Dosso and Nianaber, 1986; Dosso et al., 1989; 1990; Chen et al., 1989, 1990). These studies of the subducting Juan de Fuca plate are associated with the international EMSLAB and LITHOPROBE programs still underway. A second example of modelling induction

in a region of active subduction is found in the model studies of New Zealand by Chen et al. (1990).

The work in this thesis deals with laboratory analogue models of (i) the Bohai Bay region of China, and (ii) the Japan-Korea-China region. Geophysical study of the Bohai Bay region, on the east coast of China, is of considerable interest as the region contains thick sediments in which abundant petroleum resources have been found. Examples of recent geophysical studies of this region are seen in the work of Chen (1974), Qi et al.(1981), Liu and Liu (1983), Liu et al.(1984), Teng et al. (1985) and Kao (1990). According to the MT surveys of Liu and Liu (1983) and Liu et al. (1983) in the Beijing-Tainjin-Tangshan region near Bohai Bay, there is evidence of a conductive asthenosphere of 0.5-1 Sm^{-1} at depths ranging from 50-100 km in this region, in addition to conductive structures in the crust. Based on short period geomagnetic variation measurements which show enhancements and sign reversals of the vertical magnetic fields at the tips of the Shandong and the Liaodong peninsulas (on the two opposite sides of Bohai Bay), Qi et al. (1981) suggest a model of a highly conductive uplift anomaly under the Bohai Bay region.

Japan, with its complex but typical island arc tectonic structure, is a region that provides challenges to wide ranging geophysical studies. Since the early work of Rikitake and Yokoyma (1953) which drew attention to the anomalous behaviour of the vertical component of the geomagnetic variations in central Japan, many detailed investigations of the local characteristics of geomagnetic anomalies have been carried out in Japan. The regions studied include central Japan (Rikitake, 1959; Honkura, 1975; and Utada et al., 1986), northern Honshu (Kato et al., 1971; Research Group for Crustal Resistivity Structure, Japan (RGCRSJ), 1983; Yuku-

take et al., 1983; Ogawa et al., 1986; Ogawa, 1987, 1988), Hokkaido (Nishida,1976), and the Chugoku district (Miyakoshi, 1979). Conductivity anomalies beneath various parts of Japan have been reviewed in a number of studies (e.g., Rikitake, 1966; Rikitake and Honkura, 1973, 1986; Honkura,1978; Yukutake, 1985). Extensive analytical and numerical model calculations were carried out in an attempt to interpret field data in terms of conductive substructure of the Japan region. It has been noted (Rikitake and Honkura, 1973; Honkura, 1978) that geomagnetic variations in many regions of Japan are seriously affected by electric currents induced in the surrounding oceans, and thus some local geomagnetic variation anomalies can be attributed to the coastal effects, which include cape (or peninsula), island, bay, and channelling effects.

With the aid of the analogue model, the electromagnetic field response for the Bohai Bay region and the Japan-Korea-China region are studied in an attempt to delineate the field perturbations due to such coast effects for the complex coastlines and the continent, and thus possibly permit more accurate interpretations of field measurements in terms of geological and tectonic structures of the regions.

1.3 Summary of Work in This Thesis

In this thesis, electromagnetic induction in the Bohai Bay region and the Japan-Korea-China region is studied using 3D laboratory analogue model simulations. For the Bohai Bay region, model measurements of the in-phase and quadrature electric and magnetic field components are carried out for a simulated period range of 3-60 min for E- and B- polarizations of a uniform horizontal inducing source field. Included in the model simulation are the complex coastline, ocean bathymetry of

the Bohai Bay region, and a conductive substratum at depth of 80 km (based on the MT survey results of Liu and Liu, 1983). In the model study of the Japan-China-Korea region, measurements for traverses over the region are carried out for the period range 15-180 min, for a simulation of two cases of a conductive substratum underneath the region. For the first case, a conductive substratum at a depth of 1900 km (simulated by the graphite plate lining the bottom of the modelling tank), for the second, a conductive substratum at a simulated depth of 70 km (following a geophysical model proposed by Utada et al., 1986). The laboratory analogue model ocean coast effect responses, in terms of induction arrows,are used to remove (approximately) the coast effect in field site measurements available in the continental Bohai Bay region of China and the island region of Japan.

To study how coast effect responses could be removed from coastal field site measurements with some validity, 2D numerical models of EM induction in continental and island coastal regions for an anomalous conductor in the form of an upwelling or a depression in the asthenospheric conductive substratum at depth are studied to determine constraints on ocean-anomalous conductor separation distances that would permit, to within an acceptable approximation, a simple vector subtraction of the coast effect response. It is found, that if the distance of the ocean-conductor is at least as great as the the coast effect response range Y_R (defined as the distance from the ocean where the $|B_z/B_{yn}|$ coast effect response is reduced to a value of 0.2), then the coast effect can be removed by vector subtraction to yield a response that approximates the conductor alone.

Difference induction arrows, obtained by subtracting the 3D laboratory analogue model coast effect responses from the field site responses, are examined

and employed in the interpretation of the field measurements available for a number of coastal sites in the Bohai Bay (China) and the Japan Island regions.

Chapter II

LABORATORY ANALOGUE MODELLING

2.1 Model Scaling Conditions

A brief summary of EM induction theory is introduced here in order to obtain the model scaling conditions. Electromagnetic fields are described by Maxwell's equations (SI units)

$$\nabla \times \mathbf{E} = -\partial \mathbf{B}/\partial t, \tag{2.1}$$

$$\nabla \times \mathbf{B} = \mu \mathbf{j} + \mu\varepsilon\, \partial \mathbf{E}/\partial t, \tag{2.2}$$

$$\nabla \cdot \mathbf{E} = \rho/\varepsilon, \tag{2.3}$$

$$\nabla \cdot \mathbf{B} = 0, \tag{2.4}$$

together with Ohm's law

$$\mathbf{j} = \sigma \mathbf{E}, \tag{2.5}$$

where E and B are electric field and magnetic field (magnetic flux density) vectors, j the electric current density, ρ the volume density of charge in the medium, σ the conductivity, μ and ε the permeability and the permittivity respectively.

The conductivity in the upper regions of the earth ranges from 10^{-4} Sm^{-1} for some rocks to 4 Sm^{-1} for seawater. The permeability, for most materials in the earth, does not differ significantly from the free space value, and thus in the present work is assumed constant as $\mu \simeq \mu_o = 4\pi \times 10^{-7}$ H/m. Since the variations of the natural geomagnetic field contain low frequencies, i.e. $\varepsilon\omega << \sigma$, the

displacement current term in Maxwell's equation (2.2) can be ignored. In other words, the EM induction in the earth is a diffusion problem, rather than a wave propagation problem.

If the media of the earth are assumed to be linear and isotopic, the field variables and parameters in the model and geophysical system may be related by simple linear transformations as

$$E_g = K_E E_m, \tag{2.6}$$

$$B_g = K_B B_m, \tag{2.7}$$

$$\varepsilon_g = K_\varepsilon \varepsilon_m, \tag{2.8}$$

$$\mu_g = K_\mu \mu_m, \tag{2.9}$$

$$\sigma_g = K_\sigma \sigma_m, \tag{2.10}$$

$$L_g = K_L L_m, \tag{2.11}$$

$$t_g = K_t\, t_m, \tag{2.12}$$

where the subscripts g and m refer to the geophysical and model values, and the dimensionless constants K_E, K_B, K_ε, K_μ, K_σ, K_L, K_t are the scaling factors for the electric field, magnetic field, electric permittivity, magnetic permeability, conductivity, length and time respectively. If only non-ferromagnetic media are considered in both model and geophysical systems, then it is reasonable to set K_μ=1 (or $\mu_m = \mu_g$). By substituting equations (2.6-2.12) into Maxwell's equations (2.1-2.5) and comparing them for the two systems, it is readily shown that, under these assumptions, the necessary and sufficient conditions for a valid analogue model are

$$(\sigma_g/\sigma_m)(L_g/L_m) = K, \tag{2.13}$$

$$(f_g/f_m)(L_g/L_m) = 1/K, \tag{2.14}$$

where f is the frequency of the time harmonic field, and $K = K_E / K_B$ is the impedance scaling factor. By combining (2.13) and (2.14), K can be eliminated, if the impedance scaling is not of interest, and the scaling condition becomes

$$(\sigma_g/\sigma_m)(f_g/f_m)(L_g/L_m)^2 = 1. \tag{2.15}$$

It should be noted that since equations (2.13) and (2.14) contain four unknowns, any two of the four scaling factors can be chosen arbitrarily. In practice, the conductivity scaling factor σ_g/σ_m, and the length scaling factor L_g/L_m are constrained by the model materials, the area of geophysical interest and the size of the analogue facility. Thus the frequency scaling factor f_g/f_m and the impedance scaling factor K are determined respectively by (2.13) and (2.14).

2.2 The Laboratory Analogue Model Description

The analogue modelling facility, including the modelling tank system, the overhead source field, the field detectors and recording equipment, has been described in detail by Dosso (1966a, 1973) and will be introduced here only for the purpose of completeness.

A schematic diagram of the analogue modelling tank and source system used in the present work is shown in Fig. 2.1. The fiberglass lined plywood tank of dimension 2.44m×1.68m×0.76m deep is filled with concentrated salt solution of conductivity $\sigma = 21 Sm^{-1}$ to a depth of 0.63 m. The bottom of the tank is lined with a 5 cm thick graphite plate to minimize the effect of the concrete floor of the laboratory and the earth below, which are unknowns as far as the conductivity is concerned. In some model studies, this graphite plate is used to simulate a highly

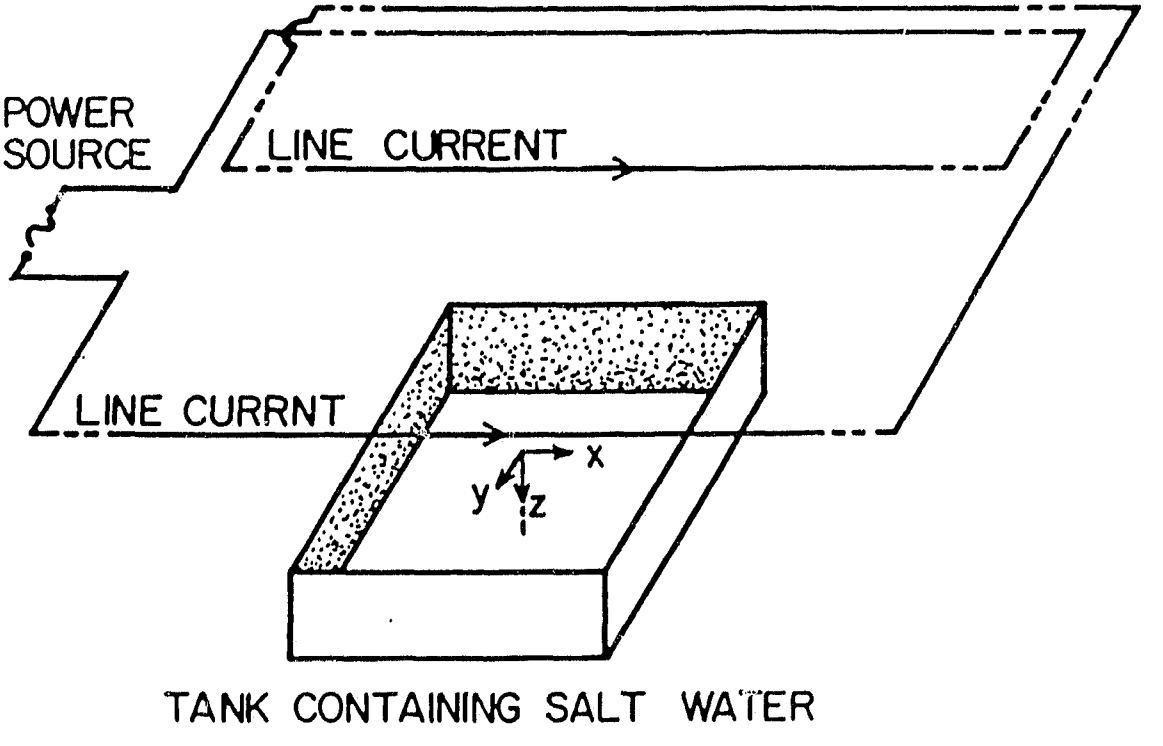

Figure 2.1: Laboratory analogue model facility.

conductive layer at depth in the earth. In order to reduce the edge effects due to the finite size of the tank, stainless steel plates line the two tank walls (parallel to the y-direction) and are electrically connected by a heavy copper wire outside the tank, so that the electrical currents induced in the tank flow parallel to the inducing electric field right to the edges of the tank.

The current for the source field is provided by a signal generator (Hewlett Packard 3325A frequency synthesizer with desired sine wave-form and frequency) and a power amplifier (STAX DA-100M amplifier). Equal currents flowing in parallel along a pair of wires (shown in Fig.2.1) separated by a distance of 2.4 m (twice their height of 1.2 m above the surface of the salt solution in the tank) provide a reasonably uniform field, simulating the external inducing field of the ionosphere.

The electric and magnetic detectors are schematically illustrated in Fig. 2.2. The magnetic fields are measured by a low inductance air-cored coil which, mounted at the end of a lucite tube, consists of a 0.1 cm long coil (250 turns of #42 wire), with inside and outside diameters of 0.235 cm and 0.635 cm respectively. The coils used in the horizontal and vertical magnetic field detectors are designed to be identical, but mounted with their axes directed in the desired horizontal and vertical directions respectively. The horizontal electric field detector consists of three equally spaced copper pins just protruding through the sealed end of a lucite tube. The two outer pins are connected to the signal inputs of a low noise pre-amplifier (PAR CR-4), while the centre pin is connected to a common ground so as to provide a suitable input to a differential amplifier. The three pins of the probe are in contact with the surface of the salt solution in the tank. The

output from the pre-amplifier provides the voltage difference between the two outer pins and thus permits a determination of the electric field for the known electrode separation.

The electric and magnetic field sensors, mounted on the carriage that is driven by a variable-speed motor along the wooden beam mounted above the tank, measure the field components at the surface of the salt solution which simulates the uniform host earth. The position of each field point is defined by a potential measurement along a resistive wire mounted on the beam along which the carriage moves during a traverse over the analogue model. The signals from the sensors are amplified and transmitted to the analyzing and recording equipment shown in the schematic (Fig. 2.2.) and recorded in analogue form on X-Y plotters and in digital form using a micro computer (IMS 8000).

The model ocean, consisting of a graphite plate ($\sigma = 1.2\times10^{5}$ Sm^{-1}) shaped and machined according to the coastline and bathymetric contours of a given model, is suspended at the surface of the salt solution ($\sigma = 21$ Sm^{-1}) in the tank. The model magnetic (B_z, B_x, B_y) and electric (E_x, E_y) field components at the surface of the model are recorded for two perpendicular polarizations of the source field. The field polarizations are taken to be defined as E- and B- polarizations for the case of the electric field of the source in the x- and y-directions respectively as indicated for a model map of a given region. It is noted that the E- and B- polarization directions are arbritary, and they can be rotated and decomponented into any other set of perpendicular polarization direction. For each polarization, the source field is held constant for all measurements (in-phase B_y=1 nT, quadrature B_y=0 nT for E-polarization; and in-phase B_x =1 nT, quadrature B_x =0 nT for

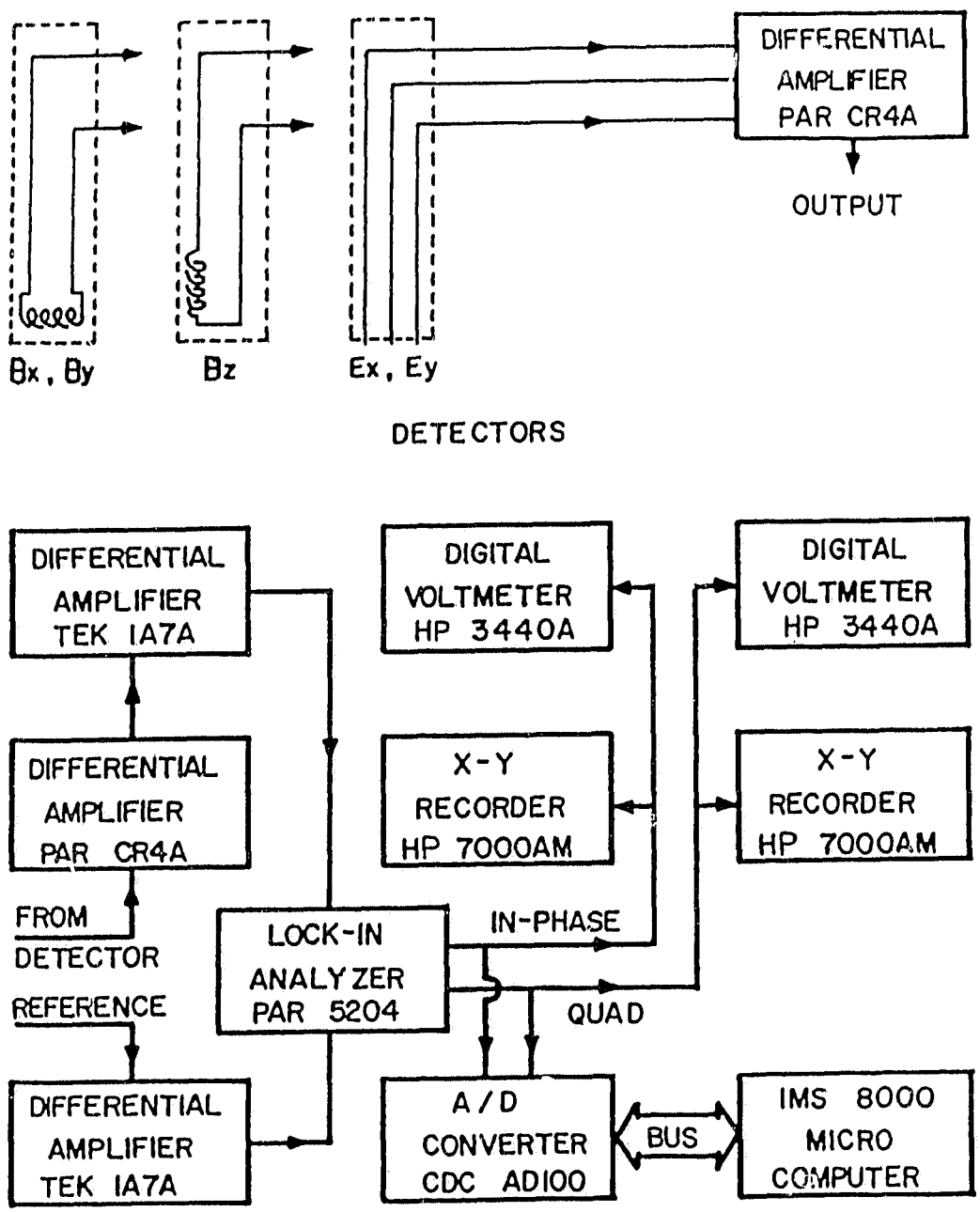

Figure 2.2: The field detectors and measurement instrumentation.

B-polarization) at a model land reference location in the model tank well away from the continental coastline. The time variation of the source field is taken to be $\exp(i\omega t)$ so that the quadrature component leads the in-phase component by 90^{o}.

2.3 The Analogue Model of The Bohai Bay Region

A simplified map of the Bohai Bay region used in the construction of the laboratory model is shown in Fig.2.3. The area includes the shallow Bohai Bay, the Yellow and the East China Seas, and the deeper Japan Sea. Major coastal features include a number of bays, two straits (the Bohai and the Korea-Japan straits) and the three peninsulas (Shandong, Liaodong and Korea).

This model will be referred to as the Bohai model. The linear scaling factor, for the Bohai model, is chosen to be $L_g/L_m=10^6$, so that an area of 1.4m×1.4m in the laboratory model, represents an area of 1400km×1400km in the geophysical case. Since the conductivity contrast for graphite and ocean water is $\sigma_g/\sigma_m=3\times10^{-5}$, the frequency scaling factor is constrained to be $f_g/f_m = 3.3\times10^{-8}$, thus, as an example, a frequency of 25 kHz in the laboratory simulates a geomagnetic variation with a period of 20 min. The impedance scaling for the present model, according to Eq. (2.12) or (2.14), is determined as K=30.

The shallow ocean (0.05 km depth) in the expansive Bohai Bay is underlain by conductive sediments (unpublished well log record for 3 km depth) to an average depth of approximately 5 km (Ma et al., 1984). The conductivity of the sediments was taken as $0.36 Sm^{-1}$ (one-tenth that of sea water). Since modelling materials to simulate the actual sediment-ocean conductivity contrast are not readily avail-

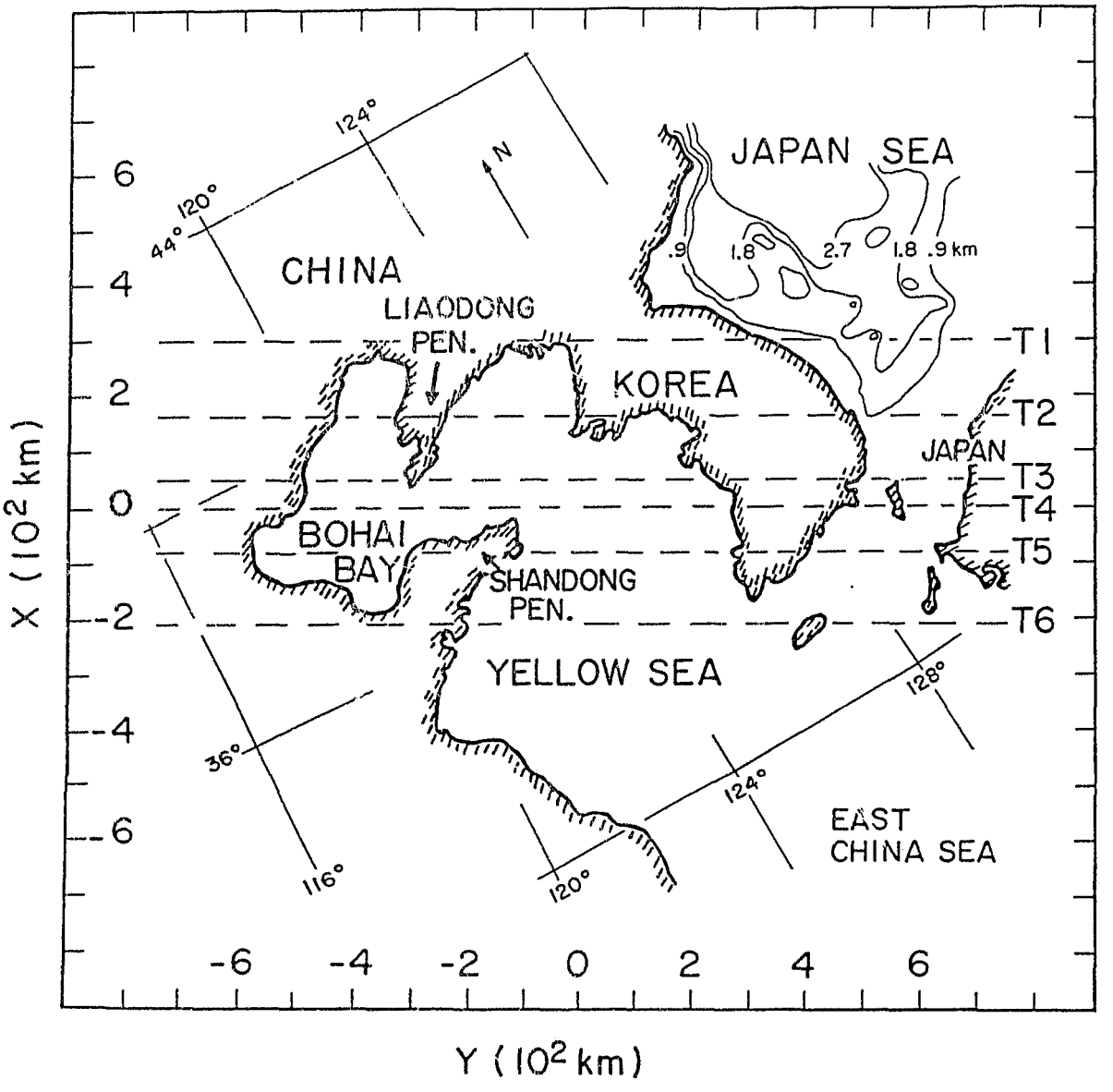

Figure 2.3: Simplified map of the Bohai Bay region with bathymetric contours, showing locations of the traverses for the model measurements.

able, an expedient discussed elsewhere (Dosso and Nienaber, 1986) is to scale the conductances (rather than the conductivity) and simulate the ocean-sediment combination as an equivalent ocean of increased depth. This results in a 0.5 km depth ocean in Bohai Bay to be simulated in the model by graphite plate of 0.5 mm thickness (near the limit of minimum thickness for possible physical construction). It is realized, that replacing the sediments by an equivalent ocean in the model will effect the electromagnetic responses somewhat at very short periods, since the bulk of the conducting material is nearer the surface. The highly conductive upper asthenosphere, taken to be at a depth of 100 km, was simulated by a 1.5 cm thick graphite plate suspended at a depth of 10 cm below the model ocean. The choice of the 80 km depth asthenosphere was based on the results of magnetotelluric surveys in the Bahai Bay region reported by Liu and Liu (1983) and Liu et al. (1983). In their work MT measurements at 30 sites in the Beijing-Tainjin-Tangshan region were used to determine apparent resistivities which were then fitted to 1D models to determine the conductivity structure. In addition to structures in the crust, their interpretation indicated a 0.5-1.0 Sm^{-1} asthenosphere at depths ranging from 50-100 km. The larger value of 100 km, rather than an intermediate depth, was chosen for the analogue model since the conductivity simulated using a graphite plate was somewhat higher than the Liu et al. (1983) values. The larger depth would somewhat offset the effects of the higher conductivity used. The 5 cm thick graphite plate that permanently lines the bottom of the modelling tank simulates a 3.6 Sm^{-1} conductive layer at a depth of 630 km.

2.4 The Analogue Model of The Japan-Korea-China Region

This second model will be referred to as the Japan model. Figure 2.4 shows a simplified map of the Japan-Korea-China region used as a pattern in constructing the scaled laboratory model. To ensure that the ocean effects, for sites on the Japan islands and on the continent in coastal regions, would be adequately represented in the model, a simulation of a portion of the ocean extending some 1500 km eas of Japan was included in the model. Included in the simulation also is the deep Pacific Trench off-shore Japan. The model of Fig.2.4 covers an area of 1.4m×1.4m, which for the $L_g/L_m = 3\times 10^6$ scaling factor chosen for the Japan model, represents an area of 4200km ×4200km. As was the case for the Bohai model, the conductivity scaling factor (determined by the modelling material used to simulate the land and oceans) is $\sigma_g/\sigma_m=3\times 10^{-5}$. Employing this factor and the linear scaling of 3×10^6, the frequency and impedance scaling are constrained to be $f_g/f_m =3.7\times 10^{-9}$ and K=90 respectively. For this scaling, a frequency of 75 kHz in the laboratory, simulates a geomagnetic variation with a period of 60 min, and 1 cm in the model simulates a length of 30 km in the geophysical scale. The model scale factors for the Bohai and the Japan models are listed in Fig. 2.5.

The region modelled in the Bohai model is also included in the Japan model and is shown by the dashed square section between T4 and T8 in Fig. 2.4. In order to carry out a valid model study of Japan it was necessary to include a much larger portion of the ocean than that of the Bohai model so that the Japan model could adequately represent the effects of the expansive Pacific Ocean on field measurements on Japan.

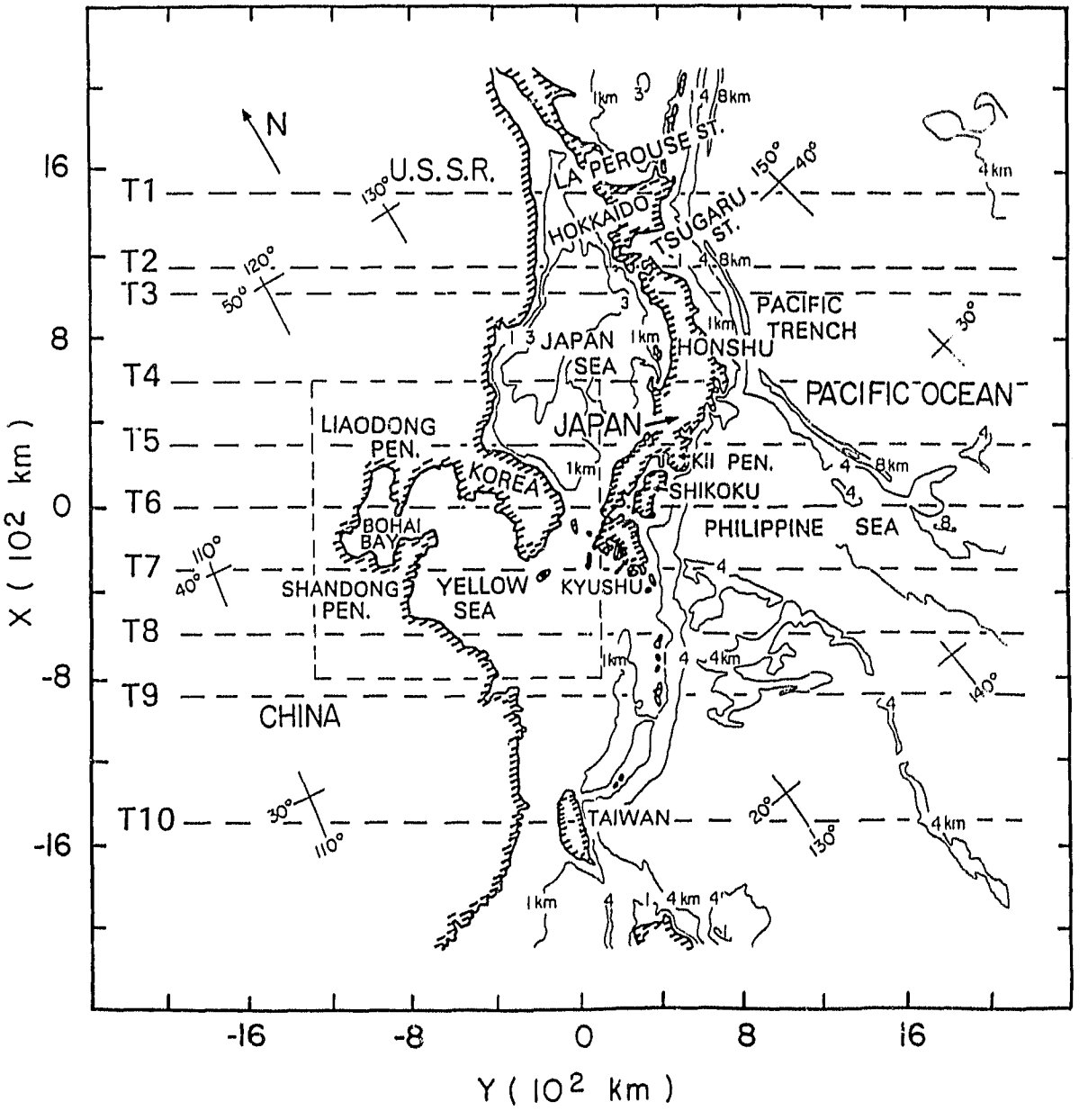

Figure 2.4: Simplified map of the Japan-Korea-China region with bathymetric contours, showing locations of the traverses for the model measurements.

$$\left(\frac{\sigma_g}{\sigma_m}\right)\left(\frac{L_g}{L_m}\right) = K$$

$$\left(\frac{f_g}{f_m}\right)\left(\frac{L_g}{L_m}\right) = K^{-1}$$

(1) THE BOHAI MODEL

$$\sigma_g / \sigma_m = 3\times10^{-5}$$

$$L_g / L_m = 10^6$$

$$f_g / f_m = 3.3\times10^{-8}$$

$$K = 30$$

(2) THE JAPAN MODEL

$$\sigma_g / \sigma_m = 3\times10^{-5}$$

$$L_g / L_m = 3\times10^6$$

$$f_g / f_m = 3.7\times10^{-9}$$

$$K = 90$$

Figure 2.5: Scale factors for the analogue models of the (1) Bohai Bay region and (2) Japan-Korea-China region.

In the Japan island arc region, it is known that the Pacific and Philippine oceanic plates are both actively subducting the islands. The conductivity anomalies beneath various parts of the Japan islands have been discussed in a number of studies (e.g. Rikitake, 1966; Rikitake and Honkura, 1973, 1986; Honkura,1978; RGCRSJ, 1983; Yukutake, 1985; Utada et al, 1986; Ogawa et al, 1986). Two dimensional analytical and numerical model calculations were used to interpret field data in the Japan region. For example, for the central Japan area where the coastlines are adjacent to the Pacific Ocean on the east and the Japan Sea on the west, three conductivity models have been proposed in these studies. These include: the Rikitake (1969) model in which the conductive substratum at 50km depth is depressed to a depth of 200 km beneath central Japan; the Honkura (1975) 2D model in which a 0.5 Sm^{-1} conductive layer (at a depth of 30 km and a thickness of 50 km) exists under both the Pacific Ocean and Japan Sea, but not under Japan, is underlain by a 0.01 Sm^{-1} conductive substratum; and the Utada et al. (1986) 2D model which includes a 0.1 Sm^{-1} conductive layer 40 km thick beneath the Pacific Ocean, and extending part way beneath Japan, at a depth of about 30 km, as well as a local 0.1 Sm^{-1} conductivity anomaly at a depth of 20 km under central Japan, with the entire structure underlain by a conductive (0.01 Sm^{-1}) substratum at a uniform depth of 70 km. Although the three models differ in structure and conductivity, they do have the common feature of a highly conductive anomaly underneath the Pacific Ocean, associated with the subducting structures of the Philippine oceanic plate.

Another example for the study of anomalous conductivity structure is the northern Honshu region of Japan where the Pacific Oceanic plate is subducting the

island at the east coast, and the Pacific trench is only a few hundred kilometers off shore. The west coastline of the region, on the other hand, is adjacent to the back-arc sea, the Japan Sea where the volcanoes are active. Extensive GDS and MT sounding along a number of east-west profiles across the region have been carried out since 1970 (Tanaka, 1972; RGCRSJ, 1983; Ogawa et al., 1986). The sea floor MT measurements at the Northwest Pacific ocean were made by Yukutake et al.(1983) in order to investigate the electrical conductivity structure of the subduction zone and to obtain the vertical profile of the conductivity beneath the Pacific Oceanic plate near the subduction zone. According to the Research Group for Crustal Resistivity Structure of Japan (RGCRSJ, 1983), it is known that the active volcanoes are distributed on the back-arc side of the island behind the so called volcanic front that runs along the island-arc axis. The measured heat flow values are higher on the back-arc side, and lower on the Pacific side. On the other hand, according to explosion seismology (Research Group for Explosion Seismology, 1977), the seismic foci distributions under the Japan island clearly depict the subducting structure of the Pacific oceanic plate with a roughly 45 degree dipping angle. The general conductivity structure under this region, according to the 2D model of Ogawa et al.(1986), is that the highly conductive layer ($0.01 Sm^{-1}$) at depth of 30 km under the Japan Sea is subducting the island almost to the east coast, while the Pacific oceanic plate ($0.01\ Sm^{-1}$) at depth of 80 km is subducting the island from the east.

In the present Japan analogue model study, the electrical and magnetic fields were first measured for the model with no deep conductivity structure included (except the 5 cm thick graphite plate that permanently lines the bottom of the

modelling tank, which simulates a $3.6Sm^{-1}$ conductive layer at a depth of 1890 km). The purpose of the measurements was to examine the ocean effect alone for the entire model region. A 1.5 cm thick graphite plate then was placed under the model ocean to simulate the effect of the conductive layer proposed by Utada et al. (1986), that is, σ=0.01 Sm^{-1} and d=70 km. The method to simulate the conductance rather than the conductivity of a proposed layer structure by a graphite plate has been fully discussed in previous analogue model work (Hebert, 1982). By applying this method to simulate a conductive layer at 70 km depth in the present Japan model, the depth of the graphite plate for the periods of 15, 30, 60, and 120 min was determined to be 4.4, 6.6, 8.2 and 11.2 cm (simulating 130, 200, 250 and 340 km) respectively. Detailed measurements for both electric and magnetic fields for a range of periods 15-120 min were carried out. For some traverse regions where the field measurements are available (for instance, for the central Japan and the northern Honshu regions), the magnetic fields were also measured for a range of plate depths for two perpendicular field polarizations. In these regions the analogue model data are amenable to comparison with the available field data.

2.5 The Chapter Summary

In this chapter, a brief summary of EM induction theory is introduced in order to obtain the model scaling conditions. It is shown that for a valid analogue model, the necessary and sufficient conditions are

$$(\sigma_g/\sigma_m)(L_g/L_m) = K, \qquad (2.13)$$

$$(f_g/f_m)(L_g/L_m) = 1/K, \qquad (2.14)$$

where the parameters f, L, σ represent frequency, length, and conductivity respectively, and $K = K_E / K_B$ is the impedance scaling factor. For the Bohai model, the length scaling factor L_g/L_m, and the conductivity scaling factor σ_g/σ_m are chosen to be 10^6 and 3×10^{-5} respectively. The frequency scaling factor f_g/f_m and the impedance scaling factor K, determined by the above scaling conditions, are 3.3×10^{-8} and 30 respectively. The Bohai model includes the shallow Bohai Bay, the Yellow Sea, the East China Seas and the deeper Japan Sea. For the Japan model, the length scaling factor L_g/L_m, the conductivity scaling factor σ_g/σ_m, the frequency scaling factor f_g/f_m and the impedance scaling factor K are 3×10^6, 3×10^{-5}, 3.7×10^{-9} and 90 respectively. Included in the Japan model are the Asian continental coastline, the Japan Islands, the Japan Sea and the Pacific Ocean.

A general description of the laboratory analogue modelling facility is presented. For a given model, a suitably shaped graphite plate simulates the ocean and salt solution in the large tank simulates land. A 1.5 cm thick graphite plate, placed beneath the model ocean, simulates the effect of a conductive substratum at depth.

Chapter III

ANALOGUE MODEL RESULTS FOR THE BOHAI BAY REGION OF CHINA

In the complex Bohai Bay coastal region of China (Fig.2.3), the effects of the prominent peninsulas, as well as the bays and ocean straits will play major roles in the field responses, particularly at short periods (Chan et al. 1981a; Dosso et al. 1986; Hu et al. 1986). Delineating the characteristics of these anomalous responses is of importance, since the responses may, in part, mask the responses of geological structure of interest.

In this study, measurements of the electric and magnetic field components for E- and B-polarizations were carried out along 15 traverses parallel to the y-axis over the Bohai Bay model for simulated source periods of 3, 5, 10, 20, 60 min. Traverses T1-T6 (Fig. 2.3) were chosen to examine the responses of the main coastal features in the modelled region. In the figures showing the field components of the traverses over the model, dashed lines represent responses over land and solid lines represent responses over the ocean. Geophysical, rather than model parameters, are used throughout.

3.1 Model Field Components for E-Polarization

3.1.1 Traverses for E-Polarization

For E-polarization of the source field, electric current induced in the Yellow Sea and the Japan Sea will tend to flow in the x-direction. A large part of the induced current will be channelled through the Korea-Japan strait. The channelling effects will be complicated by the small islands located within the strait. Current will also be deflected by the Korean peninsula and diffuse into the continent. To examine the fields due to these effects, results for E-polarization for six traverses (T1-T6) for a simulated 3 min period are shown in Fig. 3.1.

Traverse T1 shows the effects of the east coastline of Korea and the ocean depth gradient in the Japan Sea. In this traverse, in-phase B_x shows a particularly large positive anomalous response over the coastline which indicates that current induced in the Japan Sea is deflected by the Korean east coast which has an angle of roughly 45^o with the electric field of the inducing source. Both in-phase B_y and B_z also show large enhancements at this location in response to current deflection. Traverse T2 generally shows a similar response for the east coast of Korea, except that the anomaly in B_x is decreased since the angle the coastline makes with the inducing field is much reduced. Anomalies in the in-phase B_y and B_z components are increased relative to those for T2 due to the channelling of current through the Korea-Japan strait. Also, larger B_y and B_z anomalies are expected where the coastline is parallel to the inducing field. The channelling effects observed here agree with the model results (Dosso et al. 1986) for an idealized island situated near a cape coastline. Continuing down the east coast, it is seen that the results along T3, T4, and T5 all show the effects of current con-

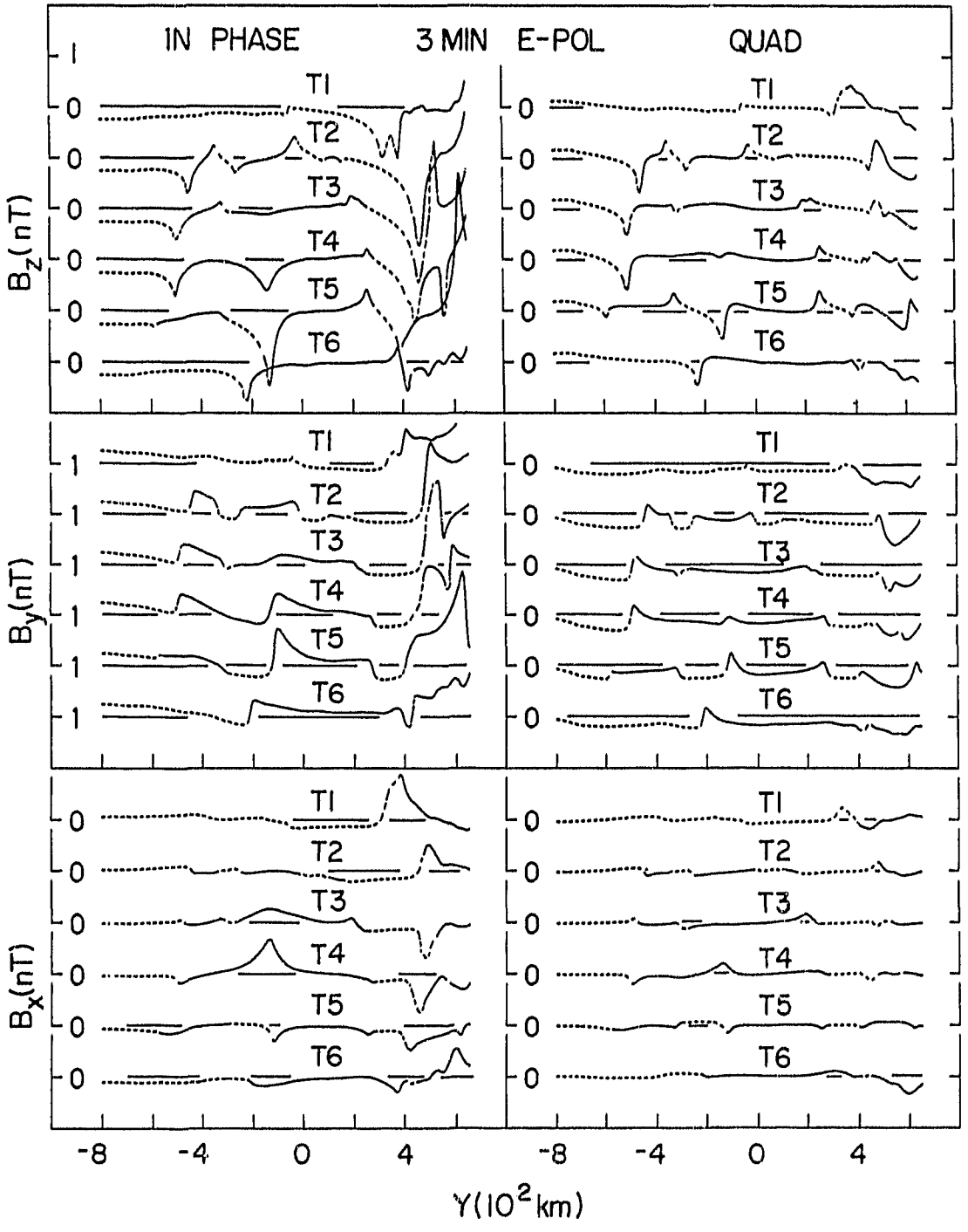

Figure 3.1: In-phase and quadrature magnetic fields for traverses T_1 to T_6 for E-polarization at 3 min.

centration due to channelling through the strait, with the in-phase B_x coastal anomaly changing sign in response to the changing direction of the y-component of the current as it is channelled through the strait and into the Yellow Sea. The form of in-phase B_z over the Korea-Japan strait shows the effects of current channelling most clearly, with the field reversing as though the profile traversed a perpendicular line current. Generally, the anomalies on the west coast of the Korean peninsula are small due to minimal induction in the shallow Yellow Sea for E-polarization. This is also the case along much of the Yellow Sea coastal region, including Bohai Bay. It is noted that the Liaodong and the Shandong peninsulas do lead to significant anomalies due to current deflection at this short period of 3 min. Traverse T5 shows large in-phase and quadrature B_z anomalies at the eastern Shandong peninsula coastline, and these anomalies are significant inland over the peninsula, and would be important in interpreting field measurement at such locations. One notable feature is the large B_x anomaly in the Yellow sea region (T4) opposite in sign to the B_x anomaly near Japan. While the latter indicates SW-NE current flow in the Korea-Japan strait, the former indicates that the dominant current flow in the Yellow Sea is SE-NW as it flows near and around the Shandong peninsula.

The in-phase and quadrature E_x and E_y along traverses T1 to T6 for 3 min are shown in Fig. 3.2. As expected for E-polarization of the source field, the induced current flowing in the x-direction will first encounter the southern coast of the Korean peninsula. Some of the current will be deflected to the +y direction, being funnelled through the Korea-Japan strait. While some will be deflected to the -y direction, flowing along the conductive pass of the Yellow sea. These currents

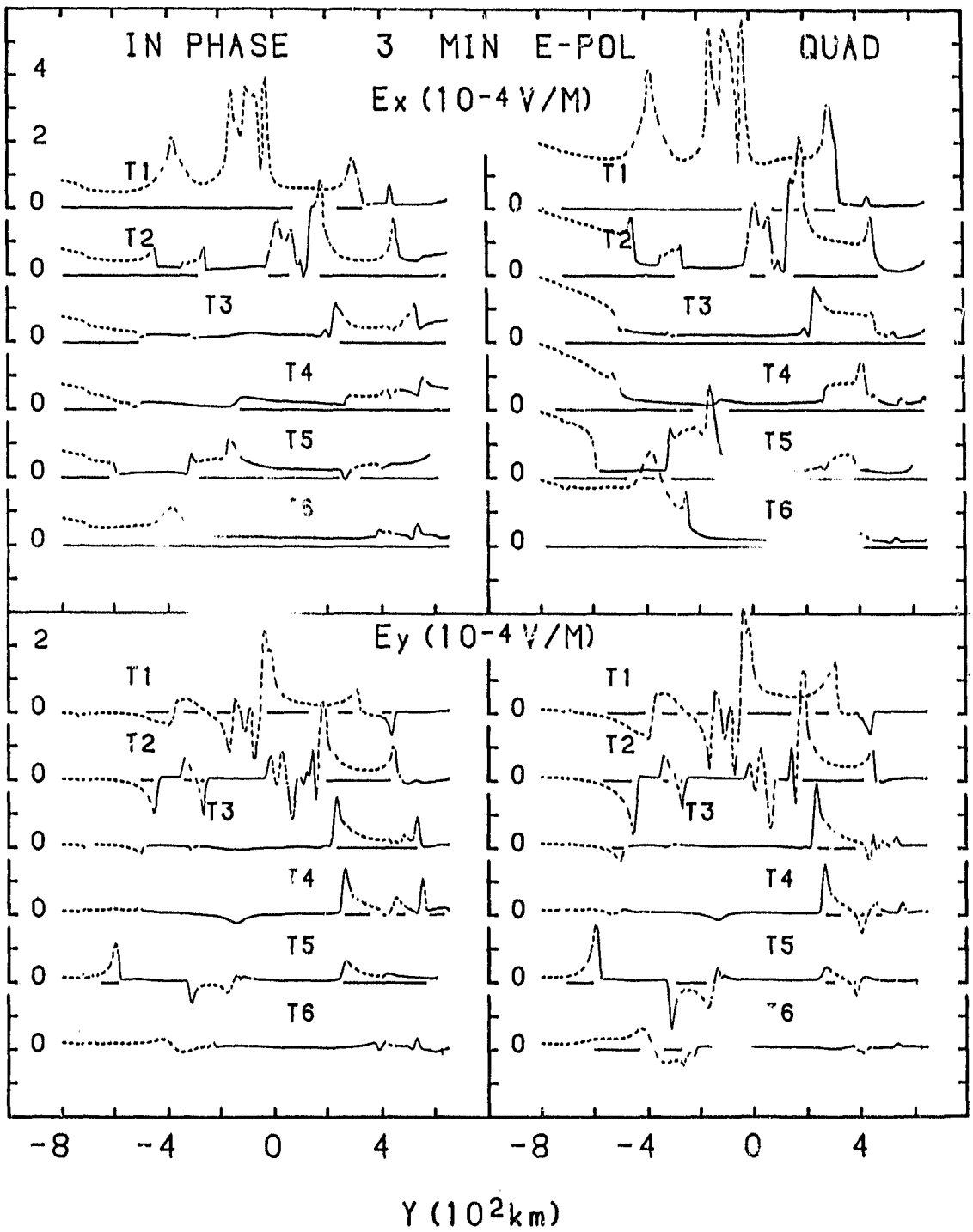

Figure 3.2: In-phase and quadrature electric fields for traverses T_1 to T_6 for E-polarization at 3 min.

deflected in opposite directions account for the reversal of quadrature E_y for T3, T4 and T5 in the Korean peninsula region. At the T1 China-Korea coast region, induced current will encounter the coastline and then be diffused into the resistive continent which leads to large anomalous response of E_x and E_y for T1. It is seen that E_x at the continent area of T3 and T4 gradually decreases approaching the coast of Bohai Bay, while E_y has minimal response over the coast, due to the bay effect.

3.1.2 Frequency Response for E-Polarization

Traverses T2 and T5 were selected to examine the responses (as a function of period) of the bays, capes, and peninsulas that would be important in any interpretation of field observations in these coastal regions. Results provided for both E- and B- polarizations for a range of periods readily permit determination of induction arrows (or transfer functions) appropriate for comparisons with field observations. Such comparisons will be discussed in a later chapter.

The in-phase and quadrature B_z, B_y and B_x along T2 are shown in Fig. 3.3 for six periods for E-polarization. Since the ocean is generally very shallow here, induction will be important only for very short periods. Note that the 0.5 km depth ocean is 0.1δ (skin depth $\delta = (2/\sigma\omega\mu)^{1/2}$) for 3 min period variations. Thus, as expected, the results of Fig. 3.3 show that any small field anomalies in the shallow bay region observed along T2 at 3 min become negligible with increasing period. However, both in-phase and quadrature fields for all components show substantial anomalies over the east coastline of Korea in response to the increased current density resulting from local induction as well as from deflection of current by the local coastline, and the channelling of current through the

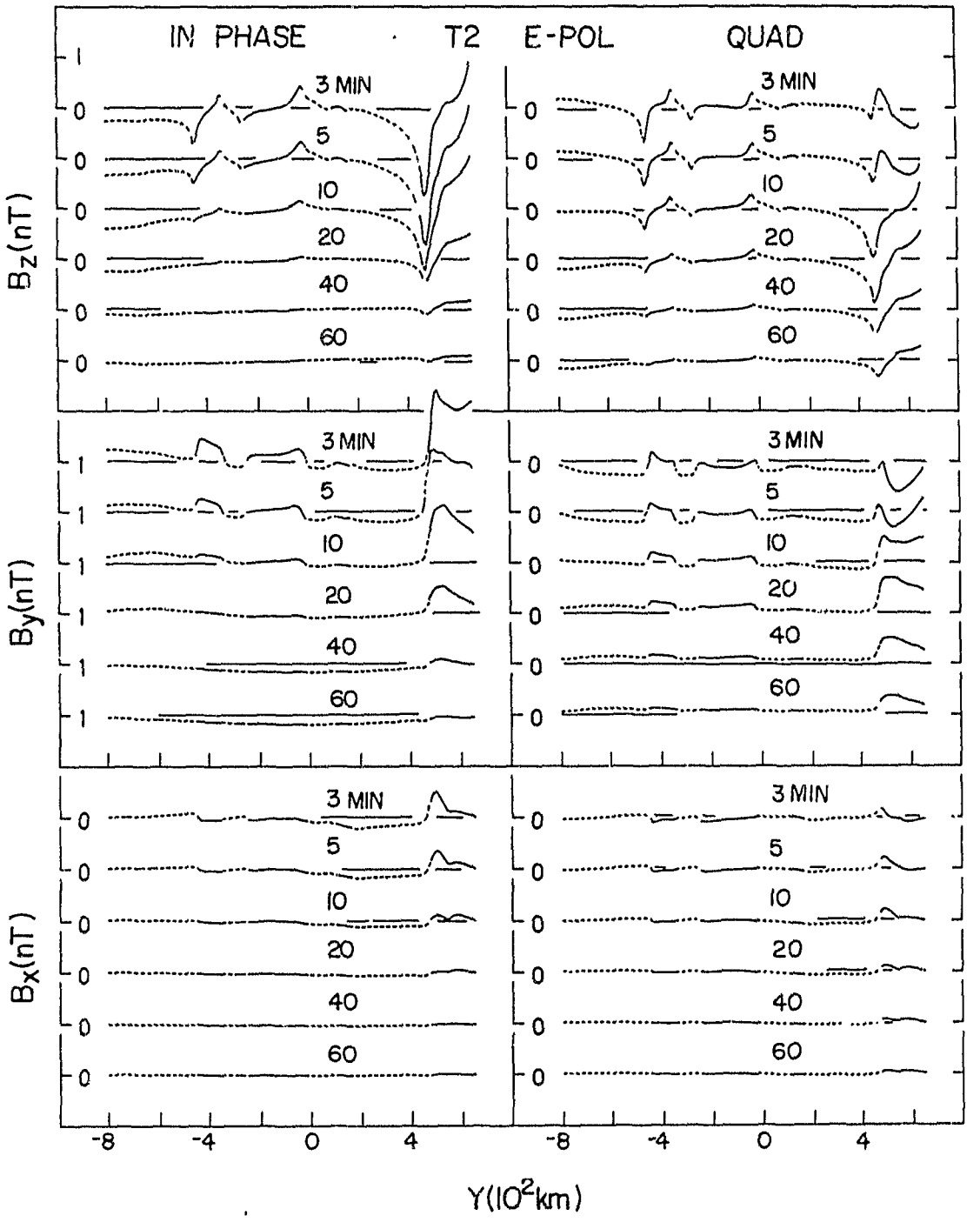

Figure 3.3: In-phase and quadrature magnetic fields for traverse T_2 for E-polarization at periods from 3 to 60 min.

Korea-Japan strait. These anomalies, too, fall off with increasing period. It is noted that over the Korea-Japan strait quadrature B_z and B_y anomalies at long periods are of opposite sign to those at short periods. This will lead to a rotation of the quadrature induction arrows with increasing period. Quadrature B_z and B_y anomalies at the east coast of Korea are significant over the entire period range, while the in-phase responses are negligible beyond 40 min.

Other significant anomalies along traverse T2 are the large gradients in B_z and the enhancements of B_y over the northern part of Bohai Bay at short periods due to local induction in the ocean, the cape effect, and the deflection of current to either side of the Liaodong peninsula. These anomalies fall off rapidly with increasing period, since the .5 km ocean is too shallow for induction at long periods. It is interesting to note from the shapes of the curves in Fig. 3.3 that the quadrature responses at longer periods tend to closely mimic the in-phase responses at shorter periods. For example, the quadrature B_z response off-shore Korea at 60 min over the deeper ocean on the east coast of Korea is very similar to the in-phase response at 20 min. Relative enhancement of the quadrature response is characteristic of current flowing at increased depth. The similarity of shape to the in-phase response is expected since the current channelled at increasing depths with period (due to induction at increasing depths in the deep ocean) will continue to have a line current form at the longer period. As the effective depth of the current increases, the quadrature response will be enhanced and the in-phase response decreased.

Figure 3.4 provides the frequency responses for the magnetic fields along traverse T5 for E-polarization. Large in-phase and quadrature B_z anomalies

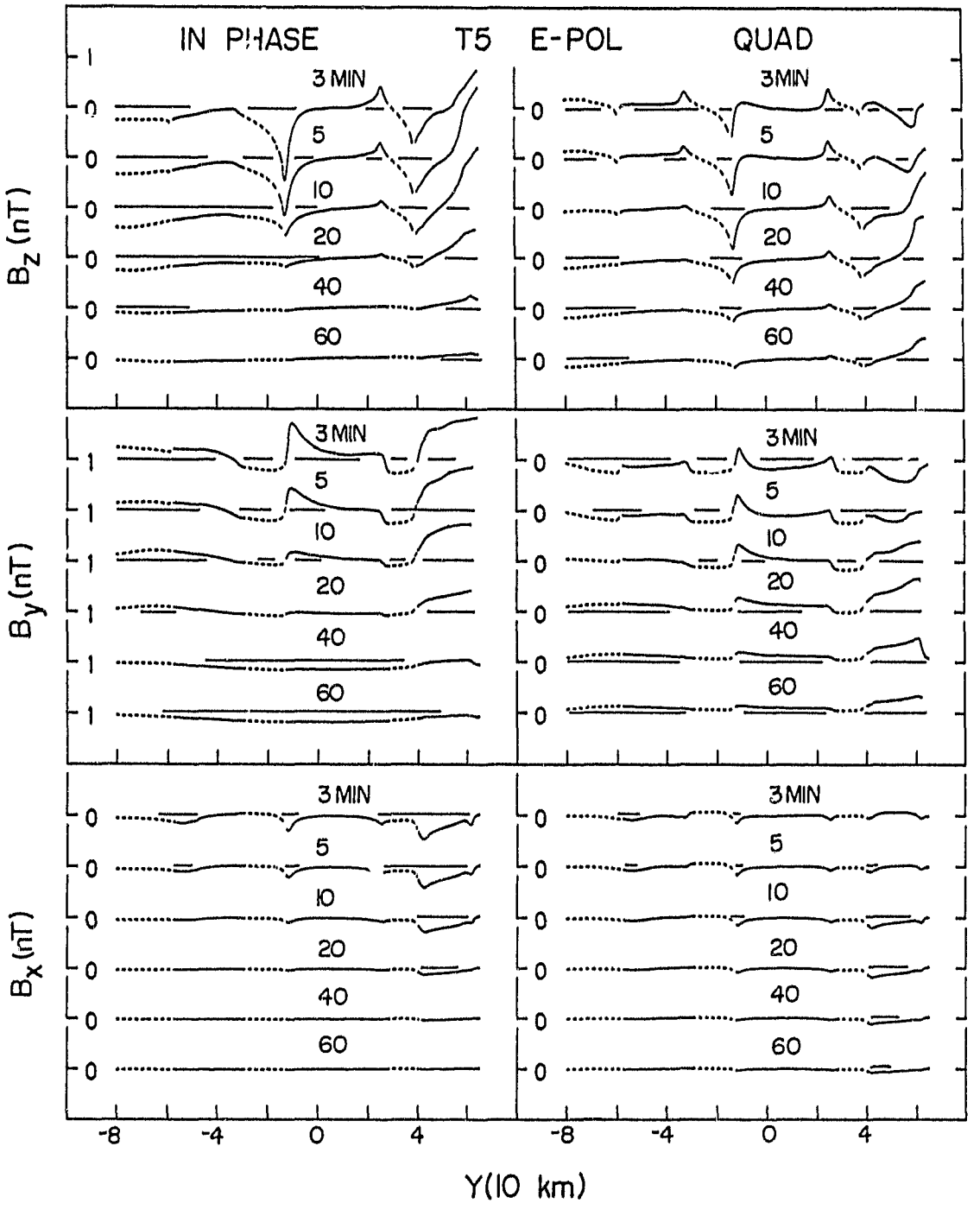

Figure 3.4: In-phase and quadrature magnetic fields for traverse T_5 for E-polarization at periods from 3 to 60 min.

observed at the Shandong peninsula are due to the cape effect. This cape effect leads to large in-phase and quadrature B_z field gradients over the Shandong and the Korean peninsulas with the quadrature gradients remaining significant over the entire period range. The B_z and B_y responses indicate that the deflection of current at the Korean peninsula is more significant than that at the Shandong peninsula. Clearly, the interpretation of any field station measurements for sites on these peninsulas, or for local off-shore sites, would have to take into account these cape effects, particularly at short periods.

Figure 3.5 shows the frequency responses of the electric fields for traverse T2. In the continent area the E_x responses increase rapidly as the period decreases, as expected. The quadrature E_x in general is larger than the in-phase component by a factor of 3 over the land area, indicating a phase lag (less than 45^o) between electric and magnetic fields. It is seen that large E_x and E_y occur at the coastlines of the Korean peninsula in response to the enhanced current density resulting from diffusion and deflection of the current in that region. The electric fields over the Bohai bay region show somewhat smaller responses than those over the Korean peninsula due to the bay effect. It is also seen that E_y changes sign cross the Liaodong peninsula in response to the change of the current direction along the y-axis as it encounters the peninsula and is deflected by the tip of the peninsula.

Figure 3.6 shows the in-phase and quadrature electric fields for traverse T5. The most significant anomalous response along T5 is that over the Shandong peninsula where strong current deflection has occurred. The responses of E_x and E_y decrease rapidly with increasing period, so that both the in-phase and quadrature

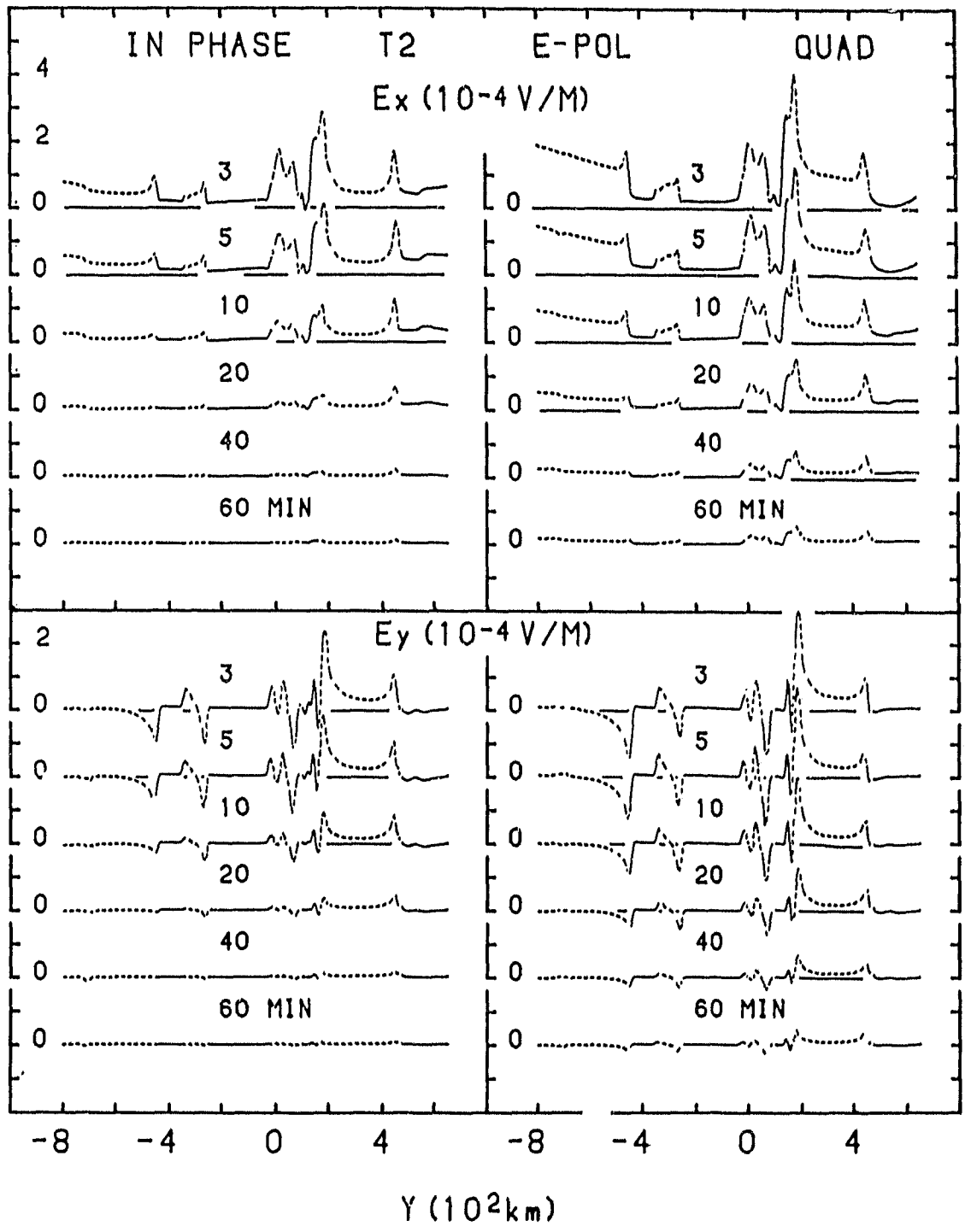

Figure 3.5: In-phase and quadrature electric fields for traverse T_2 for E-polarization at periods from 3 to 60 min.

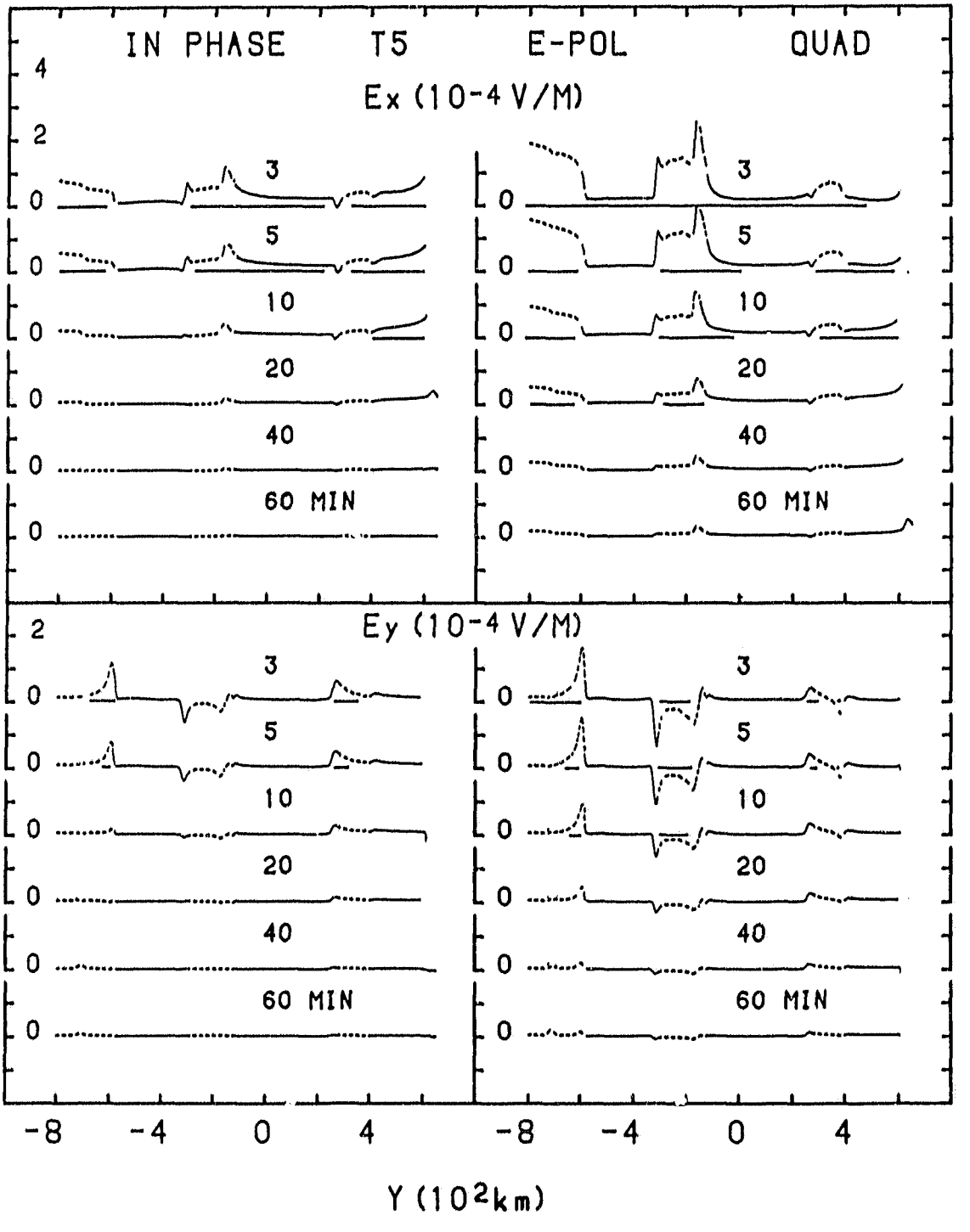

Figure 3.6: In-phase and quadrature electric fields for traverse T_5 for E-polarization at period from 3 to 60 min.

components are negligible at 60 min. In comparing Fig. 3.5 with Fig. 3.6, it is seen that E_y in the T2 area of Bohai bay is opposite in sign to that at the T5 area of the bay, clearly indicating the effect of induced current expanding into the bay region.

3.2 Model Field Components for B-Polarization

3.2.1 Traverses for B-Polarization

The responses of the modelled region for B-polarization of the source field (electric field of the inducing source in the y-direction in Fig. 2.4) are shown in Fig. 3.7 for traverses T1-T6 for 3 min. For this polarization of the source field, electric currents induced in the Japan Sea and the open Yellow Sea tend to flow in the y-direction to be in part deflected and channelled by the coastlines, and in part diffused into the continent. In general, the shapes of the coastlines provide a more abrupt obstacle to the y-direction flow of induced current than was the case for E-polarization. The results for T3 and T4 at the eastern coast of Korea in Fig. 3.7 show the effects of some current channelling through the Korea-Japan strait, but much less than observed for E-polarization. Current induced in the East China Sea is in part funnelled into the Yellow Sea and eventually into Bohai Bay where it diffuses into the continent. The peninsulas (Korea, Shandong, and Liaodong) provide obstacles to the current funnelling and lead to local current concentrations at the tips of the peninsulas for B-polarization. Large in-phase B_z and B_x anomalies over the tip of the Liaodong peninsula (T3) are observed due to such local current concentration. Traverse T4, which by-passes the peninsulas (Liaodong and Shandong), shows the effects of current deflection and channelling

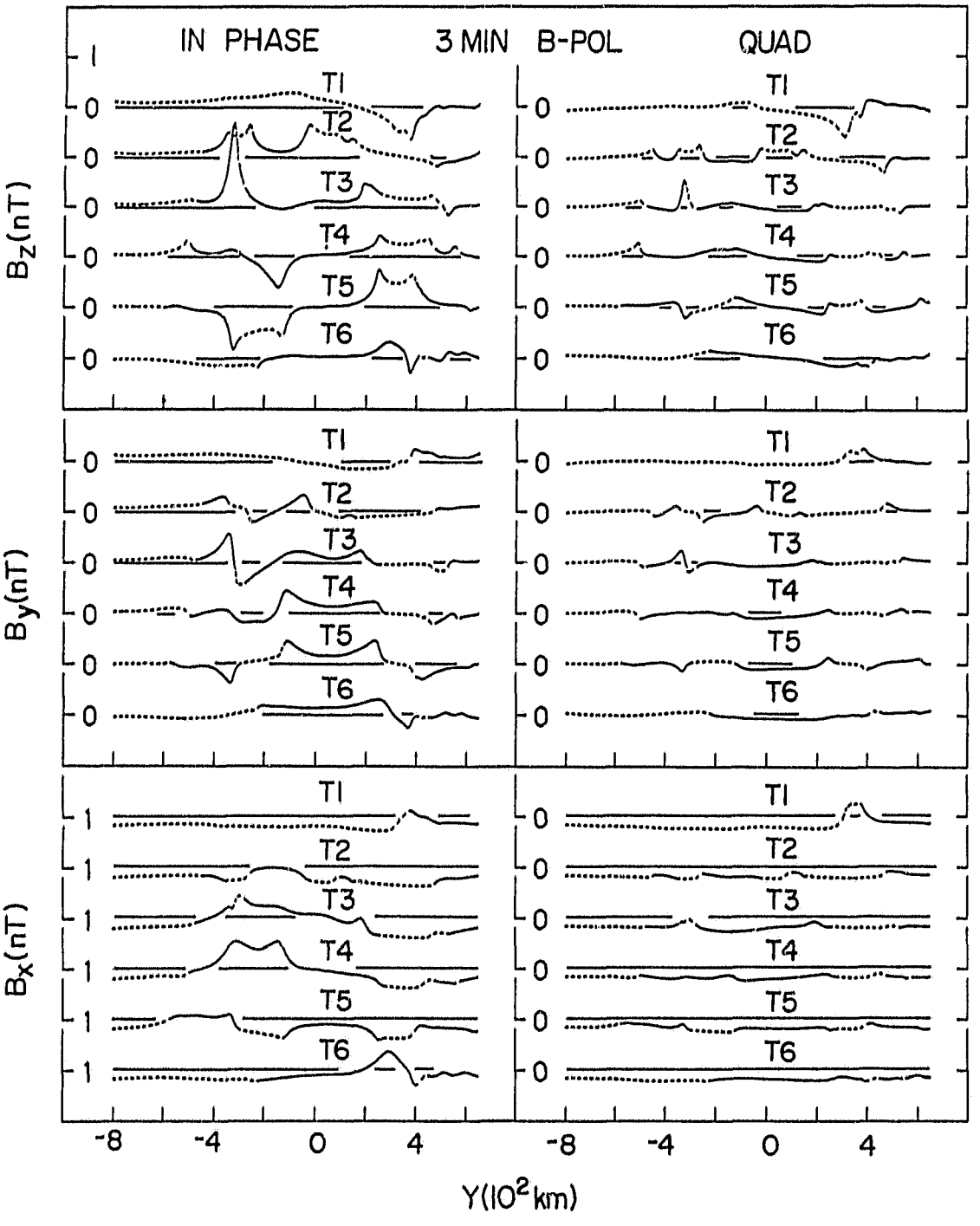

Figure 3.7: In-phase and quadrature magnetic fields for traverses T_1 to T_6 for B-polarization at 3 min.

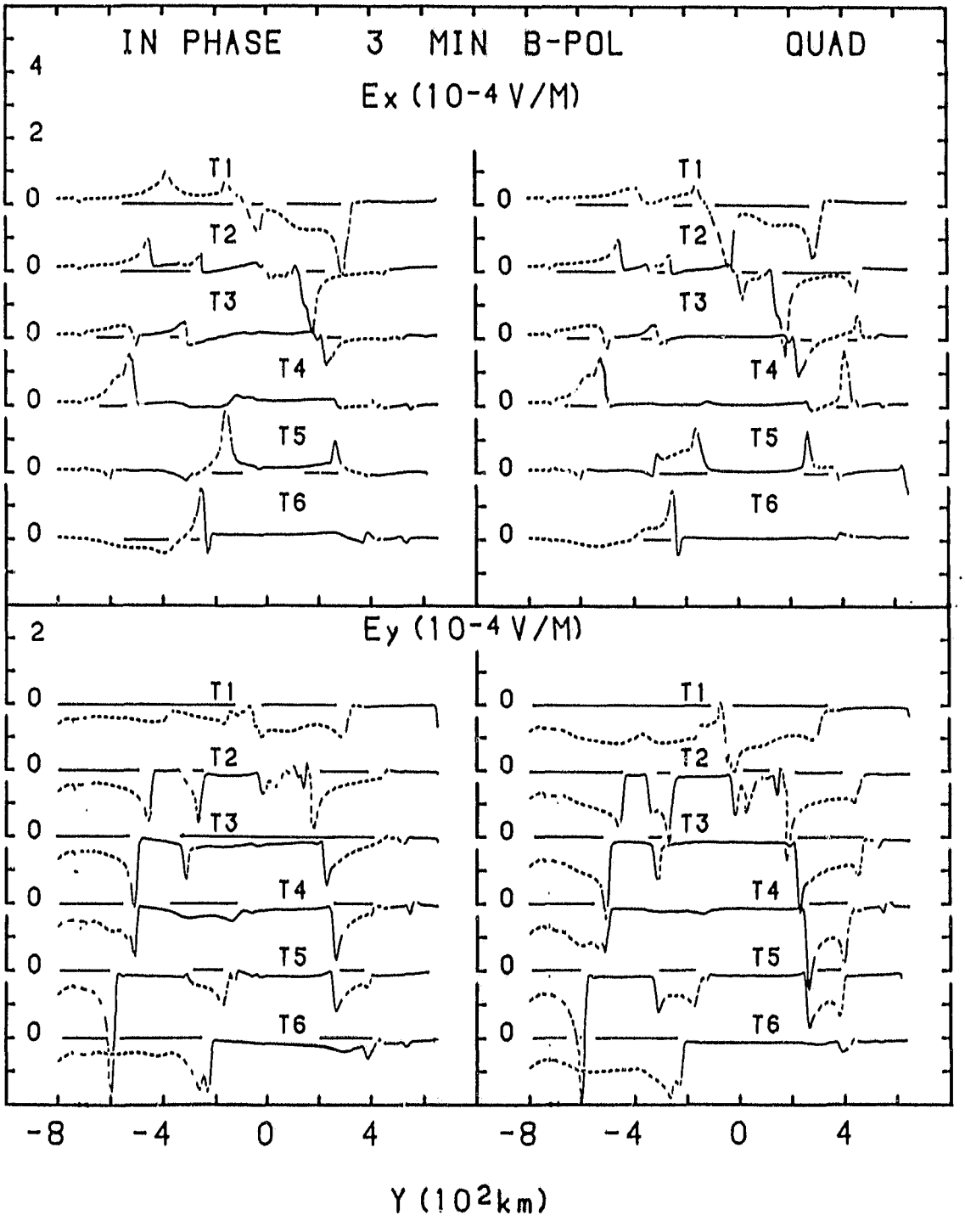

Figure 3.8: In-phase and quadrature electric fields for traverses T_1 to T_6 for B-polarization at 3 min.

through Bohai strait, showing significant anomalies in all three in-phase components. In comparing the results for E- and B-polarization, it is noted that the east coast of the Korean peninsula and the Korea-Japan strait show a strong response for E-polarization, whereas the Liaodong and the Shandong peninsulas show the major responses for B-polarization. In both cases current channelling and deflection plays an important role. The B_z reversal observed for traverse T5 in crossing the Yellow Sea is roughly the same for both E- and B- polarizations, since the conductor generally lies at 45^o to the inducing field, and thus channels current effectively for both polarizations.

Figure 3.8 shows the in-phase and quadrature electric fields for traverses T1 to T6 for B-polarization for 3 min period. As induced current flowing in y-direction encounters the continent, current diffusion is expected to occur which yields large negative anomalies in E_y along the west coast of Korea shown in T4, T5 and T6, and at the Bohai bay coast shown in T2, T3, T4 and T5. In addition to the current diffusion, evidence of current deflection also is seen along the east coast of Korea where quadrature E_x on traversers T1 and T2 are negative, while E_x on traverses T3 and T4 are positive, indicating the effect of current deflected to either the +x or -x direction to follow the east coast of Korea. Large in-phase and quadrature E_x are also observed along T5 in response to the current deflection around the tip of the Shandong peninsula.

3.2.2 Frequency Response for B-Polarization

In-phase and quadrature magnetic fields along traverses T2 and T5 are shown in Figs. 3.9 and 3.10 respectively For B-polarization, current induced in the oceans will be deflected to the left and right by the eastern Korea coastline, leading to current concentration at the coastline and the resulting vertical and horizontal field anomalies. Current deflected around the tip of the Korean peninsula, and current induced in the Yellow Sea, will follow the conductive path into the Bohai Bay region and diffuse into the continent. In general, large field anomalies should not be expected along T2 in the shallow sea region since the coastlines represent an effective obstacle to current flow in the y-direction. Moderate anomalies along T2 are observed at the west coast of Korea and over the Liaodong peninsula at short periods only. Along T5 in Fig. 3.10 significant cape responses are observed at the Korean and the Shandong peninsulas, with the maximum in the quadrature B_z response in each case occurring at roughly 10-20 min.

Figures 3.11 and 3.12 provide the frequency responses of the electric fields for T2 and T5 respectively. As expected, large negative response of in-phase and quadrature E_y occur at the Bohai bay coast and the Liaodong peninsula in response to the effect of current diffusion into the resistive land. Along the west coast of Korea, both current deflection and diffusion are expected to be important since the strike of the coastline is roughly 45° relative to the direction of the inducing field. Evidence of these effects is clearly indicated by the large negative responses of both E_x and E_y over the Korean peninsula. For T5, the most significant anomaly is the enhanced positive E_x over the Shandong peninsula, showing the effect of current deflection there. It is seen that the electric field responses are maxi-

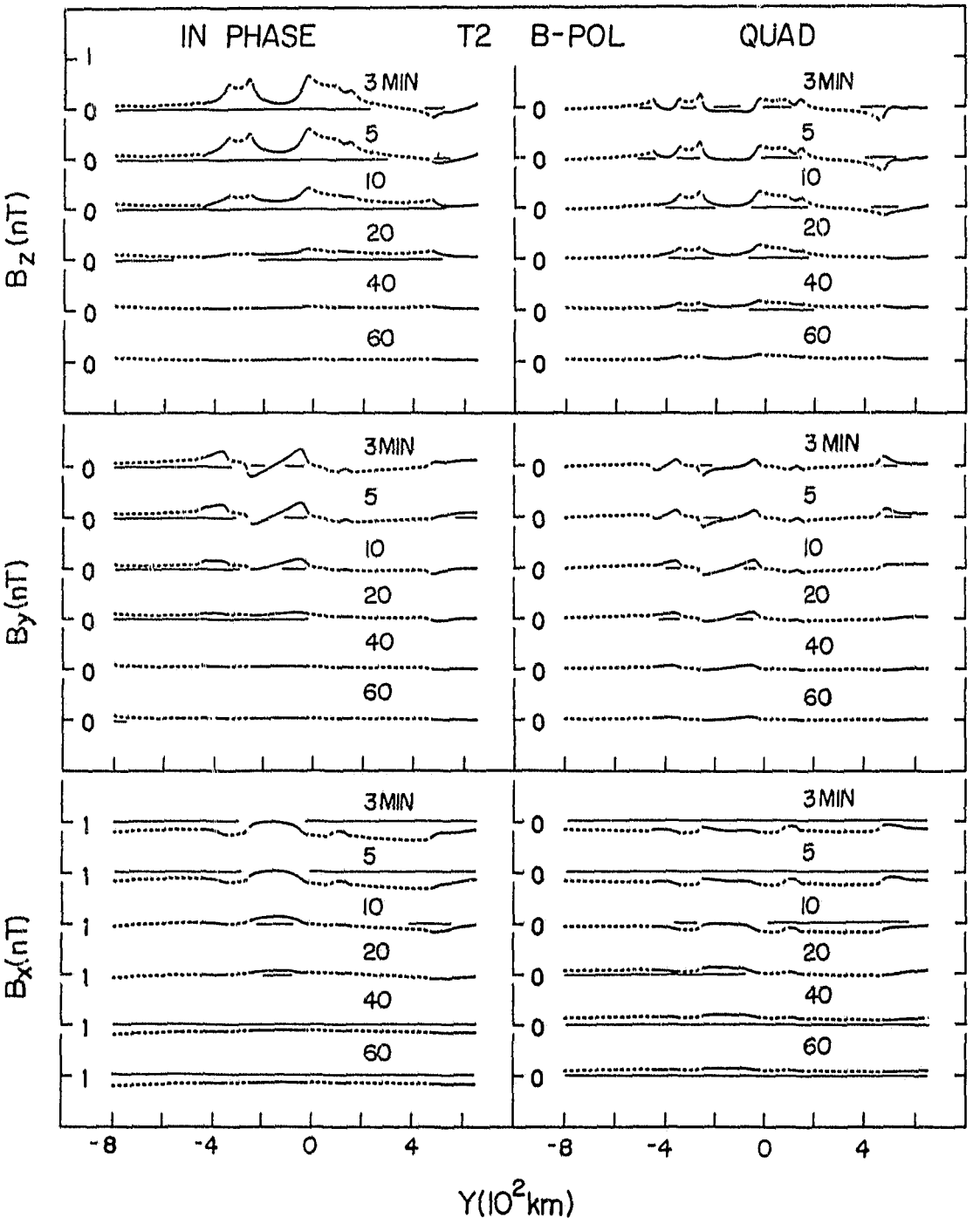

Figure 3.9: In-phase and quadrature magnetic fields for traverse T_2 for B-polarization at periods from 3 to 60 min.

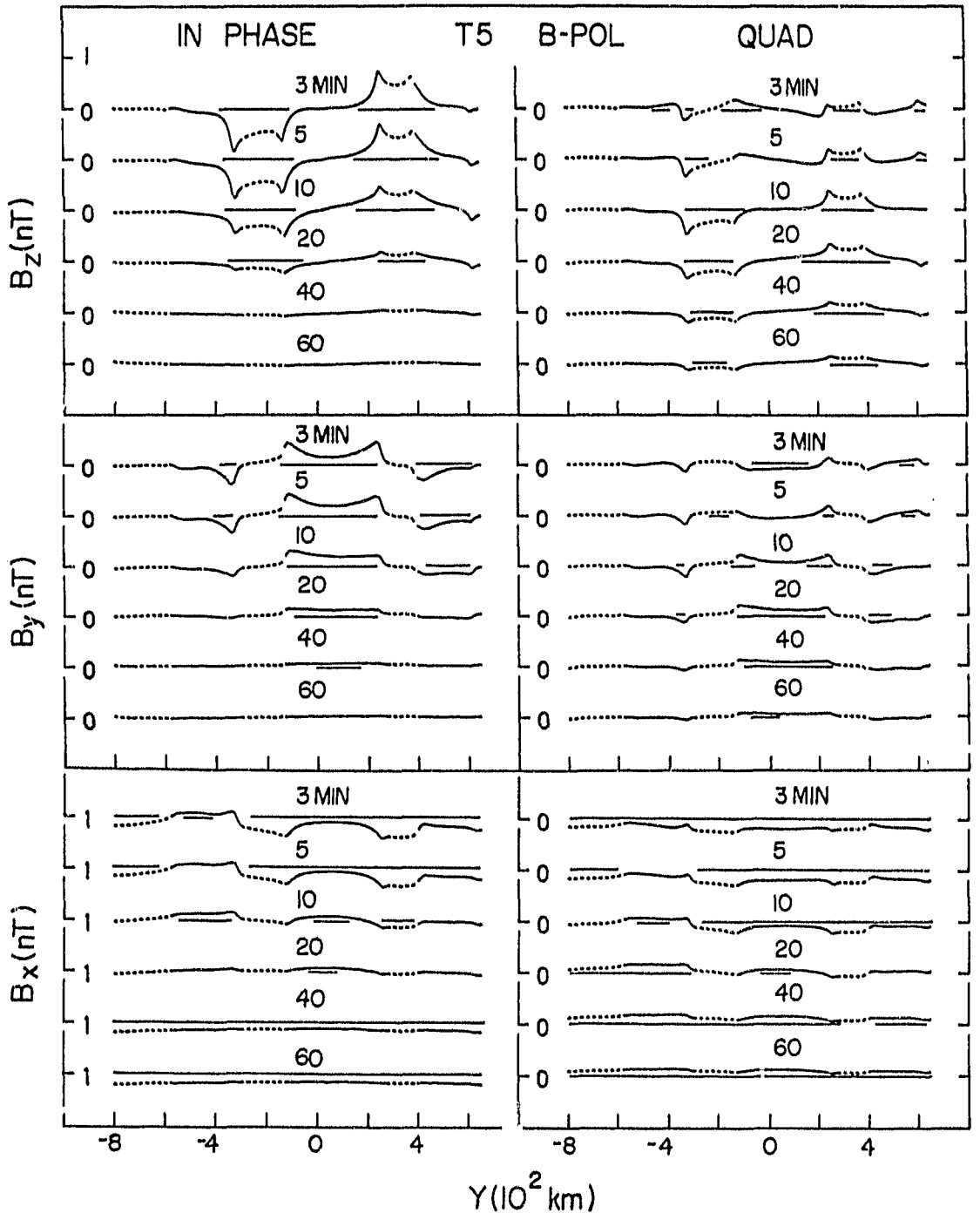

Figure 3.10: In-phase and quadrature magnetic fields for traverse T_5 for B-polarization at period from 3 to 60 min.

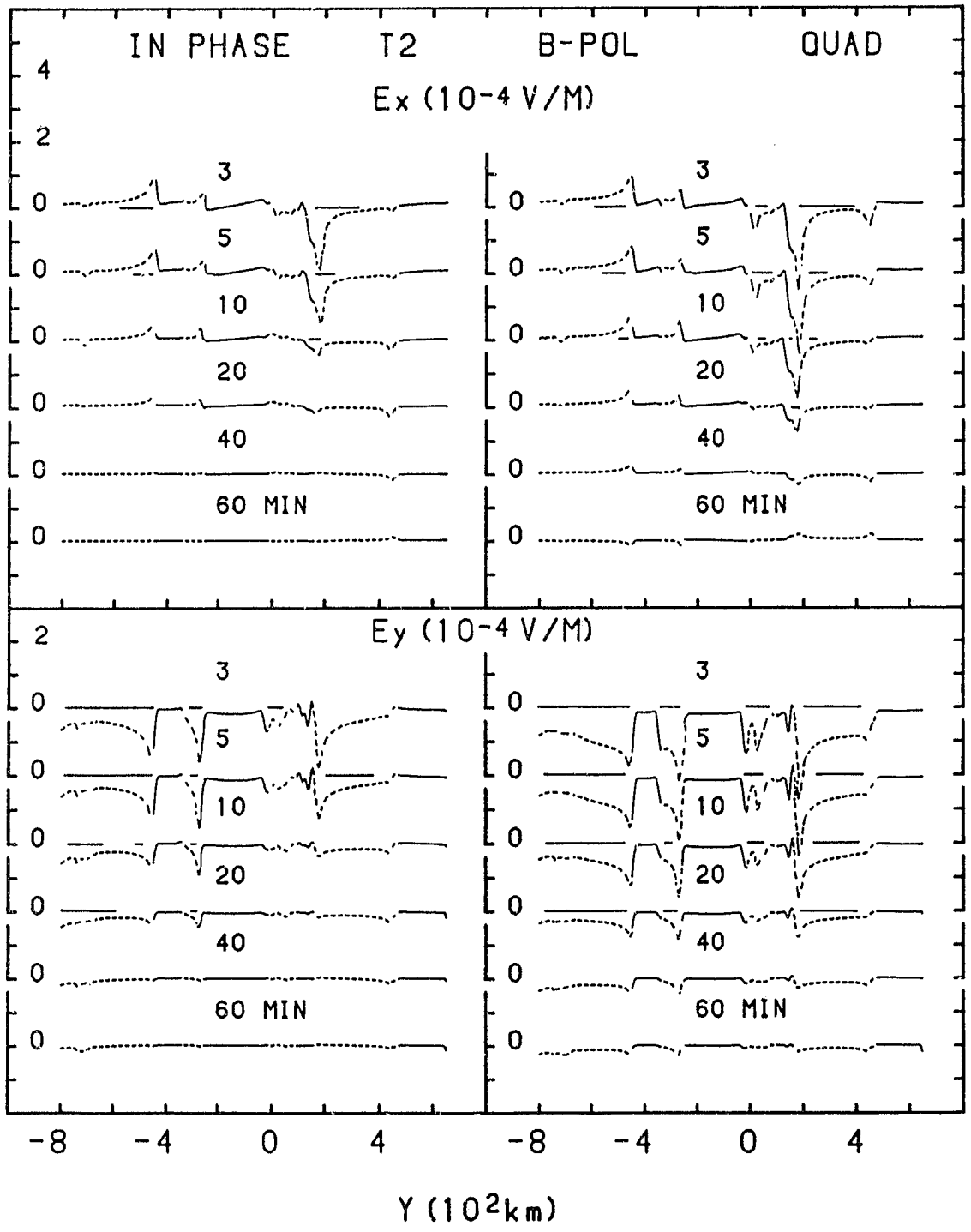

Figure 3.11: In-phase and quadrature electric fields for traverse T_2 for B-polarization at periods from 3 to 60 min.

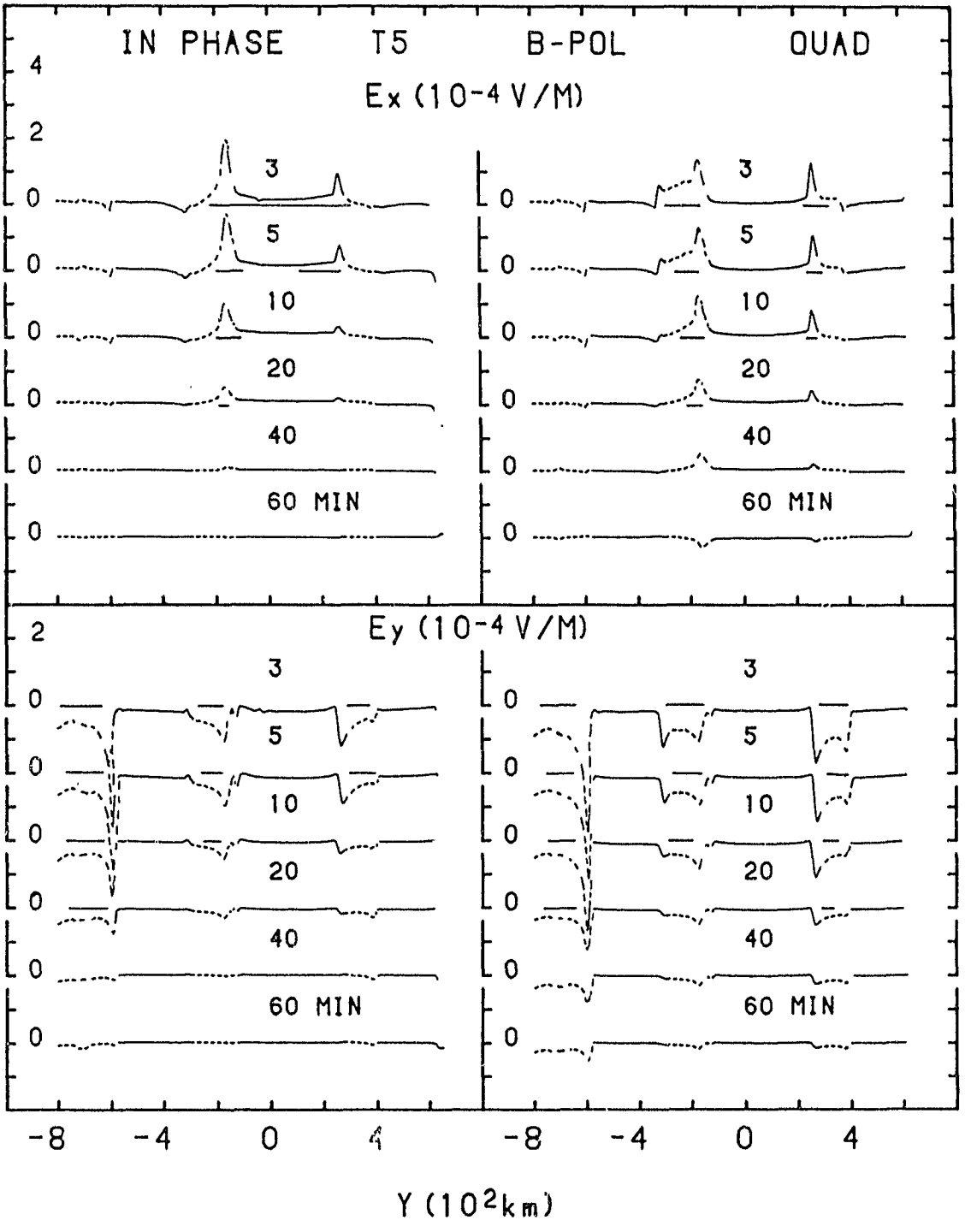

Figure 3.12: In-phase and quadrature electric fields for traverse T_5 for B-polarization at periods from 3 to 60 min.

mum at the short period of 3 min, similar to that observed for E-polarization. With increasing period, the responses decrease to become negligible at 60 min for both in-phase and quadrature components.

3.3 Contours and Three Dimensional Views of Model Field Components

3.3.1 Field Contours for E- and B-Polarizations

To provide a broader view of the in-phase and quadrature magnetic field components for the entire region of the model, E_z and B_y field contours of 3 min for E-polarization are given in Figs. 3.13 and 3.14 respectively. Clearly from Figs. 3.13 and 3.14, large in-phase B_z and B_y field gradients are observed along the eastern Korea coastline due to the effects of current deflection by the curved coastline and current channelling through the Korea-Japan strait. As well, particularly large field gradients are seen at the tip of the Shandong peninsula due to the cape effect at this short period.

Figures 3.15 and 3.16 show B_z and B_x contours at 3 min for B-polarization respectively. Large in-phase B_z and B_x gradients are observed at the Bohai strait and at the southern tip of the Korean peninsula as was the case for E-polarization. Significantly large field gradients for in-phase B_z also exist over the Shandong peninsula. It is noted that a large B_z anomaly over the tip of the Liaodong peninsula occurs for B-polarization (Fig. 13), while little response is observed over the region for E-polarization. Thus the comparison of the B_z contours for the two polarizations shows that there is considerable current flow in the Yellow Sea region for both polarizations, but current flow in the Bohai strait primarily for B-polarization.

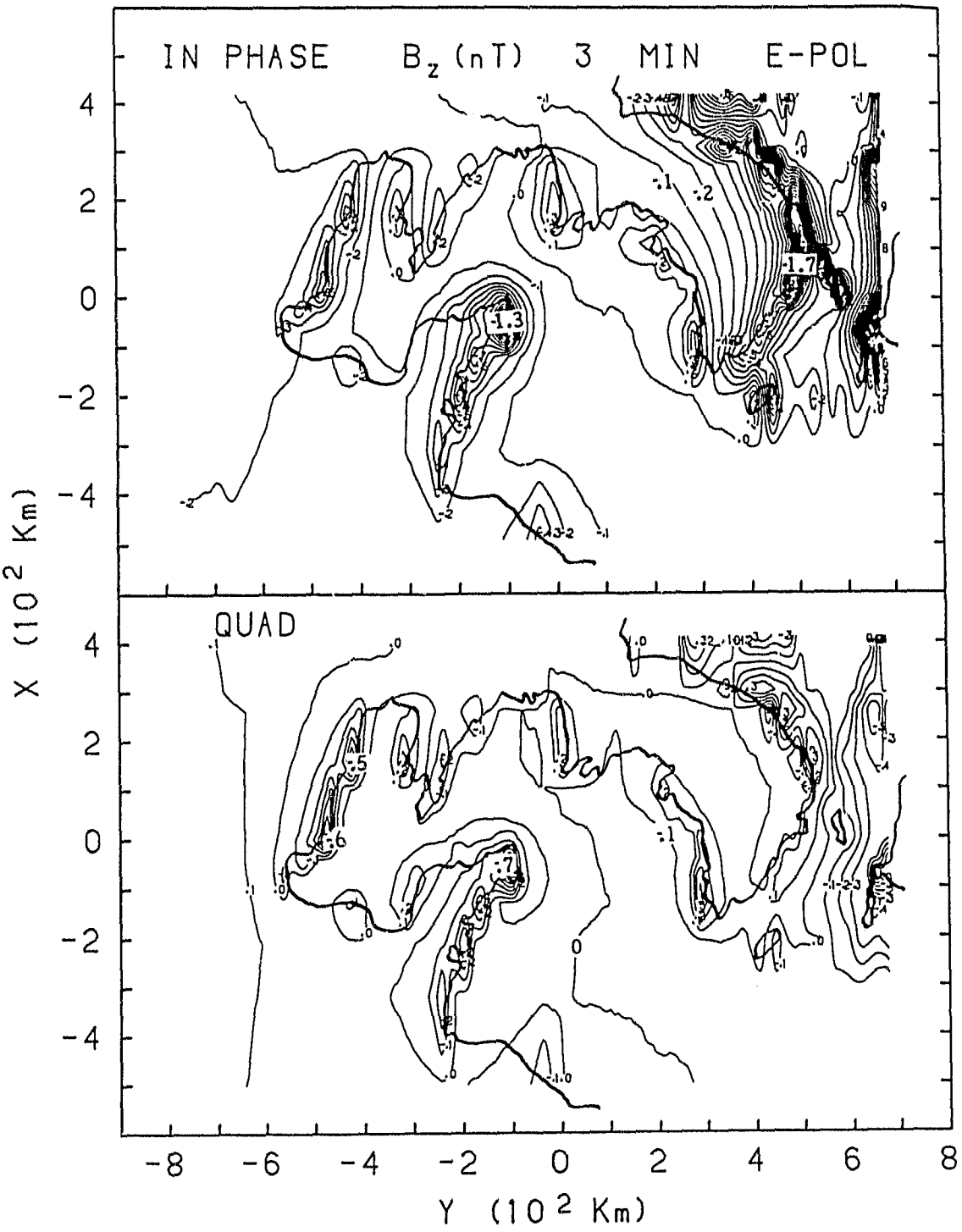

Figure 3.13: In-phase and quadrature B_z field contours at 3 min for E-polarization.

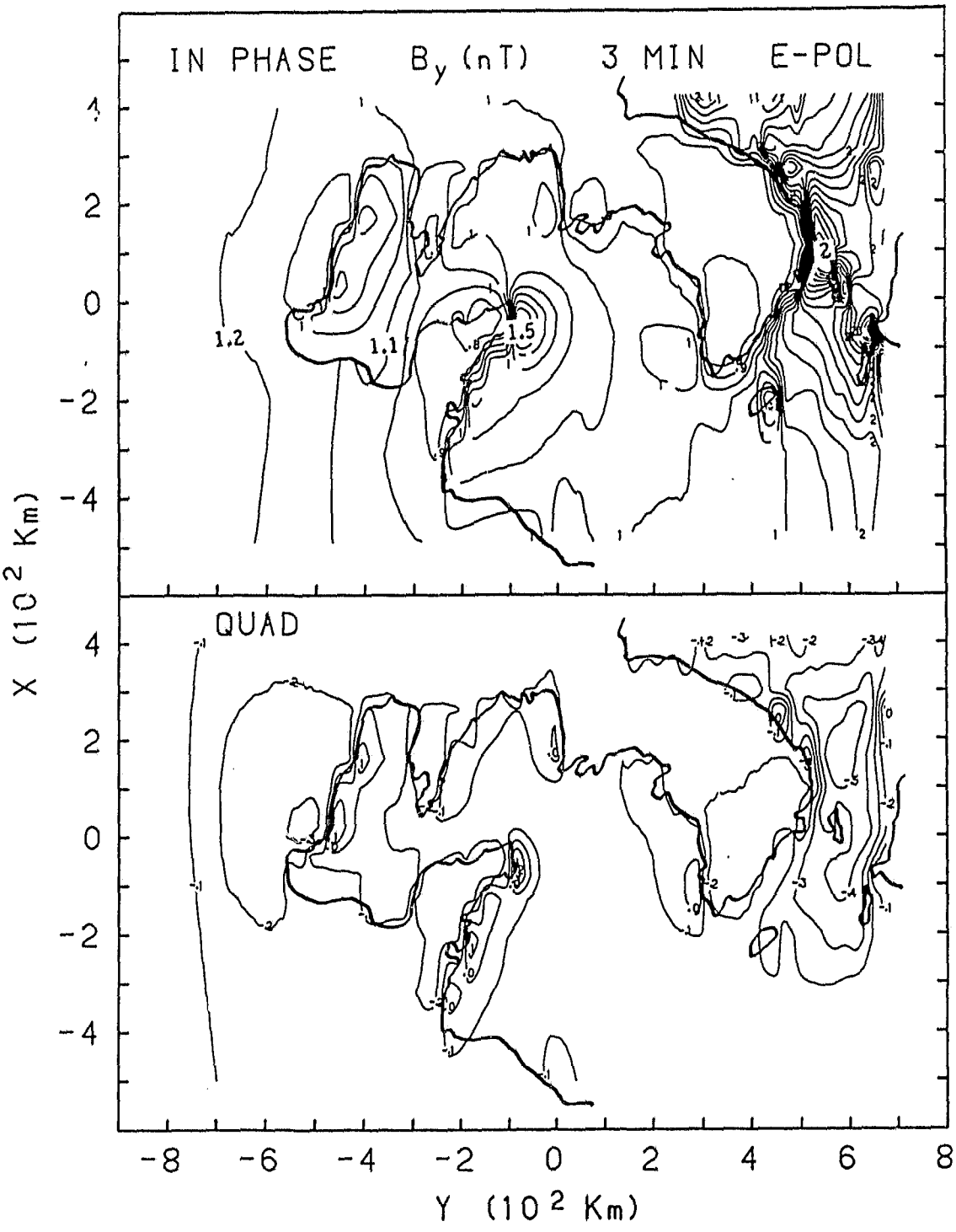

Figure 3.14: In-phase and quadrature B_y field contours at 3 min for E-polarization.

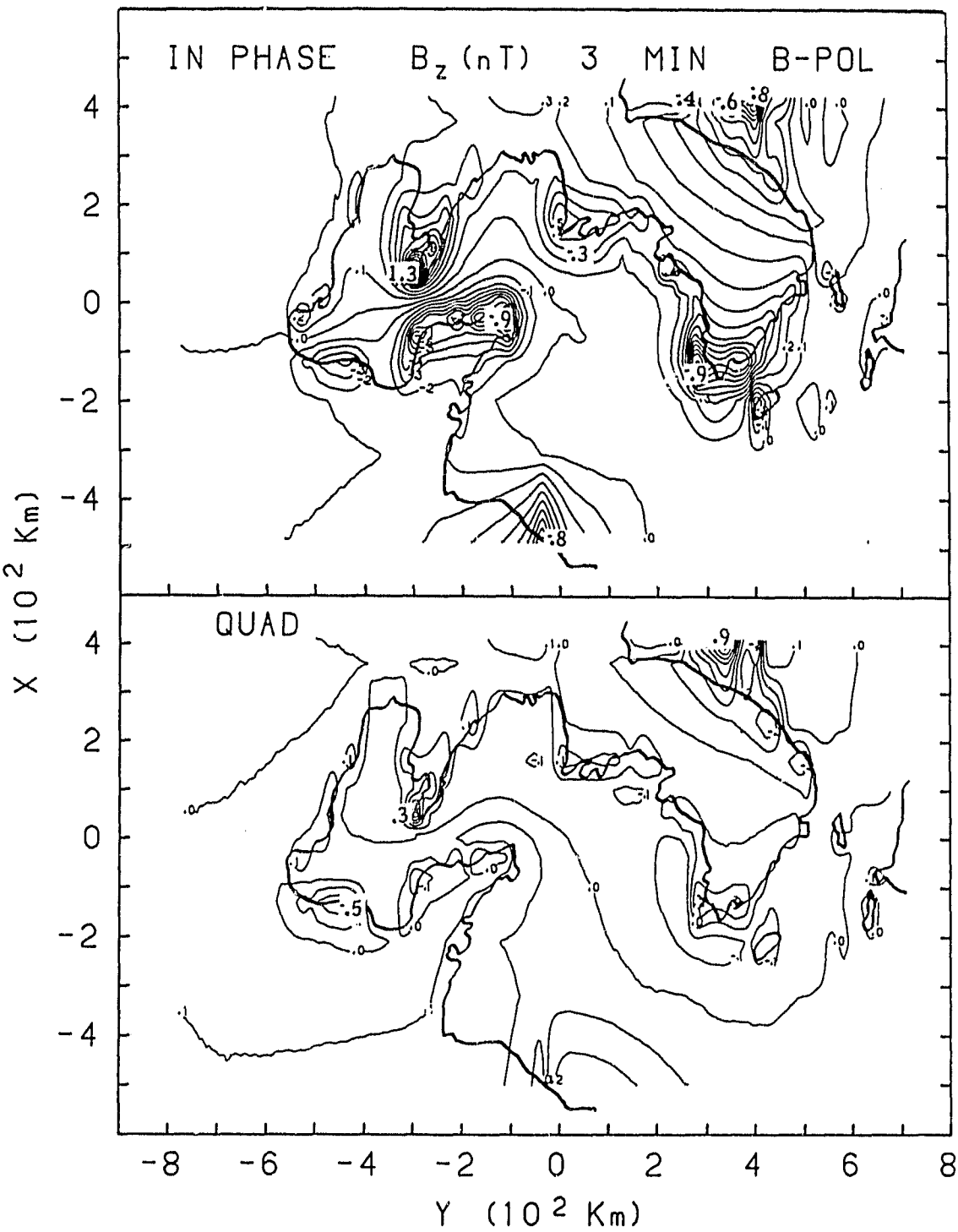

Figure 3.15: In-phase and quadrature B_z field contours at 3 min for B-polarization.

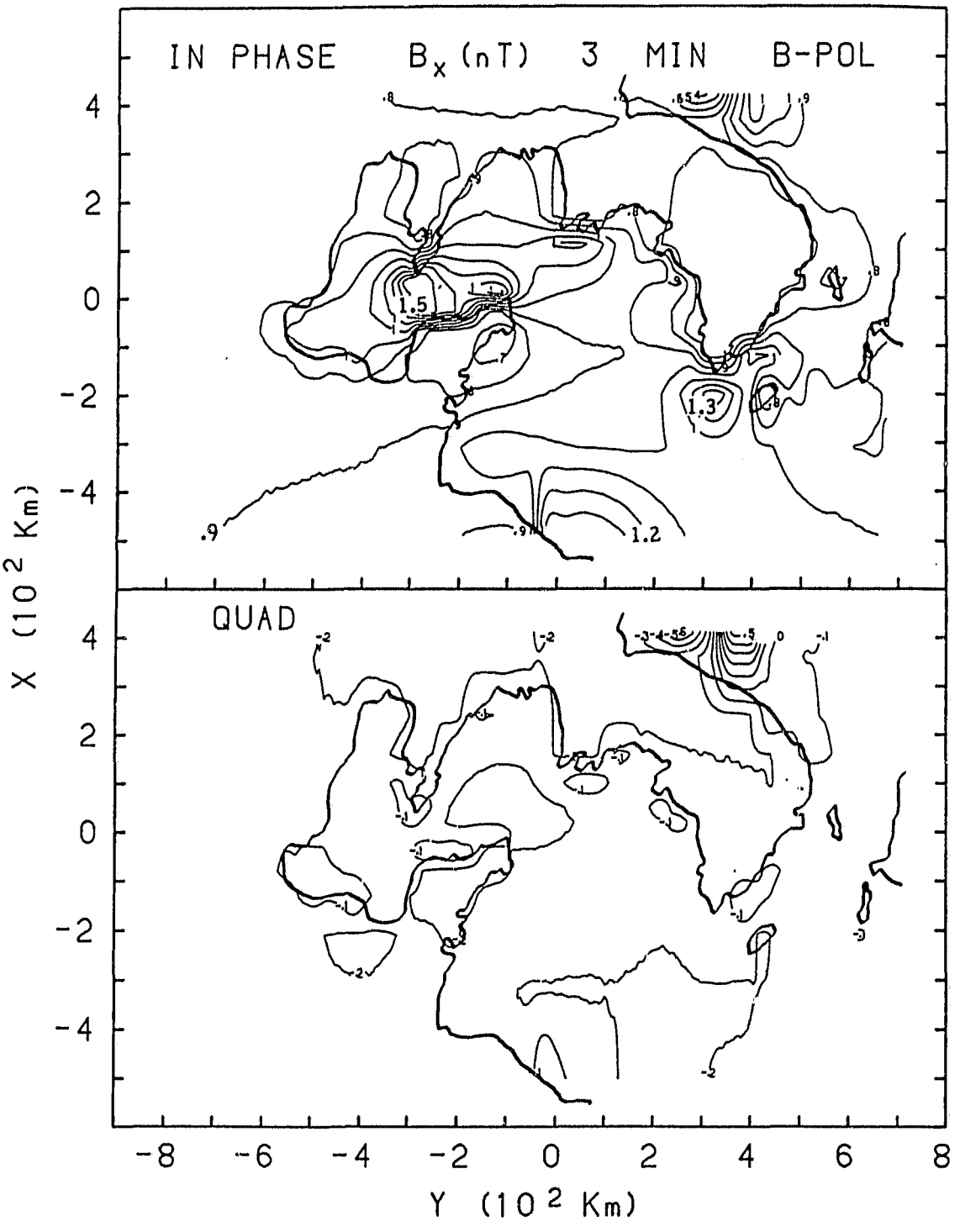

Figure 3.16: In-phase and quadrature B_x field contours at 3 min for B-polarization.

3.3.2 Three Dimensional Views of Model field Components

To provide another general view of the electromagnetic field responses in the modelled region, detailed traverse measurements were used to construct three dimensional (3D) views for magnetic and electric field components. Figs. 3.17, 3.18 and 3.19 show the 3D views of B_z, B_y and E_x respectively for 3 min for E-polarization (the 3D views of B_x and E_y for E-polarization are provided in appendix A). From the results of B_z and B_y shown in Figs. 3.17 and 3.18, it is seen that large anomalies occur where the coastlines are parallel to the source field due to increased current density concentrated along the coastlines. Significantly large in-phase B_z and B_y responses occur at the Korea-Japan strait due to the channelling effect. The much enhanced in-phase magnetic fields over the Shandong peninsula and along the eastern coast of Korea again show the effects of current deflection (as discussed in previous sections that dealt with the model traverses and contour plots). In Fig. 3.19, general enhancements of E_x are observed along the coastlines of Bohai bay. Large E_x components on shore in the China-Korea coastal region and part of the eastern coast of the Korean peninsula indicate the effect of current diffusion into the resistive continent.

Three dimensional views of B_z, B_x and E_y are shown in Figs. 3.20, 3.21 and 3.22 respectively at 3 min for the B-polarization. The 3D views for B_y and E_x are given in appendix B and will not be discussed here. Similar to the case of E-polarization, the anomalous responses are large where current is deflected by coastlines not perpendicular to the electric field of inducing source. The in-phase B_z component (Fig. 3.20) is large over the tip of the Korean peninsula in response to current deflection. The channelling effect over the Bohai strait is clearly indi-

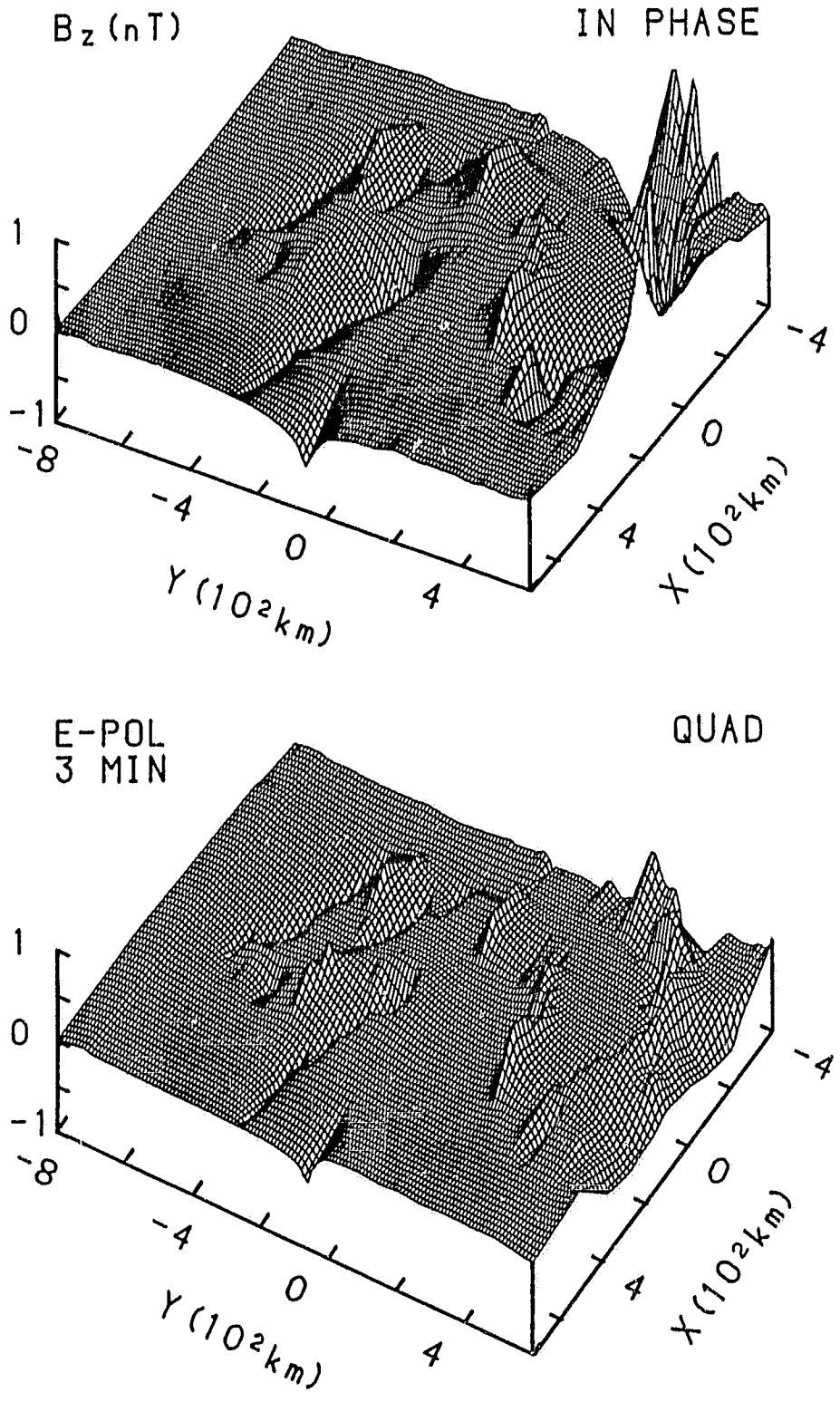

Figure 3.17: Three dimensional view of B_z for E-polarization at 3 min.

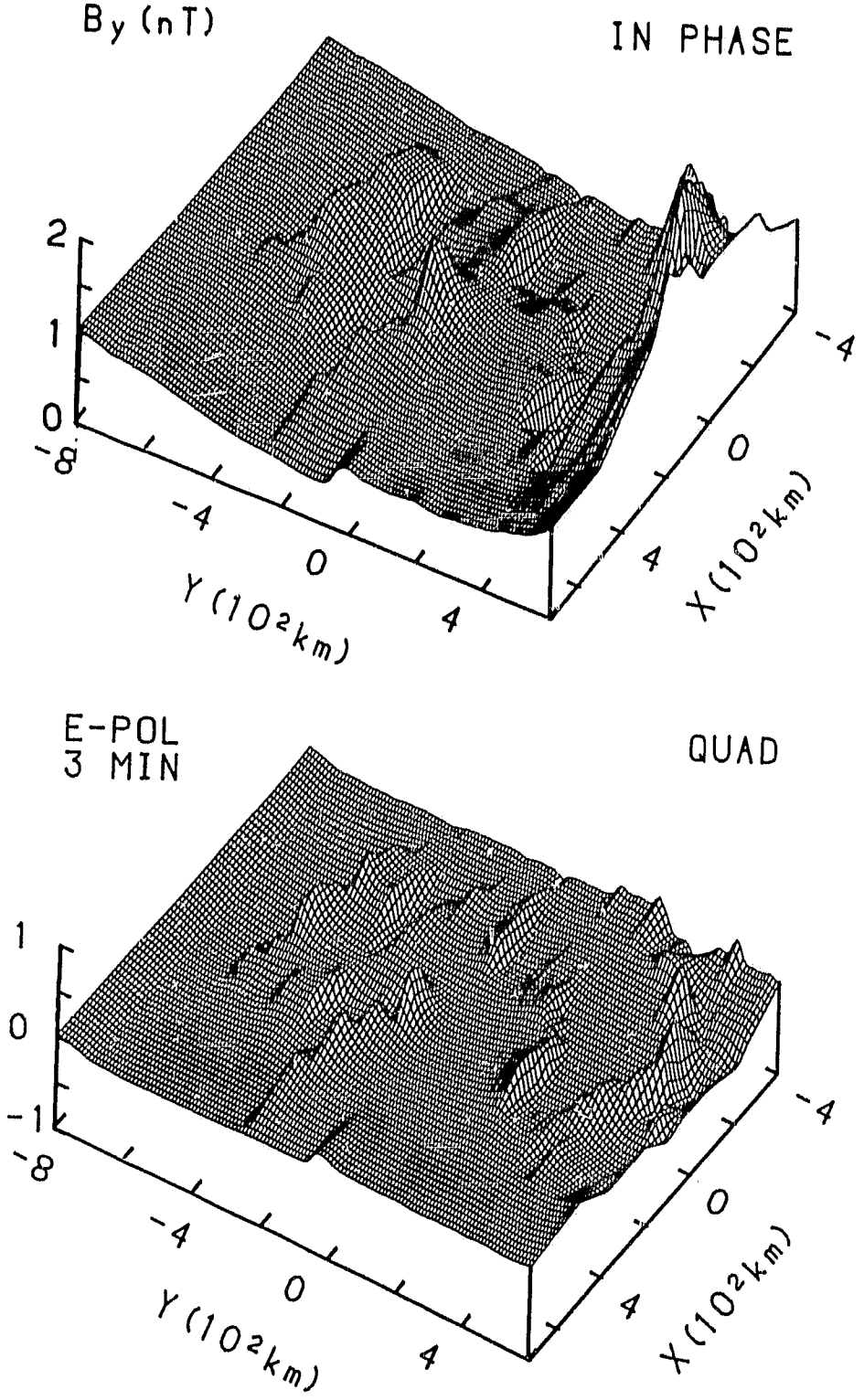

Figure 3.18: Three dimensional view of B_y for E-polarization at 3 min.

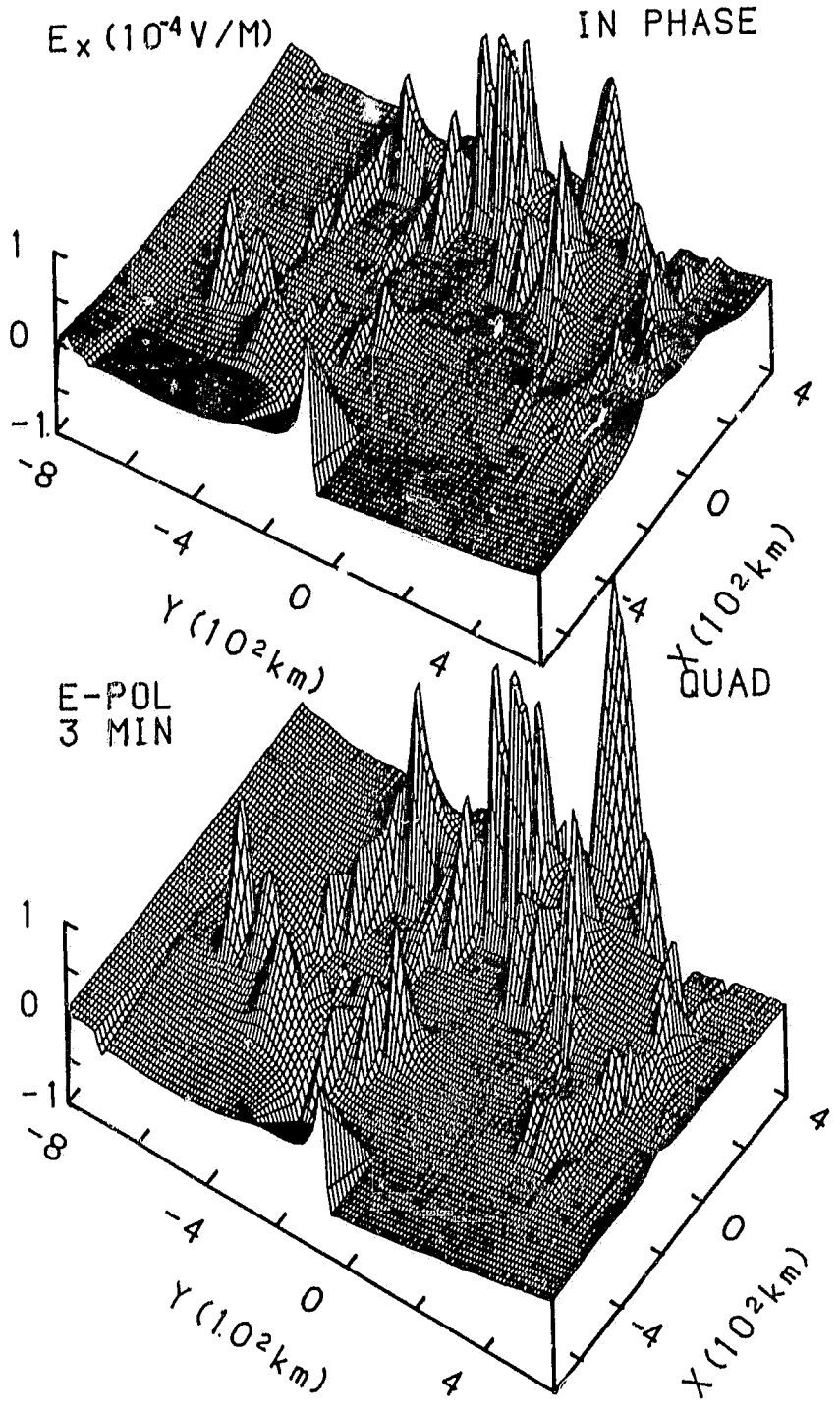

Figure 3.19: Three dimensional view of E_x for E-polarization at 3 min.

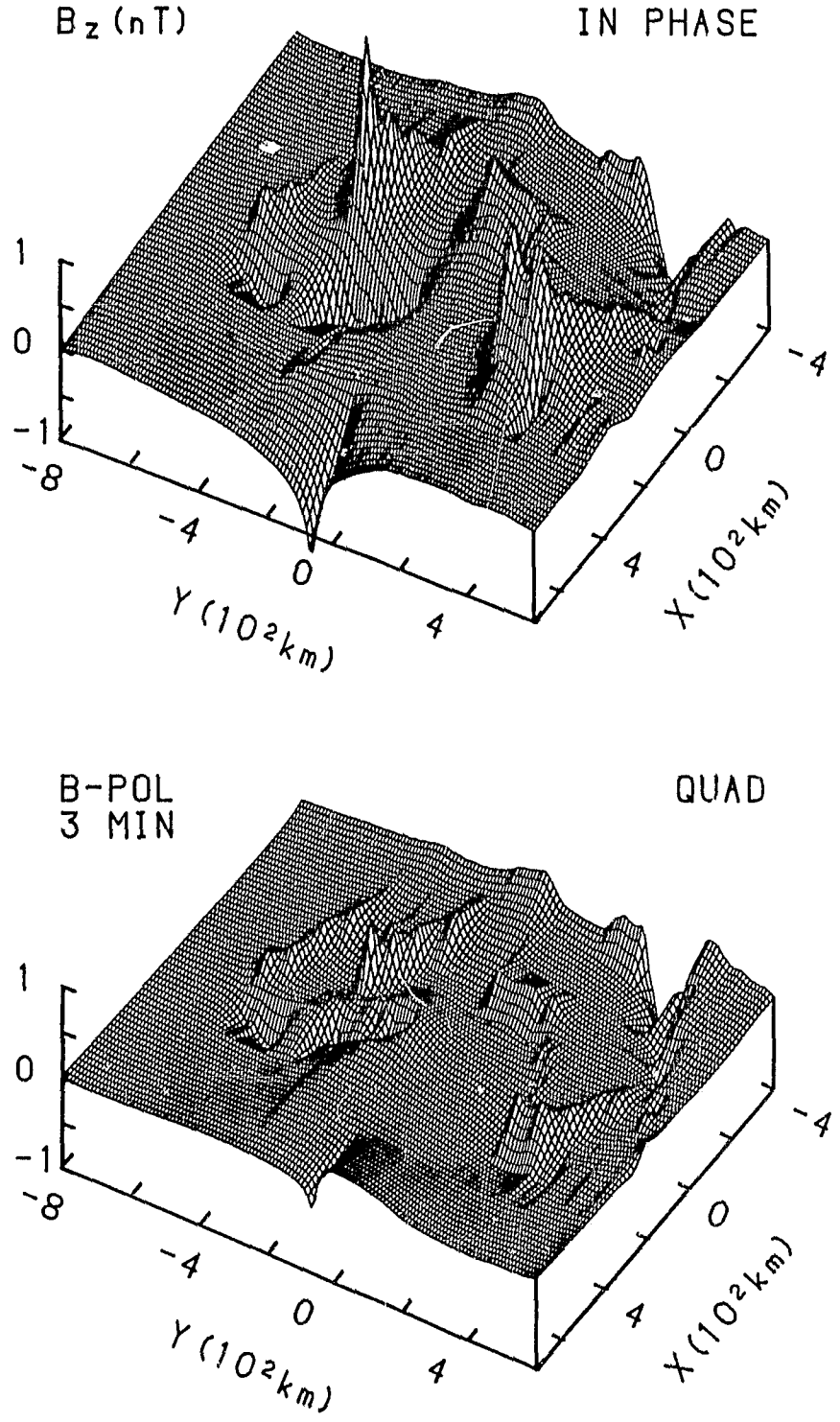

Figure 3.20: Three dimensional view of B_z for B-polarization at 3 min.

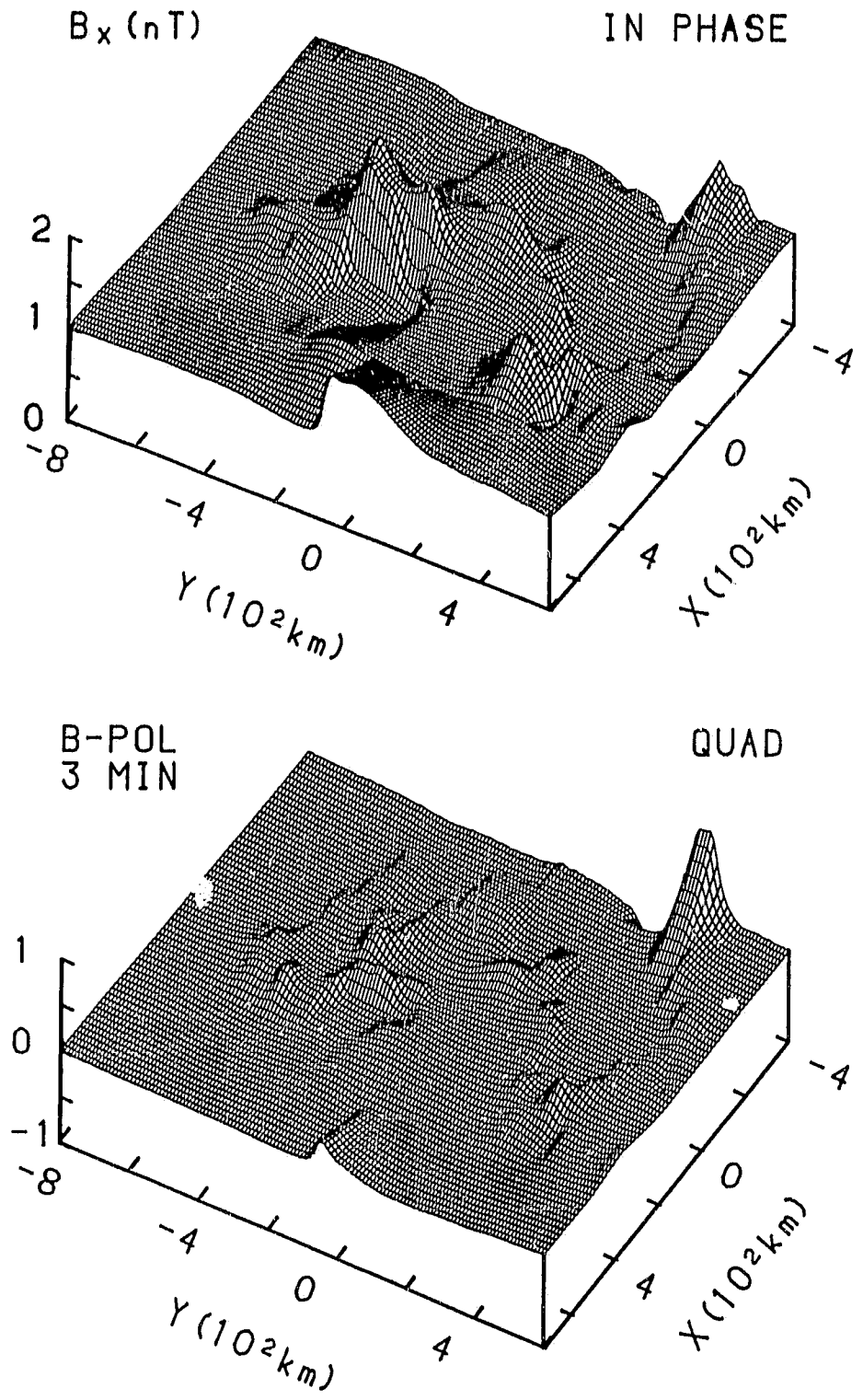

Figure 3.21: Three dimensional view of B_x for B-polarization at 3 min.

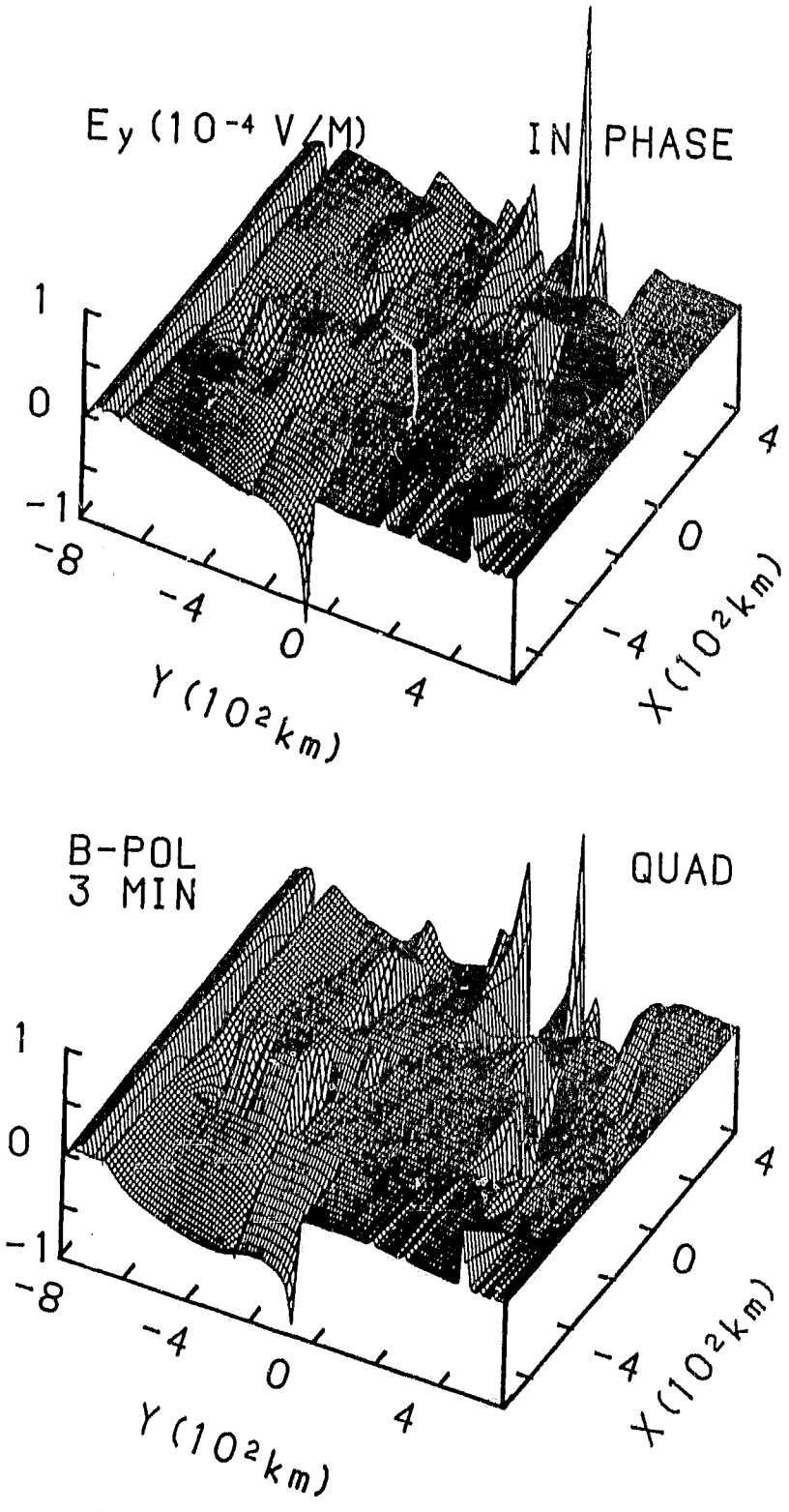

Figure 3.22: Three dimensional view of E_y for B-polarization at 3 min.

cated by very enhanced positive and negative responses on either side of the strait. Both in-phase and quadrature B_z show a large negative response indicating that the relatively deep Japan Sea plays an important role in the electromagnetic response in the region. Comparing the results in Figs. 3.17 and 3.20, it is noted that B_z is large along the east coast of Korea for both E- and B-polarizations. This is expected since the coastline here is roughly 45^o relative to the direction of the inducing field for both E- and B-polarizations. In Fig. 3.21, again, both in-phase and quadrature B_x show large anomalies along the eastern coastline of Korea, and a much enhanced in-phase B_x occurs at the Bohai strait. The three dimensional views of E_y shown in the Fig. 3.22 basically support the observations noted for the traverses, that is, large negative responses of both in-phase and quadrature E_y occur at Bohai Bay, the Shandong and Liaodong peninsulas, and the eastern coast of Korea in response to current deflection.

3.4 Induction Arrows

The model magnetic field measurements for two independent source fields (E-and B-polarizations) were used to calculate transfer functions (see equation (1.2) in Chapter 1). Since the time variation of the fields is described by $\exp(i\omega t)$ for the present analogue model study, the induction arrows then were obtained from the transfer functions by reversing the signs for both in-phase and quadrature components.

Figure 3.23 shows the induction arrows at 3 min for traverses T1-T6. For such a short period, it is expected that the local Bohai bay should have a significant contribution to the current induction. On the continent of China, the in-phas-

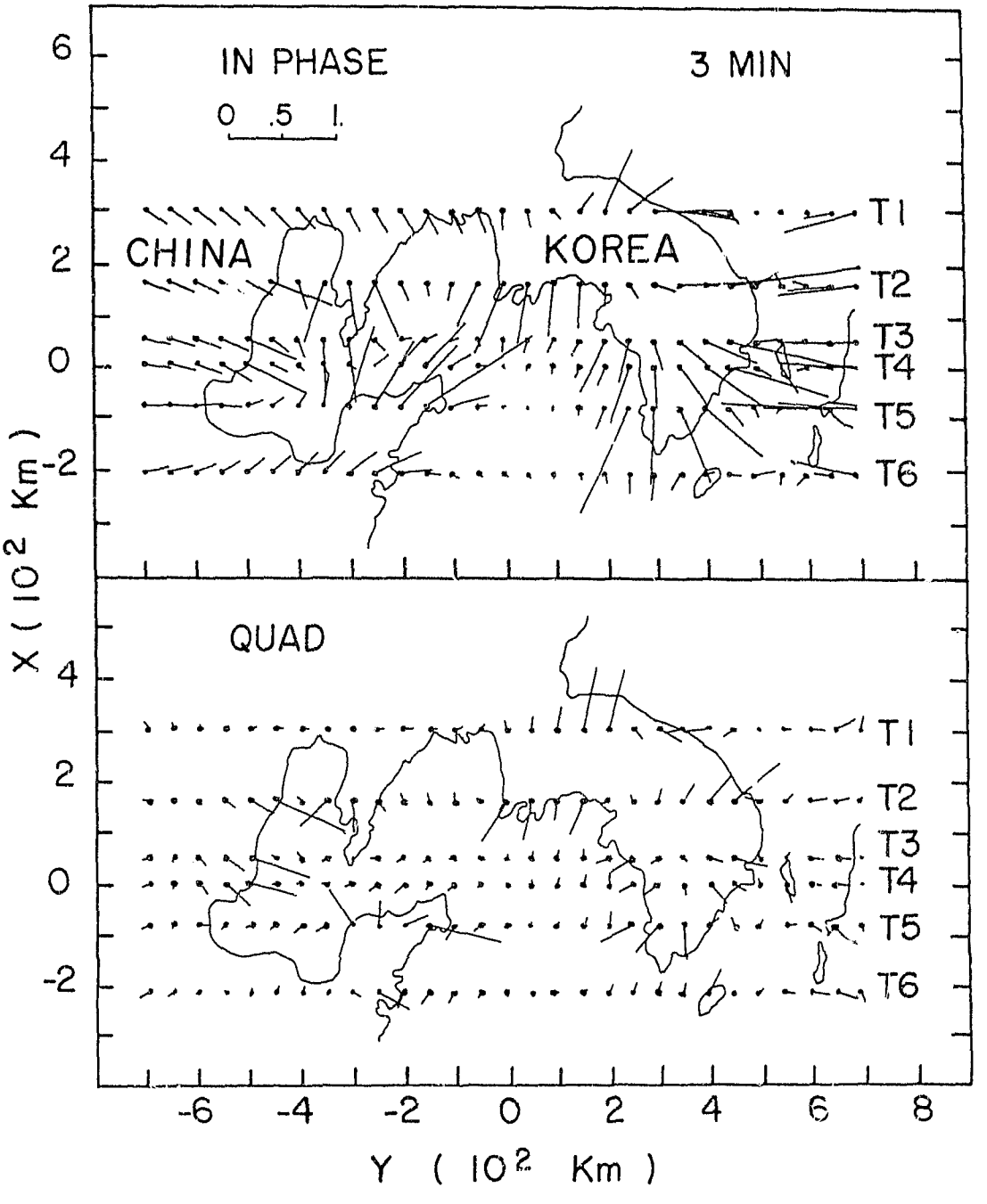

Figure 3.23: In-phase and quadrature induction arrows along traverses T_1 to T_6 at 3 min.

induction arrows, pointing towards Bohai Bay, increase in length as the coastline is approached, then decrease seaward from the coast. Along the flanks of the bay (T2-T4), it is found that, both in-phase and quadrature arrows are relatively large due to current channelled through the Bohai strait and diffused into the continent. The in-phase and quadrature arrows along T5 over the coastline region are particularly small, due to the bay effect. The very enhanced in-phase arrows at the tips of both the Liaodong and Shandong peninsulas show the importance of the cape effect. Since the Shandong peninsula provides an abrupt obstacle to the current induced in the open Yellow Sea, the current is deflected around the tip of the peninsula before it is channelled through the Bohai strait. Such a current deflection effect is clearly indicated by the direction and the enhanced induction arrows at the peninsula. Similarly, large induction arrows are also seen at the tip of the Korean peninsula. For the locations along the west coastline of Korea, it is noticed that, the in-phase arrows all roughly point towards the open Yellow Sea which provides evidence that at short periods the large open ocean plays an important role for the current induction in the area of the Korean peninsula. For locations along the east coast of Korea, the in-phase arrows are roughly perpendicular to the coastline. The Korea-Japan strait, connecting the open Yellow Sea and the Japan Sea, provides a conductive path for the induced current from south to north. A typical channel effect is seen here, that is, the induction arrows at both sides of the strait point to the strait in response to the concentrated current density due to the channelling effect. Comparing the in-phase and quadrature arrows in Fig. 3.23, it is found that quadrature arrows in general are of smaller amplitude. Right at the coast, the quadrature arrows are roughly perpendicular to the coastline.

Along the traverses T2-T5 at the Bohai bay region it is seen that the quadrature arrows are oppositely directed on either side of the coastline, so as to point towards each other and towards the coastline. Further landward, the quadrature arrow undergoes a second reversal at some distance from the coastline which is, according to Agarwal and Dosso (1990), dependent on the period and somewhat characteristic of the conductivity and depth of a conductive layer at depth, which in the present model is at a depth of 80 km.

To demonstrate the change of induction arrow direction and amplitude with increasing period, induction arrows for 20 and 60 min are shown in Figs. 3.24 and 3.25 respectively. Both the in-phase and quadrature induction arrows over the entire region are attenuated as the period increases, with the in-phase arrows showing the more rapid decrease. For the locations along the west coastline of Korea, all the quadrature arrows now point (or tend to point more) towards the open ocean. From Figs. 3.23, 3.24 and 3.25, it is interesting to note that the quadrature induction arrows tend to closely mimic the in-phase arrows at shorter period. For example, the quadrature arrows at 20 min are very similar to the in-phase arrows at 3 min, and quadrature arrows at 60 min are similar to the in-phase arrows at 20 min.

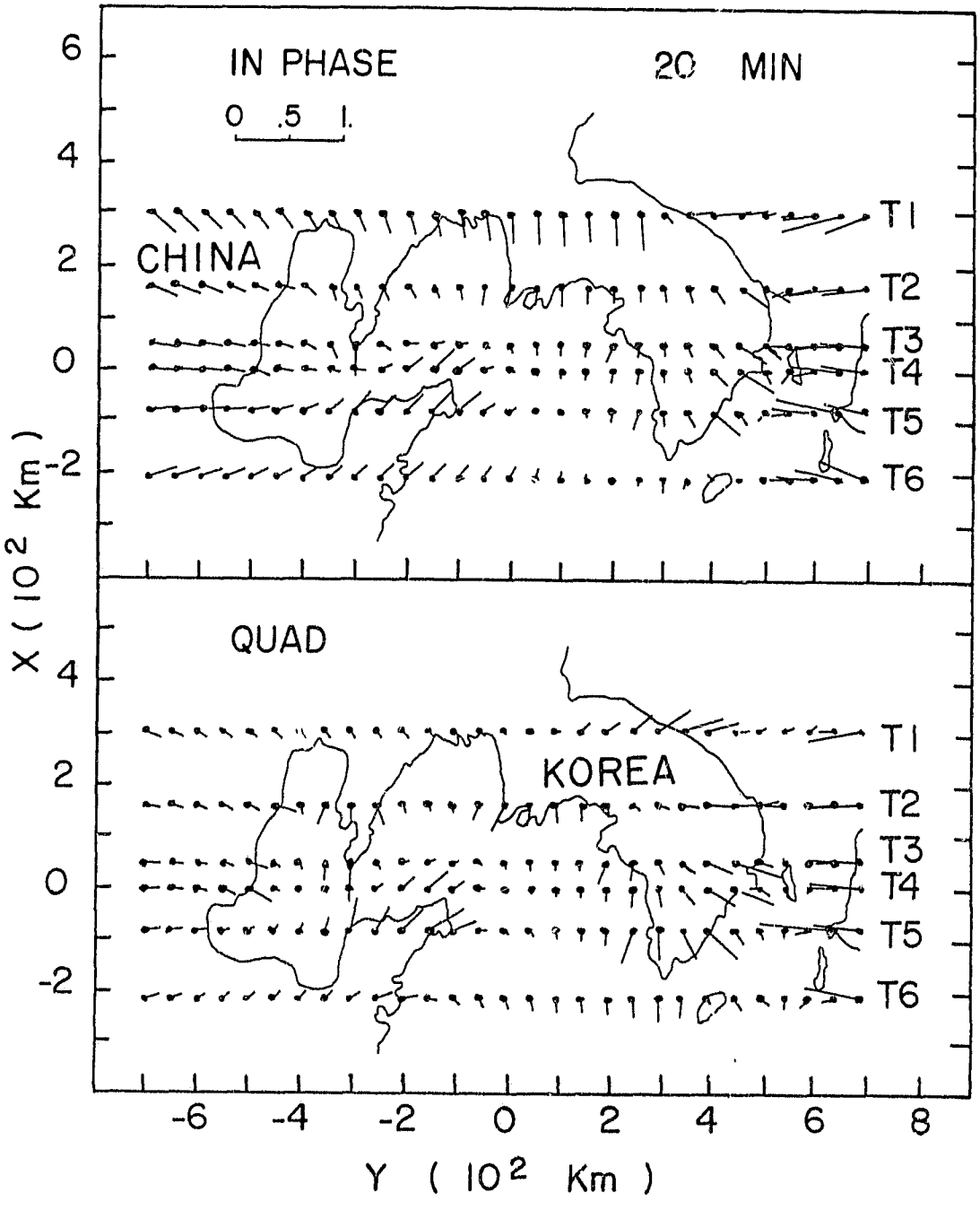

Figure 3.24: In-phase and quadrature induction arrows along traverses T_1 to T_6 at 20 min.

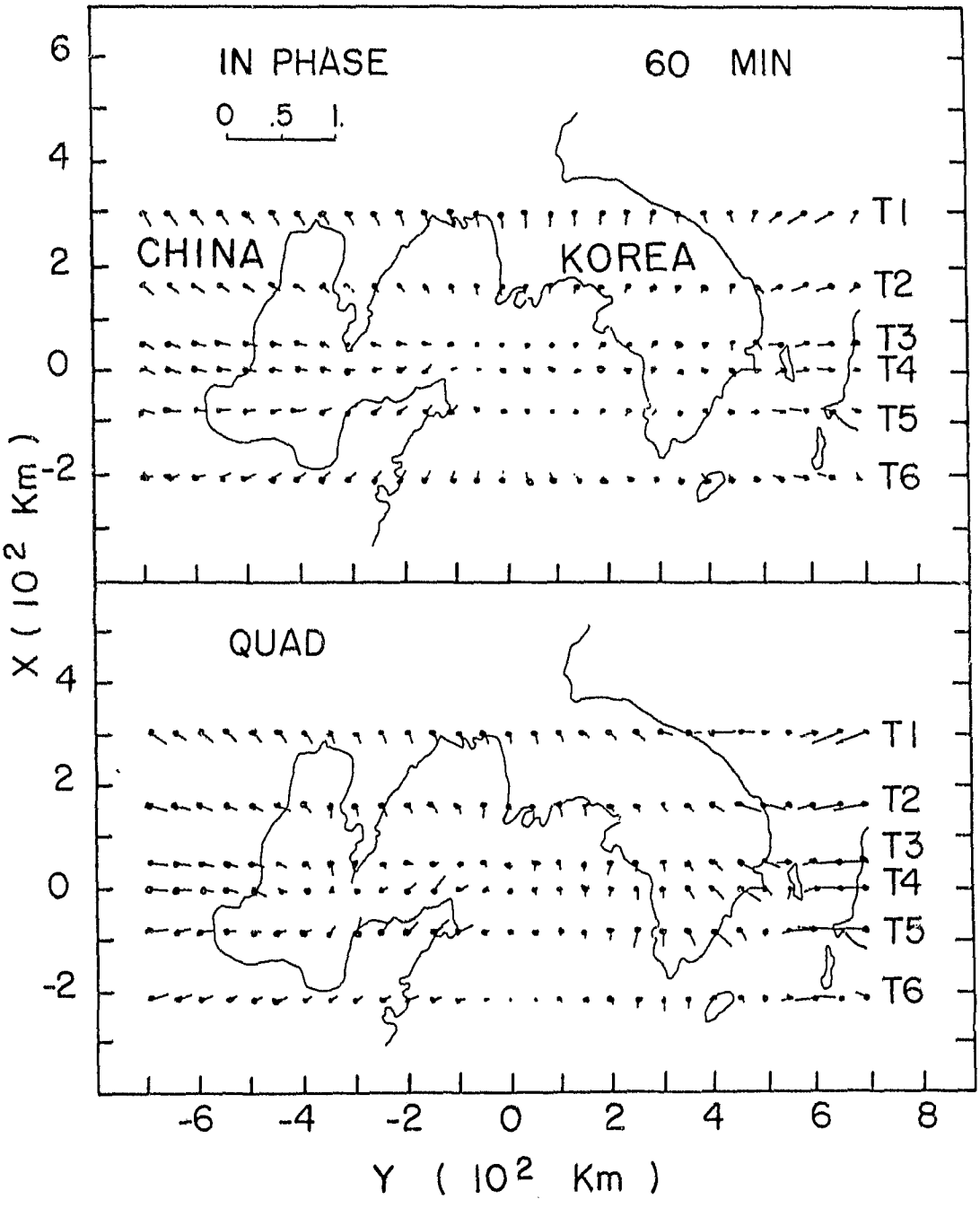

Figure 3.25: In-phase and quadrature induction arrows along traverses T_1 to T_6 at 40 min.

3.5 The Chapter Summary

In this chapter, the behaviour of the electric and magnetic field variations over the Bohai Bay coastal region of China is described in detail. The model source frequencies simulate naturally occurring geomagnetic variations of periods 3-60 min. In-phase and quadrature B_x, B_y, B_z, E_x and E_y measurements for the modelled region are presented for an approximately uniform overhead horizontal source field for E- and B-polarizations. Large anomalous in-phase and quadrature model magnetic fields are observed over the Korea-Japan strait for E-polarization and over the Bohai strait for B-polarization due to current channelling through the straits. Large responses over the peninsulas in the shallow coastal areas occur at short periods but decrease abruptly with increasing period. The model induction arrows show that induction in the shallow local Bohai Bay is important at short periods. In general, the analogue model results indicate that the effects of peninsulas, straits, bays and irregularities in the costliness play an important role in determining the electric and magnetic field responses both on-shore and off-shore for this complex Bohai Bay coastal region.

Chapter IV

ANALOGUE MODEL RESULTS FOR THE JAPAN-KOREA-CHINA REGION

The scaled laboratory analogue model of the Japan-Korea-China region has been described in chapter II. The in-phase and quadrature horizontal electric (E_x, E_y), the vertical (B_z), and horizontal magnetic (B_x, B_y) fields for a grid of traversover the model (Fig. 2.4) for a simulated period range of 15-180 min were sured for two perpendicular source fields (E- and B-polarizations). Detailed and magnetic field measurements were carried out for 45 traverses over laboratory model. Eight of these traverses (T1-T8 shown in Fig. 2.4) ted to examine the EM responses for the Japan island arc region and the Bay region of China. The latter region, included in the dashed square section between T4 and T8 in Fig. 2.4, was the topic of chapter 3 which examined the EM responses of the shallow Bohai Bay. Detailed measurements were also carried out over a period range of 15 - 120 min for the present Japan model with a 1.5 cm thick graphite plate underneath which simulates a proposed conductive layer under Japan (Utada et al., 1986). Since the primary interest of this chapter is to study the effect of electromagnetic induction due to the ocean alone, the model measurements with no graphite plate included will be used through out this chapter.

4.1 Model field components for E-Polarization

4.1.1 Traverses For E-Polarization

For E-polarization of the source field, electric current in the oceans induced in the +x-direction (Fig. 2.4) will tend to flow roughly parallel to the west and east coastlines of Japan. Off the east coast, in the T4 region in particular, current will tend to be concentrated due to the cape effect, as it is deflected to flow around the convex shaped coastline, while off the concave shaped west coastline, current density will be reduced due to the bay effect. Thus, for most of the island arc coastlines, current density would be reduced off the west coast and enhanced off the east coast, at least relative to the current density expected off a straight coastline parallel to the electric field of the inducing source (E-polarization). This current density distribution would generally lead to greater B_z coast effects on the eastern than on the western coastal regions of Japan. This is certainly seen to be the case for both the in-phase and quadrature B_z at 60 min for traverses T3, T4 and T5 in Fig. 4.1. The east coast anomaly is the largest for the coastal region of the T4 traverse, where the current density is expected be the most enhanced due to coastal location, as well as the proximity of the deep Pacific Trench (also simulated in the model). The current densities at both the east and west coasts are also affected by the coastline irregularities, the small islands, and the straits (Korea-Japan, Tsugaru, and La Perouse). The strait effects (or channel effects) due to current induced in the more distant deep oceans being funnelled through the straits, account for the large B_z enhancements at the westerly coast regions along the T1, T3, and T6 traverses (Fig. 4.1). For E-polarization, induced electric current in the ocean south of Japan is channelled through the Korea-Japan strait,

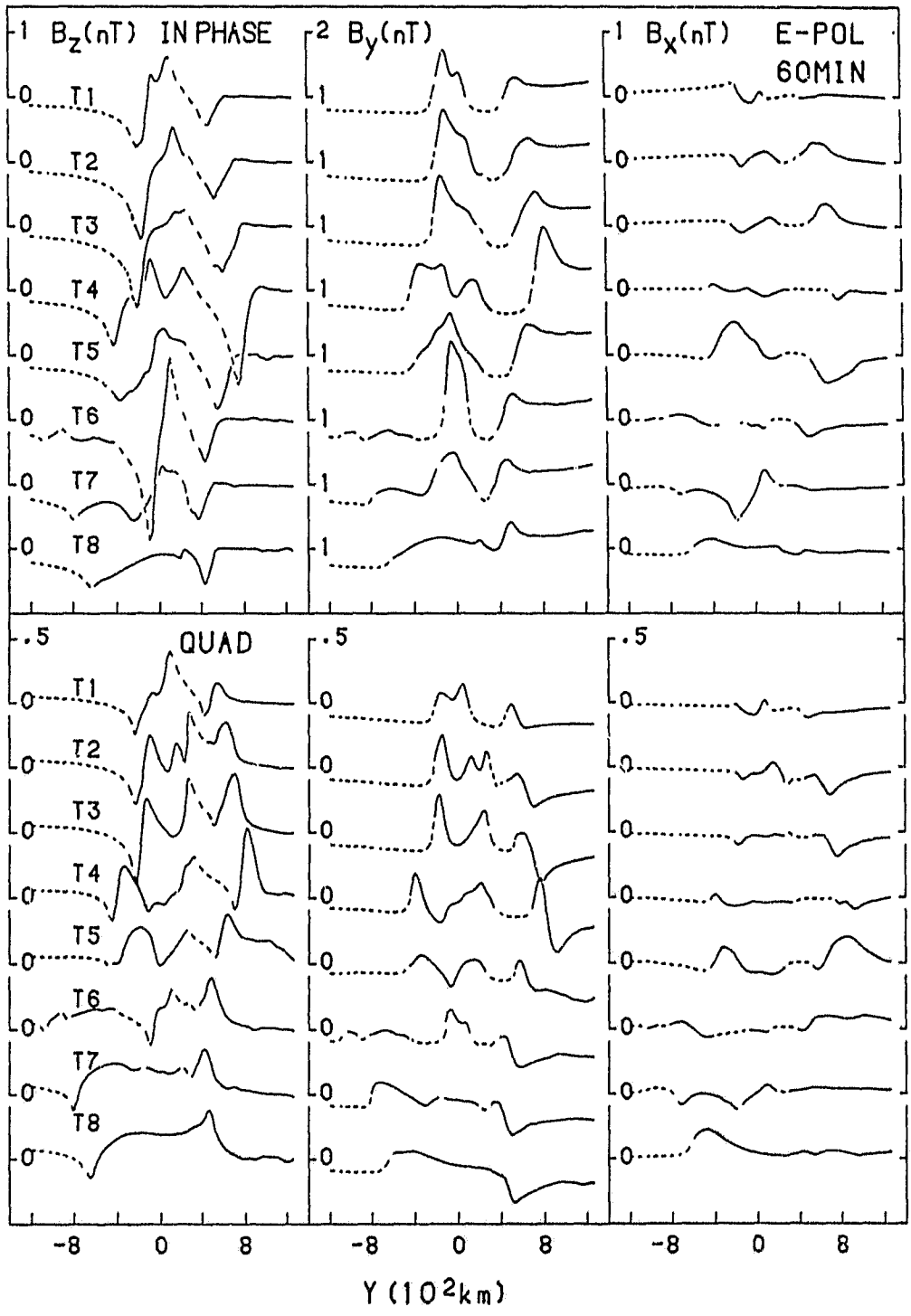

Figure 4.1: In-phase and quadrature magnetic fields for traverses T_1 to T_8 for E-polarization for 60 min.

expands into the Japan Sea, then is confined by the converging continental and Japan coastlines, to be channelled through Tsugaru and La Perouse straits, and finally expanded into the Pacific Ocean. The greatly enhanced current concentrations resulting from channelling through the straits leads to the large B_z responses observed in the neighborhood of the T1, T2, and T6 traverses both at the Japan and the continental coastal regions. The largest in-phase B_z channel response, as would be expected, occurs at the Korea-Japan strait (T6) where the geometries of the coastlines are seen to be particularly effective in enhancing local current concentration. The observed quadrature B_z responses, though of much smaller magnitude than the in-phase responses, also show the effects of changing current concentrations at the straits, bays, and capes along the Japan coastlines. Thus, as expected, the highly irregular coastlines on either side of the narrow Japan islands lead to large in-phase B_z anomalous fields at most coastal locations, and thus to large B_z gradients along traverses over Japan for all on-shore locations for E-polarization. As well, significant quadrature B_z gradients are observed along all traverses over Japan. Hence, the effects of the oceans can be expected to be significant component in the transfer function (or induction arrow) responses for any field site measurements on Japan.

In Figure 4.1, the off shore in-phase B_y responses, too, reflect the x-components of the current enhancements at the straits (T1, T2, and T6), as well as the current enhancements due to deflections at the concave coastline (east), with T6 showing the largest strait effect, and T4 showing the largest cape effect. The quadrature fields show responses similar to the in-phase responses, but are of smaller magnitude. For E-polarization, B_x is expected to be small (or zero),

except in regions where induced current flowing in the oceans in the x-direction is deflected by the ocean bathymetry and the coastline, with a resulting y-component of current. Current deflections account for the off-shore in-phase B_x anomalies on the east coast for T2 and T3, where the anomalies are positive, and for T5, where the anomalies are negative, as current is deflected by the concave coastlines. At the apex of the concave coastline (T4) the B_x anomaly is minimal, as expected, since little current deflection occurs. The in-phase B_x anomalies of opposite sign just off the southern tip of Korea (T7), clearly show the effects of current being deflected to the left and to the right.

Figure 4.2 shows the in-phase and quadrature E_x and E_y along traverses T1 to T8 for 60 min period. For E-polarization, both in-phase and quadrature E_x are large over the land and small over the ocean, which will lead to the apparent resistivity (perpendicular to the coast) being enhanced over the resistive land and reduced over the conductive ocean, as expected. For the T2, T3, and T4 traverses, both in-phase E_x and E_y show minimal responses over the Japan islands. As the Korea-Japan strait is approached, E_x is greatly enhanced in magnitude on both sides of the strait and over the strait as well, as shown in T6. E_y shows a sign reversal across the strait, similar to the response of the magnetic field B_z. In contrast with the large in-phase E_y observed along the U.S.S.R.-China continental coastlines, the in-phase electric field E_y shows small response over the entire Bohai bay area (T6 and T7) in response to the reduction of the induced current density due to the bay effect.

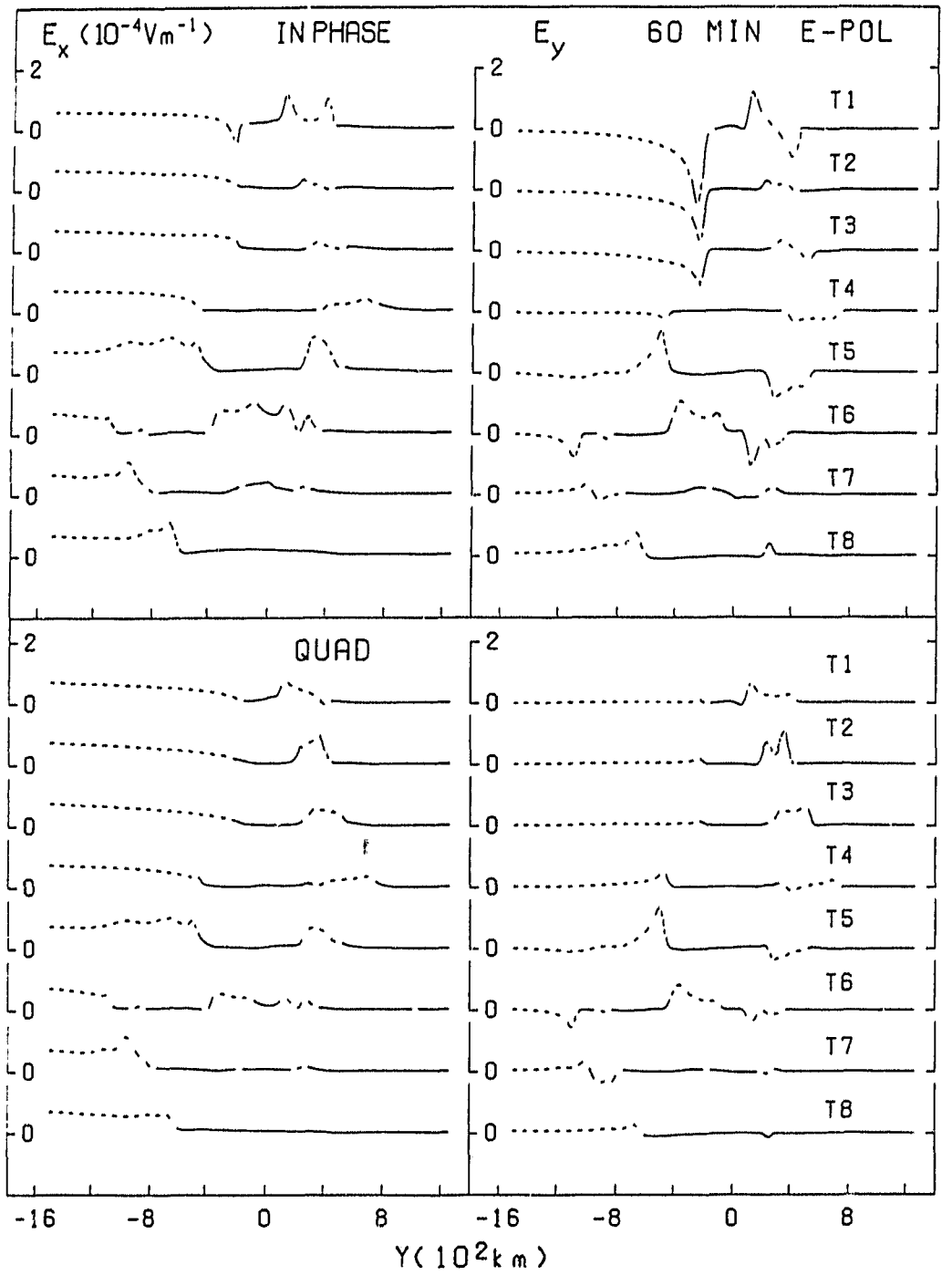

Figure 4.2: In-phase and quadrature electric fields for traverses T_1 to T_8 for E-polarization at 60 min.

4.1.2 The Frequency Response For E-Polarization

To examine the dependence on period, the in-phase and quadrature electromagnetic field components for the period range 15 min to 180 min were studied for traverse T3, crossing the northern Honshu of Japan and extending to the Pacific trench, for traverse T5, profiling the central Japan region, and for traverse T6, traversing the Bohai Bay region and the Korea-Japan strait. The three traverses were selected because field site measurements are available in the Japan and Bohai Bay regions of these traverses.

The in-phase and quadrature B_x, B_y and B_z along T3 are shown in Fig.4.3 for 8 periods for E-polarization. Since the induced current tends to flow in the x-direction, which is roughly parallel to the local U.S.S.R.-China coastline, large anomalous responses of B_z and B_y are observed at the coastline. It is seen that in-phase B_z reaches maximum response at about 60 min, while quadrature B_z is maximum at a period of approximately 150 min. The quadrature B_z experiences a sign reversal as the period increases. According to Rokityansky (1982), the period at which the amplitude of quadrature B_z is minimum and the amplitude of in-phase B_z is maximum, is called the characteristic period. It is seen that for the B_z response over the U.S.S.R.-China coastline, the characteristic period is between 30 to 60 min. Over Japan, in-phase B_z behaves very much as expected for a typical island, however with much enhanced amplitude on the east coast, which becomes more prominent as the period increases. This is in agreement with actual field data interpretation, since field data over the northern Honshu region (Ogawa et al., 1986) showed that the coast effect at the west coast (Japan Sea) of Japan was much smaller than that at the east coast (Pacific Ocean). Continuing east-

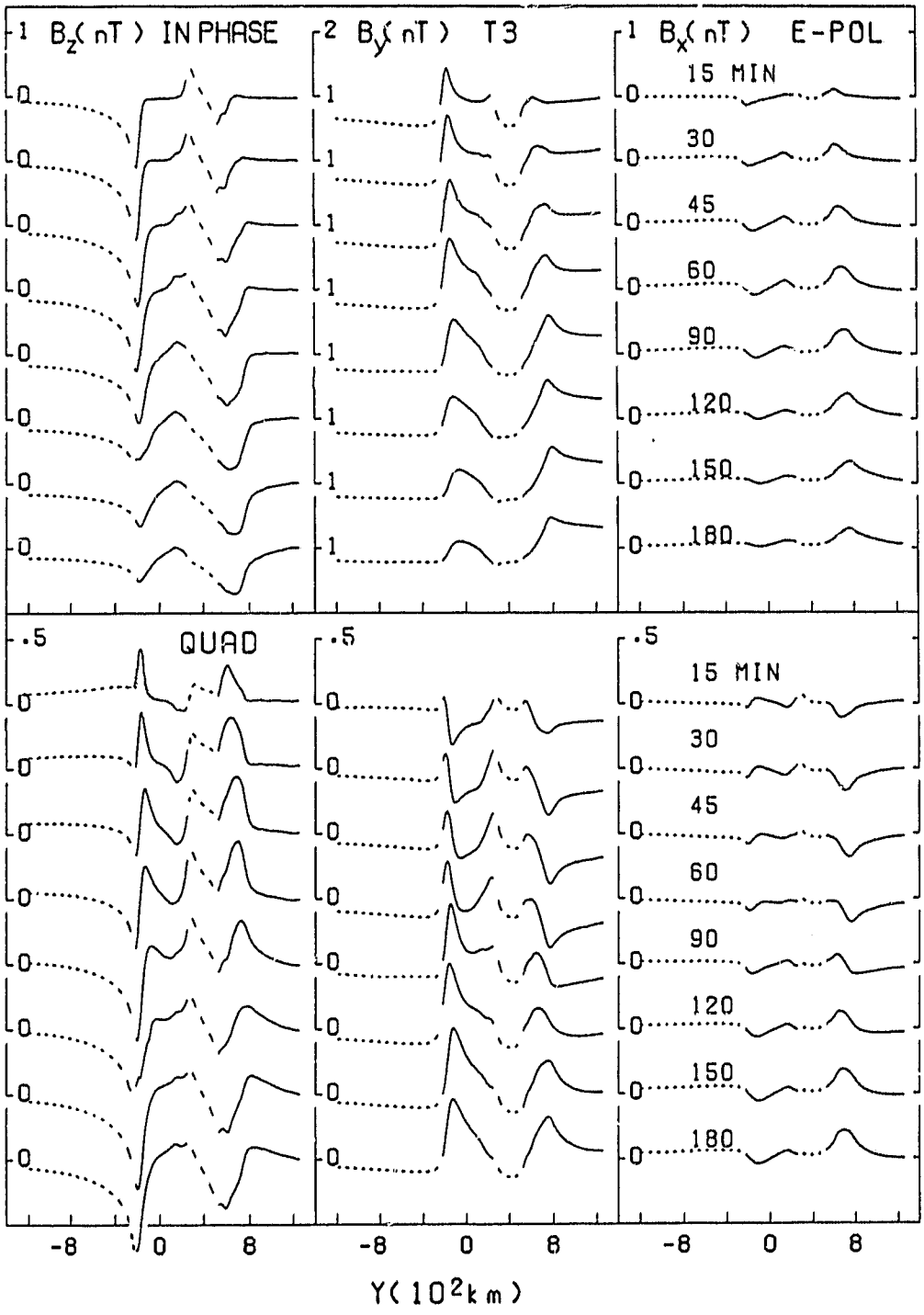

Figure 4.3: In-phase and quadrature magnetic fields for traverse T_3 for E-polarization at periods from 15 to 180 min.

ward to the deep ocean along T3, it is seen that both in-phase and quadrature B_x show the effect of induced current concentration along the deep Pacific Trench. The magnetic field B_x, showing negligible effects over the mainland coastline and the Japan island, has notable anomalous response over the trench, which has an angle of roughly 45° relative to the direction of the source field. The maximum B_x response occurs at 60 min for the in-phase and at 150 min for the quadrature component. As the period increases, the maximum anomalous B_x gradually shifts towards the deeper ocean, indicating that more induced currents are concentrated in the deep ocean at the longer periods. The quadrature B_x here, similar to the quadrature B_z over the U.S.S.R.-China coastline, also shows a sign reversal over the period range, but at a longer characteristic period, 90 min.

The in-phase and quadrature magnetic field responses along traverse T5 for periods ranging from 15-180 min for E-polarization are shown in Fig. 4.4. It is rather surprising that the B_y and B_x fields over Japan show negligible change over the entire period range, although the anomalies over the ocean at either side of Japan do show some interesting features. In-phase B_x, which for E-polarization should be zero except for the effects of current deflection, shows at 15 min, a positive anomaly off the coast of Korea and a negative anomaly off the inner coast of Japan, while at longer periods only a positive anomaly is observed. This can be explained as being due to the increasing portion of the current that is channelled into the Japan Sea at long periods, following the deeper ocean near the Korea coastline, rather than the shallow ocean near Japan. It is noted that the in-phase B_y and B_x responses over the Japan Sea are maximum in the 60-90 min range, the same period range at which the quadrature anomalies show minima and

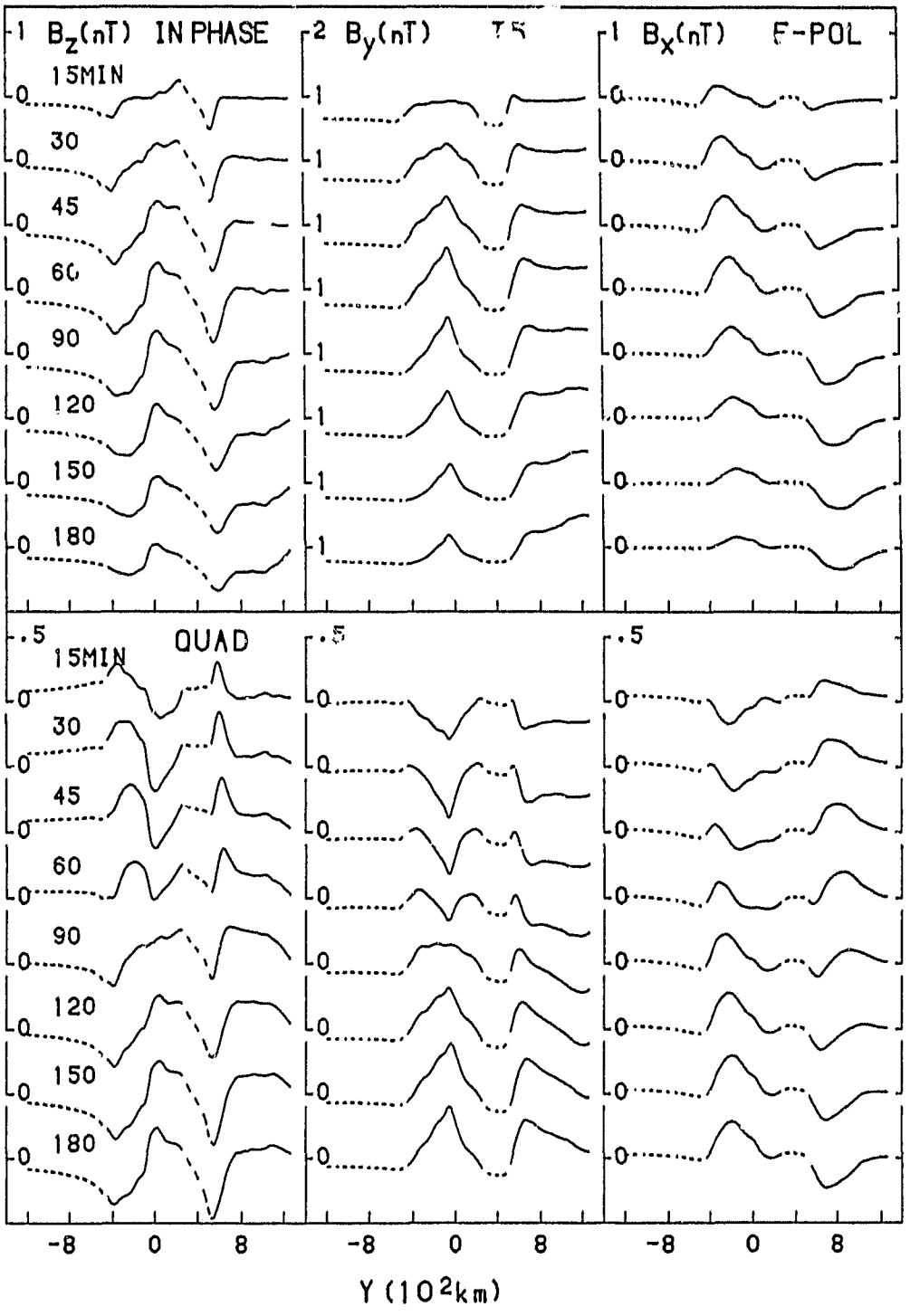

Figure 4.4: In-phase and quadrature magnetic fields for traverse T_5 for E-polarization at periods from 15 to 180 min.

undergo a change in sign. This behavior, characteristic of the depth of the local ocean and the conductive layer (simulated by the graphite plate at the bottom of the modelling tank), is observed to have little (if any) effect on the B_y and B_x fields directly over Japan for both polarizations for the T5 traverse region. The results of Fig. 4.4 generally indicate that the effects of the oceans on the magnetic field responses for on-shore Japan (T5 region) are important at all periods, and that the characteristics of the anomalies are not strongly dependent on period. Thus the oceans should play a major role in determining the induction arrow (or transfer function) responses at both short and long periods for most field sites on Japan.

The B_z fields over Japan for E-polarization show a somewhat stronger dependence on period than was noted for the B_y and B_x fields, with the in-phase B_z response at the outer coast being maximum at roughly 90-120 min. At short periods, in-phase B_z is positive at the inner coast and negative at the outer coast, while at periods greater than 120 min it is negative over the entire Japan section of the traverse. Also, the gradient of the in-phase B_z field is seen to be small and roughly constant over Japan at short periods, while at periods greater than 45 min the gradient (seaward) becomes increasingly negative, so that at 90 min, quadrature B_z is negative on the inner coast and positive on the outer coast, with the magnitude of the field at the inner coast decreasing, and at the outer coast increasing, with increasing period.

Figure 4.5 shows the magnetic field frequency response along T6 for E-polarization. As described earlier, current induced in the oceans in the x-direction is in part deflected by the Korean peninsula and the Japan island, or in

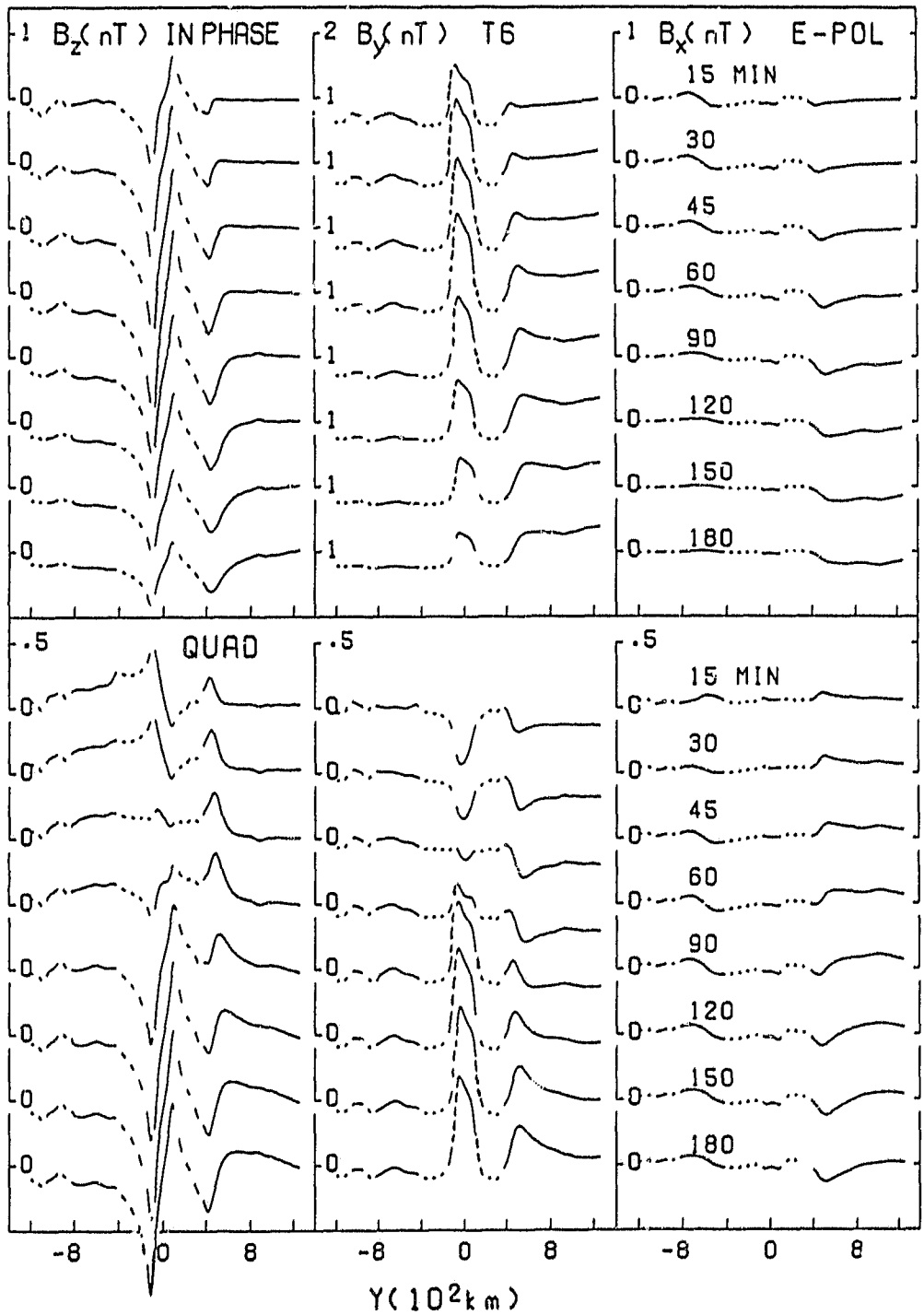

Figure 4.5: In-phase and quadrature magnetic fields for traverse T_6 for E-polarization at periods from 15 to 180 min.

part channelled into the Korea-Japan strait. A typical channelling effect is observed over the Korea-Japan strait for the entire period range, with B_z reversing its sign from negative at the Korean peninsula to positive at the Japan island, and B_y showing enhancement across the strait. In contrast, B_x shows little anomalous response over the area. As the period increases the in-phase components over the strait first increase, reach a maximum at roughly 60 min, then gradually fall off at longer periods. The quadrature components, however, first decrease with increasing period, approach a minimum at about 60 min, then following a reversal of sign, increase to a maximum at 180 min. Comparing B_z and B_y over the strait with those over the east coast of Japan, it is rather interesting to note that the characteristic period is longer for the latter case. This agrees with Agarwal and Dosso (1990) who found the characteristic period to be dependent on ocean depth. The responses of the magnetic field are relatively small over the Bohai bay area, which can be attributed to the minimal induction in the shallow ocean, and the bay effect.

The electric field E_x and E_y for T3 for 15-180 min period are shown in Fig. 4.6. It is noted that well inland, both in-phase and quadrature E_x increase with decreasing period. Along the U.S.S.R.-China coastline, large E_y anomalies are observed due to current concentration in the ocean near the coastline. Similar to the magnetic field responses observed for T3 of Fig. 4.2, in-phase E_y increases to reach a maximum, then decreases with increasing period, and quadrature E_x experiences a sign reversal at 90 min. Over the Japan island, the electric field shows a somewhat interesting feature in that both in-phase E_x and E_y reverse sign at roughly 90 min.

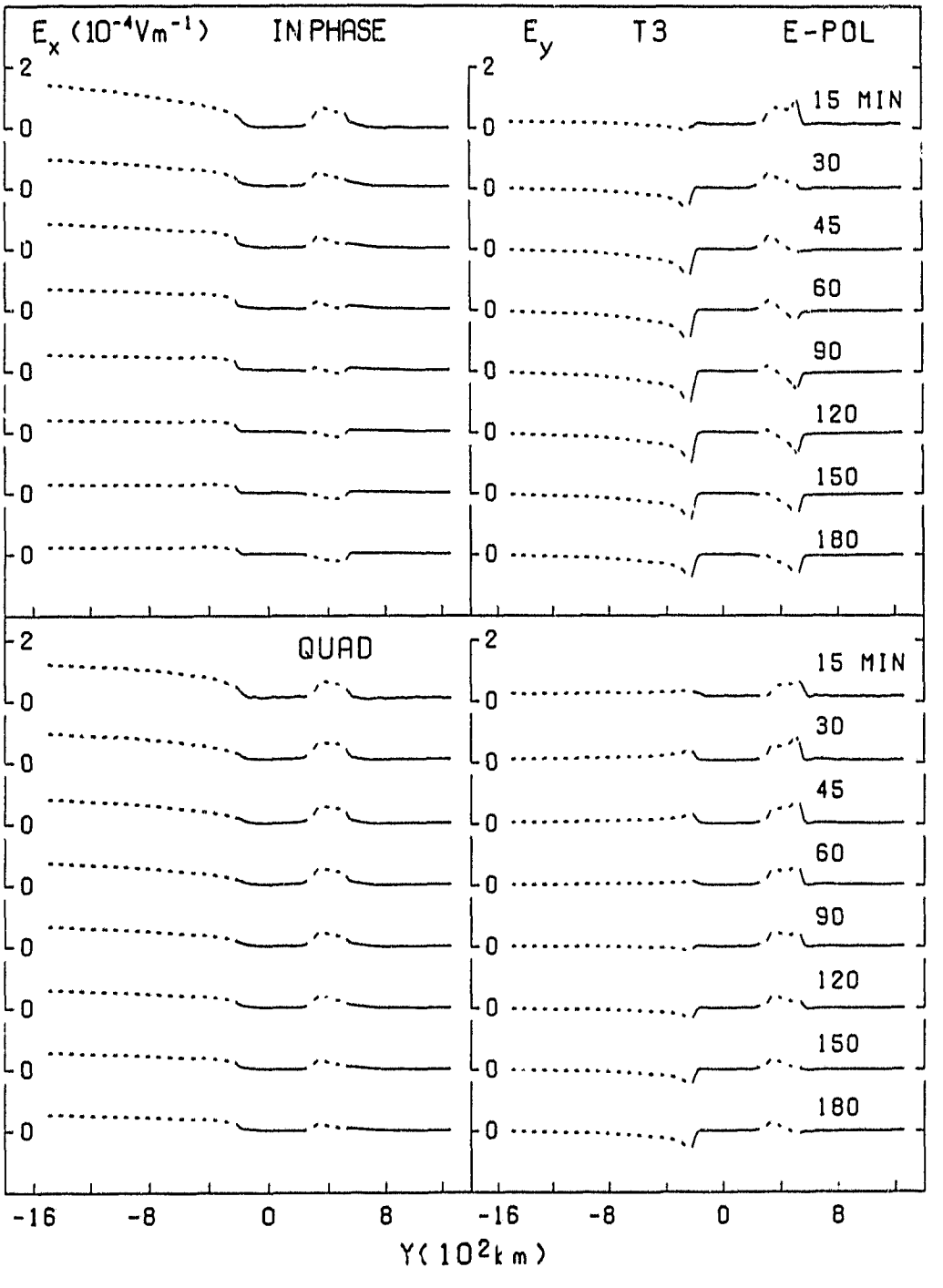

Figure 4.6: In-phase and quadrature electric fields for traverse T_3 for E-polarization at periods from 15 to 180 min.

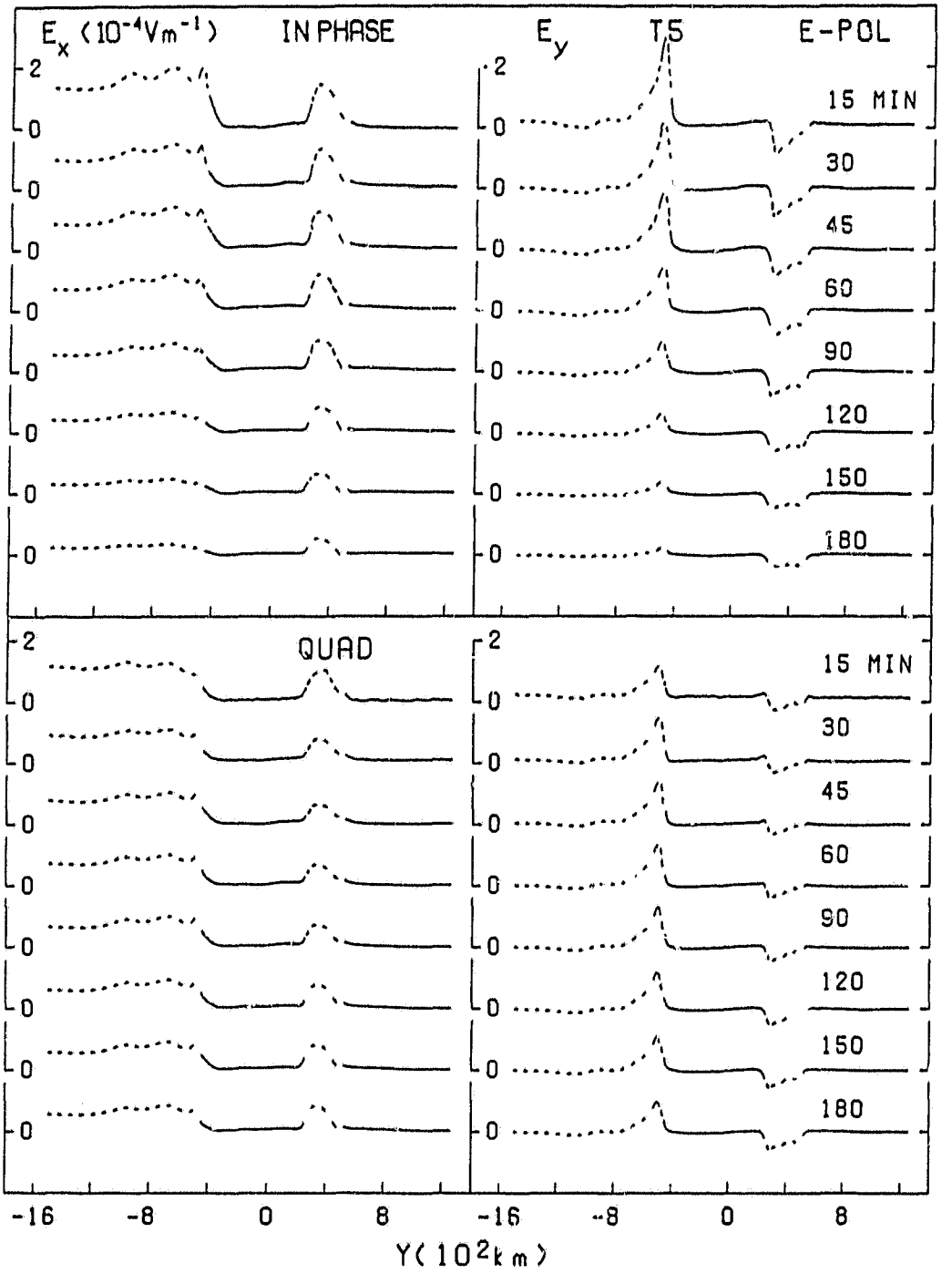

Figure 4.7: In-phase and quadrature electric fields for traverse T_5 for E-polarization at periods from 15 to 180 min.

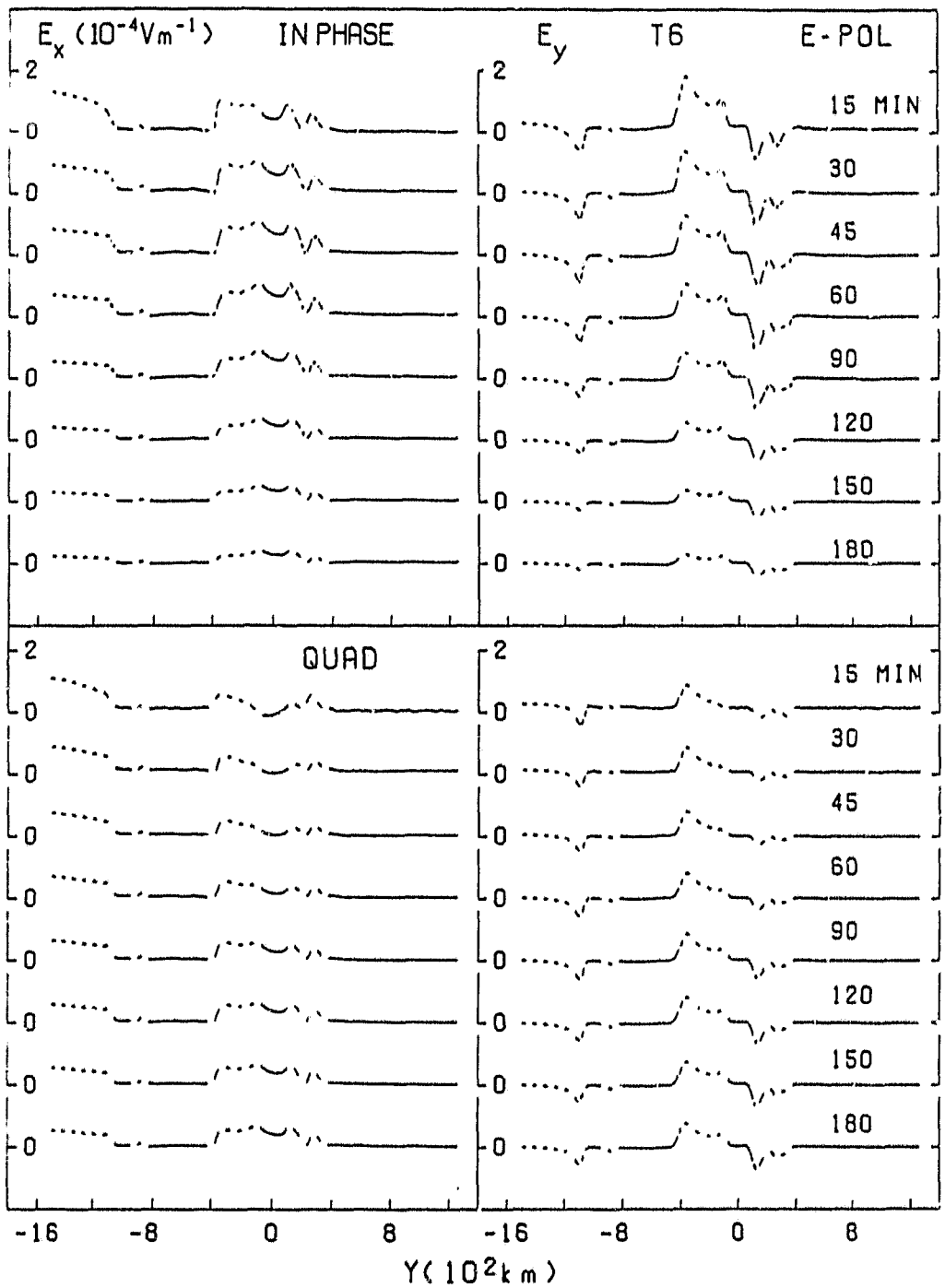

Figure 4.8: In-phase and quadrature electric fields for traverse T_6 for E-polarization at periods from 15 to 180 min.

Figures 4.7 and 4.8 show frequency responses of E_x and E_y for T5 and T6 respectively. The electric fields for traverse T5, which crosses the Korea coast and the Japan island, show the effects of current concentration along the continental coastline and current diffusion into the resistive island, which leads to a large E_y at the coast of Korea and enhanced E_x over the Japan island. Both responses fall off gradually with increasing period. In Fig. 4.8 traverse T6 shows the effect of current concentration over the Korea-Japan strait. It is seen that in-phase E_x and E_y show prominent responses over either side of the strait at short periods and fall off with increasing period, while quadrature E_x and E_y responses are significant for the entire period range. In general, the electric field response observed here are consistent with the results of magnetic field responses over the Japan island, Bohai bay and the Korea-Japan strait.

4.2 Model Field Components For B-Polarization

4.2.1 Traverses For B-Polarization

For B-polarization, the current induced in oceans will tend to flow in the y-direction (Fig. 2.5), and thus will encounter the coasts of Japan and the continent. At the convex island arc coastline (outer coast), some current will diffuse into the island, while some will be deflected to the right (+x) or left (-x), depending on the location. These currents deflected in opposite directions account for the positive in-phase and quadrature B_y anomalies for T2 and T3 in Fig. 4.9, and the negative anomalies for T5, T6 and T7 just off-shore the outer Japan coastline. The in-phase and quadrature B_z as well respond to this current deflection by the island arc coastline. At the outer coast region of the T2 and T3 traverses, induced

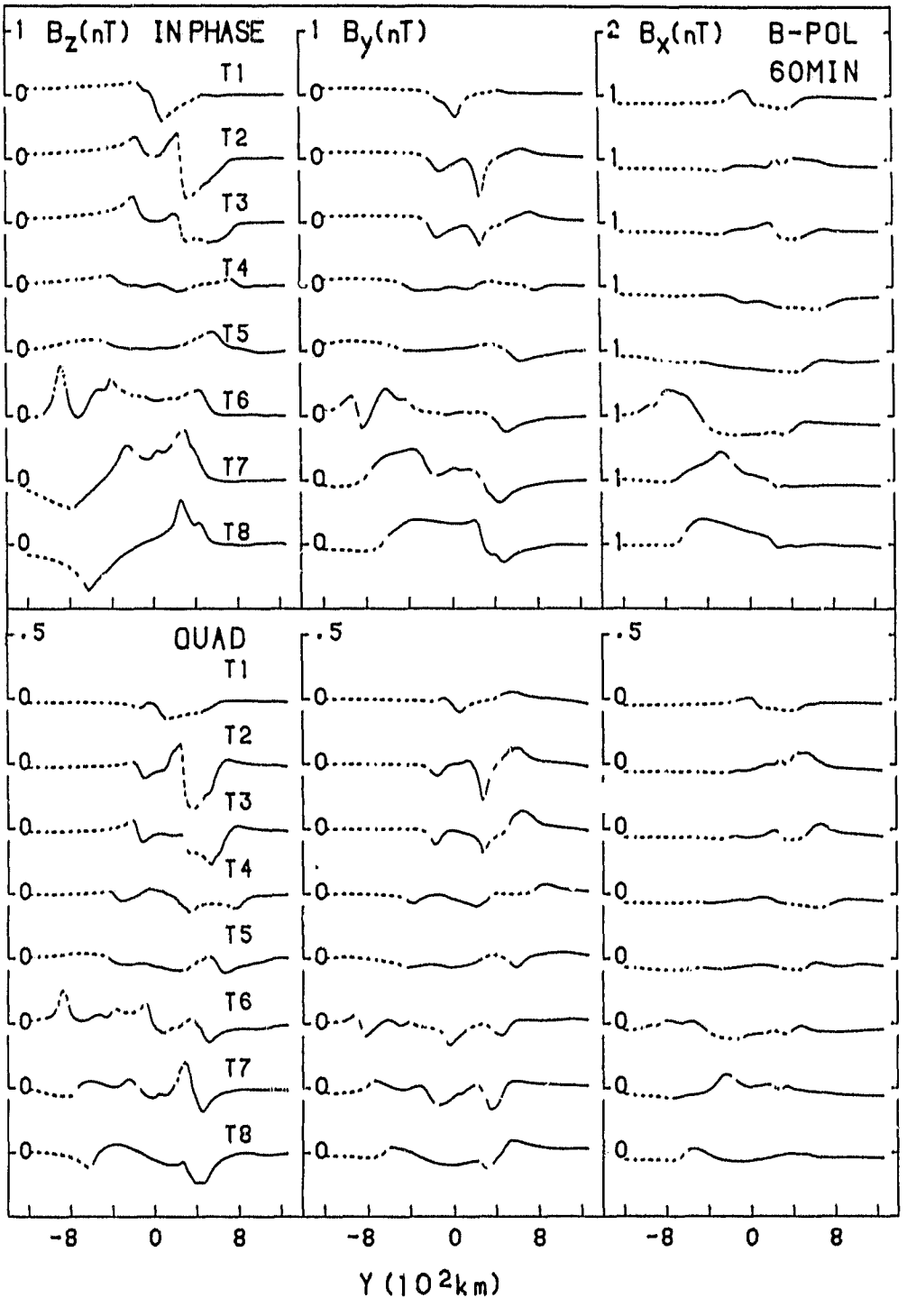

Figure 4.9: In-phase and quadrature magnetic fields for traverses T_1 to T_8 for B-polarization at 60 min.

current flowing towards Japan encountering the coastline, will first be deflected in the +x direction to yield outer coast field anomalies, then will be channelled to the left through Tsugaru strait to yield anomalies of opposite sign at the inner coast, as indicated by both B_z and B_y. For the T7 and T8 traverses, induced current in the Pacific Ocean will be deflected around the southern tip of the island arc, with some flowing into the Yellow Sea and Bohai Bay, and some channelled through the Korea-Japan strait and into the Japan Sea. Evidence of these current distributions are clearly seen in the off-shore B_z, B_y and B_x enhancements.

Although generally the field responses (Fig. 4.9) for B-polarization, are much smaller than those for E-polarization (Fig. 4.1), the B_z responses in particular are more complex for B- than for E-polarization. For E-polarization the character and the gradient of the B_z responses change little from traverse to traverse, while for B-polarization both change radically, including sign changes in the field gradients from traverse to traverse. The magnetic field responses at short periods, for example 15 min (not shown here), are very similar to those at 60 min for each polarization (Fig. 4.1 and 4.9), with the differences that the in-phase responses are generally somewhat smaller, and the quadrature responses somewhat larger than the corresponding responses at 60 min. In addition, the anomalies are more localized at the shorter periods than at longer periods. The strong similarity in the responses over a wide period range demonstrates the dominant effects of the oceans and the geometry of the complex coastlines at all periods.

Figure 4.10 shows the electric fields E_y and E_x at 60 min along traverses T1 to T8 for B-polarization. The behaviour of the electric field seen here is generally consistent with that expected for the induced electric currents as discussed for

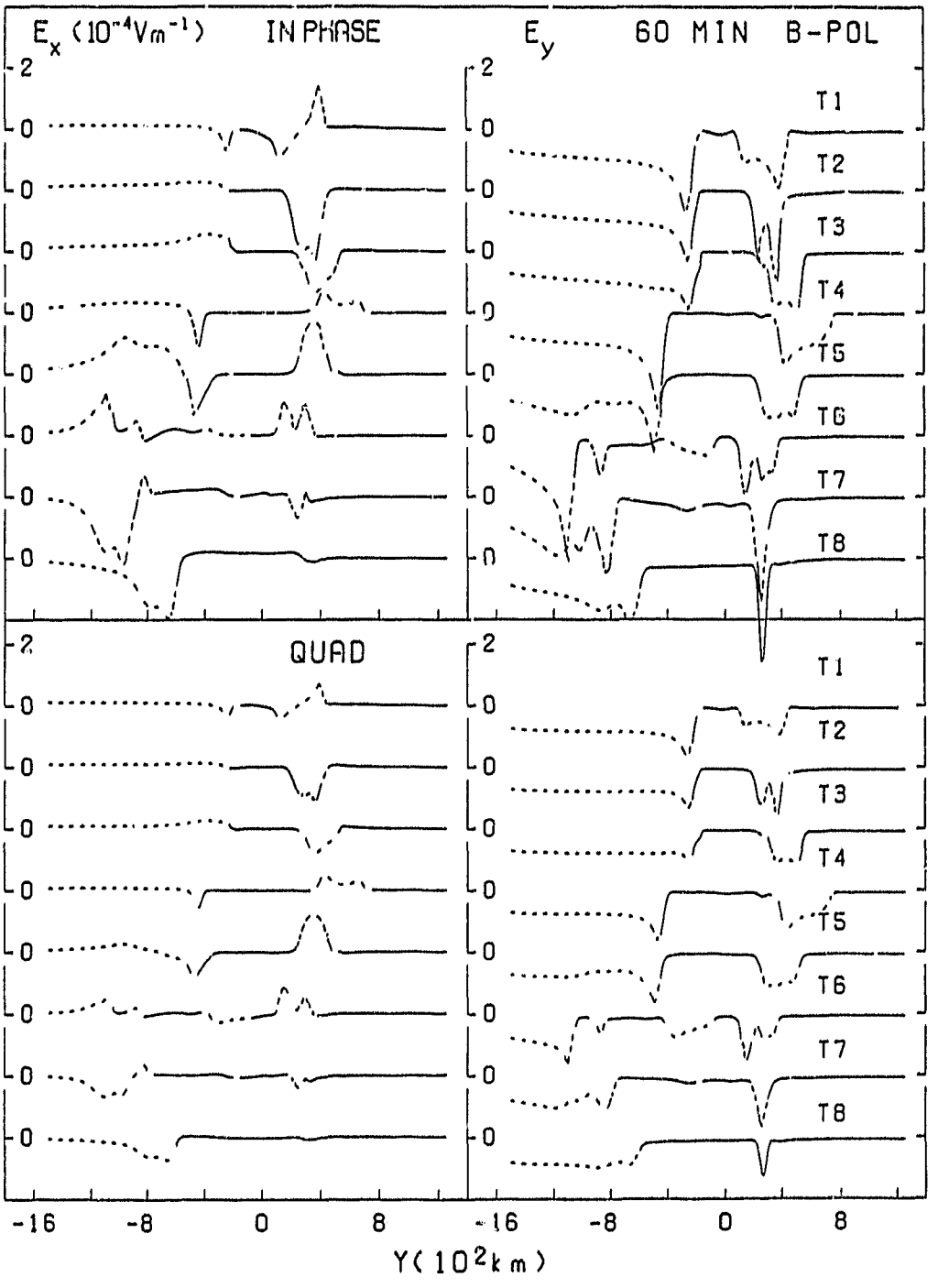

Figure 4.10: In-phase and quadrature electric fields for traverses T_1 to T_8 for B-polarization at 60 min.

the magnetic field. Along the island arc of Japan, both in-phase and quadrature E_x show negative response for T2 and T3, and positive for T5 and T6, which provides evidence that induced current in the y-direction is deflected into the +x or -x direction by the convex shaped Japan coastline. Large anomalous E_y is also observed along the continental coastline (T1-T8).

4.2.2 The Frequency Response For B-Polarization

The in-phase and quadrature B_z, B_x, and B_y along traverse T3 at periods 15-180 min for B-polarization are shown in Fig. 4.11. For this polarization, the currents induced in the deep Pacific Ocean tend to flow in y-direction and will be funnelled through Tsugaru strait (which is along the T3 region traverse). The enhanced current concentration resulting from the channelling effect leads to the large negative B_z responses observed in the northern Honshu region for a range of periods. The responses observed along T3 clearly indicate that Tsugaru strait, although shallow, plays an important role for the fields over the Honshu region of Japan. To be funnelled into Tsugaru strait, the induced currents are deflected around the tip of northern Honshu, accounting for the large anomalous response in B_y. The continental coastlines have very little effect on the magnetic field due to the coastline being roughly perpendicular to the source field direction. Quadrature B_y shows a noticeable response over the deep trench.

The in-phase and quadrature B_z responses along T5 for B-polarization shown in Fig. 4.12 are small at all periods. The fact that the magnitudes of the anomalies change little with period indicates that the current deflection at the island arc (concave) coastline, which leads to the B_z anomaly, occurs at all periods. This should be expected in view of the large depth of the off-shore ocean, a depth sufficient for significant current induction even at long periods.

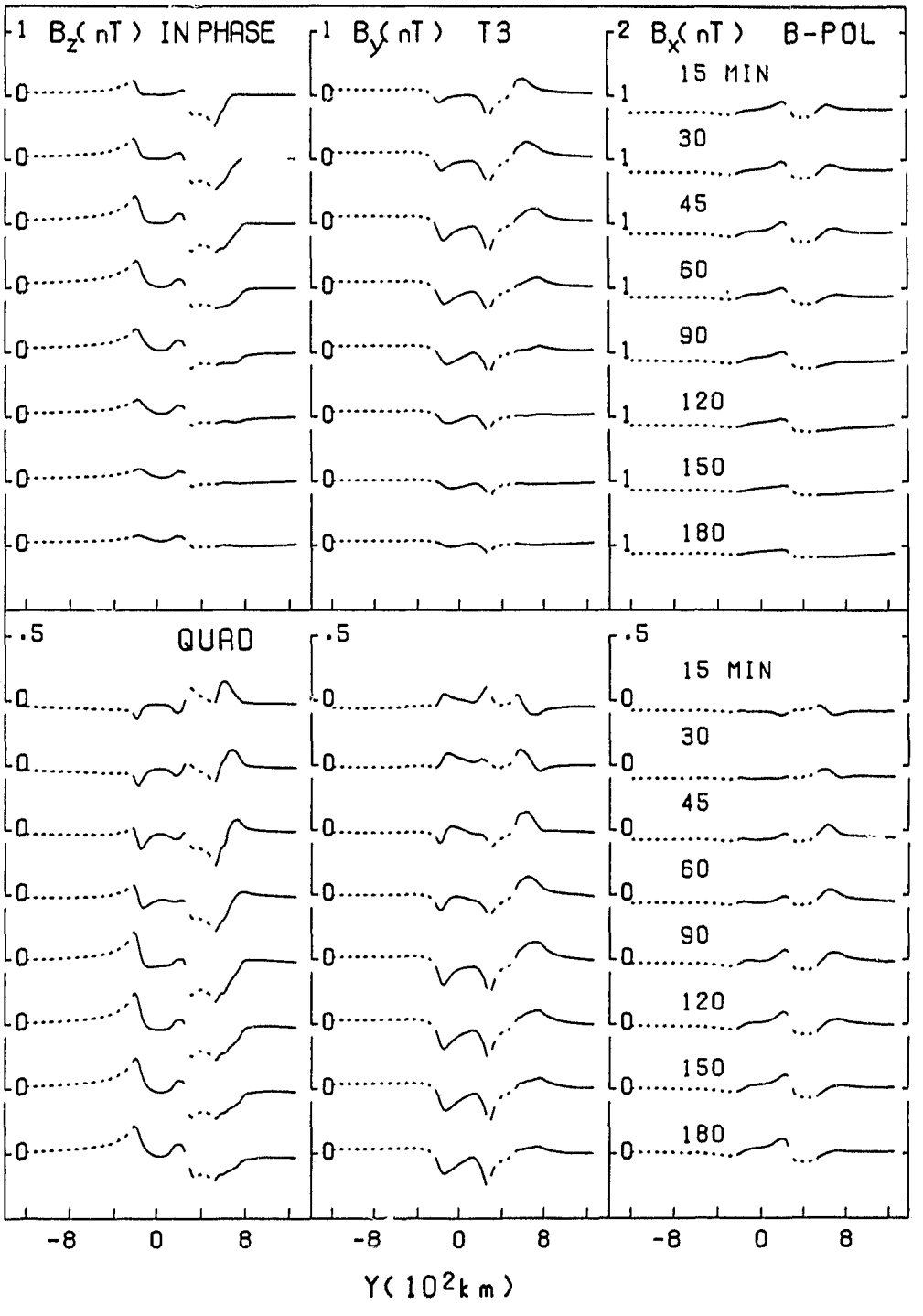

Figure 4.11: In-phase and quadrature magnetic fields for traverse T_3 for B-polarization at periods from 15 to 180 min.

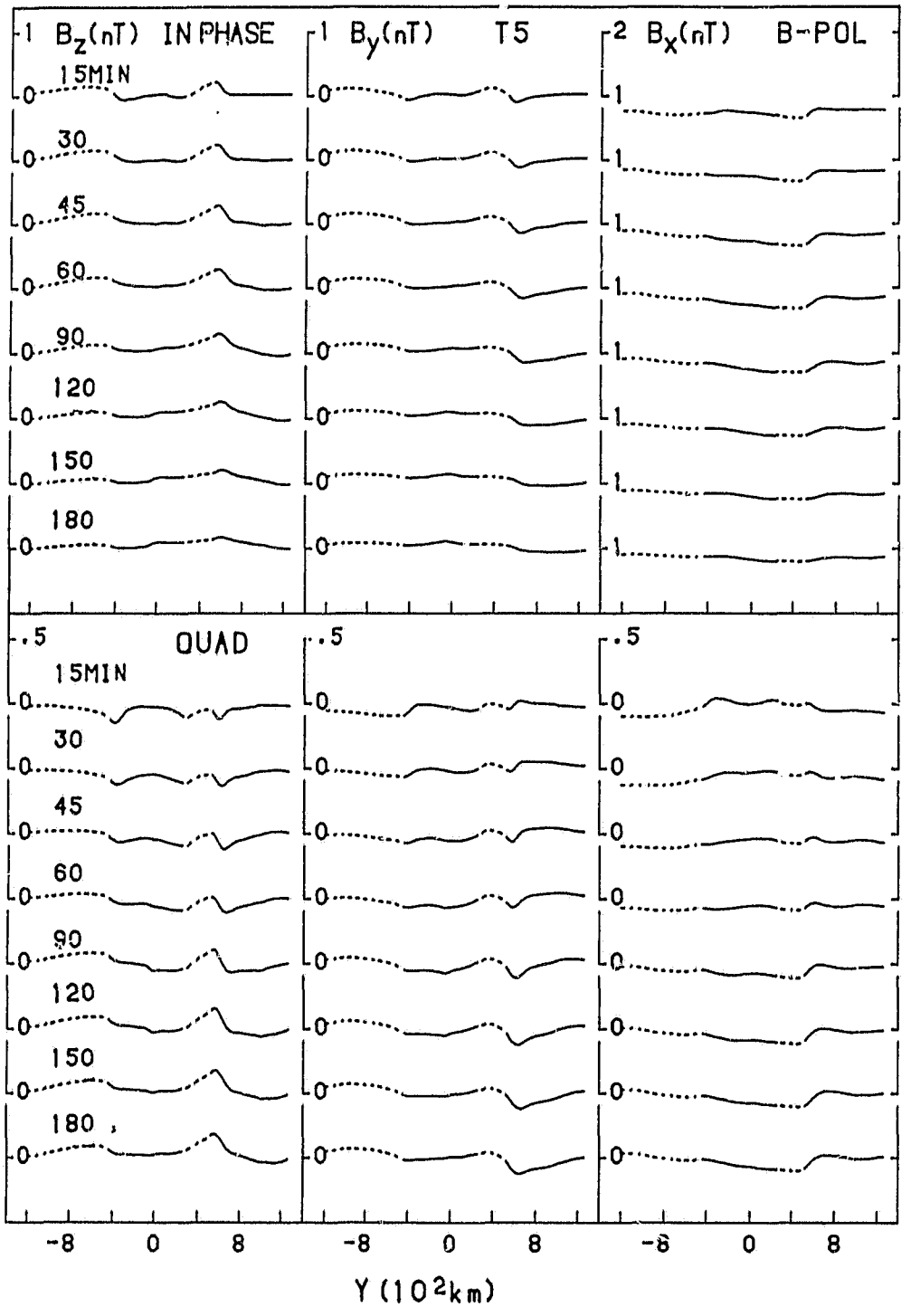

Figure 4.12: In-phase and quadrature magnetic fields for traverse T_5 for B-polarization.

Figure 4.13 shows the magnetic fields along traverse T6 for B-polarization. The responses along traverse T6 are generally small except for the region over the Liaodong peninsula where large anomalous B_z and B_y occur in response to strong deflection of current around the tip of the Liaodong peninsula. Since the Japan coastline provides a more abrupt obstacle to the y-direction flow of induced current than was the case of E-polarization, it is expected that anomalous responses will be relatively small.

The frequency responses for the electric fields for T3, T5 and T6 are provided in Figs. 4.14, 4.15, and 4.16 respectively. For traverse T3 (Fig. 4.14), E_y and E_x show large negative anomalies over the continental coastline and the Japan island. The responses over both regions decrease with increasing period for the in-phase components, and increase to a maximum at 150 min, then decrease with increasing period for the quadrature component. For traverse T5 (Fig. 4.15), both in-phase and quadrature E_y show negative enhancements over the Japan island, while E_x shows positive enhancement, indicating the effect of current deflection. It is seen that large positive E_x occurs along T5 well inland. This can be explained in terms of induced current deflected along the Korea coast (which has an angle of roughly 45° relative to the x-direction) being diffused into the continent. In Fig. 4.16 the electric fields show anomalous responses over the Bohai bay coast, the tip of the Liaodong peninsula and the Korea-Japan strait. The significantly large negative response of E_y over the Bohai Bay coastline is due to current diffusion, with the maximum in-phase response at 15 min and the maximum negative quadrature response at roughly 120 min for both E_x and E_y.

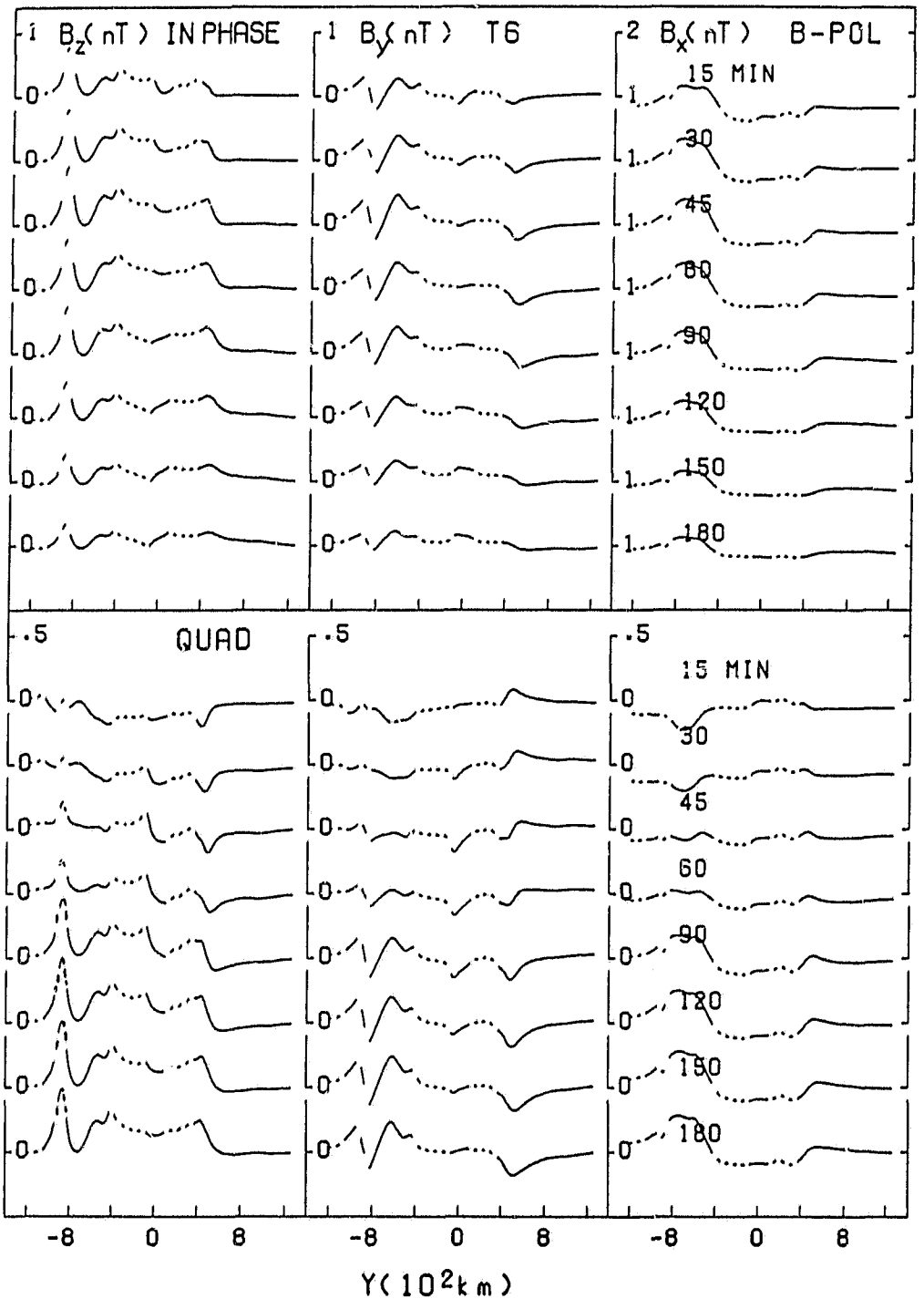

Figure 4.13: In-phase and quadrature magnetic fields for traverse T_5 for B-polarization at periods from 15 to 180 min.

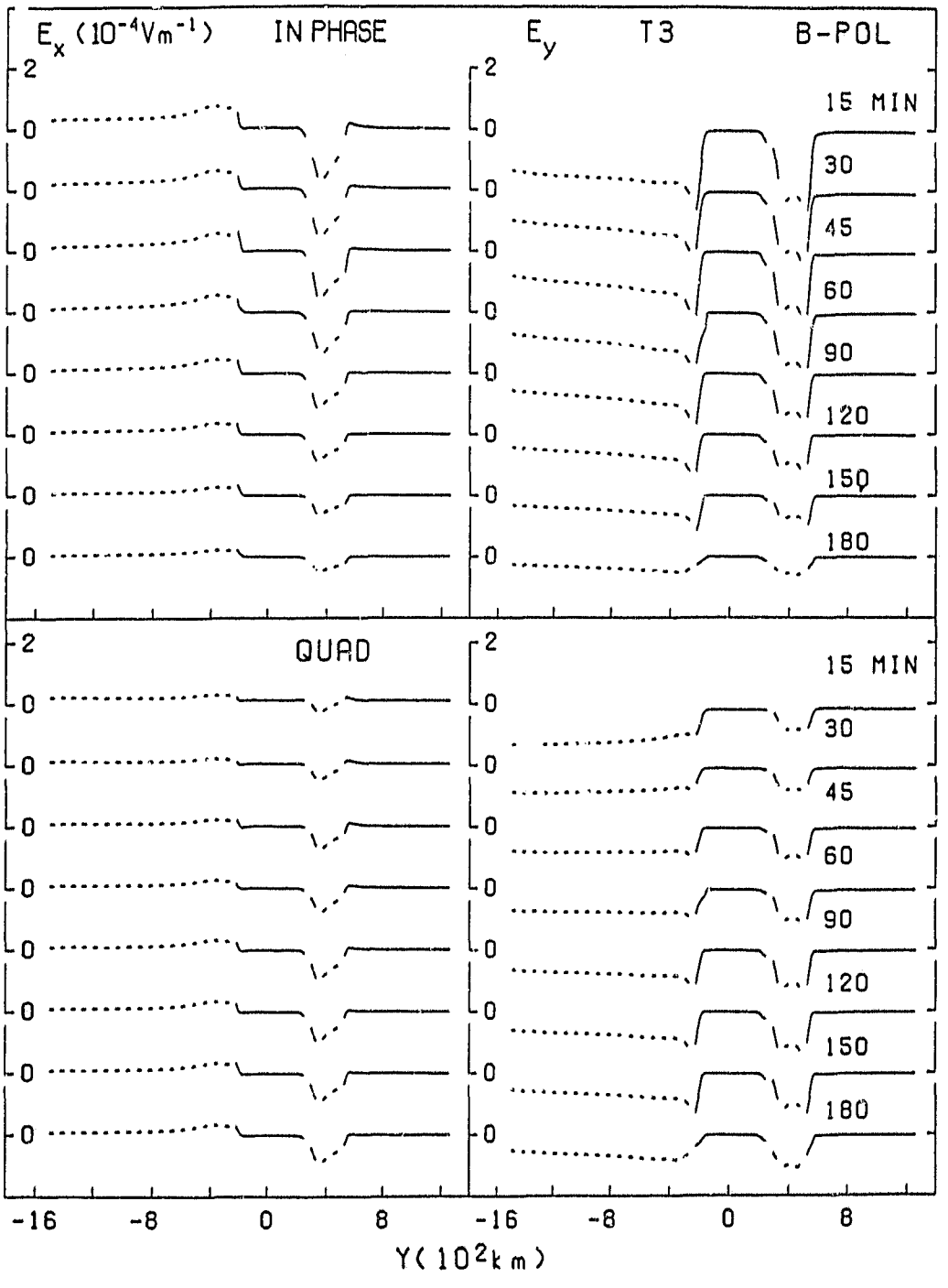

Figure 4.14: In-phase and quadrature electric fields for traverse T_3 for B-polarization at periods from 15 to 180 min.

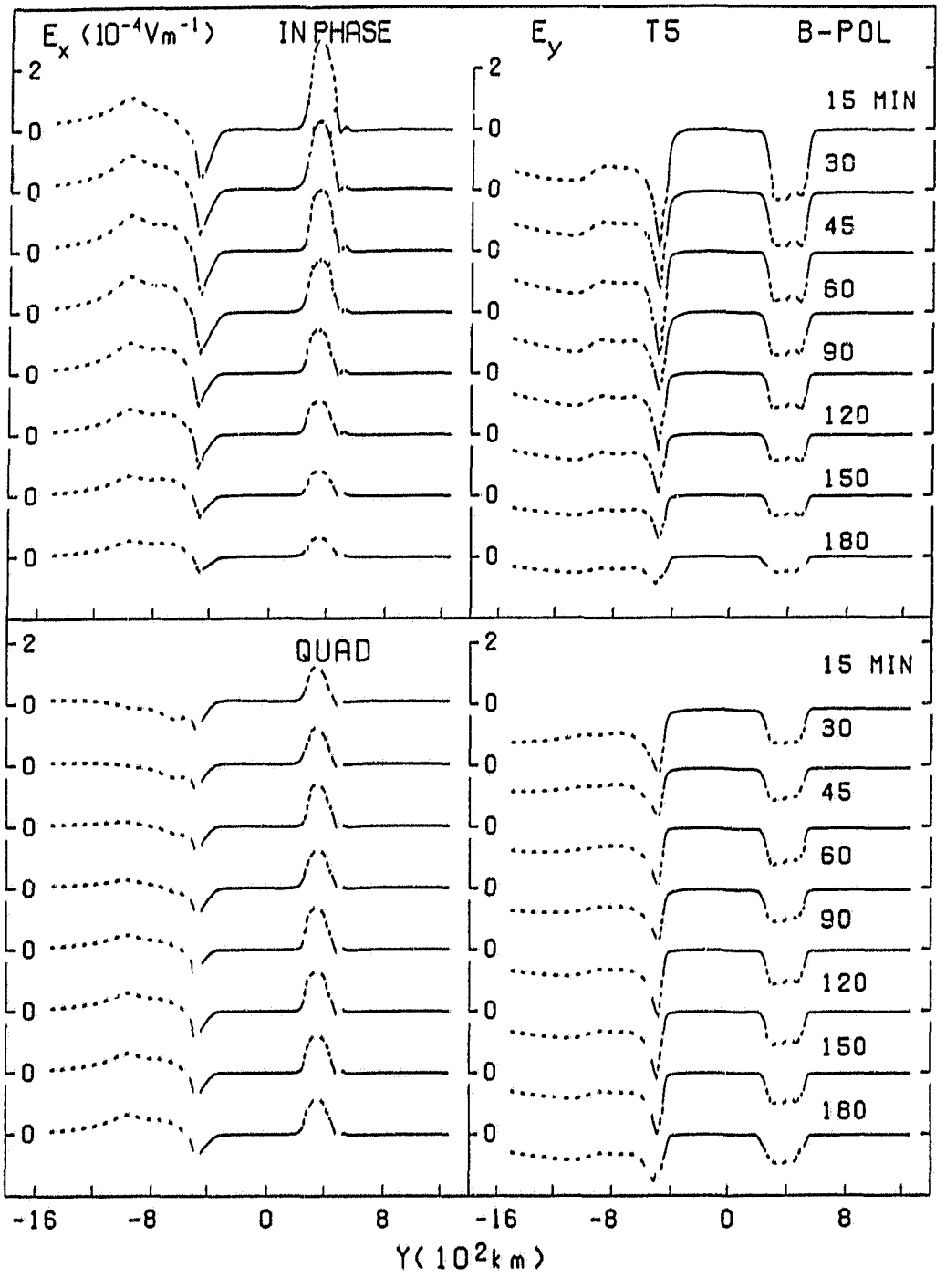

Figure 4.15: In-phase and quadrature electric fields for traverse T_5 for B-polarization at periods from 15 to 180 min.

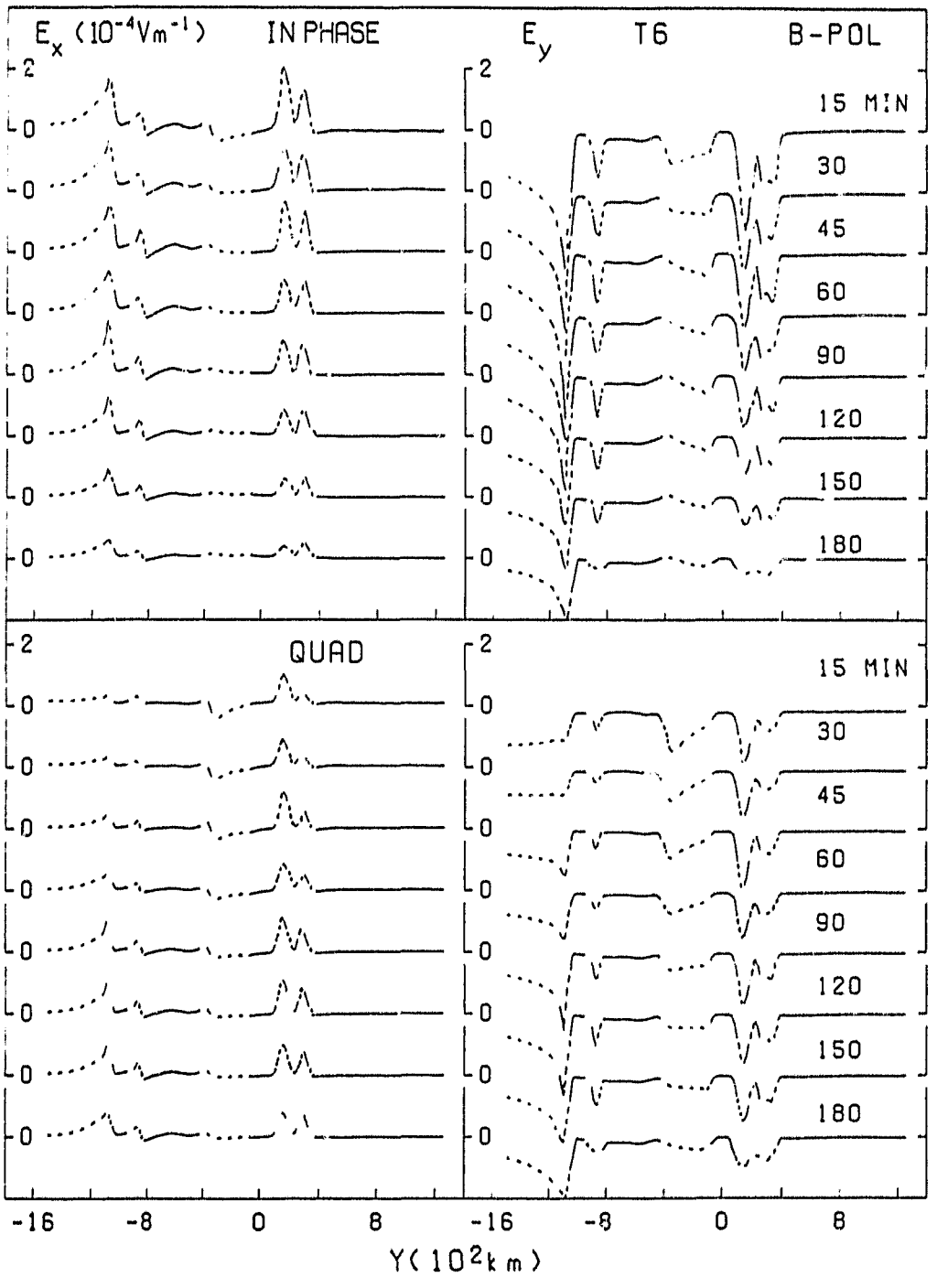

Figure 4.16: In-phase and quadrature electric fields for traverse T_6 for B-polarization at periods from 15 to 180 min.

4.3 Contours and Three Dimensional Views of Model field Components

4.3.1 Field Contours For E-Polarization

To provide an overview of the model in-phase and quadrature magnetic field components, particularly for the region around Japan, B_z field contours at 60 and 120 min for E-polarization are shown in Fig. 4.17 and 4.18. Clearly, for E-polarization large in-phase B_z field gradients are observed at all on-shore Japan sites. Over much of the Japan region, the contour lines for both in-phase and quadrature B_z tend to follow the island arc shape, accounting for the very similar B_z responses from traverse to traverse noted in Fig. 4.9. Off shore, at the outer coast, large gradients are observed due to the current, induced in the deep ocean south of Japan, being deflected around the convex island arc. Some of this current is funnelled through the Korea-Japan strait, leading to very large in-phase B_z gradients on either side of the strait (the southern tip of Japan and the Korean peninsula), and to large gradients both in the continental coastal area of the Japan Sea and the inner coastal region of Japan. In the central region of the Japan Sea two sets of closed contour lines account for the two anomalies of opposite sign noted in Fig. 4.17. Large field gradients, too, are observed at the La Perouse and Tsugaru straits in response to the current concentrations there due to current channelling for E-polarization. It is rather surprising that a much greater anomalous in-phase B_z occurs along the U.S.S.R.-China coastline than that along the west coast of Japan, which will lead to large in-phase induction arrow at the U.S.S.R.-China coastline and relatively small arrows at the west coast of Japan. The quadrature B_z contours, though showing much smaller gradients than observed for the in-phase components, follow very similar patterns, again accounting for the similar responses observed from traverse to traverse in Fig. 4.1.

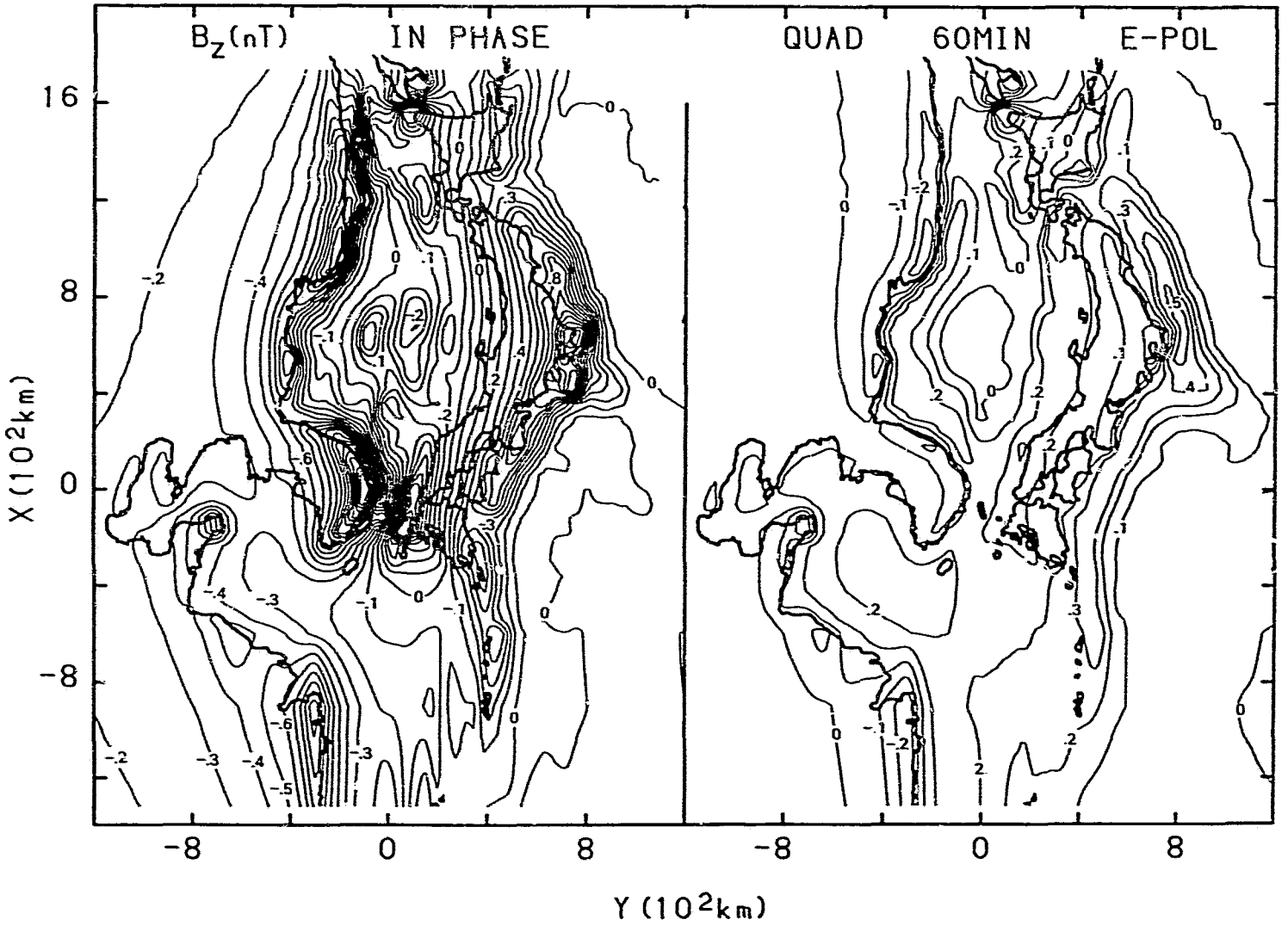

Figure 4.17: In-phase and quadrature B_z field contours for E-polarization at 60 min.

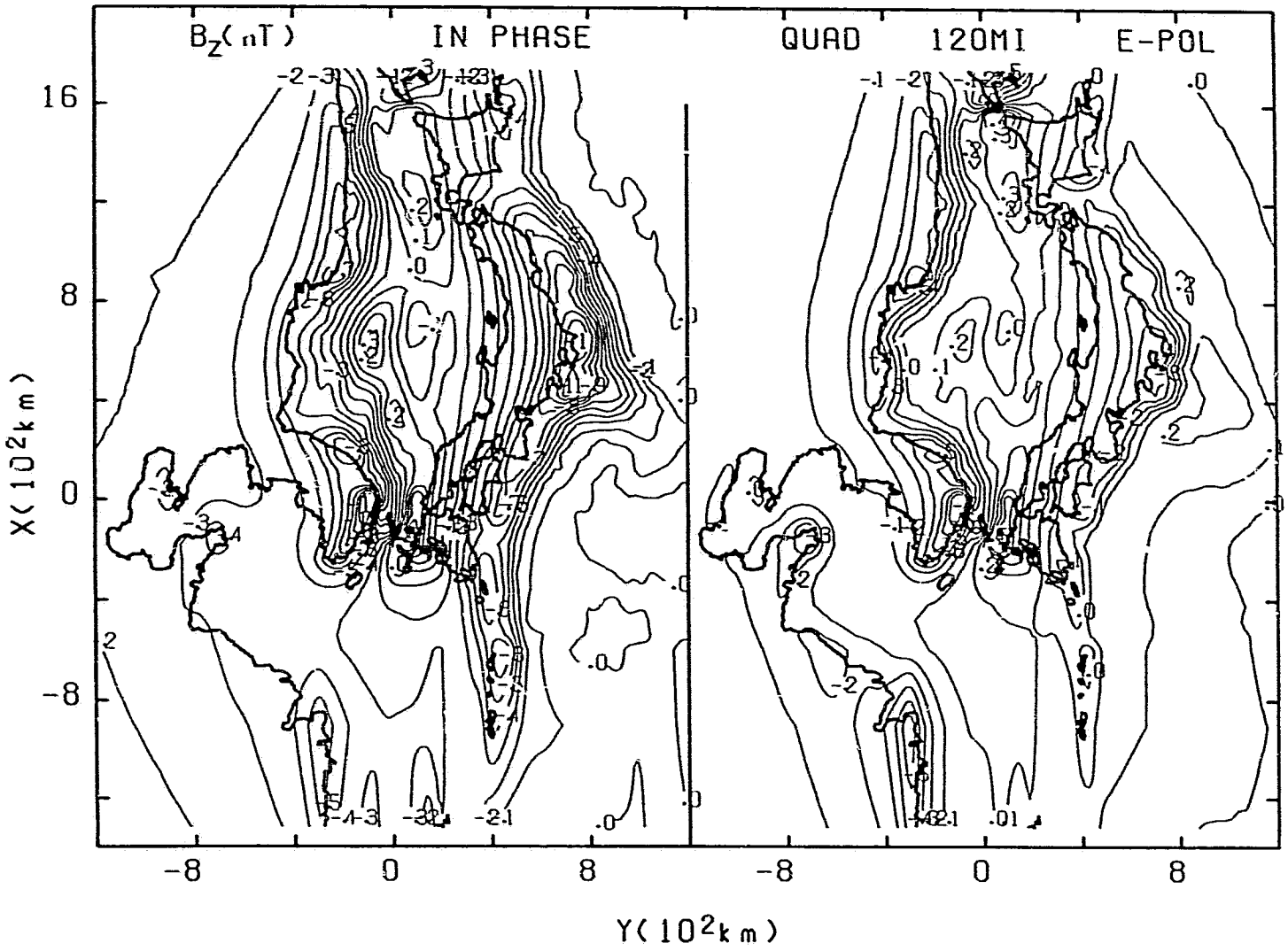

Figure 4.18: In-phase and quadrature B_z field contours for E-polarization at 120 min.

As mentioned previously in the discussion of the frequency response, in-phase B_z reaches a maximum response at 60 min while quadrature B_z reaches a maximum at a longer period. The contour plot of Fig. 4.18 shows full agreement with this result. At 120 min, enhanced B_z responses have shifted from the in-phase to the quadrature, with reduced in-phase and enhanced quadrature components. For instance, the two sets of closed contour loops which map the in-phase B_z in the Japan Sea almost vanish but appear in the quadrature component.

Figures 4.19 and 4.20 show B_y contours for 60 and 120 min. The in-phase B_y contours at 60 min (Fig. 4.19) show large gradients seaward along the general coastlines, and thus the contour lines very closely delineate the shape of the coastlines over the region. Similar to the case of B_z, greatly enhanced anomalous B_y occurs off shore from the U.S.S.R.-China coast, in response to current concentration there. Large gradients in B_y are observed at the convex shaped east coast of Japan due the cape effect, while relatively small gradients are observed at the west coast of Japan due to the bay effect. A strong channelling effect is indicated by the dense contours for the in-phase component over the Korea-Japan strait. For 120 min, the anomalous in-phase B_y peak is shifted seaward where the contour lines again depict the ocean bathmetry. Evidence of this can be found, in particular, in the B_y response along the Pacific Trench. The quadrature B_y over the entire region shows a much smaller field gradient than the in-phase component, but increases, while the in-phase part decreases with increasing period. This is related to the phase rotation of induced current at depth.

Figures 4.21 and 4.22 show B_x contours for 60 and 120 min periods. It has been shown in the previous discussion, that B_x shows large anomalous response

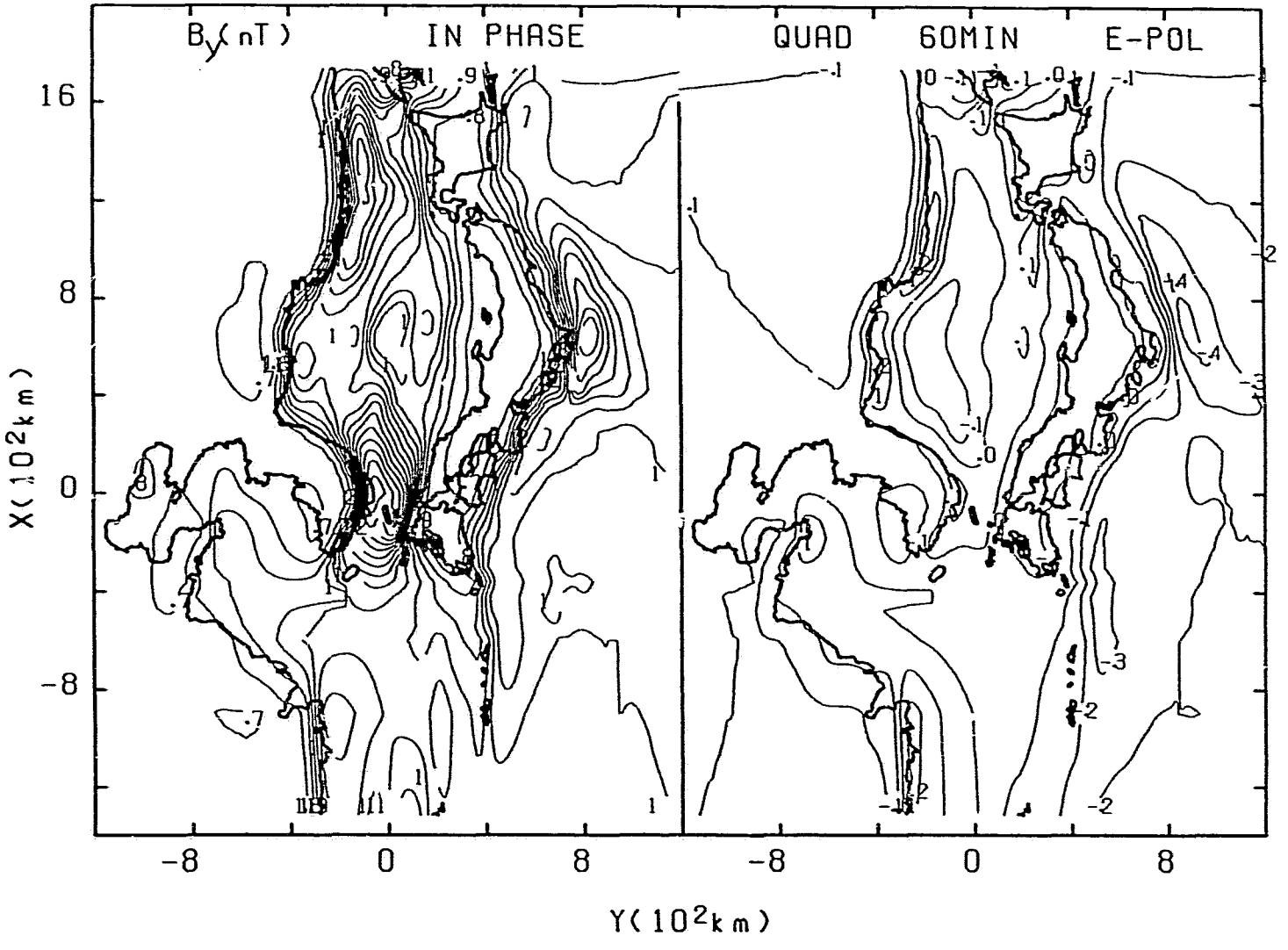

Figure 4.19: In-phase and quadrature B_y field contours for E-polarization at 60 min.

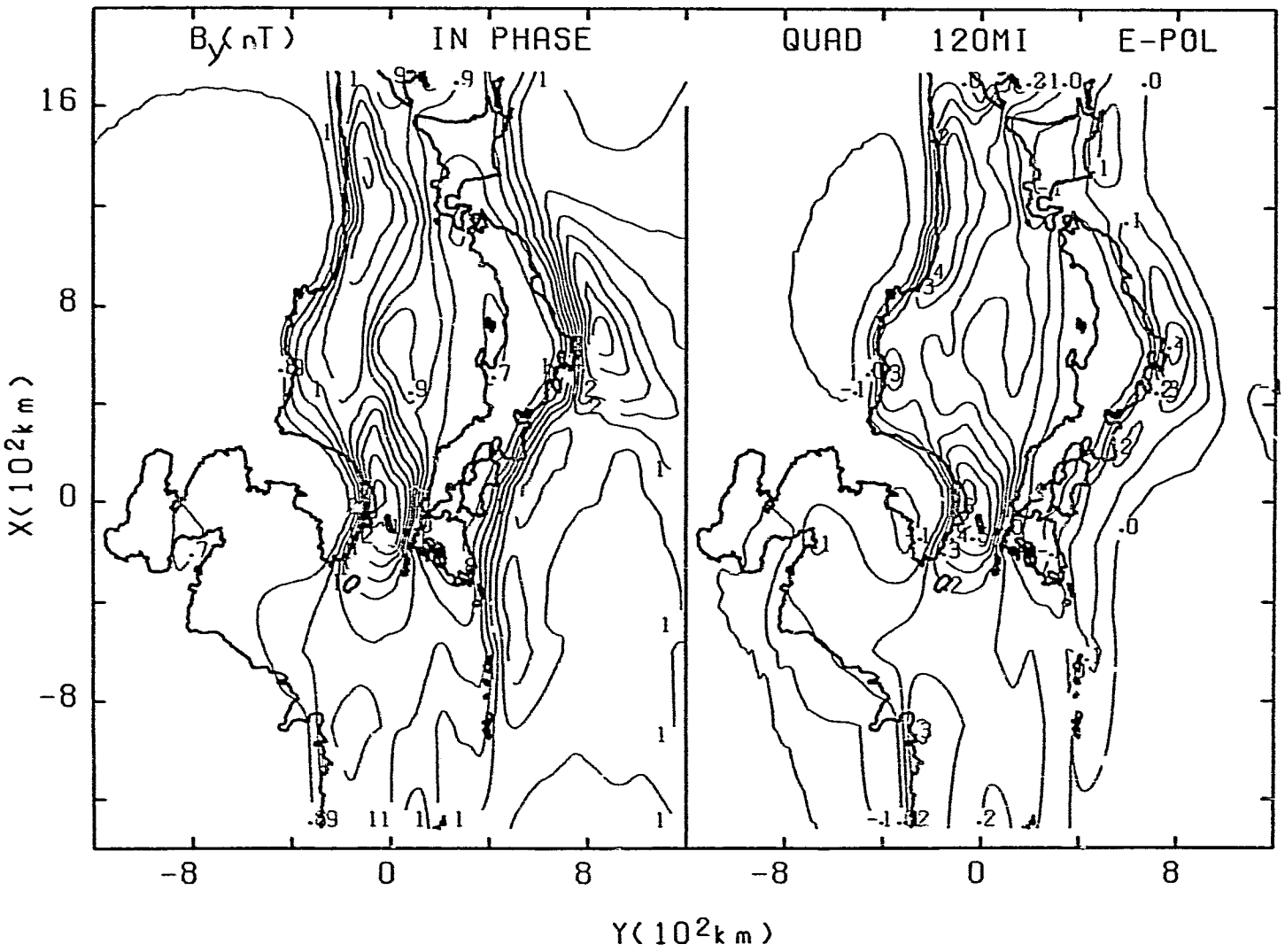

Figure 4.20: In-phase and quadrature B_y field contours for E-polarization at 120 min.

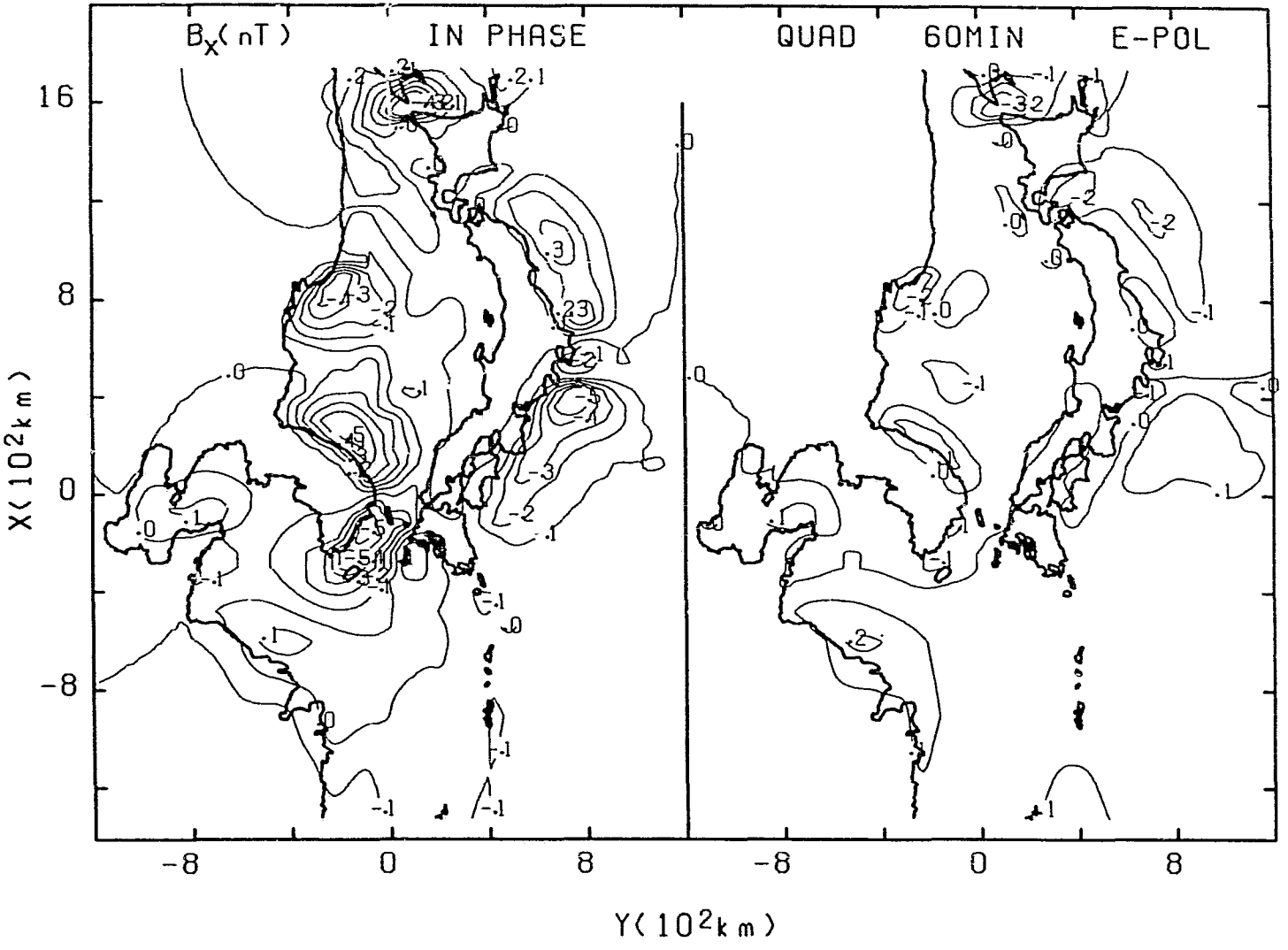

Figure 4.21: In-phase and quadrature B_x field contours for E-polarization at 60 min.

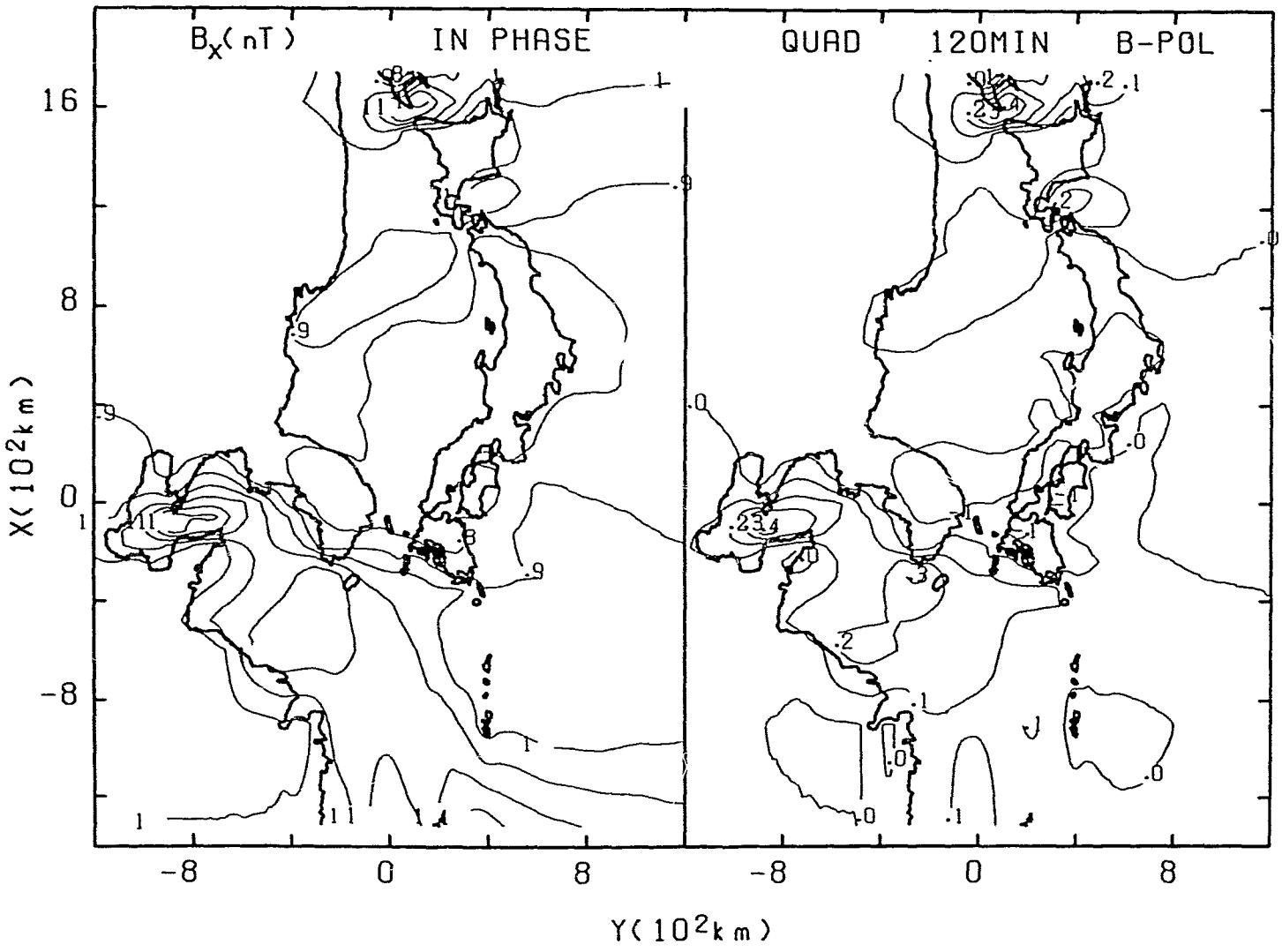

Figure 4.22: In-phase and quadrature B_x field contours for E-polarization at 120 min.

where the coastline (or structure) has roughly a 45° angle relative to the source field. This certainly accounts for the contour loops of the in-phase B_x over the Pacific Trench, the Korean peninsula, and the La Perouse strait at 60 min. As the period increases to 120 min, it is found that the contour loops vanish, except for those over the trench area where current deflection occurs at depth in the deep ocean. The widely spaced contours for both in-phase and quadrature B_x over continent and ocean, away from the coast, indicate a fairly constant field (almost zero for B_x).

4.3.2 Field Contours For B-Polarization

The B_z field contours for B-polarization are shown in Fig. 4.23 and 4.24 for 60 and 120 min. Figure 4.23 shows large B_z field gradients in the Yellow Sea in response to current, funnelled into the Yellow Sea and Bohai Bay, and in Tsugaru and La Perouse straits. In general, except in the neighborhood of the straits, relatively small field gradients are observed directly over Japan both for the in-phase and quadrature B_z. These observations fully agree with the results shown for B-polarization in Fig. 4.2. As the period increases from 60 to 120 min, it is found (Fig. 4.24) that the in-phase B_z is slightly attenuated while quadrature B_z is enhanced, very similar to that observed for the case of E-polarization, again related to phase rotation of the induced current.

Figures 4.25 and 4.26 show the B_x field contours at 60 and 120 min. The in-phase B_x over the continent, for the B-polarization, has a value of roughly 1 nT, while quadrature B_y is approximately zero, as established by the normalization procedure at a reference point at a simulated range of 1500 km inland. For the B-polarization case, the Japan islands provide obstacles to the induced current

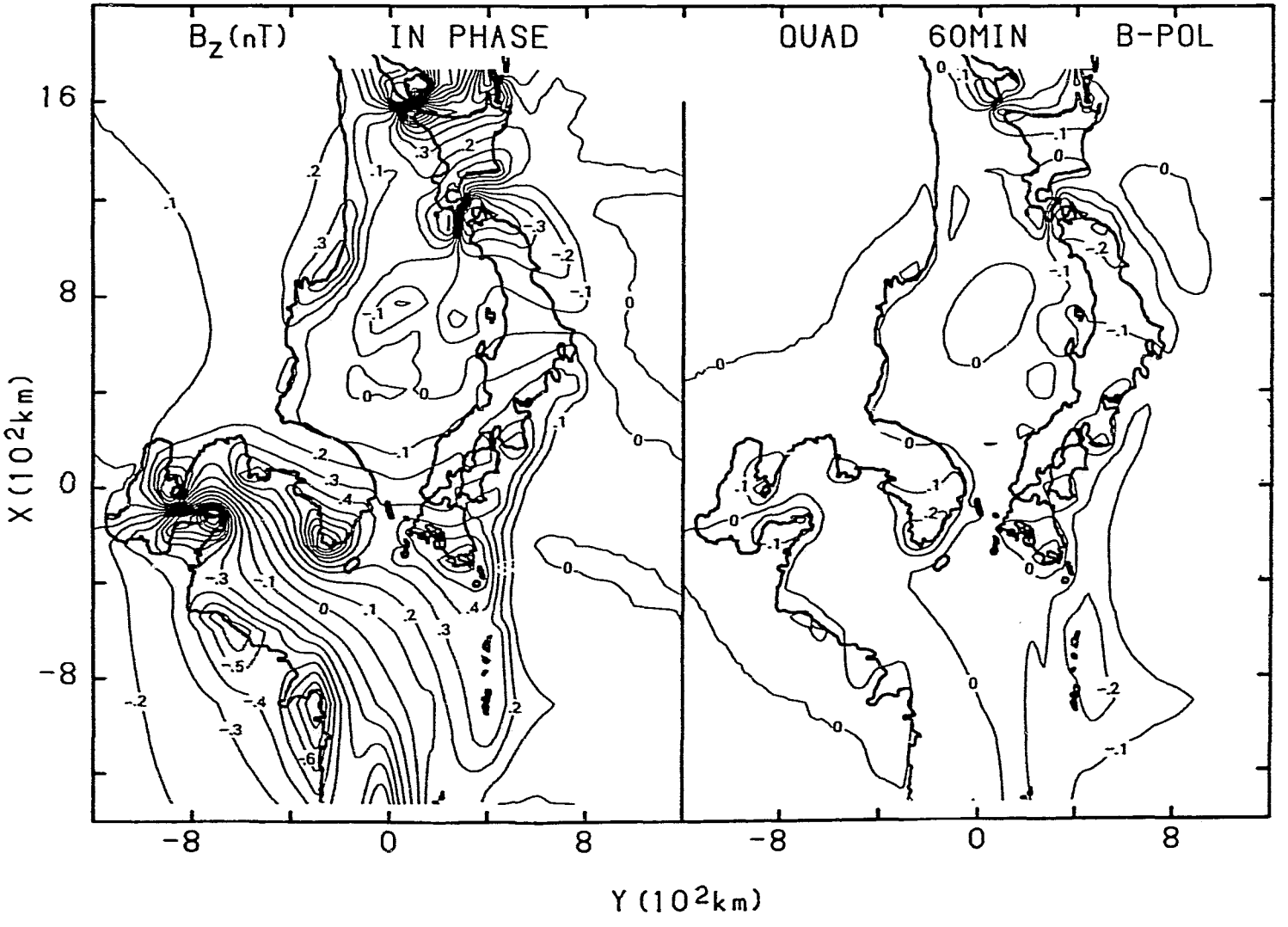

Figure 4.23: In-phase and quadrature B_z field contours for B-polarization at 60 min.

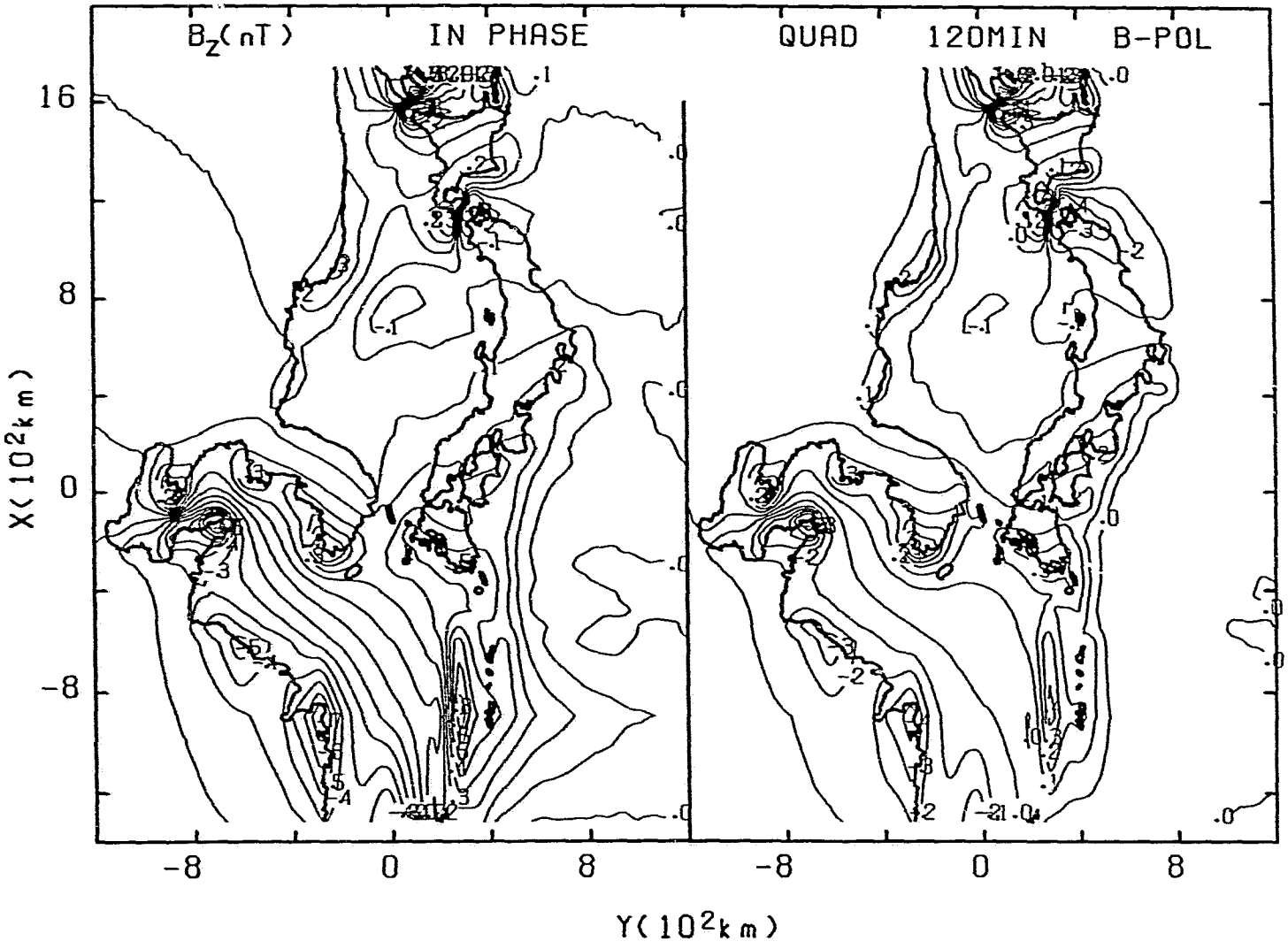

Figure 4.24: In-phase and quadrature B_z field contours for B-polarization at 60 min.

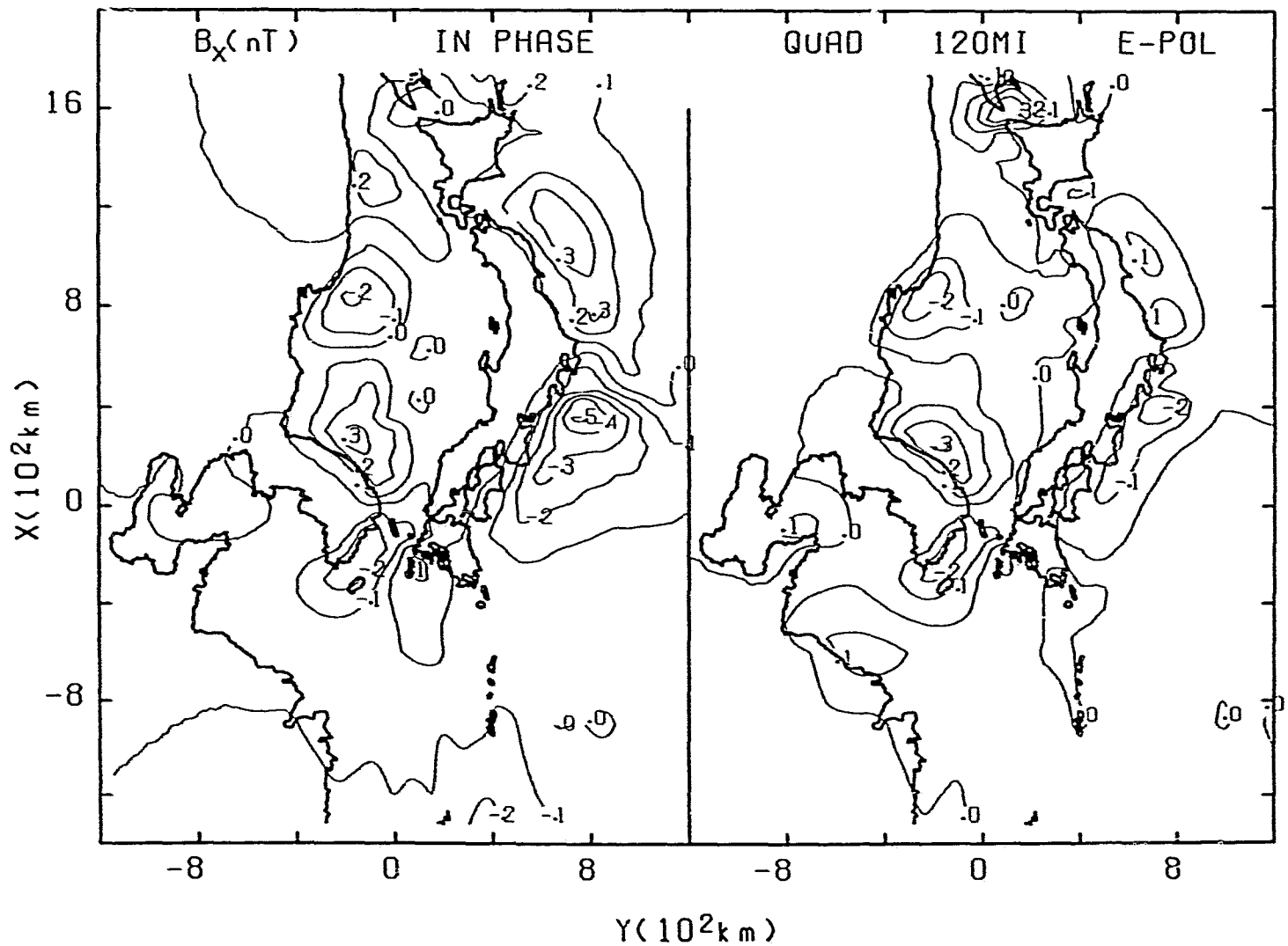

Figure 4.25: In-phase and quadrature B_x field contours for B-polarization at 60 min.

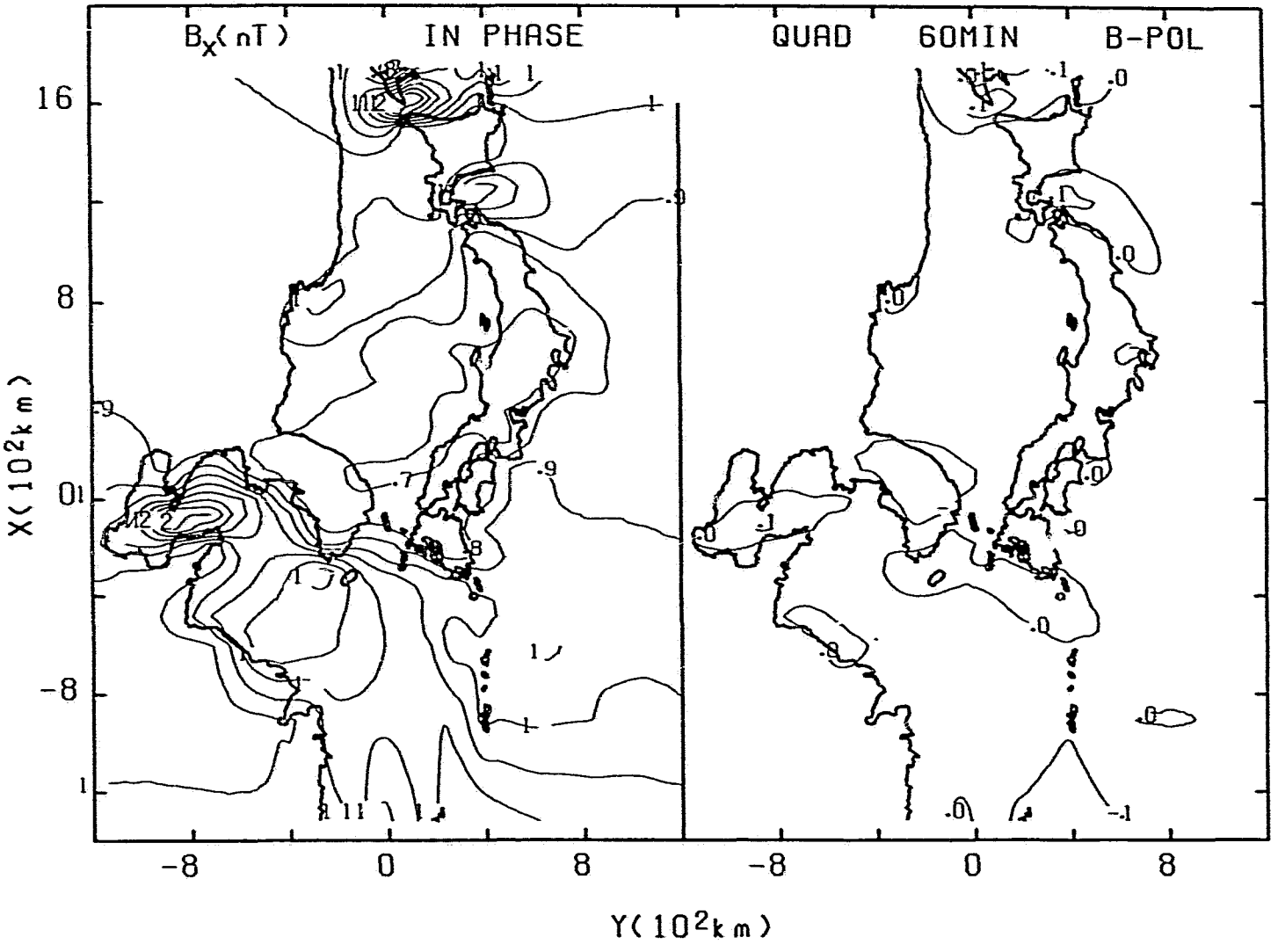

Figure 4.26: In-phase and quadrature B_x field contours for B-polarization at 120 min.

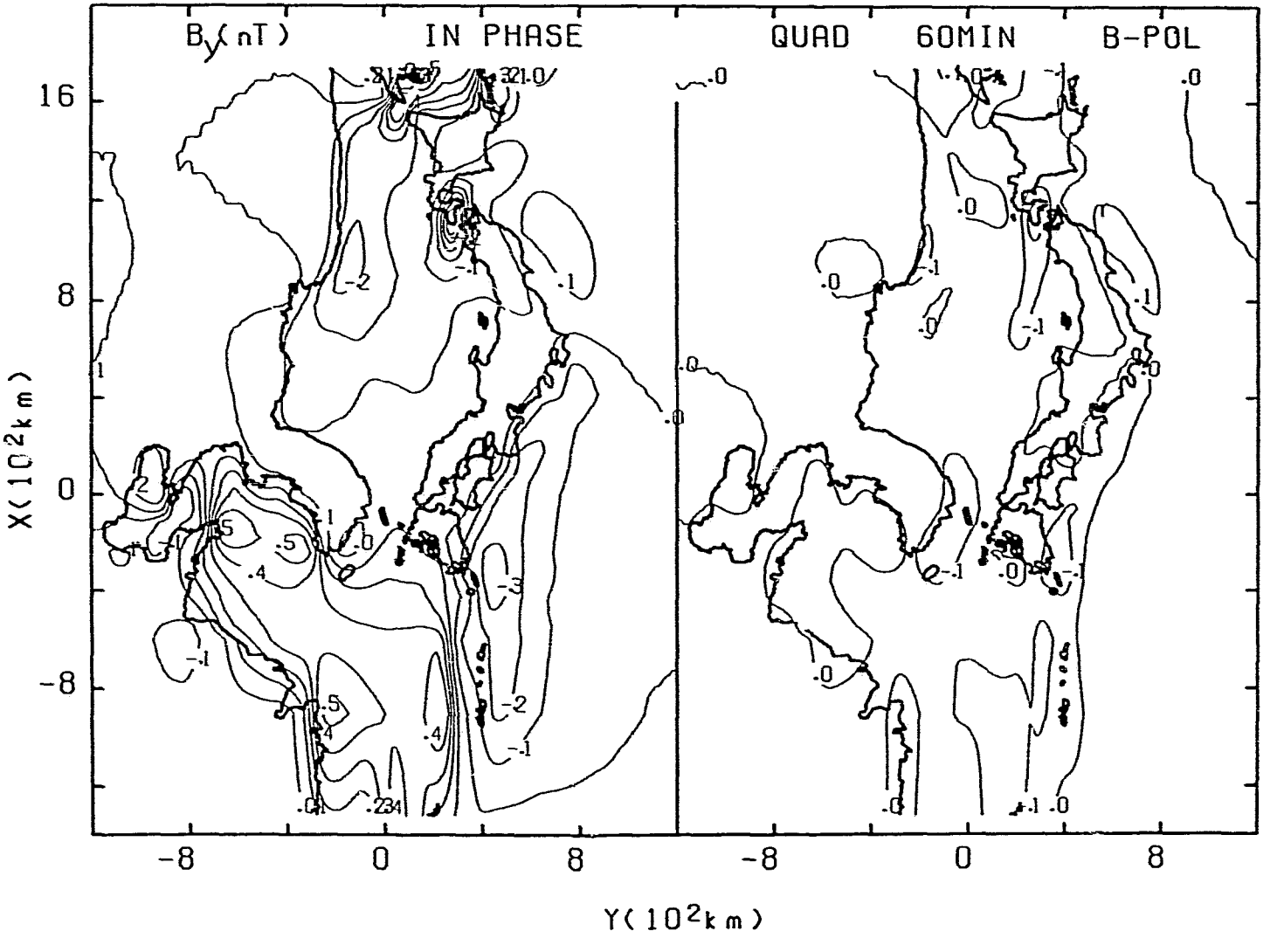

Figure 4.27: In-phase and quadrature B_y field contours for B-polarization at 60 min.

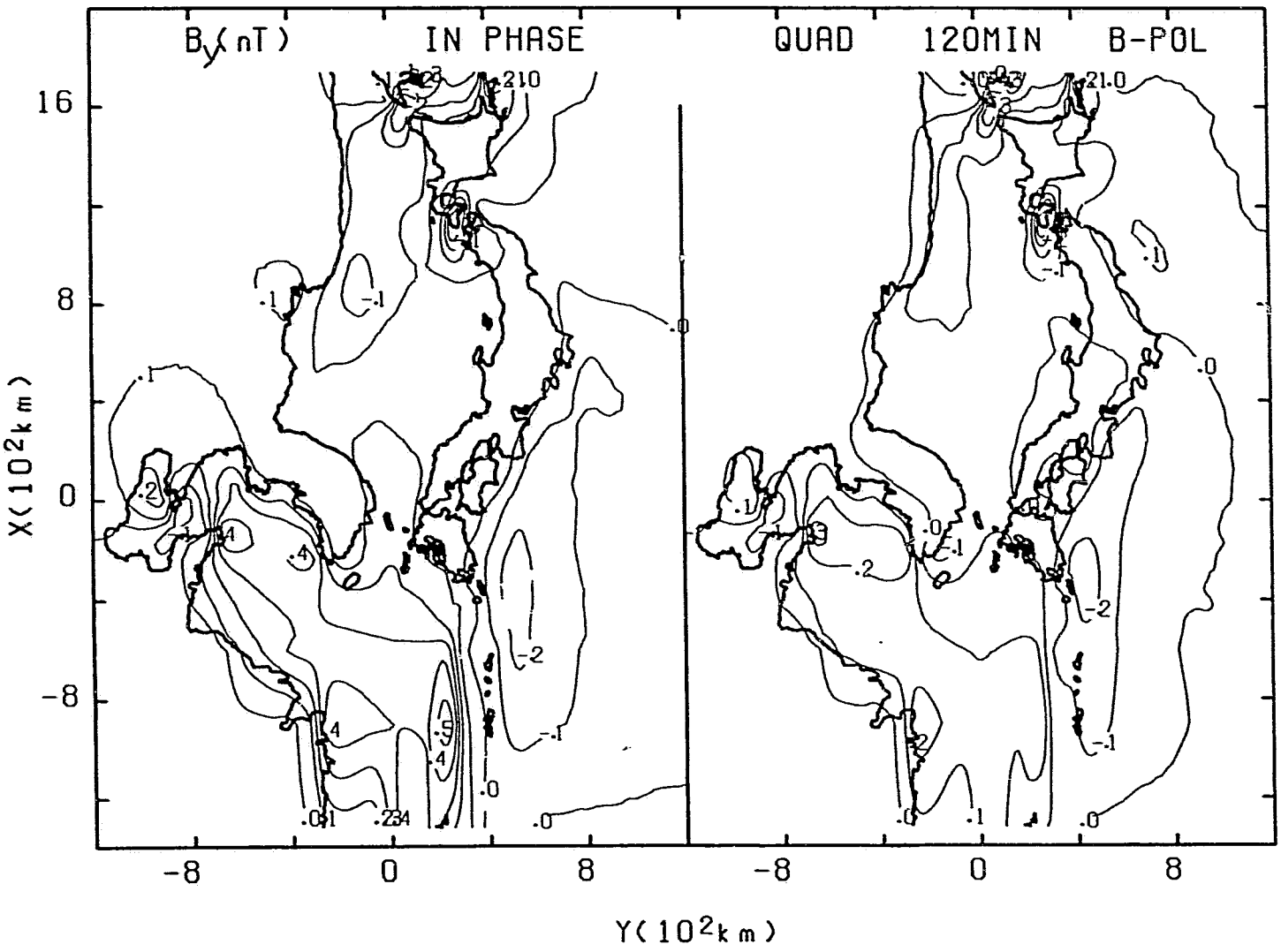

Figure 4.28: In-phase and quadrature B_y field contours for B-polarization at 120 min.

flowing in the y-direction. However, the Tsugaru and La Perouse straits provide two narrow current passages connecting the local Japan Sea with the open Pacific Ocean. Thus as expected, both B_z and B_x show anomalous responses over the straits. The current induced in the deep ocean, also flowing in the Yellow Sea, being deflected around the tips of the Korea, Shandong and Liaodong peninsulas, lead to large contour loops of in-phase B_x at the Bohai strait.

The B_y field contours for 60 and 120 min are shown in Figs. 4.27 and 4.28. The contour lines of in-phase B_y are dense over the tips of the Shandong, Liaodong and Korea peninsulas in response to the current deflections. The highly concentrated contour loops over the La Perouse and Tsugaru straits again indicate the current channelling effect.

4.3.3 Three Dimensional Views of field components for E-polarization

Figures 4.29 , 4.30 and 4.31 show three dimensional views of B_z, B_y and E_x respectively for 60 min for E-polarization. (The three dimensional views of B_x and E_y are given in Appendix A and will not be discussed here). In Fig. 4.29 the in-phase B_z responses show a trench-like shape over the east coast of Japan where large current concentration occurs. The quadrature B_z has, in general, smaller amplitudes over the coastline but with a positive response, while the in-phase B_z is negative, which will result in a direction reversal between the in-phase and quadrature induction arrows at the east coast of Japan. Further seaward, notable anomalous responses for both in-phase and quadrature B_z are observed following the shape of the Pacific Trench in response to the current concentration at depth. At the Korea-Japan strait, the current channelling effect is clearly indicated by the much enhanced positive and negative responses over each side of the strait. In

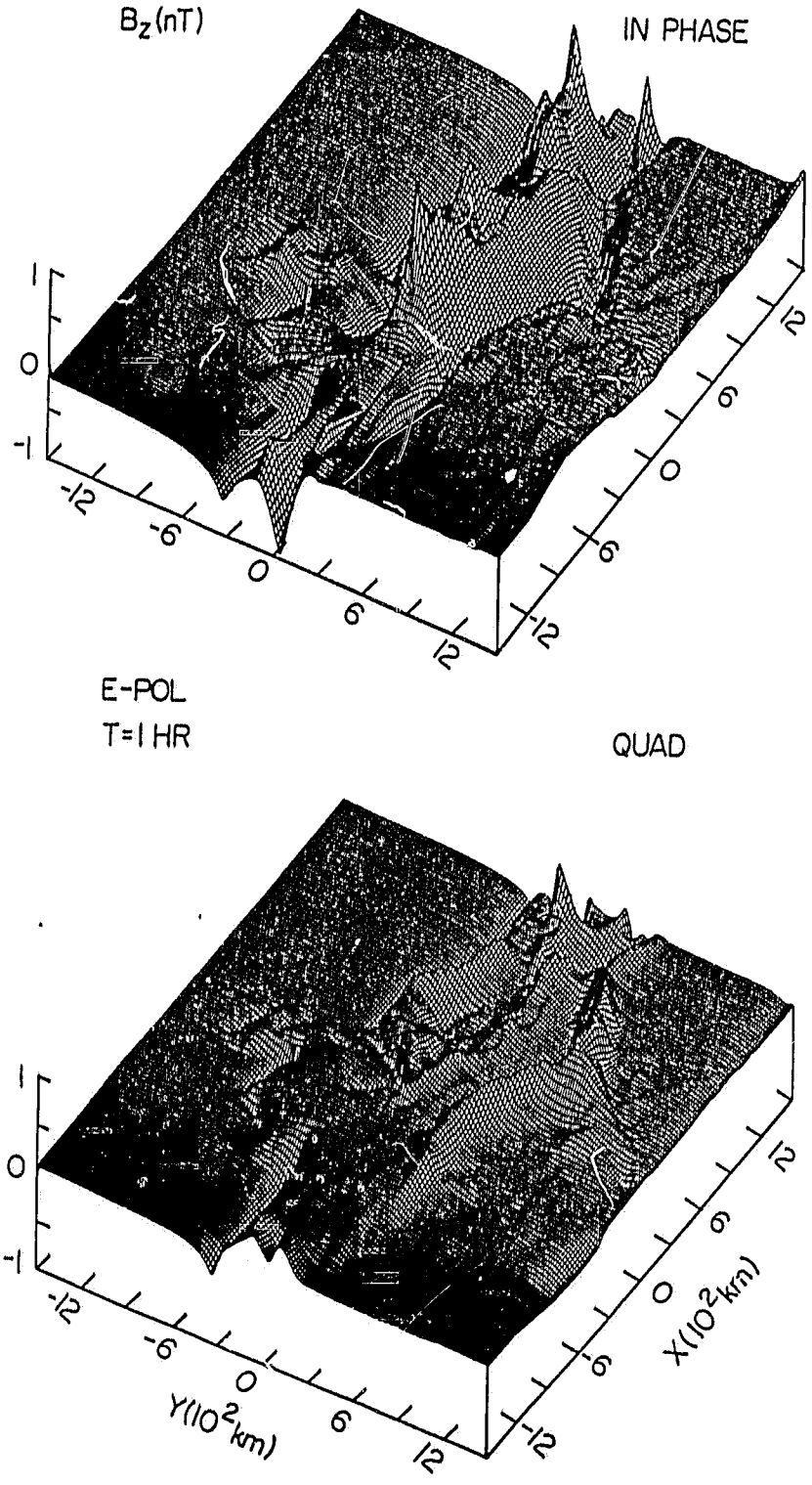

Figure 4.29: Three dimensional view of B_z for E-polarization at 60 min.

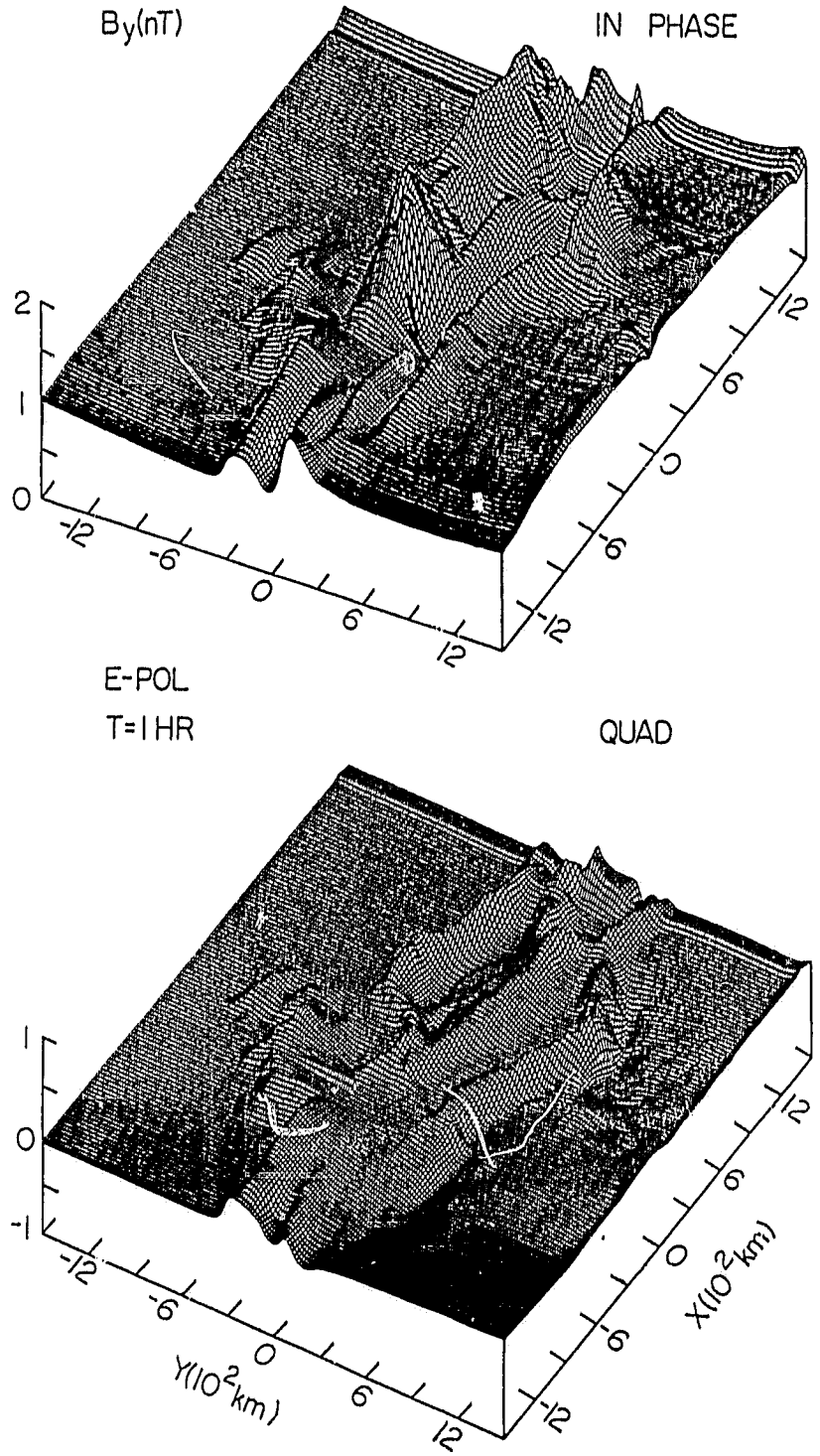

Figure 4.30: Three dimensional view of B_y for E-polarization at 60 min.

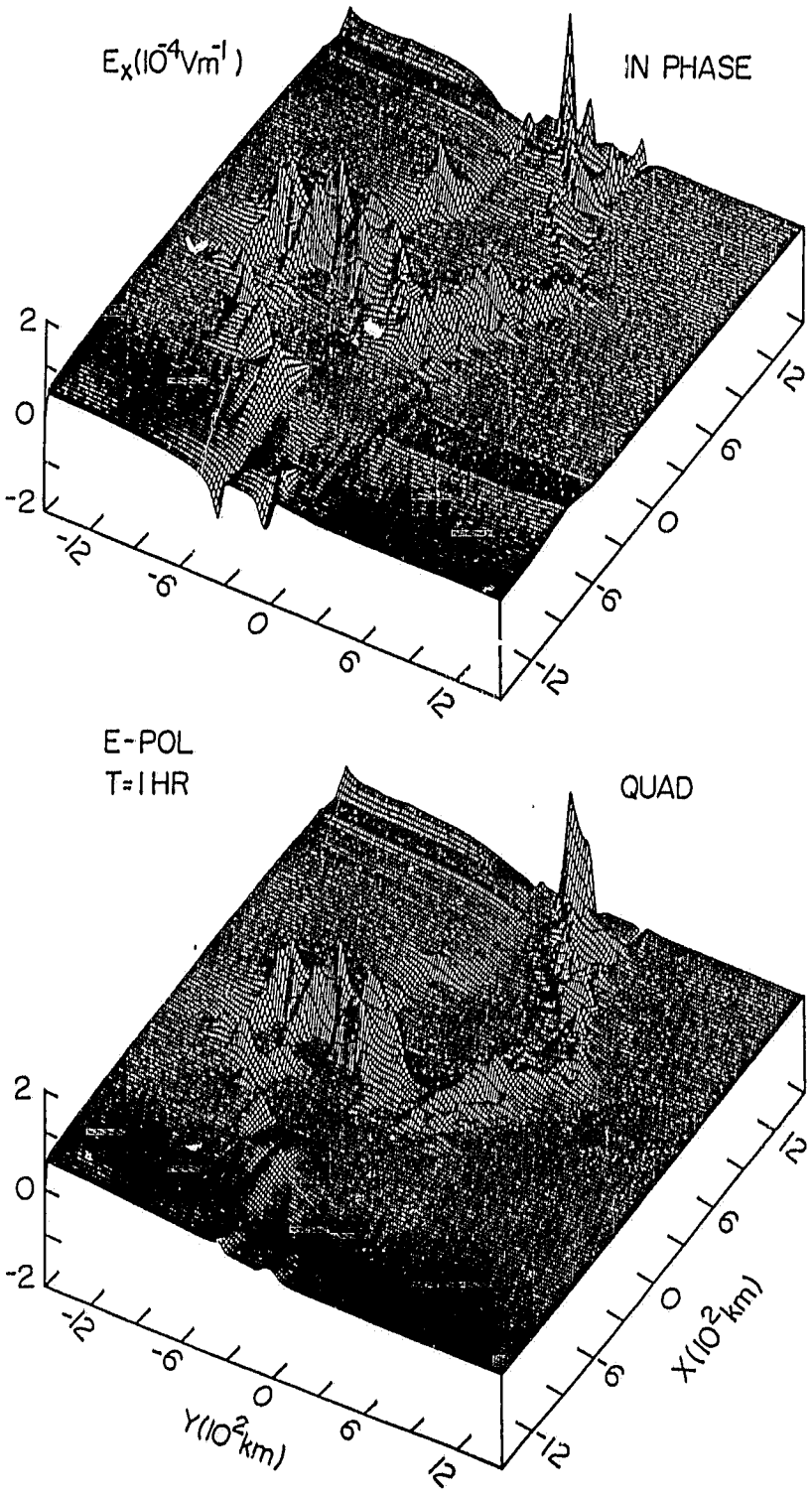

Figure 4.31: Three dimensional view of E_x for E-polarization at 60 min.

contrast, the responses of B_z over the Bohai bay area are much smaller, due to the relatively shallow ocean there and the bay effect.

Fig. 4.30 provides a 3D view of B_y for 60 min for E-polarization. B_y usually shows enhancements where induced current density is enhanced. Thus the large in-phase B_y along the U.S.S.R.-China coastline, the east coast of Japan, and the Korea-Japan strait once again are due to current concentrations there. The three dimensional view of E_x for 60 min for E-polarization is given in Fig. 4.31. Large negative enhancements are seen over the entire U.S.S.R.-China coastline and the east coast of Japan for both in-phase and quadrature components. E_x shows particularly large anomalies at the La Perouse and Korea-Japan straits, indicating the presence of current concentration there.

4.3.4 Three Dimensional Views of field components for B-polarization

The three dimensional views of in-phase and quadrature B_z, B_x, and E_y are shown in Figs. 4.32, 4.33, and 4.34 respectively for B-polarization for 60 min period. The three dimensional views of B_y and E_x for the B-polarization are given in the Appendix B. It is seen from Fig. 4.32 that in-phase B_z shows a positive response at the Liaodong peninsula and a negative response at the Shandong peninsula, indicating the effect of current deflection around the tips of the peninsulas and current channelling through the Bohai bay strait. Similarly, large anomalous B_z occurs at Tsugaru strait in response to such current concentration. In Fig. 4.33 both in-phase and quadrature B_x show very small anomalies at the continental coastline as well as at the Japan coast, while for the case of E-polarization, the responses are very prominent. It is observed that anomalies at the coastline are large where current is deflected by coastlines. In-phase B_x shows large responses

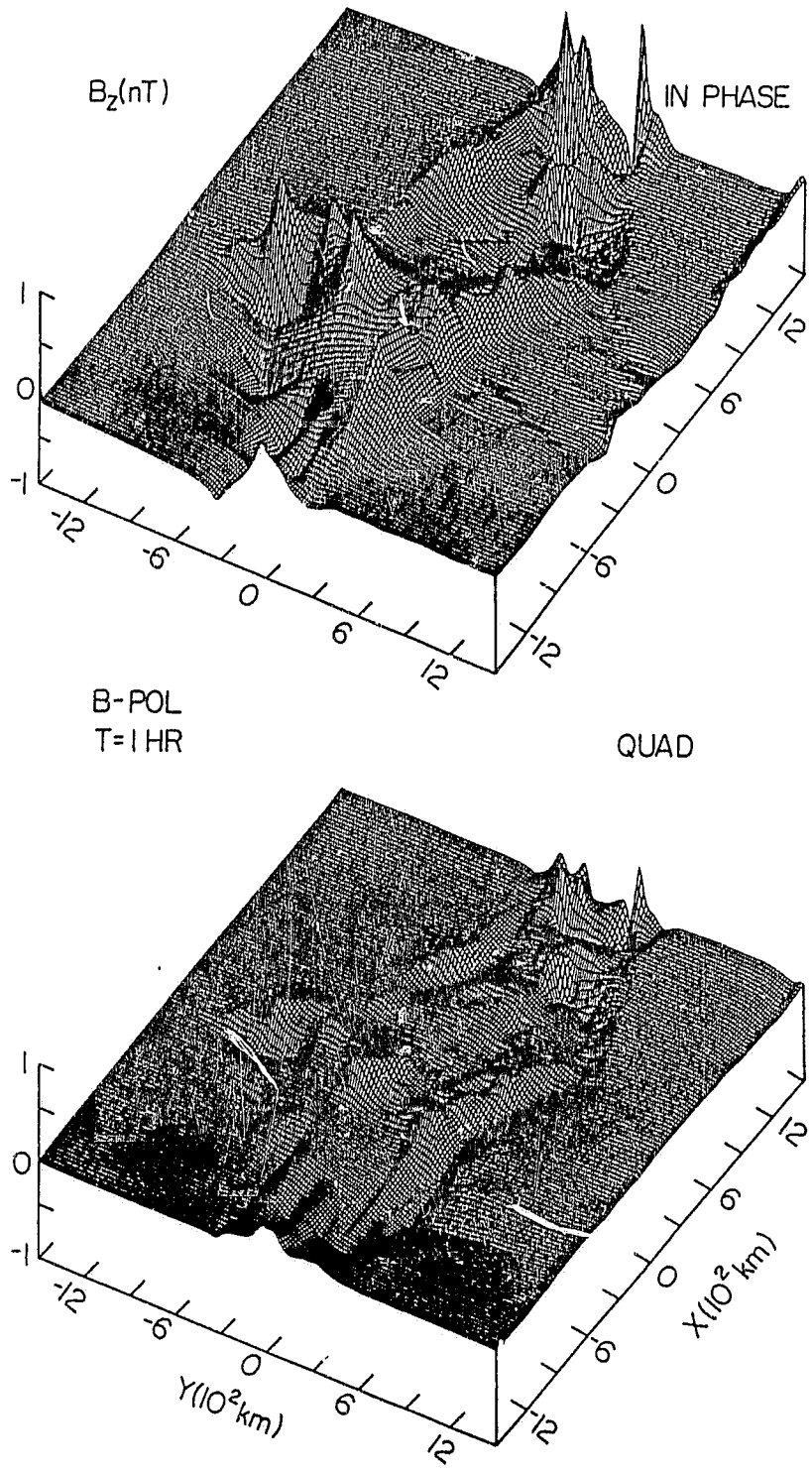

Figure 4.32: Three dimensional view of B_z for B-polarization at 60 min.

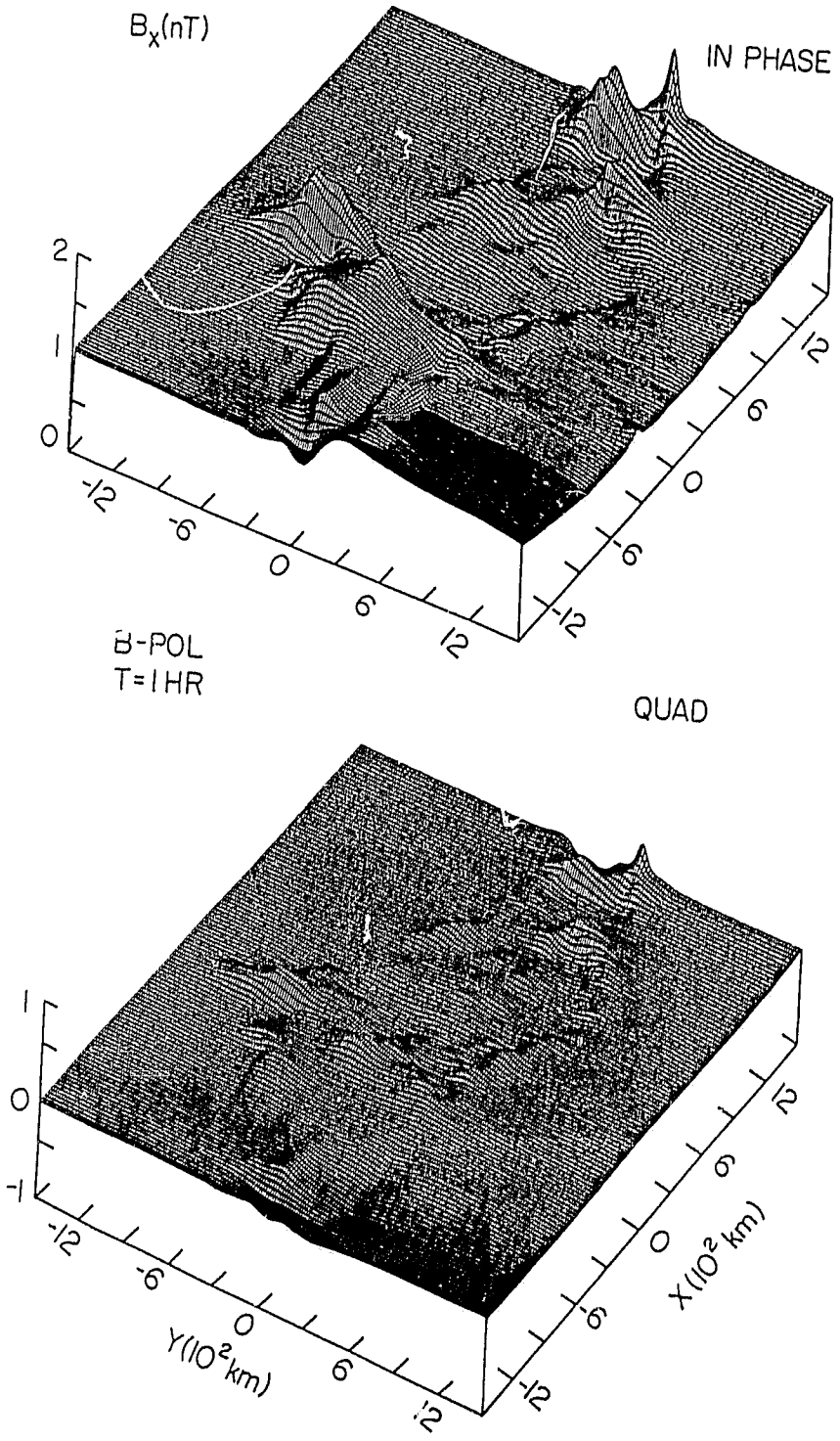

Figure 4.33: Three dimensional view of B_x for B-polarization at 60 min.

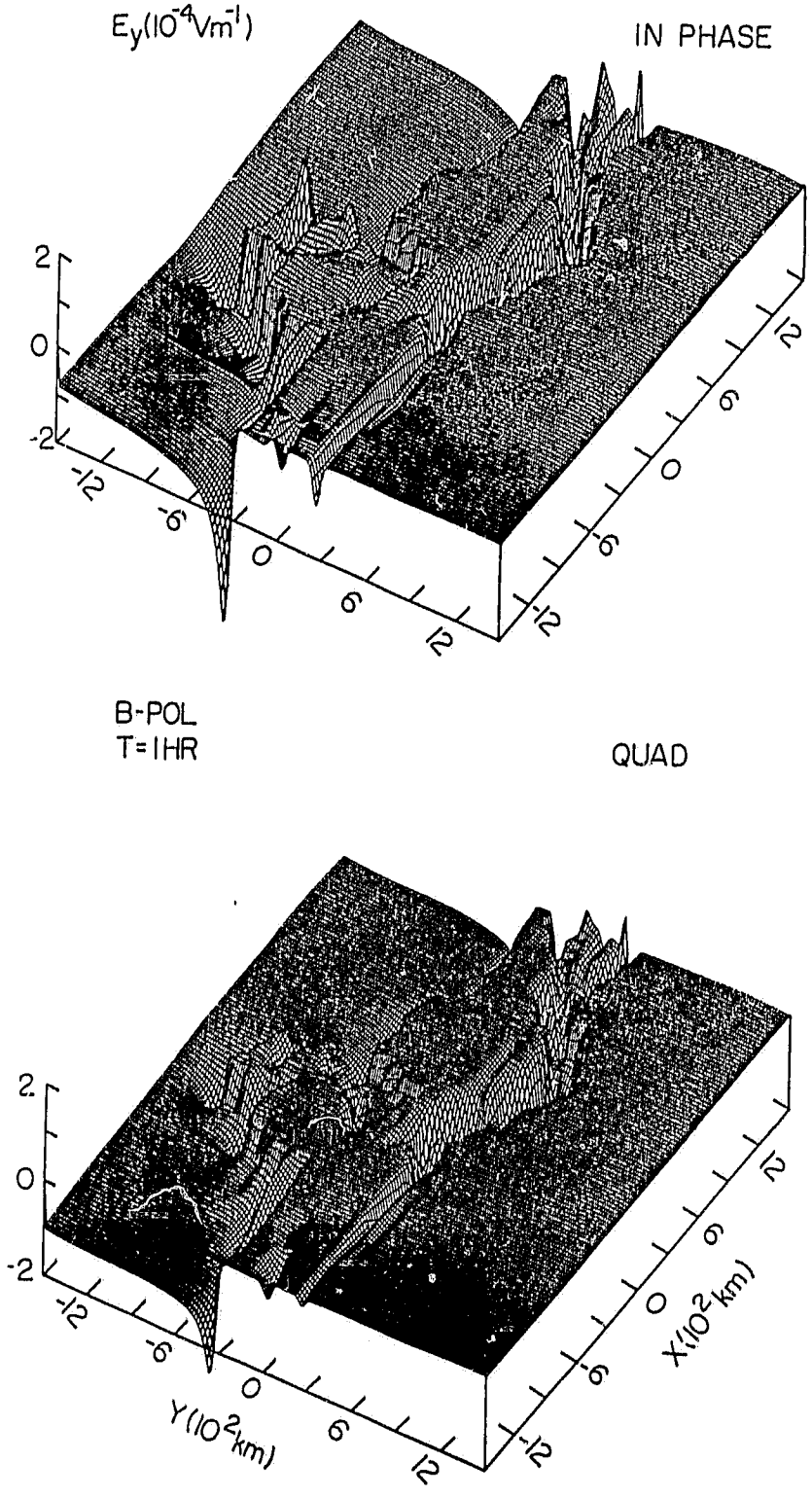

Figure 4.34: Three dimensional view of E_y for B-polarization at 60 min.

over the Liaodong and Shandong peninsulas and the La Perouse and Tsugaru straits which are consistent with the results of B_z for this polarization. Figure 4.34 shows the 3D view of E_y. Unlike the E_x responses for E-polarization, both the in-phase and quadrature E_y show a trench-like shape along the continental coastline, while E_x has positive response over the coast for E-polarization. As expected for B-polarization, E_y is small over the conductive ocean and large, but negative, over land.

4.4 Induction Arrows

In order to delineate the ocean effects and thus to aid in the interpretation of field site measurements on the Japan island arc region, induction arrows over the entire model area are examined. The responses for periods of 15, 60 and 120 min are selected since most of the available field measurements are in this range. (The method used to calculate induction arrows was discussed in chapter 1).

Figure 4.35 shows both the in-phase and quadrature induction arrows at 15 min for T1 to T8. It is seen that the in-phase arrows have substantial lengths and point seaward at the locations where current concentrations due to current deflection occur; for example, at tip of the Korean peninsula, the convex shaped east coastline of Japan, and the Korea-Japan strait. In contrast, the quadrature arrows at this short period tend to point away from the deep ocean everywhere, and are of much smaller magnitude. This agrees with the result of previous analogue and numerical studies, that although the in-phase arrow points towards current concentrations, the quadrature arrow at very short periods tends to point away from the current concentrations. At 60 min (Fig. 4.36), the in-phase induction arrows

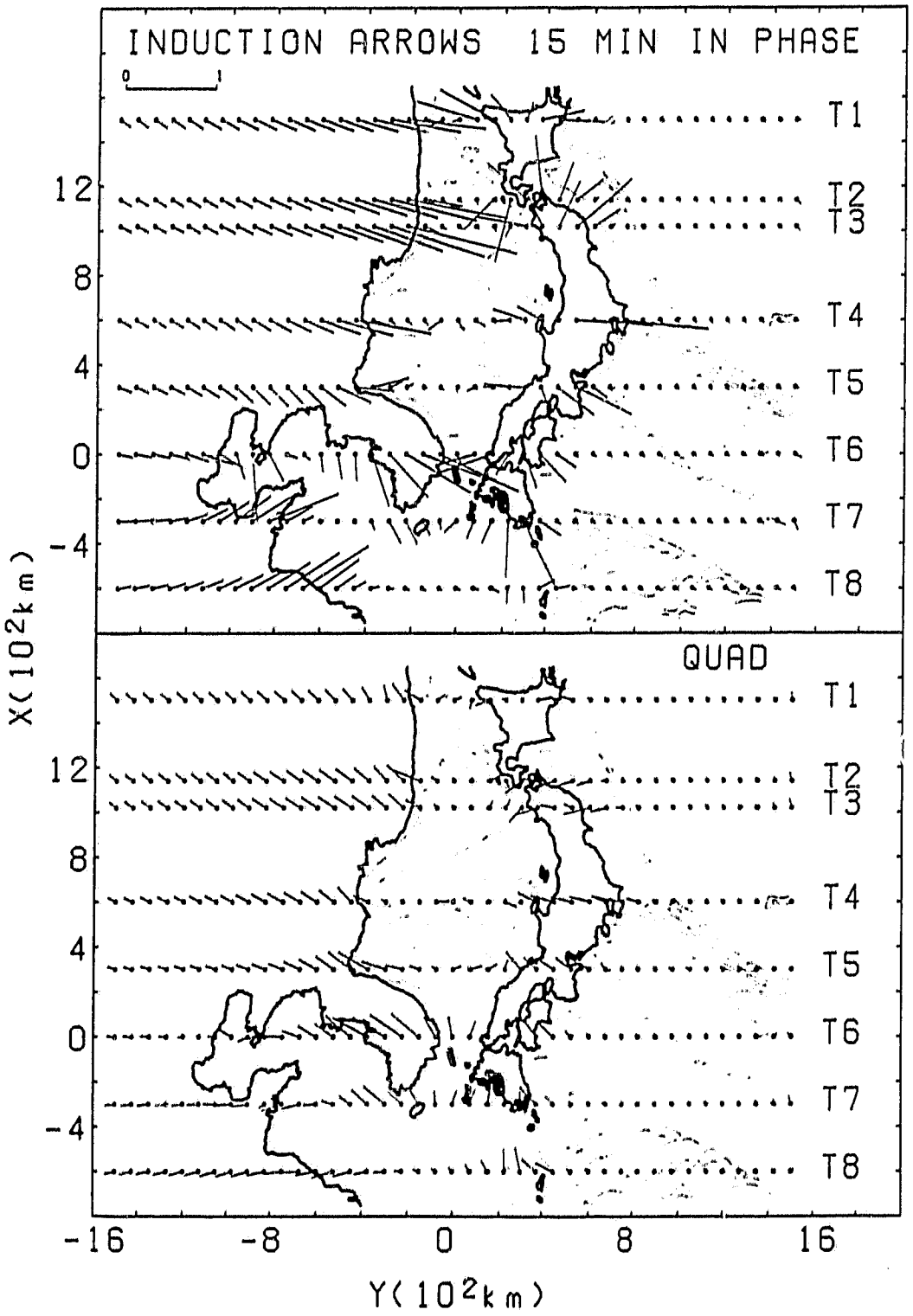

Figure 4.35: In-phase and quadrature induction arrows along traverse T_1 to T_8 at 15 min.

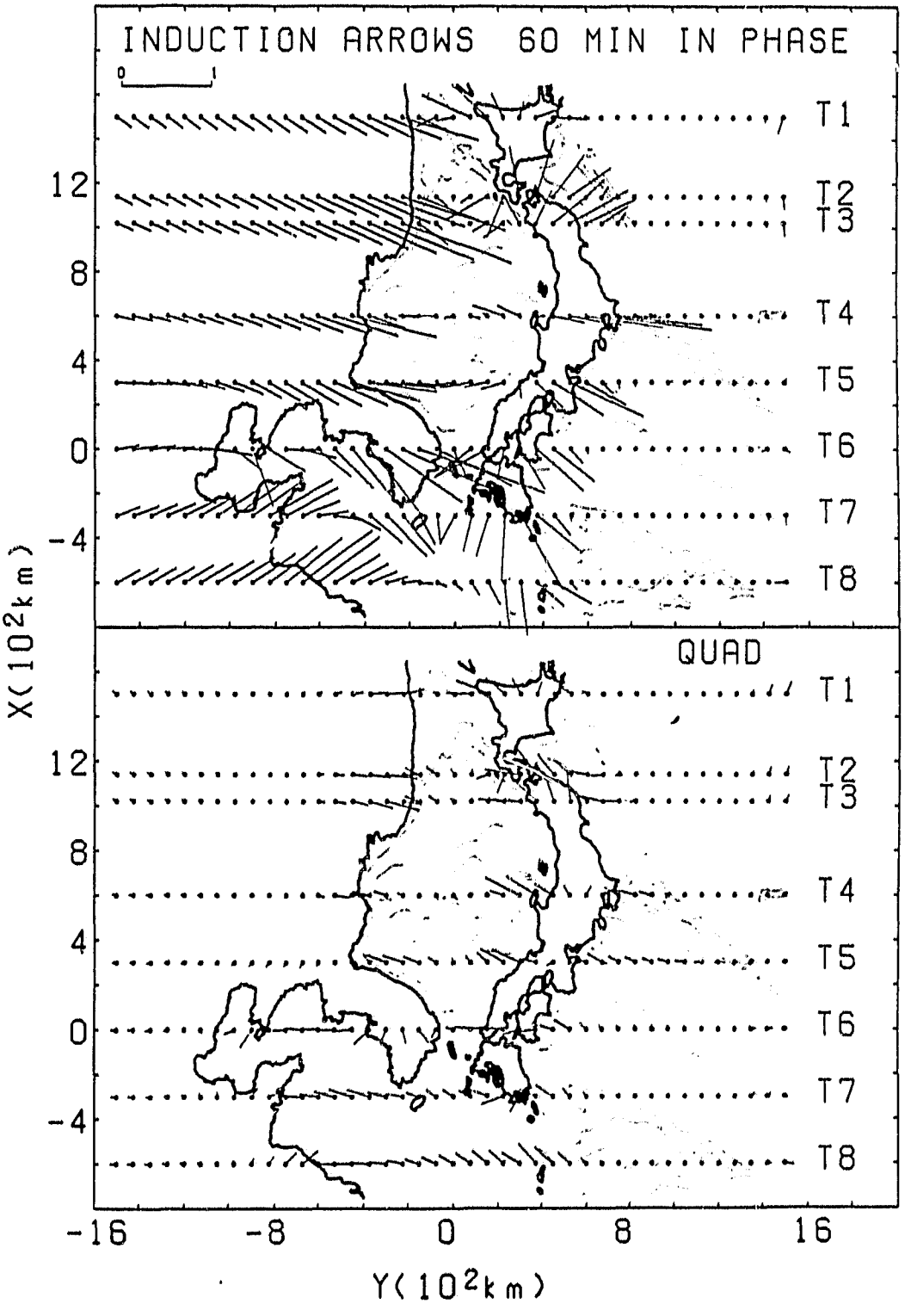

Figure 4.36: In-phase and quadrature induction arrows along traverse T_1 to T_8 at 60 min.

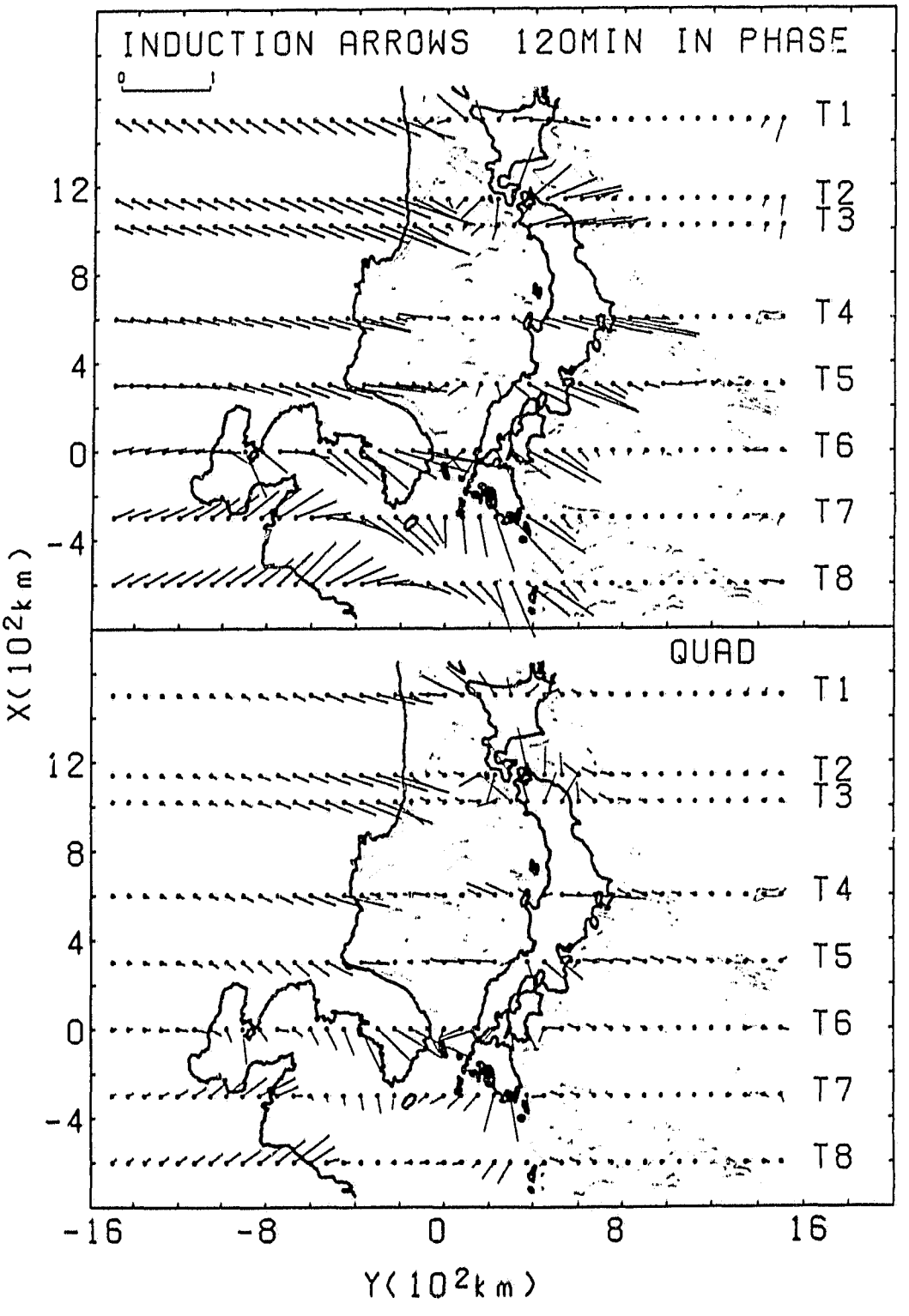

Figure 4.37: In-phase and quadrature induction arrows along traverse T_1 to T_8 at 120 min.

are slightly increased in length while the quadrature arrows have reversed direction and now point towards the current concentration. It is rather interesting to note that the quadrature arrows along the U.S.S.R.-China coastline point seaward to the local Japan Sea while the quadrature arrows along the east coast of Japan still point landward, which provides evidenc that the rotation of the quadrature arrow is characteristic of ocean depth (Agarwarl and Dosso 1990). As the period increases to 120 min (Fig. 4.37), the in-phase arrows over the coastlines of the Asian continent and the Japan islands are generally reduced while the quadrature arrows are continually enhanced, which fully agrees with the results shown earlier (sections 4.1.2 and 4.2.2) that for both E- and B- polarizations the in-phase component reaches a maximum at 60 while the quadrature component reaches a maximum at a longer period. The quadrature arrows at 120 min over the coastlines generally point seaward and roughly parallel to the direction of the in-phase arrows. It should be noted that the magnitude of the in-phase induction arrows along the east coast of Japan are much larger than those along the west coast of Japan for all periods. This is partly due to the convex and concave shapes (east and west coasts respectively) of the Japan island arc, and partly due to the Pacific Ocean being much larger and deeper than the local Japan Sea. The in-phase arrows over the ocean are generally small at the short period of 15 min, as expected. As the period increases, they are enhanced in length and tend to delineate the effect of ocean bathymetry. This certainly is seen for the induction arrows at the local Japan Sea. Along much of the Pacific Trench, it is found that the in-phase arrows are large at 120 min at distances of 200 to 300 km off the east coast of Japan, in response to the current concentration at depth, while they

are minimal for the short period of 15 min. Since no deep conductive structure is included in the present analogue model, the induction arrows presented here only delineate the ocean effect.

4.5 The Chapter Summary

In this chapter, the behaviour of the electromagnetic field components in the coastal region of Japan-Korea-China is studied. The laboratory analogue model includes a simulation of the known ocean bathymetry, the complex coastlines and the deep Pacific trench. Model measurements of the electromagnetic field components are carried out for simulated periods of 15-180 min for two mutually perpendicular polarizations (E- and B- polarization) of a uniform horizontal inducing source field. In-phase and quadrature B_x, B_y, B_z, E_x and E_y model measurements are examined in detail for a series of traverses over Japan, the Korean peninsula, and the coastal regions of China and the U.S.S.R. Large anomalous in-phase model magnetic fields are observed over the Korea-Japan strait for E-polarization and over Bohai strait, Tsugaru strait, and La Perouse strait for B-polarization due to current channelling. The significant responses observed at short periods over the peninsulas in the shallow coastal areas decrease with increasing period. Large gradients in the in-phase B_z field are observed over Japan for E-polarization for both short and long periods due to the effects of induced currents in the surrounding oceans. Thus induction arrow responses over all regions of Japan show the dominant effects of the ocean.

Chapter V

OCEAN-ANOMALOUS CONDUCTOR ELECTROMAGNETIC COUPLING

5.1 Introduction

As discussed in Chapter 1, induction arrows, characterizing induced current concentrations, are useful indicators of electrical conductivity structure within the earth. In coastal regions, however, the coast effect component, due to induction in the conductive ocean and sediments, will tend to mask an induction arrow component associated with a local anomalous conductor. Through the years, numerous simplified 2D numerical models, and recently, thin sheet 3D models (e.g. Weaver and Agarwal, 1989) have been studied with the view to delineate the coast effect. As well, laboratory analogue model studies (referred to in Chapter 1) have been carried out for a number of complex coastal regions of the world.

The motivation for the present coastal region EM induction study is to delineate the coast effect, and attempt to remove this component from the observed response at a given field site. If the coast effect component can be successfully removed, then the residue should be characteristic of any local subsurface anomalous conductor. Perhaps the simplest approach to removing the coast effect component, would be to vectorially subtract the coast effect induction arrow from the field site induction arrow, to yield a difference arrow, which is the induction arrow of the anomalous conductor alone.

As has been discussed in Chapter 1, the induction arrow (Eq. 1.3) is defined as

$$V = (-a, -b), \tag{5.1}$$

where a and b are transfer functions given by the relationship

$$B_z = aB_x + bB_y \tag{5.2}$$

between the vertical magnetic field B_z and two horizontal magnetic field components B_x and B_y. The transfer functions a and b are generally complex and frequency dependent, and thus, can be written as

$$a =(a_r + ia_i) \text{ and } b =(b_r + ib_i), \tag{5.3}$$

where r and i denote the real and imaginary (quadrature) parts. According to Eq. (5.1) the in-phase and quadrature induction arrows respectively are

$$V_r = (-a_r, -b_r) \text{ and } V_i = (-a_i, -b_i). \tag{5.4}$$

If the induction arrow for a given model consisting of an ocean and an anomalous conductor embedded in the host earth (say model 1) is

$$V_1 = V_{1r} + iV_{1i}, \tag{5.5}$$

and the induction arrow for a model not including the anomalous conductor (say model 2) is

$$V_2 = V_{2r} + iV_{2i}, \tag{5.6}$$

then the difference arrow obtained by vectorially subtracting V_2 from V_1 is

$$V_1-V_2=(V_{1r}-V_{2r}) + i(V_{1i}-V_{2i}). \tag{5.7}$$

Such a subtraction to remove the coast effect has been attempted with the aid of laboratory analogue model measurements for field sites in Newfoundland (Hebert et al., 1985), the Bohai Bay region of China (Meng et al., 1990), and several sites in Japan (Meng and Dosso, 1990). Difference arrows, thus determined,

neglect the inductive coupling between insulated conductors, which may be significant as has been emphasized by Price (1964) and Rikitake (1966). With the aid of numerical models of two-dimensional idealized conductors, Wolf (1983) investigated the mutual coupling effect for what he termed the additive case in which the anomalous conductor was located some distance from the ocean and underlain by a conductive layer, and the coupled case in which the anomalous conductor was overlain by the ocean and underlain by a conductive layer. His results indicate that simple subtraction for the additive case may be promising if the separation distance of the anomalous conductor and the ocean were sufficiently large, but that for the coupled case, strong mutual induction effects would lead to erroneous interpretation. Weaver and Agarwal (1990) employed a thin sheet numerical model to study electromagnetic induction in a rectangular surface anomaly near a coastline, and concluded that in certain regions the induction arrow is not simply the resultant of the component for the coast effect and the component for the anomalous conductor individually, unless the ocean-anomalous conductor separation distance is sufficiently large so as to have negligible coupling through mutual induction and the redistribution of the charge accumulations on their boundaries.

It is of interest to examine the constraints on ocean-anomalous conductor separation distances (for simplified subsurface anomalous conductors in the form of an upwelling or a depression in a typical upper asthenospheric conductive substratum) as a function of period, required to ensure sufficiently weak coupling that would permit (to within a given accuracy) simple subtraction of the coast effect from the observed field site induction arrows. In the present chapter 2D numerical models of EM induction for simplified anomalous conductors in the form of an

upwelling and a depression in a conductive substratum at depth in a resistive earth near continental and island coastlines are studied with the intent of determining approximate separation distances for minimal inductive coupling effects. In the next two chapters, induction arrows for a 3D laboratory analogue model will be used to subtract the coast effect from observed induction arrows for continental coastal sites in China and island sites in Japan.

5.2 2D Models Of The Coast Effect Magnetic Field Response Range

In these simplified models, the conductivities of the resistive host and ocean are taken to be $\sigma_o = 6.3 \times 10^{-4}$ Sm^{-1} and $\sigma_1 = 3.6$ Sm^{-1} respectively. For uniform horizontal inducing electromagnetic fields, the induction arrows associated with the anomalous conductor and the ocean will depend primarily on the induced vertical magnetic field (B_z) which is entirely anomalous. In the 2D numerical cases considered, the behavior of $|B_z/B_{yn}|$, where B_{yn} is the amplitude of the normal horizontal field taken to be 1 nT, as a function of distance from the coastline is studied using the numerical method of Brewit-Taylor and Weaver (1976) for E-polarization of a uniform inducing source field. Since for 2D ocean-land models the B_z response is maximum at the coastline, $|B_z/B_{yn}|$ will have a maximum at the coastline and decrease both seaward and landward. It will be demonstrated that if the coast effect response $|B_z/B_{yn}|$, at an anomalous conductor inland location has diminished to a value of 0.2, then removal of the coast effect by simple subtraction yields an acceptable approximation of the anomalous conductor

response alone. In the present work, this distance from the coast where the response $|B_z/B_{yn}| = 0.2$ is defined as the coast effect response range Y_R .

5.2.1 Continental Coast Effect Response Range

Figure 5.1 shows the coast effect field response $|B_z/B_{yn}|$ as a function of distance from the continental coast for a range of periods (5 min - 120 min) for a vertical interface ocean-land infinite depth model. The response range Y_R (already defined) for a given period is the value of Y for the intersection of the response curve for that period and the dashed line representing the 0.2 response value. As an example, Y_R shown in Fig. 5.1 for 120 min period is approximately 1650 km. For comparison $|B_z/B_y|$, where B_y is the horizontal field at each field point rather than the normal field B_{yn}, is shown for 120 min (dashed curve 5). It is seen that $|B_z/B_y| \simeq .25$ when $|B_z/B_{yn}| \simeq .2$. From the results of Fig. 5.1, it is clearly seen that Y_R increases rather uniformly with period as expected for this simplified ocean-land model, showing values of roughly 350 km and 1650 km for 5 min and 120 min periods respectively.

To demonstrate the effect of ocean depth, Fig. 5.2 shows the coast effect response for the case of a 1 km depth ocean, rather than the infinite depth ocean of Fig. 5.1. Again, the response range, taken to be the value of Y where $|B_z/B_{yn}| = .2$, increases smoothly with increasing period. The response range for 5 min (curve 1) is approximately the same in Figs. 5.1 and 5.2, but at 120 min the response range for the 1 km deep ocean is approximately 1200 km, while for the infinite depth case of Fig. 5.1, it is roughly 1650 km. As was the case in Fig. 5.1, $|B_z/B_y| \simeq .25$ (dashed curve 5 in Fig. 5.2) when $|B_z/B_{yn}| = .2$.

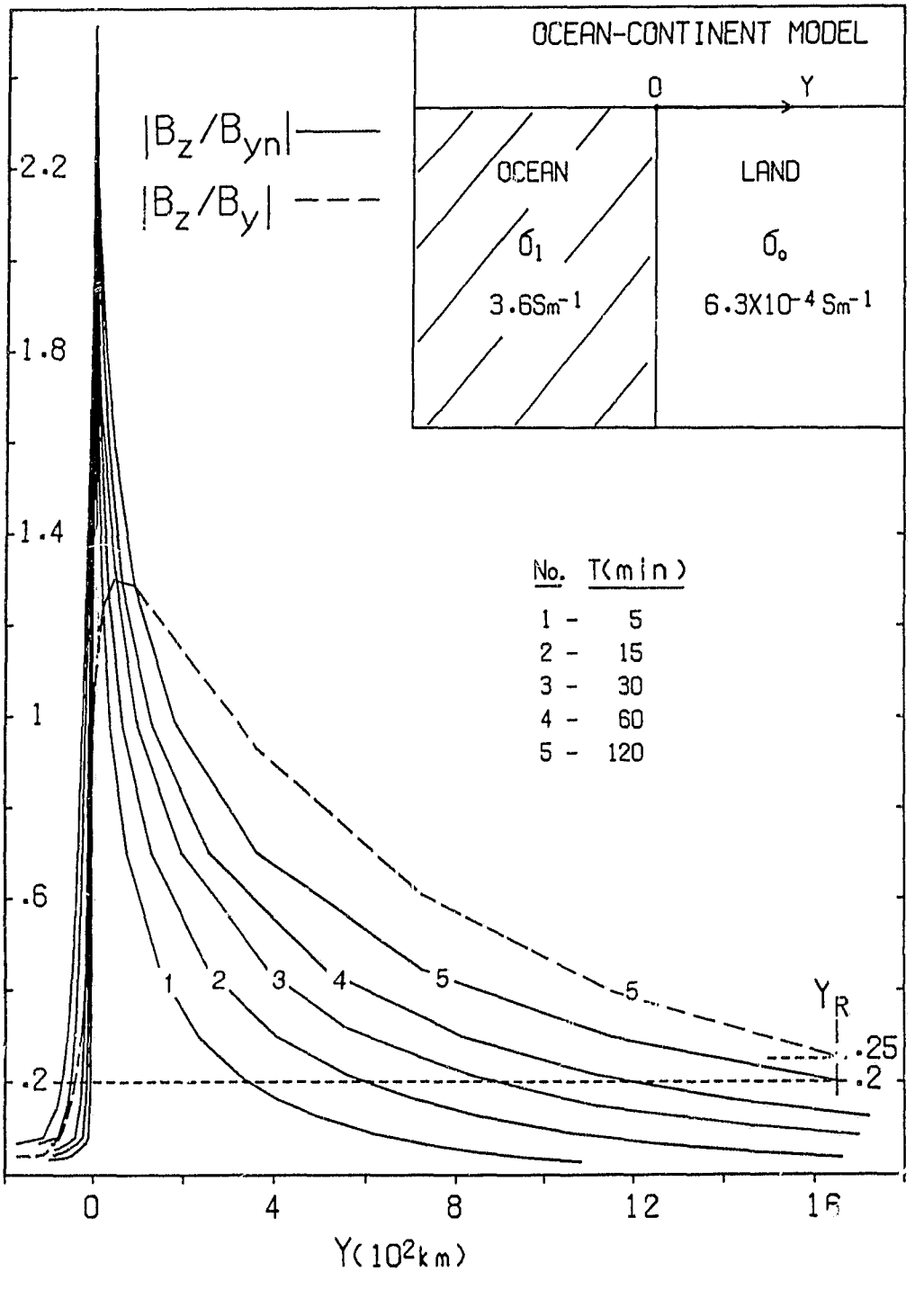

Figure 5.1: The continental coast effect magnetic field response $|B_z/B_{yn}|$ as a function of distance Y from a vertical ocean-land interface with infinite ocean depth.

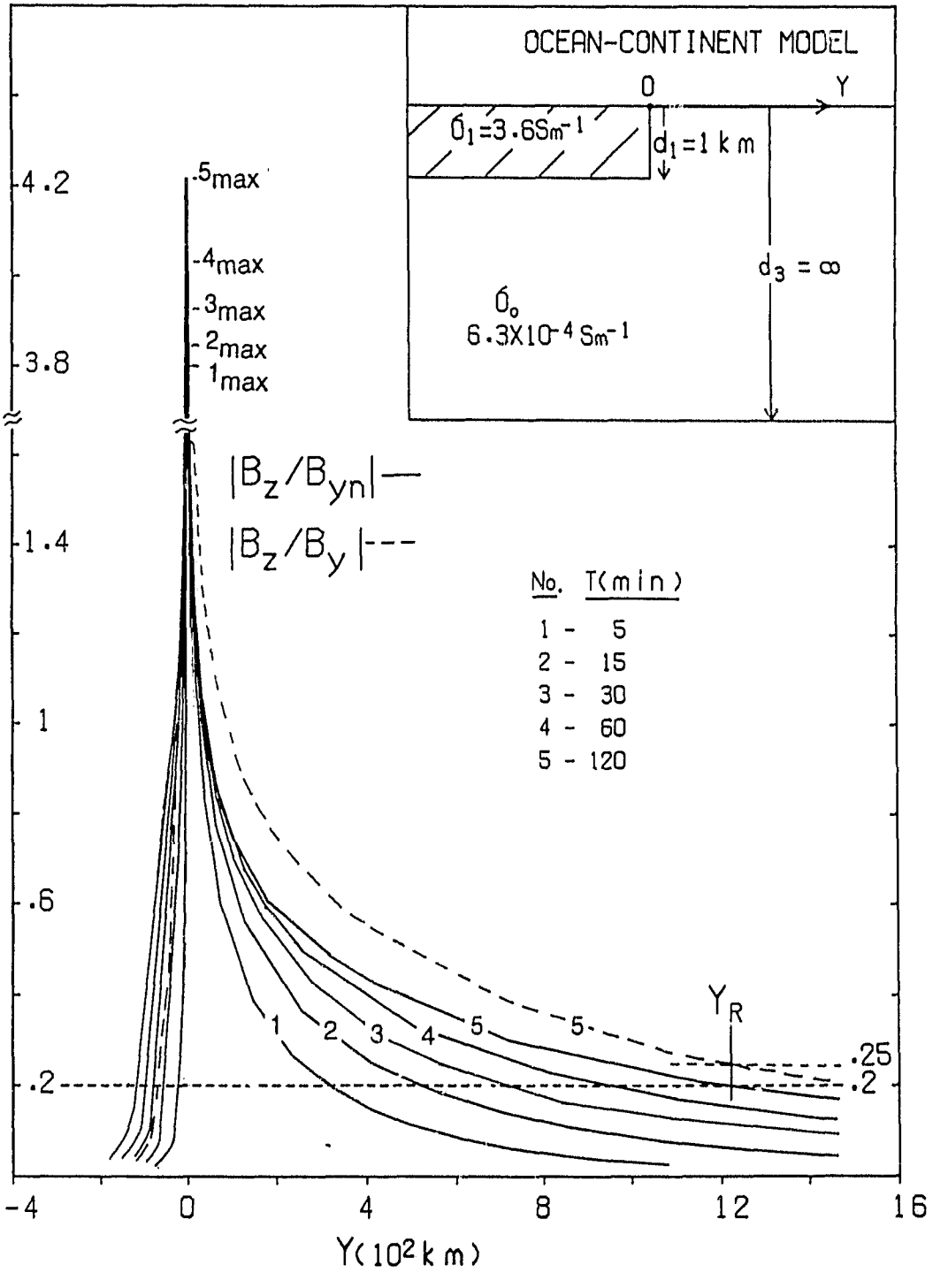

Figure 5.2: The continental coast effect magnetic field response $|B_z/B_{yn}|$ as a function of distance Y for a model with ocean depth d_1= 1 km.

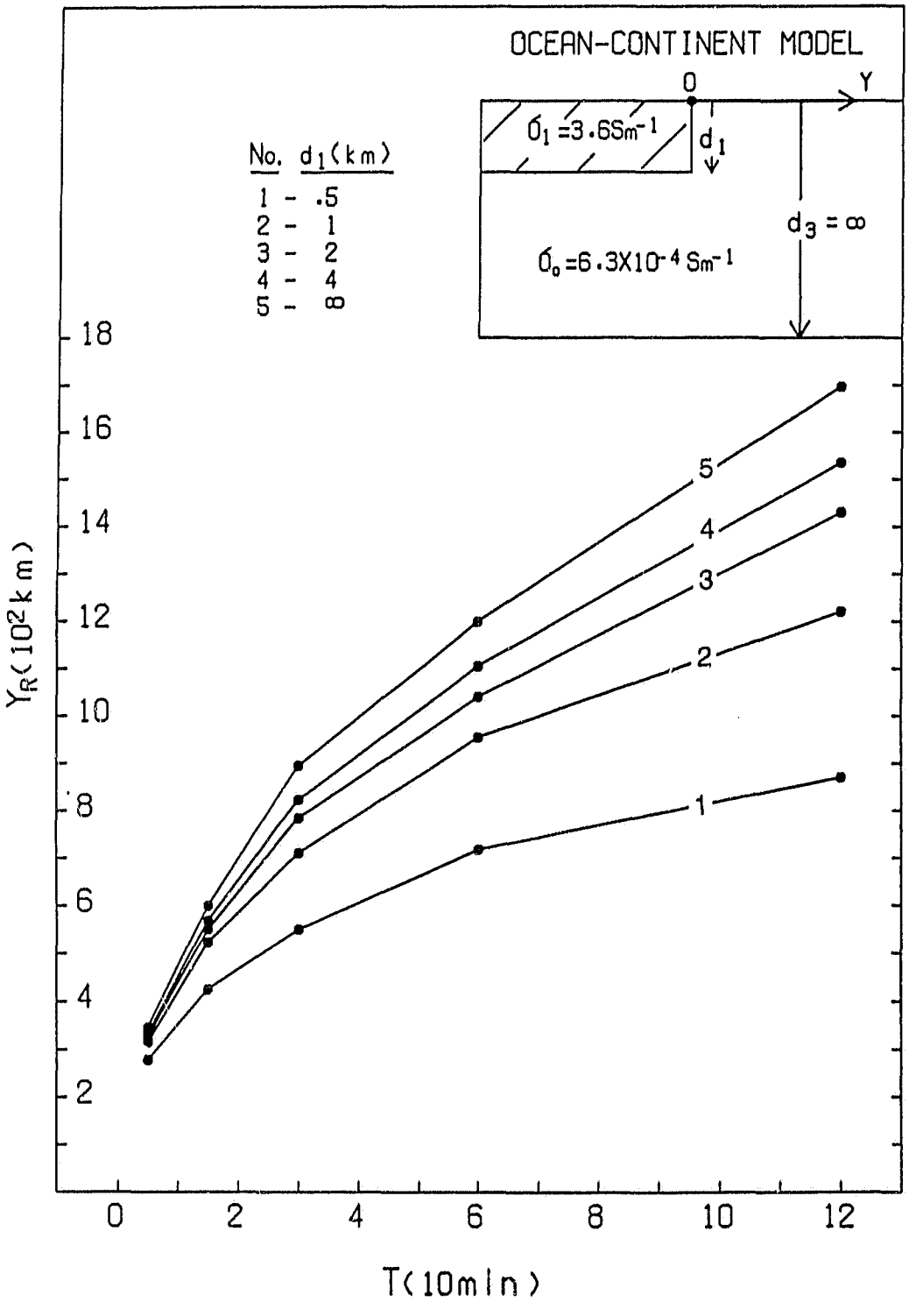

Figure 5.3: The continental coast response range Y_R as a function of period T for a range of ocean depths d_1 for an infinite depth resistive host.

Figure 5.3 examines in some detail the effect of the ocean depth (d_1) for the case of infinite depth (d_3) resistive host. The response range Y_R for each ocean depth model is seen to increase smoothly with increasing period. At 5 min period the response range is roughly 300 km for all ocean depths, while at 120 min the responses as a function of distance have diverged considerably, so that $Y_R \simeq 900$ km for the shallow ocean ($d_1 = .5$ km), and $Y_R \simeq 1700$ km for the infinite depth ocean (curve 5).

The coast effect response for a more realistic geophysical model, that includes a conductive asthenosphere substratum ($\sigma_3 = 0.1 Sm^{-1}$) at a depth of 100 km (d_3), is shown in Fig. 5.4. For this model the $|B_z/B_{yn}|$ responses, again having sharp maxima right at the coastline, show decreasing maximum values with increasing period, opposite to that observed for the infinite depth resistive host model of Fig. 5.2. A further very significant difference for the two models, is that the conductive substratum at 100 km (Fig. 5.4), which generally attenuates the coast effect, is seen to have the effect of decreasing the response range with increasing period, rather than the opposite as observed in Fig. 5.2. This opposite behaviour is expected, since the 1 km depth ocean is but a fraction of a skin depth for all periods (e.g., the skin depth ranges from 4.6 km at 5 min to 23 km at 120 min), and the infinitely thick conductive substratum at 100 km depth (shallow in terms of skin depth in the host σ_0) plays the increasingly dominant role in the response with increasing period, with the response becoming more that of a layered conductor than that of a coast effect. This leads to the response maxima at the coast, as well as the spatial responses of the coast effect, showing a monotonic decrease with increasing period. Perhaps, the most important result is that the

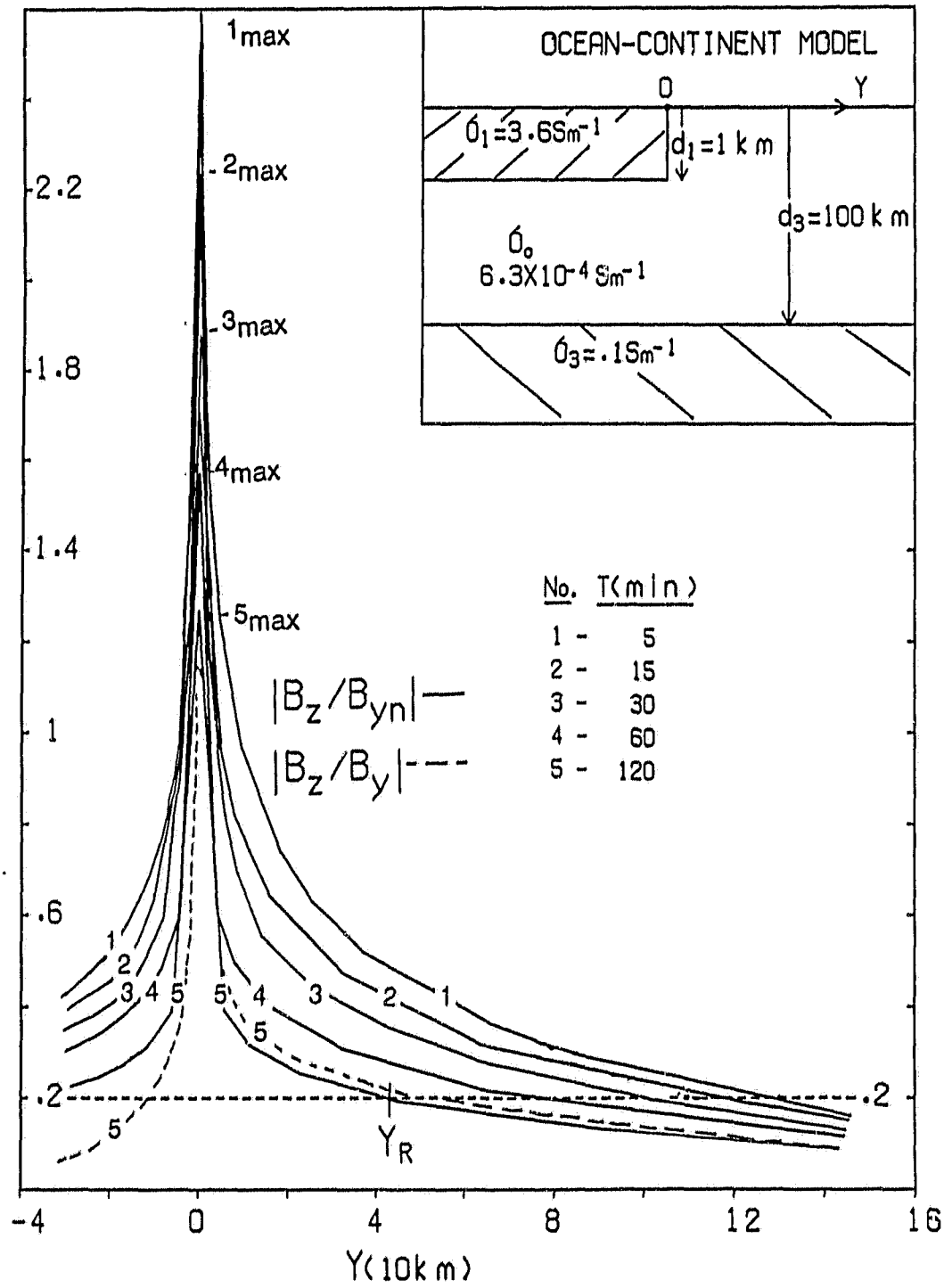

Figure 5.4: The continental coast effect magnetic field response $|B_z/B_{yn}|$ as a function of distance Y for a model with ocean depth d_1=1 km and conductive substratum depth d_3=100 km.

conductive substratum(σ_3 = 0.1 Sm^{-1}) has the effect of greatly localizing the response, so that the approximate response ranges Y_R now vary from 130 km at 5 min to 40 km at 120 min, as compared with 300 km at 5 min and 1200 km at 120 min, in the absence of the conductive substratum (Fig. 5.2). It is noted in Fig. 5.4 that landward, at 120 min, $|B_z/B_y|$ differs little from $|B_z/B_{yn}|$. It can be concluded that an underlying conductive substratum greatly reduces the range of the coastal response, and thus has the effect of reducing the separation distance required for minimal electromagnetic coupling between an ocean and an onshore anomalous conductor.

Figure 5.5 shows empirical curves of the response range Y_R as a function of period for a range of ocean depths (d_1) and conductive asthenosphere depths (d_3). For the shallow ocean models (d_1 = .5, 1 km), the response range decreases with increasing period over the entire range (5 min - 120 min) for all depths d_3, except for d_3 = 200 km for the d_1=1 km depth ocean, where Y_R shows a maximum at 15 min. The results for the 2 km depth ocean tend to show broad maxima in Y_R followed by gradually decreasing values with increasing period, while for the 4 km depth ocean the response range continues to show increases with increasing period at short periods, but becomes essentially constant for periods greater than 30 min. Thus, as the ocean depth increases, the general observation is that the response range increases for all periods. Further, as a function of increasing period, the behavior changes from sharply decreasing for shallow depths, to becoming constant for large ocean depths. In addition, the response range is seen to depend strongly on the conductive substratum depth (d_3), generally increasing markedly with increasing depth. The results of Fig. 5.5 should provide a useful guide as to

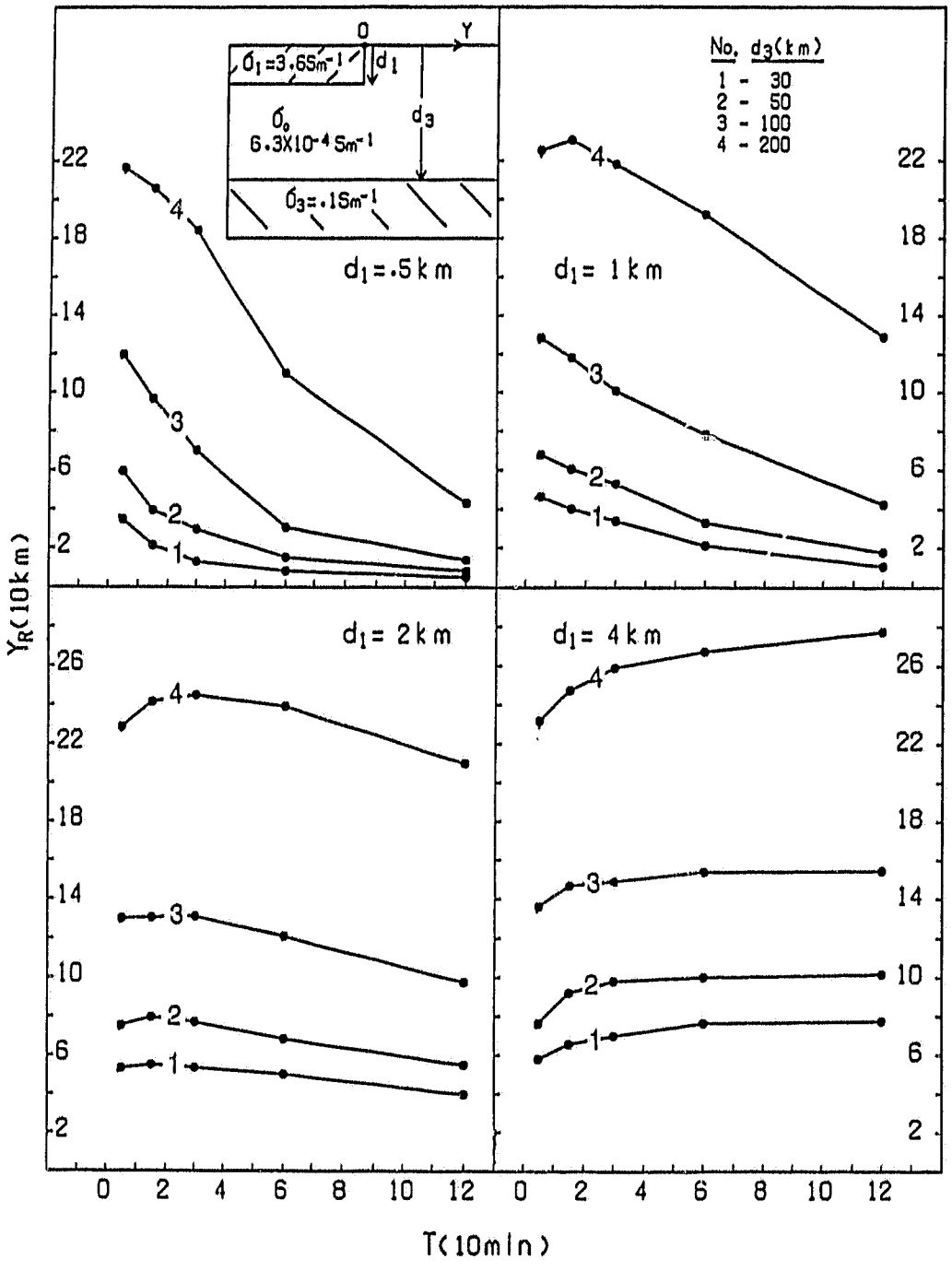

Figure 5.5: The response range Y_R as a function period T for a range of ocean depths d_1=.5, 1, 2, 4 km and d_3 = 30, 50, 100, 200 km.

the response range beyond which electromagnetic coupling of an ocean and an anomalous conductor in a continental coastal region should be small for the range of conductive asthenosphere depths expected to be encountered in the interpretation of field studies in the various regions of the earth.

5.2.2 Island Coast Effect Response Range

Figure 5.6 shows the coast effect field response $|B_z/B_{yn}|$ as a function of distance from the one of the island coastlines for a Y_i = 400 km width island for a range of periods (5 min - 120 min). The coast effect field response for the island model is found to decrease more rapidly with range than was observed for the continental model. It is also noted that the field response as a function of distance from the coast changes little with period, quite different from that observed for the ocean - continental model of Fig. 5.1. This should be expected, since for this simple 2D island model the induced vertical magnetic field must reverse sign at the midpoint of the island, and thus the amplitude response $|B_z/B_{yn}|$ must be zero at the midpoint (Y = 200 km). Further, due to this minimum value at the midpoint, the coast effect field response range Y_R should also be expected to decrease as the island width decreases. For this 400 km island width example, $|B_z/B_y|$ is seen to be less than 0.2 for the central 200 km region.

To demonstrate the effect of ocean depth, Fig. 5.7 shows the coast effect response for the case of a 1 km depth ocean, rather than the infinite depth ocean of Fig. 5.6. The response range Y_R, compared with that of Fig. 5.6, is slightly reduced (about 210 km), but again, does not depend on period very much. The coast effect response for a more realistic geophysical model, that includes a conductive asthenospheric substratum ($\sigma_3 = 0.1 Sm^{-1}$) at a depth of 100 km (d_3), is

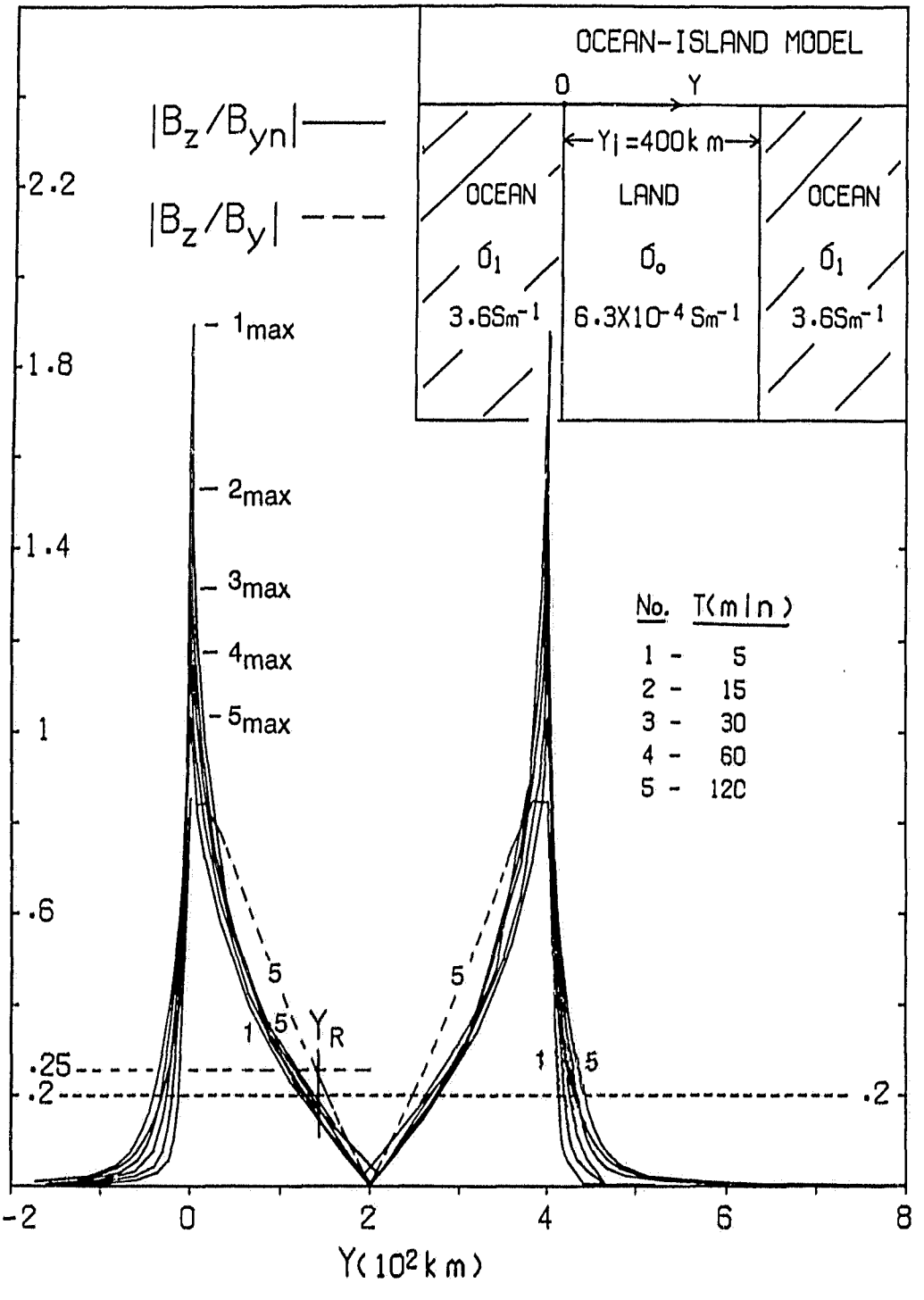

Figure 5.6: The island coast effect magnetic field response $|B_z/B_{yn}|$ as a function of distance Y from a vertical ocean-island interface.

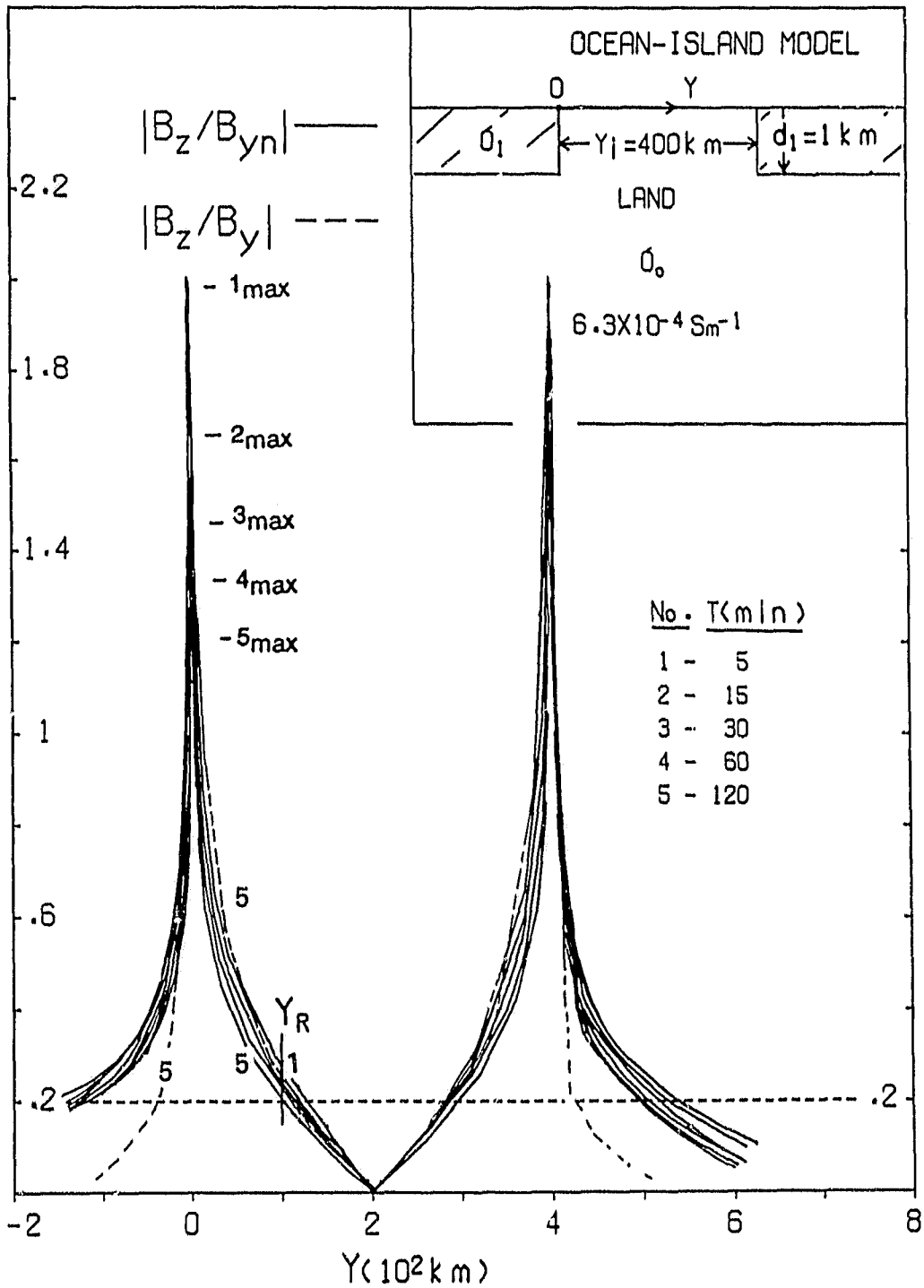

Figure 5.7: The island coast effect magnetic field response $|B_z/B_{yn}|$ as a function of distance Y for the ocean-island model with ocean depth d_1 = 1 km.

shown in Fig. 5.8. For this model the $|B_z/B_{yn}|$ responses show much reduced maxima at the coastline and thus, lead to smaller coast response range values.

The response range Y_R (as defined for the ocean-continent model in 2.1) as a function of period for island widths (Y_i = 100, 200, 300, 400, 500 km) and finite ocean depths (d_1 = .5, 1, 2, 4 km) for the case of infinite depth resistive host ($\sigma_o = 6.3 \times 10^{-4} Sm^{-1}$) is shown in Fig. 5.9. The response range Y_R is seen to decrease rather uniformly with decreasing island width for each ocean depth case. For example, at 60 min for d_1 = 2 km and Y_i = 300 km (curve 3 in the lower left of Fig. 5.9), Y_R = 80 km, while for Y_i = 200 km, the response range value is Y_R = 50 km. Similar changes in Y_R are seen for each of the other island widths. For these finite depth ocean models, the response range Y_R depends only weakly on period, except at the short periods, and particularly for the shallow ocean (d_1= .5, 1 km) models, where Y_R decreases significantly with increasing period. Further, the response range is seen to increase with increasing ocean depth. For example, at 60 min for Y_i = 300 km, Y_R = 65, 70, 80, 85 km for ocean depths d_1 = .5, 1, 2, 4 km respectively.

Figures 5.10 and 5.11 show the island coast effect response range as a function of period for the geophysically more realistic models of an underlying conductive asthenosphere ($\sigma_3 = 0.1 Sm^{-1}$) for a range of depths d_3 = 30, 50, 100, 200 km. The effect of adding the conductive substratum at depths d_3 = 30, 50 km and d_3 = 100, 200 km is examined in Figs. 5.10 and 5.11 respectively. A general observation is that the conductive substratum, which generally attenuates the coast effect, has the effect of greatly reducing the response range as compared with those observed in the absence of the conductive substratum (Fig. 5.9). As an example, at

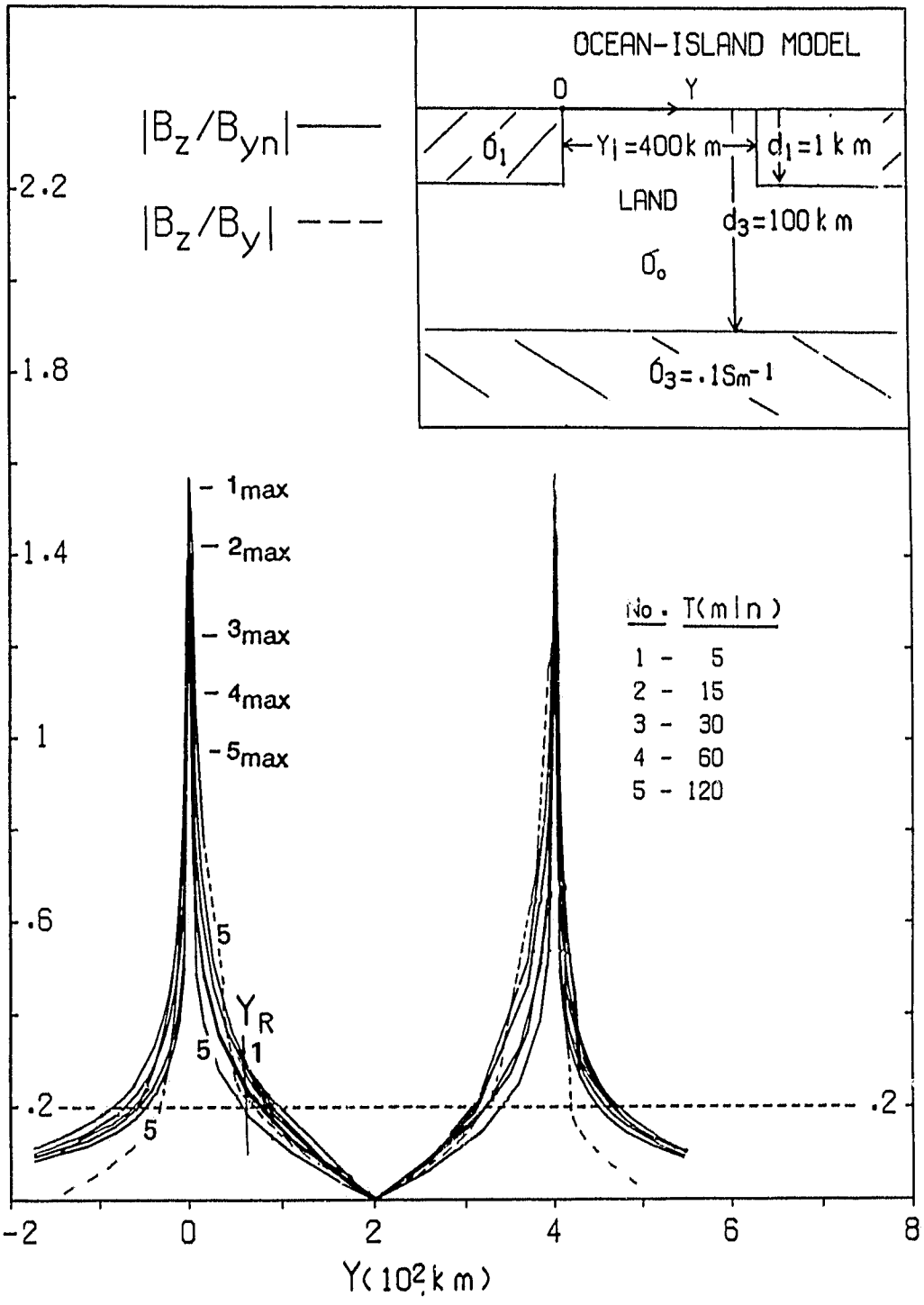

Figure 5.8: The island coast effect magnetic field response $|B_z/B_{yn}|$ as a function of distance Y for the ocean-island model with ocean depth d_1 = 1 km and conductive substratum d_3=100 km.

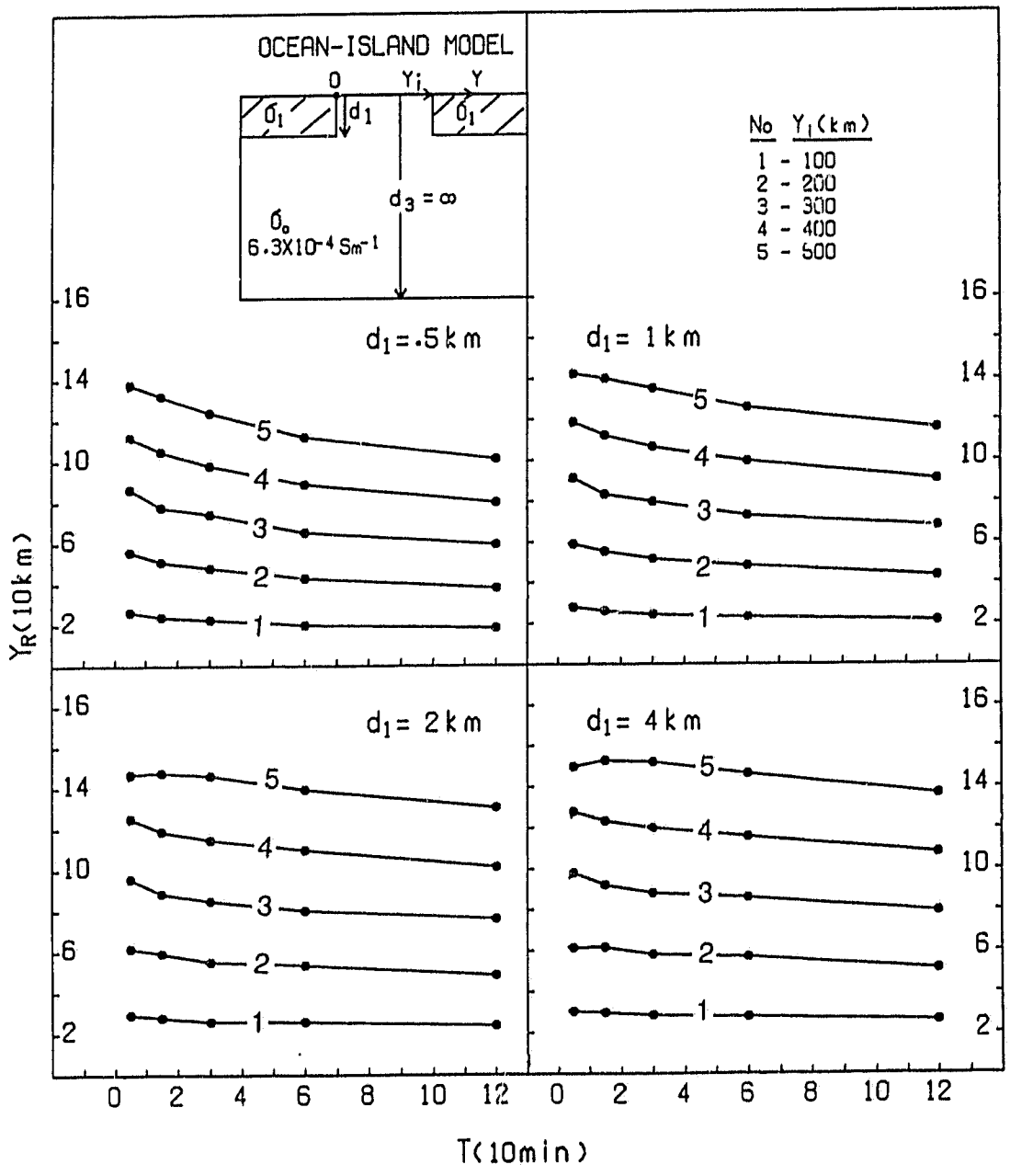

Figure 5.9: The response range Y_R as a function of period T for a range of island widths Y_i and ocean depths, for an infinite depth resistive host.

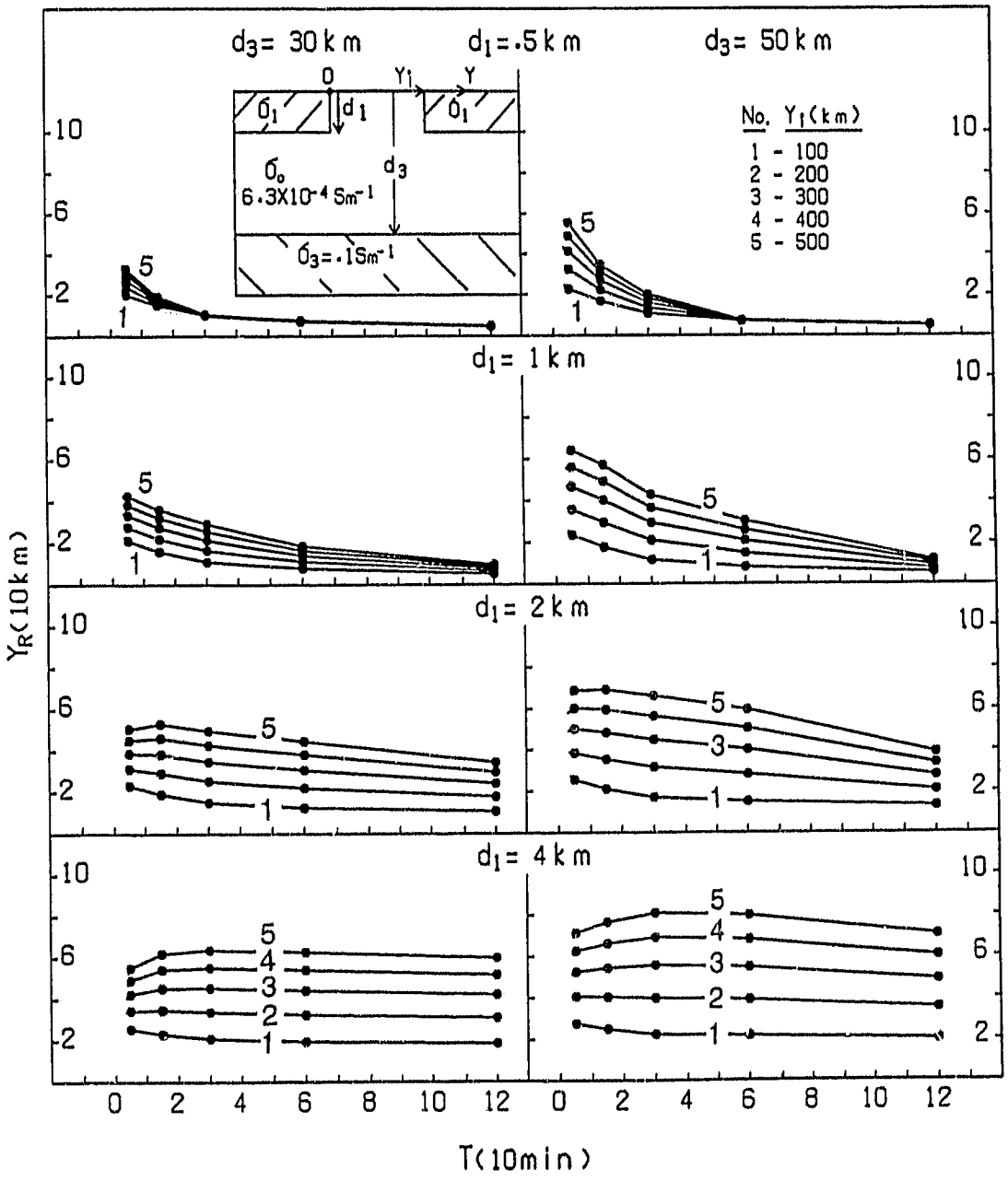

Figure 5.10: The response range Y_R as a function of period T for a range of island widths Y_i and ocean depths, for the conductive substratum depths d_3 = 30 km and 50 km.

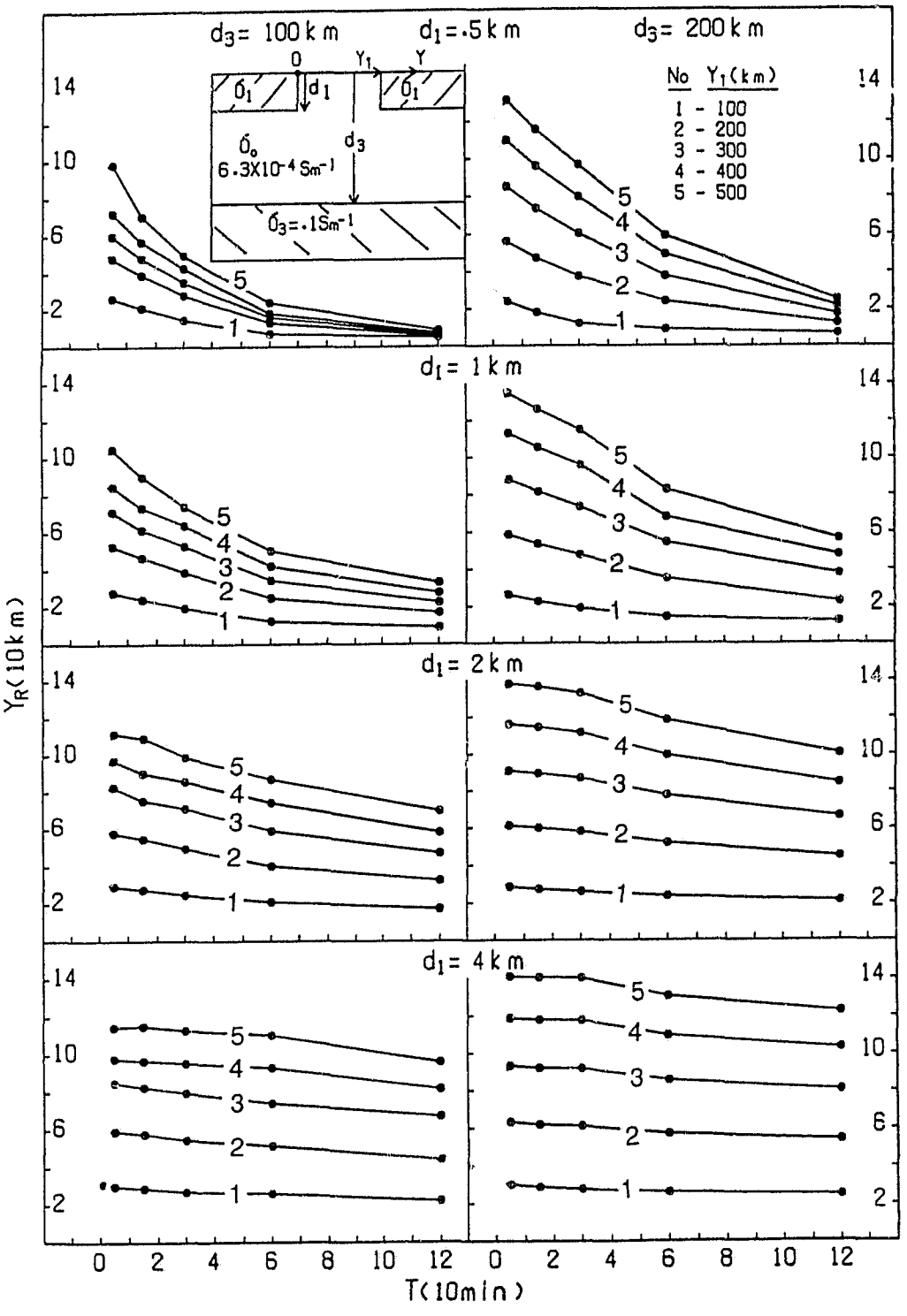

Figure 5.11: The response range Y_R as a function of period T for a range of island widths Y_i and ocean depths, for the conductive substratum depths d_3 = 100 km and 200 km.

60 min $Y_R \simeq 5$ km for the shallow ocean and shallow conductive substratum depths (d_3= 30, 50 km), as compared with $Y_R \simeq 20$ km (for Y_i=100 km) in Fig. 5.9. As the conductive substratum depth increases to d_3=200 km for the deep ocean case (d_1 = 4 km in the lower right of Fig. 5.11), the Y_R response curves approach those of Fig. 5.9 (lower right), as would be expected. It is seen in both Figs. 5.10 and 5.11, that for increasing ocean depth, the response curves show increasing dependence on ocean depth with increasing conductive substratum depth. For example, for Y_i=300 km and d_3 = 50 km (upper right in Fig. 5.10) Y_R = 5 km for d_1 = .5 km, while the response range increases to Y_R = 20, 30, and 50 km as the ocean depth increases to d_1 = 1, 2, 4 km respectively. Further, as the conductive substratum depth increases, the response range Y_R becomes more dependent on period, particularly at the longer periods for the shallow ocean cases, with Y_R decreasing sharply with increasing period. For example, for the d_3=50 km and Y_i=300 km model (upper right in Fig. 5.11), the response range at both 60 min and 120 min is Y_R = 5 km, while for the d_3 = 200 km model (upper right in Fig. 5.11), Y_R = 50 km and 15 km at 60 and 120 min respectively.

Clearly, from the results of Figs. 5.9 , 5,10 and 5.11 the island width Y_i and the conductive substratum depth d_3 are important parameters in determining the response range. Further, since the coast effect response range is seen to be generally much smaller for an island than for a continent, it should be possible to successfully remove the coast effect response from measurements at field sites much nearer the coast on an island (Figs. 5.10 and 5.11) than on a continent (Fig. 5.5).

5.2.3 Inductive Coupling for a Conductor in a Coastal Region

Figure 5.12 provides the schematics of a series of idealized models that aid in considering the effects of electromagnetic coupling for an anomalous conductor (σ_2) in the form of an upwelling conductive substratum at a horizontal distance Y from a uniform depth ocean (σ_1). The resistive host (σ_0) and conductive structure are underlain by a conductive substratum (σ_3). In a preceding section (5.2.1) it was proposed that if the ocean conductor separation were sufficiently large so that the mutual coupling were negligible, then the ocean coast effect response could simply be subtracted from the field site response to yield the approximate response of the anomalous conductor alone. A measure of the required separation distance for negligible coupling was taken to be the range for which the ocean coast effect response at the anomalous conductor location was diminished to a value of 0.2. This separation distance was defined as the response range Y_R.

In Fig. 5.12, model a includes an ocean of depth d_1, an anomalous conductor at a depth d_2 and a conductive substratum at a depth d_3, model b is the same as model a but not includes the anomalous conductor, while model c is the same as model a but does not include the ocean. In order to have some validity for the interpretation of field measurements, the resultant of a subtraction of the response of model b (ocean) from the response of model a (ocean plus conductor) should provide an acceptable response for model c (anomalous conductor and the conductive substratum). The level of validity of such a subtraction will depend on the mutual coupling of the various conductive structures (ocean, host, anomalous conductor and the underlying conductive substratum). Since the induced vertical magnetic field B_z at a point on the surface (say P) can be considered as due to

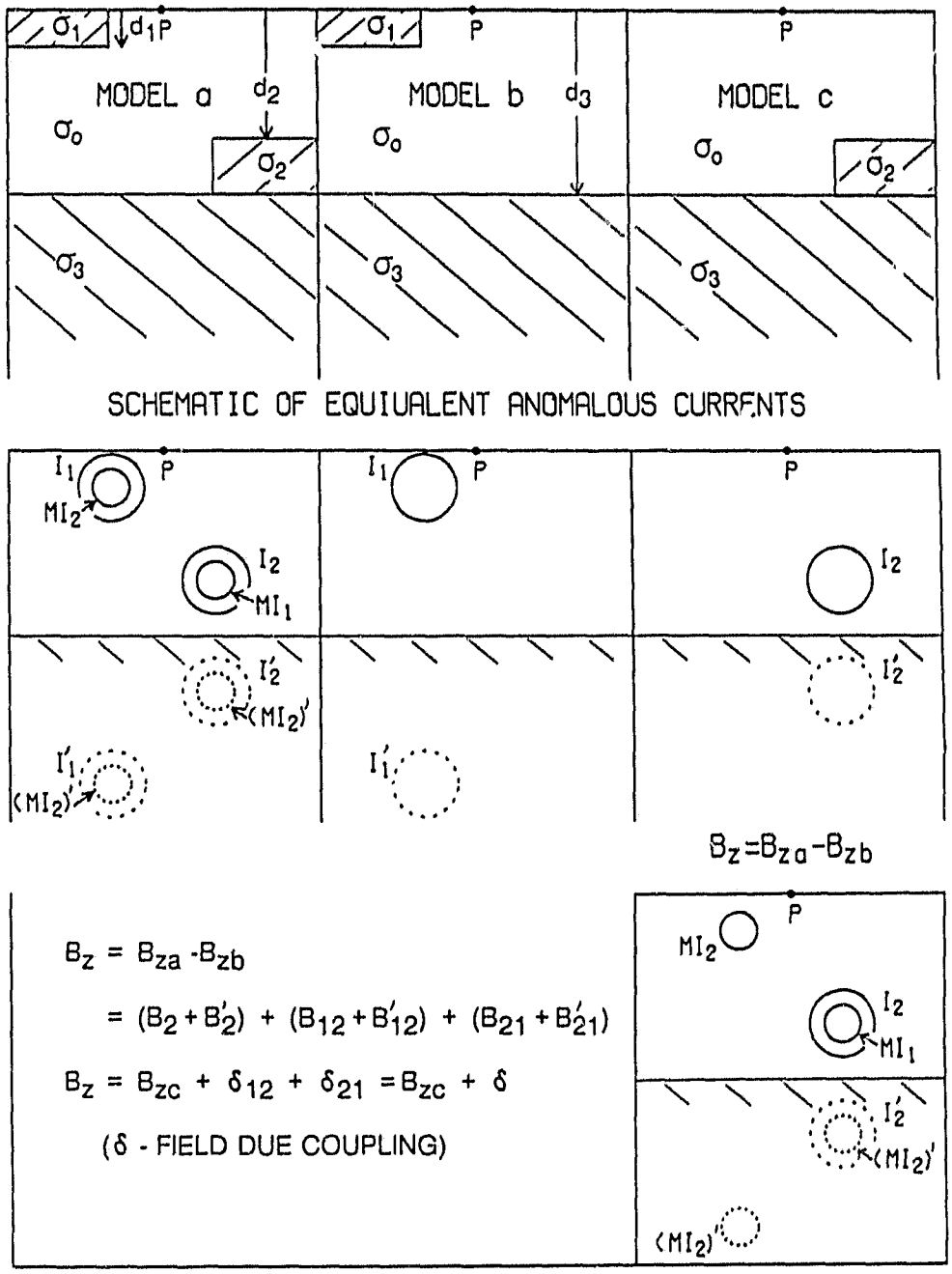

Figure 5.12: Schematic of induced equivalent anomalous currents and image currents for idealized 2-D conductivity models a, b, c.

anomalous currents (or localized current inhomogeneities) associated with conductive anomalies, the effect of mutual coupling between conductive bodies may be rationalized in terms of anomalous currents (current circuits) and their images. In the schematic of anomalous currents for model a in Fig. 5.12, the current circuits (loops in the horizontal plane of the model) labelled I_1 and I_2 symbolize regions of anomalous currents due to the ocean - host interface and the conductive anomaly - host interface respectively, and are considered as sources (taken to also include the effect of current distortion due to charge distribution on the conductive boundaries). At a given period, current in circuit I_1 induces current MI_1 in circuit I_2, while current circuit I_2 induces current MI_2 in circuit I_1, where M is the coefficient of mutual inductance between the I_1 and I_2 current circuits. The currents I_1 , I_2 , (MI_1) , (MI_2) and their complex images I'_1, I'_2, $(MI_1)'$, $(MI_2)'$ in the underlying conductive substratum lead to magnetic fields B_1, B_2, B_{12}, B_{21} and image magnetic fields B'_1, B'_2, B'_{12}, B'_{21}. Thus, at an arbitrary point P (surface of the earth in model a), the resultant anomalous vertical magnetic field for model a is

$$B_{za} = (B_1 + B_{12}) + (B_2 + B_{21}) + (B'_1 + B'_{12}) + (B'_2 + B'_{21}). \qquad (5.8)$$

Similarly, it is readily seen that the anomalous fields at point P for models b and c are respectively,

$$B_{zb} = B_1 + B'_1, \qquad (5.9)$$

$$B_{zc} = B_2 + B'_2 \ . \qquad (5.10)$$

At P, a subtraction of the anomalous field for model b from the anomalous field for model a, results in

$$B_z = B_{za} - B_{zb} = (B_2 + B'_2) + (B_{12} + B'_{12}) + (B_{21} + B'_{21}) , \qquad (5.11)$$

which is the anomalous field for model c (the desired model) plus the field due to

the mutual inductive coupling of the ocean and the anomalous conductor, and is described by the anomalous current schematic in the lower right of Fig. 5.12. Thus the subtraction of the field of model b from that of model a yields

$$B_{zd} = B_{zc} + \delta_{12} + \delta_{21} \ , \qquad (5.12)$$

where $\delta_{12} = (B_{12} + B'_{12})$, and $\delta_{21} = (B_{21} + B'_{21})$ are the contributions due to inductive coupling. Clearly, δ_{12} and δ_{21} must be small relative to B_{zc} (the response of the anomalous conductor) in order that subtraction yields an acceptable approximate response of the anomalous conductor alone. It should be pointed out that the phase relationship between a current source and its image (due to the conductive substratum) is such as to reduce the resultant vertical magnetic field at P from what it would be in the absence of the conductive substratum. This will also be the case for the component due to coupling, and its image. Thus the conductive substratum has the effect of reducing the spatial range of the components due to inductive coupling between the ocean and the anomalous conductor. The numerical results discussed in section 2.1 indicated that the effect of reducing the depth of the underlying conductive substratum is to reduce the spatial range of the ocean coast effect, that is, to reduce the response range, Y_R, in the 2D model. This decrease is expected intuitively, when summing the fields of the current source (associated with the ocean-host interface) and its image at shallower depths, for decreasing conductive substratum depths.

5.2.4 Removal of the Coast Effect Responses for 2D Models

Continental Coastal Region

The empirical curves of Fig. 5.5 will now be used to specify the response ranges Y_R to be used for numerical models of anomalous conductors in the form of an upwelling or a depression in the conductive substratum at depth in a continental coastal region, a model for which the ocean-conductor electromagnetic coupling should be sufficiently small to permit a subtraction of the coast effect response from field measurements to provide an approximate response of the anomalous conductor alone. The induction arrow components, which for 2D ocean-land models are essentially the real (in-phase) and imaginary (quadrature) components of the vertical to horizontal field ratios, will attenuate, as a function of distance from the interface, at least as rapidly as the (amplitude) coast effect field responses $|B_z/B_{yn}|$ studied in Figs. 5.1 - 5.11. In the following figures, the induction arrows presented are the in-phase and quadrature single station transfer functions (with sign reversed) for time varying fields of the form $\exp(i\omega t)$.

Figure 5.13 shows schematics of three models a, b, and c that will be used to examine the results of the subtraction of the coast effect responses from the combined coast effect and anomalous conductor responses at 60 min. The anomalous conductor is in the form of an upwelling in the conductive substratum at 100 km depth and at a horizontal distance of 80 km (equal to the response range Y_R) from the coastline of a 1 km depth ocean (i.e., the response range Y_R for 60 min from the upper right in Fig. 5.5). The numerical method of Brewit-Taylor and Weaver (1976) was used to evaluate the 2D in-phase and quadrature induction arrow responses V (V_a, V_b, and V_c) for the three models at 60 min. Positive val-

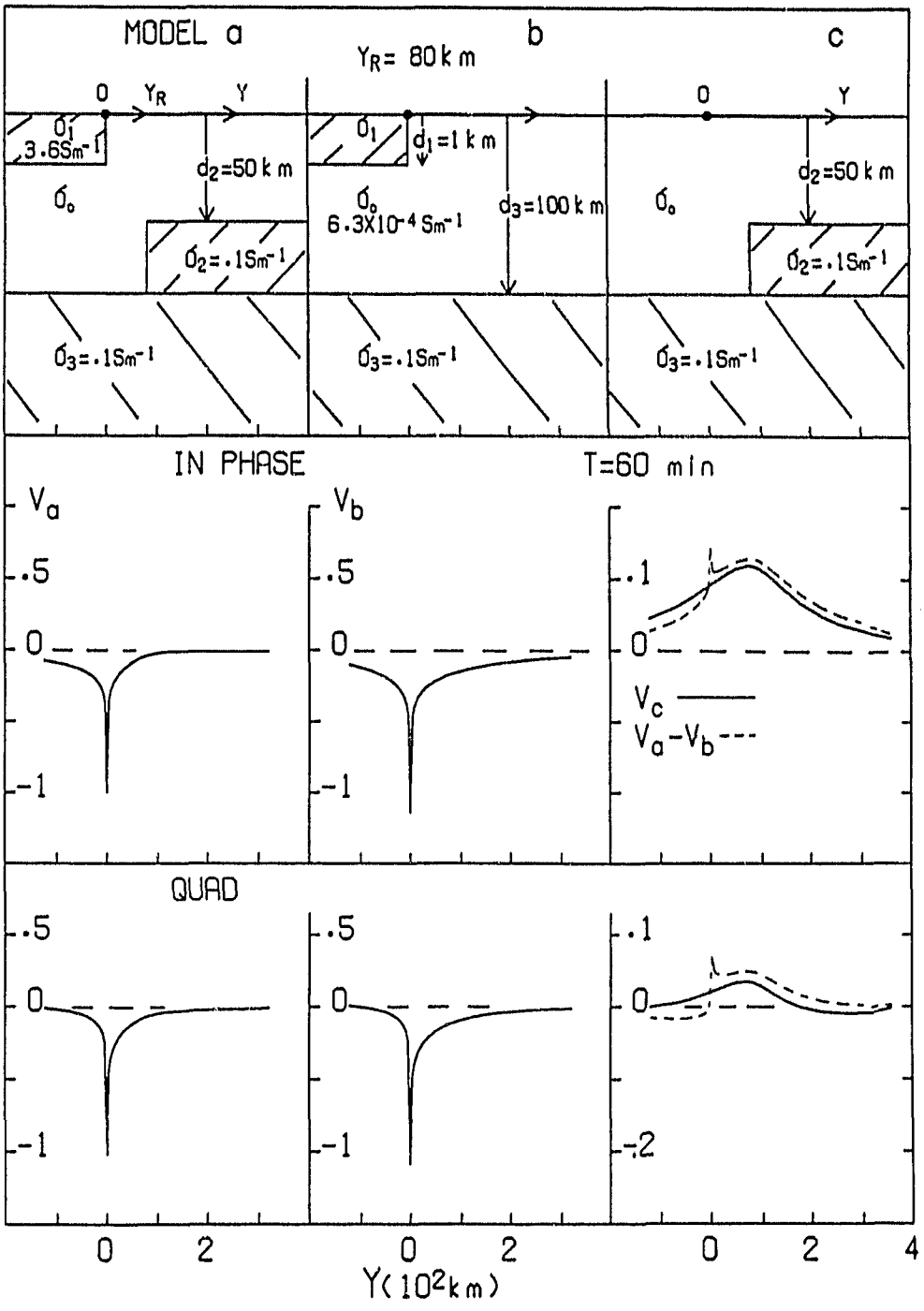

Figure 5.13: V_a, V_b, V_c for 2-D models a, b, c respectively, and (V_b - V_a) for an anomaly in the form of an upewlling in the conductive substratum (d_3=100 km) in a continental coastal region.

ues of V represent arrows pointing in the +y direction, while negative values represent arrows pointing in the -y direction. In Fig. 5.13, the dashed curve for model c is the resultant of subtracting the model b induction arrow (V_b) response from the model a induction arrow response (V_a). The small differences between these two curves is attributed to the electromagnetic coupling of the ocean and the conductor (σ_2) that is not removed in the subtraction (as discussed in the previous section). For this model, simple subtraction to remove the coast effect response would be judged acceptable, particularly for the in-phase component. The quadrature response, being very small (less than .05), would be of little value in any interpretation.

Figures 5.14 and 5.15 show 2D models and induction arrow responses at 60 min for the case of an anomalous conductor, in the form of a depression in the conductive substratum, in a continental coastal region. The depth of the ocean is the same as that for Fig. 5.12, but the depth of the conductive substratum is taken to be d_3 = 100 km and d_3 = 50 km for Figs. 5.14 and 5.15 respectively, and thus the horizontal distance from the ocean coastline to the edge of the anomalous conductor is chosen to be 80 and 40 km, approximately equal to the response range Y_R value predicted from the upper right in Fig. 5.5 (curve 2). The differences between the dashed curve and the response curve for model c (Fig. 5.14 and 5.15) again are attributed to the electromagnetic coupling of the anomalous conductor and the ocean. The results indicate that the coupling effect is small, and thus simple subtraction to remove the coast effect for this model also, appears to be acceptable, again particularly for the in-phase component.

Island Coastal Region

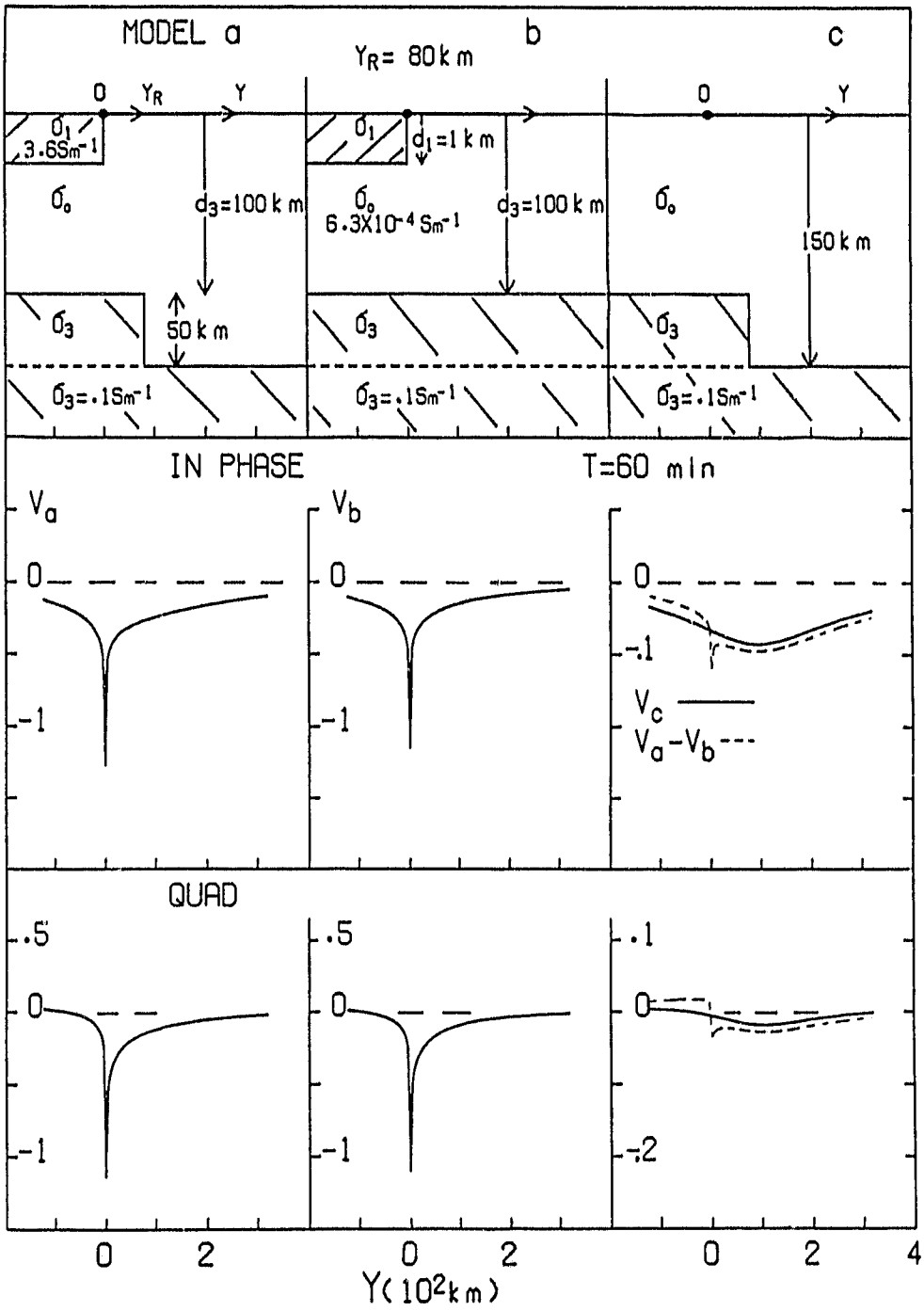

Figure 5.14: V_a, V_b, V_c for 2-D models a, b, c respectively, and (V_b - V_a) for an anomaly in the form of a depression in the conductive substratum (d_3=100 km) in a continental coastal region.

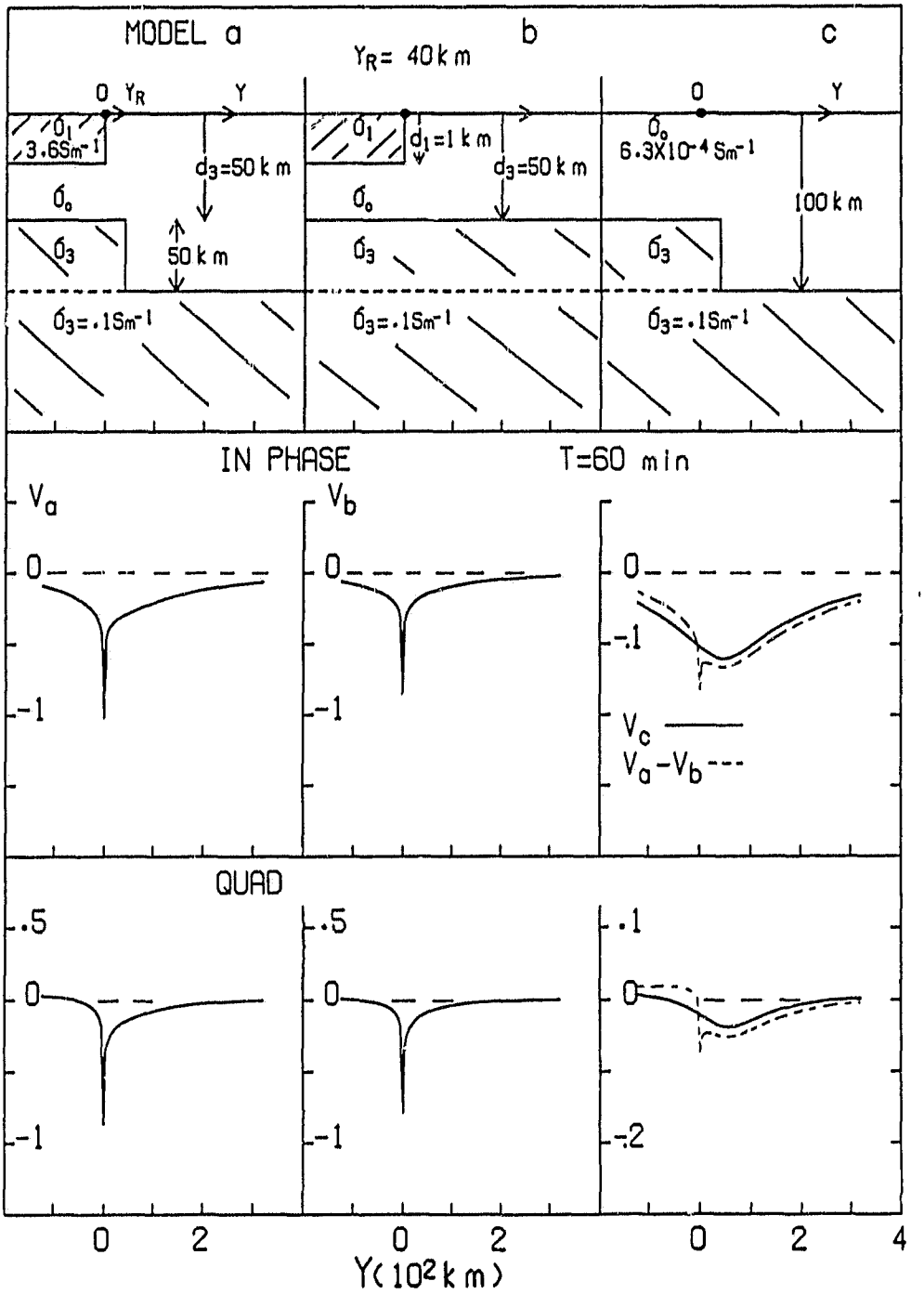

Figure 5.15: V_a, V_b, V_c for 2-D models a, b, c respectively, and (V_b - V_a) for an anomaly in the form of a depression in the conductive substratum (d_3=50 km) in a continental coastal region.

The empirical curves of Figs. 5.10 and 5.11 are used to specify the response ranges Y_R to be used for numerical models of anomalous conductors in the form of an upwelling or a depression in the conductive substratum at depth for the case of an island, a model that should permit subtraction of the island coast effect.

Figure 5.16 shows 2D models and induction arrow response curves for an anomalous conductor, in the form of an upwelling of the conductive substratum at depth, in an island coastal region. The island width is Y_i = 200 km and the horizontal distance from the ocean coastline to the edge of the anomalous conductor is chosen to be 40 km, approximately equal to the Y_R value indicated in Fig. 5.11 (curve 2 for d_1 = 2 km and d_3 = 100 km). For this upwelling conductive anomaly structure in the island coastal region, subtraction yields excellent results, except very near the coastline and over the ocean.

Figures 5.17 and 5.18 deal with a model of a conductive anomaly in the form of a depression in the conductive substratum at depths of 50 km and 100 km respectively, in an island coastal region. The island width is Y_i = 200 km and, in this case, the horizontal distance from the ocean coastline to the edge of the anomalous conductor is chosen to be 35 km for d_3 = 50 km, and 40 km for d_3 = 100 km, approximately equal to the Y_R values indicated in Fig. 5.10 (curve 2 for d_1 = 2 km and d_3 = 50 km), and in Fig. 5.11 (curve 2 for d_1 = 2 km and d_3 = 100 km). These results, too, show that the coast effect response can be subtracted to yield, with small error, the response of the conductive anomaly alone.

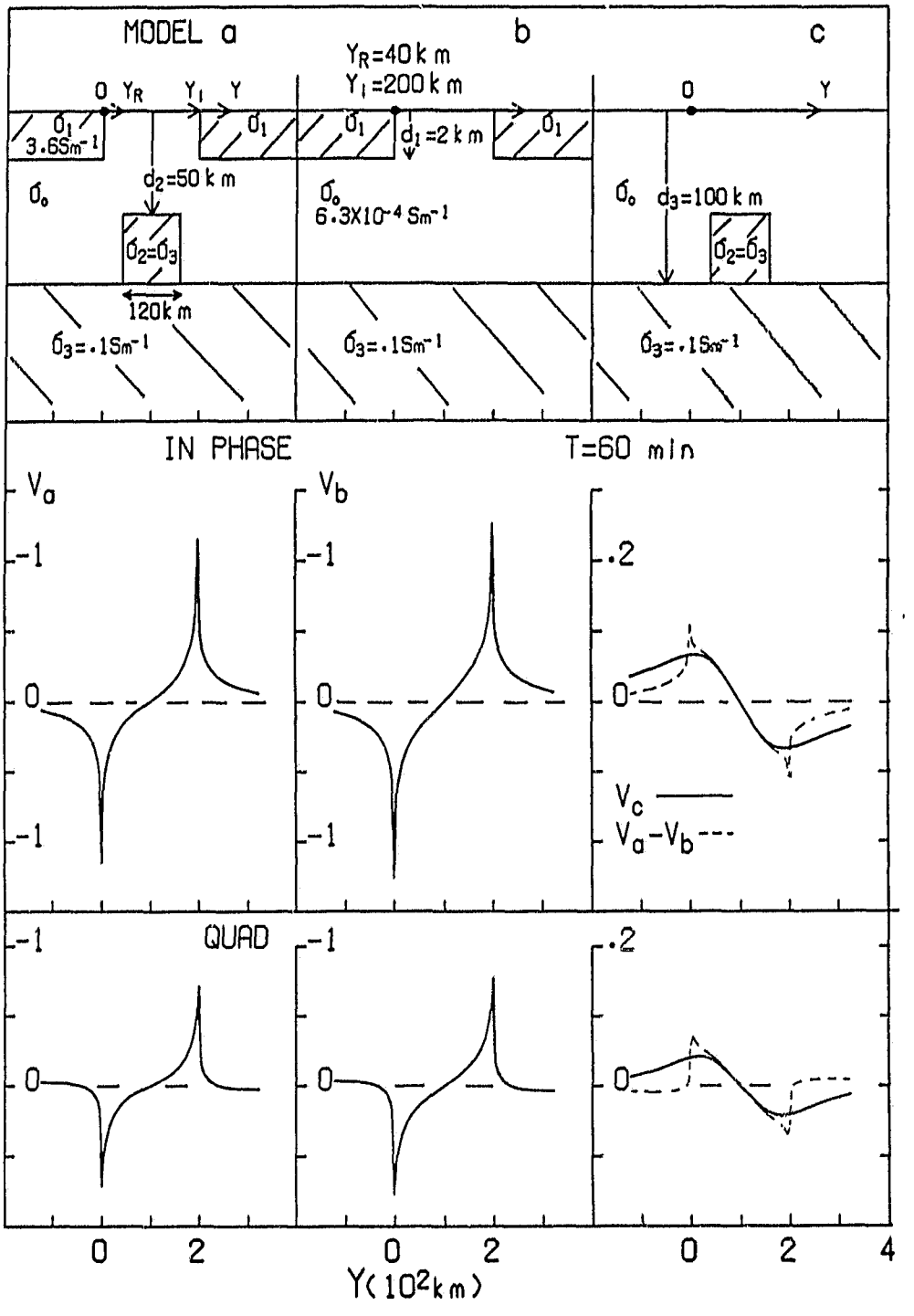

Figure 5.16: V_a, V_b, V_c for 2-D numerical models a, b, c respectively, (V_b - V_a) for an anomaly in the form of an upwelling in the conductive substratum (d_3=100 km) in an island coastal region.

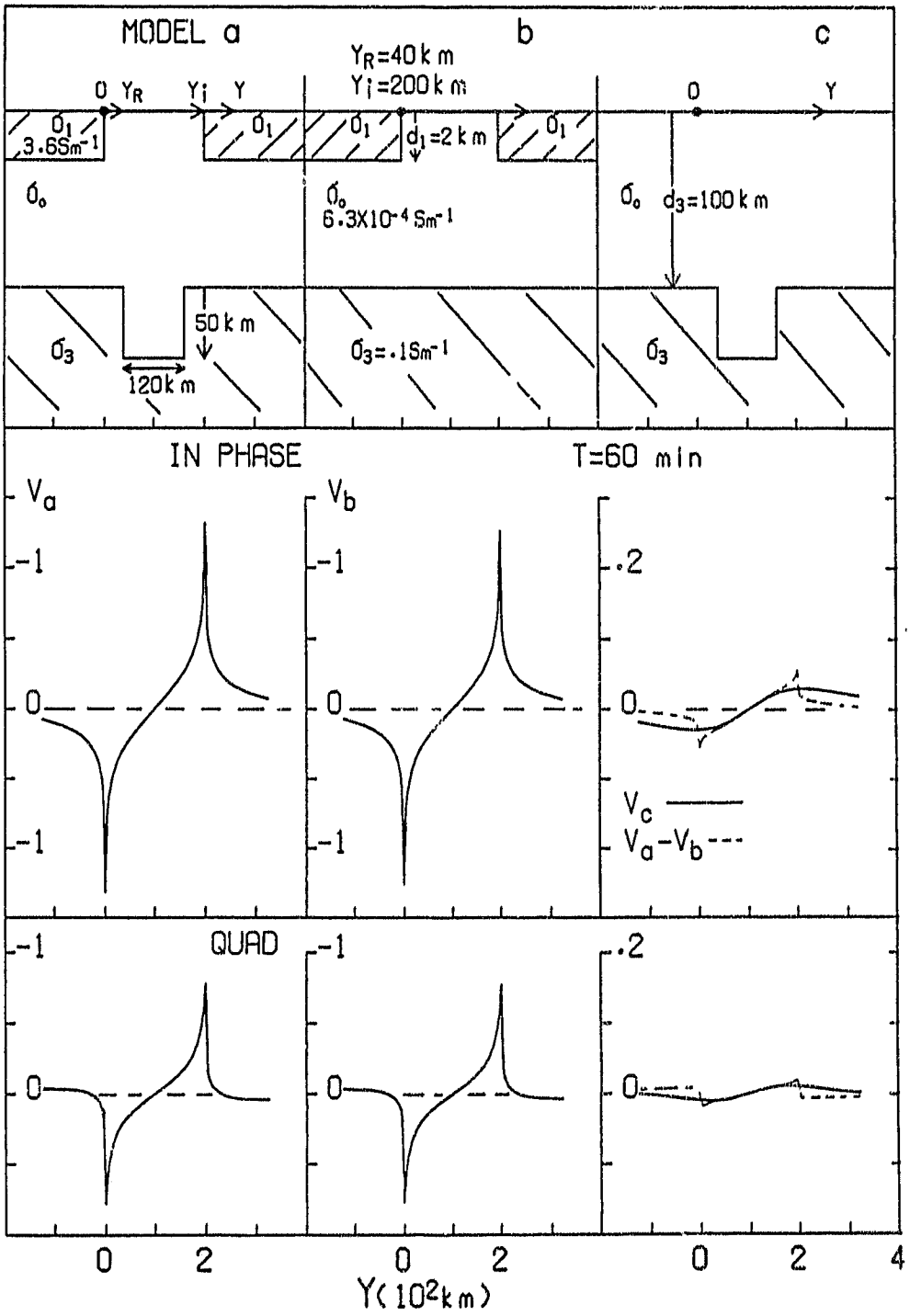

Figure 5.17: V_a, V_b, V_c for 2-D numerical models a, b, c respectively, (V_b - V_a) for an anomaly in the form of a depression in the conductive substratum (d_3=100 km) in an island coastal region.

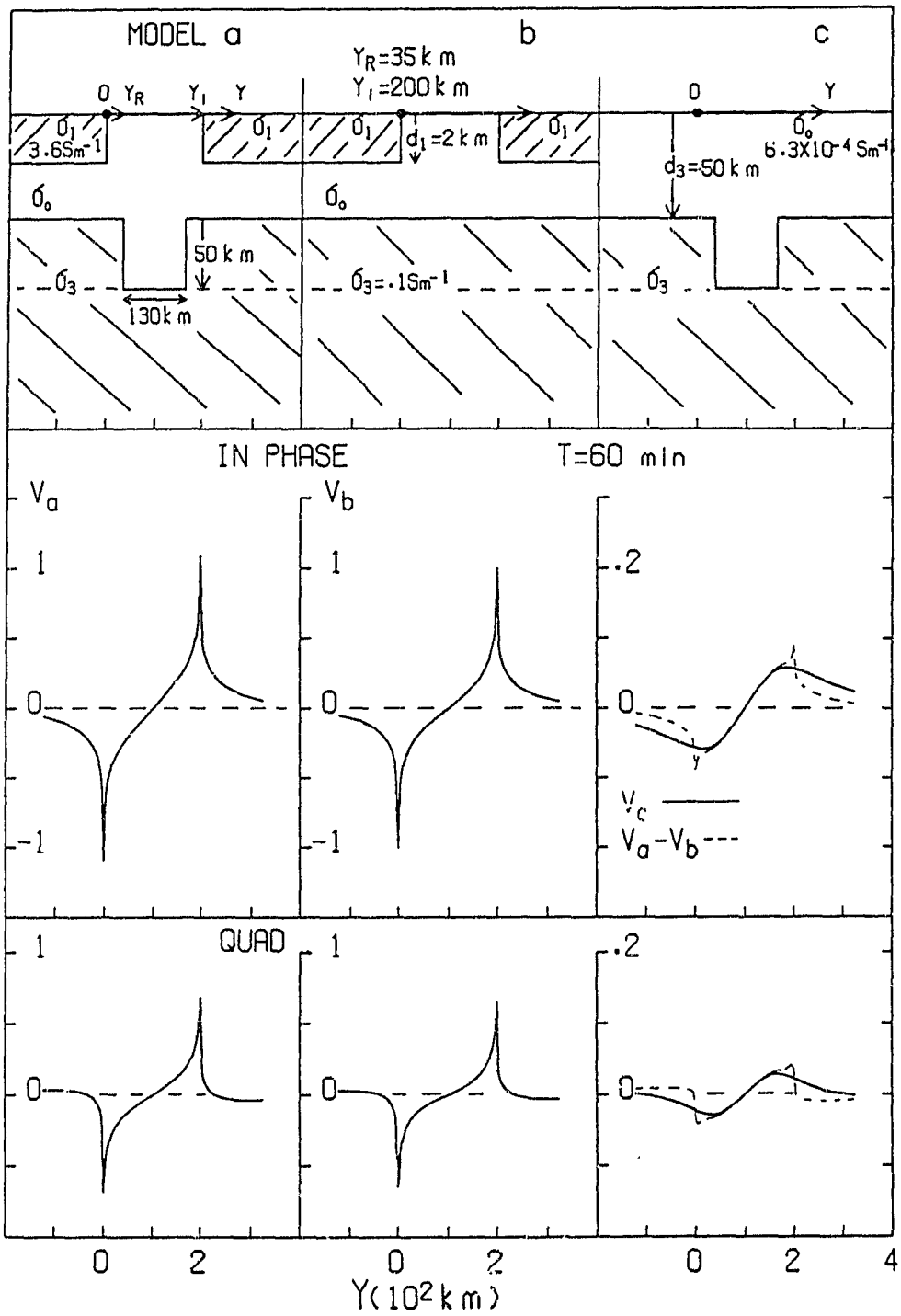

Figure 5.18: V_a, V_b, V_c for 2-D numerical models a, b, c respectively, and (V_b - V_a) for an anomaly in the form of a depression in the conductive substratum (d_3=50 km) in an island coastal region.

5.3 The Chapter Summary

The 2D numerical calculations of EM induction in continental and island coastal regions for an anomalous conductor in the form of an upwelling or a depression in the conductive substratum, show that if the ocean-conductor separation distance is at least as great as the coast effect response range Y_R (defined here to be the range where the coast effect $|B_z/B_{yn}|$ has decreased to a value of 0.2), then the coast effect can be removed by vector subtraction to yield a response, approximately that of the conductive anomaly alone. For a given period (in the range 5 - 120 min), Y_R is found to increase with increasing ocean depth, conductive substratum depth, and island width. Further, the dependance on period is found to vary from model to model, but the general trend is for Y_R to decrease with increasing period, on account of the increasing importance of the underlying conductive substratum through the skin depth effect in the host. For a typical conductive substratum depth d_3=100 km, general trends for the dependance of the response range Y_R on the ocean depth, conductive substratum depth, island width and period can be empirically generalized as a set of practical "rules of thumb" as shown in Table 5.1.

Table 5.1: COAST EFFECT RESPONSE RANGE Y_R "RULES OF THUMB"

(for a typical conductive substratum depth d_3 = 100 km)

The coast effect response range Y_R is defined to be the range where the coast effect $|B_z/B_{yn}|$ has decreased to a value of 0.2

1. CONTINENT COAST EFFECT RESPONSE RANGE

(a) $Y_R \simeq d_3$ for shallow ocean (d_1 = 1 km)

(b) $Y_R \simeq 3/2d_3$ for deep ocean (d_1 = 4 km)

2. ISLAND COAST EFFECT RESPONSE RANGE

(a) $Y_R \lesssim 1/4d_3$ for narrow island (Y_i = 100 km), and all ocean depths.

(b) $Y_R \lesssim 3/4d_3$ for wide island (Y_i = 300 km), " " " "

(c) $Y_R \lesssim 1/4Y_i$ for island widths ($Y_i \lesssim$ 500 km), " " " "

3.CONTINENT AND ISLAND COAST EFFECT RESPONSE RANGE COMPARISON

(a) Y_R (narrow island)$\lesssim 1/4Y_R$ (continent) for given ocean depths.

(b) Y_R (wide island) $\lesssim 1/2Y_R$ (continent) " " " "

4. GENERAL TRENDS IN THE RESPONSE RANGE

(a) Y_R decreases with decreasing ocean depth (d_1)

(c) Y_R " " " island width (Y_i)

(b) Y_R " " " conductive substratum depth (d_3)

(d) Y_R " " increasing period (T)

Chapter VI

ANALOGUE MODEL AND FIELD SITE RESULTS FOR THE COASTAL BOHAI BAY REGION OF CHINA

6.1 Introduction

The continent of China, situated between the subduction zone of the west Pacific Oceanic plate and the collision zone of the Himalayas, is divided into two major parts, namely the western and eastern continents, based on their geological identities (Liu, 1987). The boundary between the two is a N-S striking geotectonic zone with a width extending from the longitude of 102°E to 107°E. The western part of the continent, including the Tibetan Plateau and the Cenozoic basins of Talimu, Chaidamu, and Zhungeer, is characteritized by strong neotectonic movements, thick Cenozoic deposits in the basins, and NWW geological trends. The eastern continent adjoins Bohai Bay, the Yellow Sea and the East China Sea. Although the neotectonic features are different from region to region, the geological trends are mainly in the NNE direction, roughly parallel to the Asian continental coastline (the direction of E-polarization of the source field for the Bohai Bay model). The Bohai Bay region (in the eastern part of this continent) is roughly located on a Cenozoic rift system (Liu, 1987) where strong earthquakes have frequently occurred. The rift system, with a maximum width of 400 km at the middle, and a minimum width of 50-100 km at the north and south ends, runs about 1000km through Northern China with a NNE strike. The terrain within the rift system is

low-lying, covered by seawater in its most easterly and northeasterly parts and surrounded by mountains. It consists of a series of uplifts and depressions. The thick sediments are characteristic of rift systems with the thickness of Cenozoic deposits inside the depressions generally 6-7 km, and up to 12 km in the depression of Bohai Bay, and less than 1 km at the uplift region (Liu, 1987).

Geophysical study of the Bohai Bay region is of considerable interest as the region abundant petroleum resources have been found within the thick sediments. During the last ten years, various geophysical surveys have been carried out in the Bohai Bay region (Chen, 1974; Qi et al., 1981; Liu et al. 1984; Teng et al., 1985; Kao et al. 1990). One dimensional inversion results of MT site measurements for deep structure in the region (Liu, 1987) indicate a conductive layer at a depth of 35-40 km (with a thickness of 4-5 km and conductivity of 0.1 to 0.2 Sm^{-1}), and a conductive asthenosphere substratum at a depth of 80-90 km (with conductivity of 0.5 to 1.0 Sm^{-1}). The resistive host has a conductivity on the order of $0.001Sm^{-1}$. Based on the results of seismic data inversion, a low velocity zone, with a velocity of 7.8 km/sec is indicated at a depth of roughly 60 -70 km in the Bohai Bay region (Song, 1985). This suggests that the conductive substratum in the region may coincide with the low velocity zone. The measurement of heat flow shows that the average exceeds 1.6 HFU (10^{-6} cal/sec cm^2) inside the rift system. In particular, the heat flow values in the Bohai Bay coastal region range from 1.77 to 2.53 HFU, while in the surrounding mountains the average value is only 1.0 HFU (Liu, 1985).

The scaled 3D laboratory analogue model of the Bohai Bay coastal region (as discussed in detail in Chapter 3) can readily be used to provide ocean coast

effect responses for the continental region. These responses for the 3D laboratory models may then be used to delineate the coast effect response component in the geophysical field site observations, and if this coast effect response can successfully be subtracted, then the remaining response should be characteristic of any conductive anomaly in the earth that was not included in the laboratory simulation. Thus the response of the conductive anomaly alone could be determined. Laboratory analogue model ocean coast effect responses, in terms of induction arrows (or transfer functions), available for the Bohai Bay coastal regions will be used to attempt to remove (approximately) the coast effect in the coastal field site measurements. The subtraction of the analogue model response should have validity for cases where the electromagnetic coupling of the ocean and inland conductive anomaly is sufficiently small.

In Chapter 5, the ocean coast effect response range, and the proposed empirical criteria for permitting subtraction of the coast effect from field measurements, were analyzed for 2D models. Since an actual geophysical conductive anomaly, as well as the ocean-land interface, are generally 3D in nature, it should be advantageous to employ measurements of the coast effect response for a 3D laboratory analogue model which includes a simulation of the complex coastlines, the shelving ocean (simulating the known bathymetry), as well as the conductive asthenosphere substratum, to account for the ocean coast effect component in actual field measurements in a coastal site. The empirical response ranges (Y_R) proposed in Chapter 5 for the 2D numerical models should provide useful estimates in 3D regions, particularly at the longer periods. At shorter periods, where a coastal response for a cape or a bay coastline may differ considerably from that for a

straight coastline (Dosso et al., 1986), the 2D response range may somewhat underestimate the actual response range. In Chapter 5, 2D numerical models of EM induction in continental and island coastal regions for an anomalous conductor in the form of an upwelling or a depression in the conductive substratum at depth were studied to determine constraints on ocean-anomalous conductor separation distances that would permit, to within an acceptable approximation, a simple vector subtraction of the coast effect response. It was found that if the ocean-conductor separation distance were at least as great as the coast effect response range Y_R (defined as the distance from the ocean where the $|B_z/B_{yn}|$ coast effect response is reduced to a value of 0.2), then the coast effect could be removed by vector subtraction to yield a response, approximately that of the conductor alone.

In the present chapter, the analogue model induction arrows will be compared with field site arrows for several sites in the Bohai Bay region. The field results include those of Chen (1974), IGSSB (1986, private communication), and Kao (1990). A convenient method of viewing the model and field station results is to compare the model and field site induction arrows at the same site, so that the difference between the two can be easily observed. Difference arrows, obtained by subtracting the 3D laboratory analogue model coast effect responses from the field site responses, are examined and employed in the interpretation of the field site induction arrow responses available in this Bohai Bay region of China.

6.2 Induction arrows in the Bohai Bay region

In Fig. 6.1, the removal of the ocean coast effect, by subtracting the analogue model coast effect responses from field site responses (Chen, 1974) for three locations in the Bohai Bay region of continental China is examined for 5 and 60 min. In-phase field site induction arrows (V_f), analogue model induction arrows (V_m), and field-model difference induction arrows (V_f-V_m) are shown for three sites, two of which are roughly 50 km from the shallow Bohai Bay, and the third over 200 km from the coast. All sites are at least 200 km from the deeper ocean of the Yellow Sea. At 5 min the model and field site arrows at all three sites have directions approximately normal to the local Bohai Bay coastline, with the field site arrows rotated about 10° clockwise relative to the model arrow directions. The model arrows at A and B are about 50% larger, and at C about 70% larger, than the respective field site arrows. From the results of Chapter 3, it is known that induction in Bohai Bay is important at short period, and thus in the absence of other nearby conductors, induction arrows at coastal sites should point to Bohai Bay and shorten with distance from the coastline. Both of these features are clearly seen in Fig. 6.1. At 60 min, induction in Bohai Bay should not be so important, and any induction arrow response, in the absence of other local conductors (e.g. subsurface conductors), should be due to induction in the distant ocean. At 60 min, the model arrows at the three sites are shortened in length, with the arrow at A (nearest to Bohai Bay) decreased the most, and at C (furthest from Bohai Bay) decreased the least, as expected since the induction effects of the shallow bay at 5 min would be the greatest for site near the coast. At 60 min the analogue model arrows at the three sites have roughly equal lengths indicating

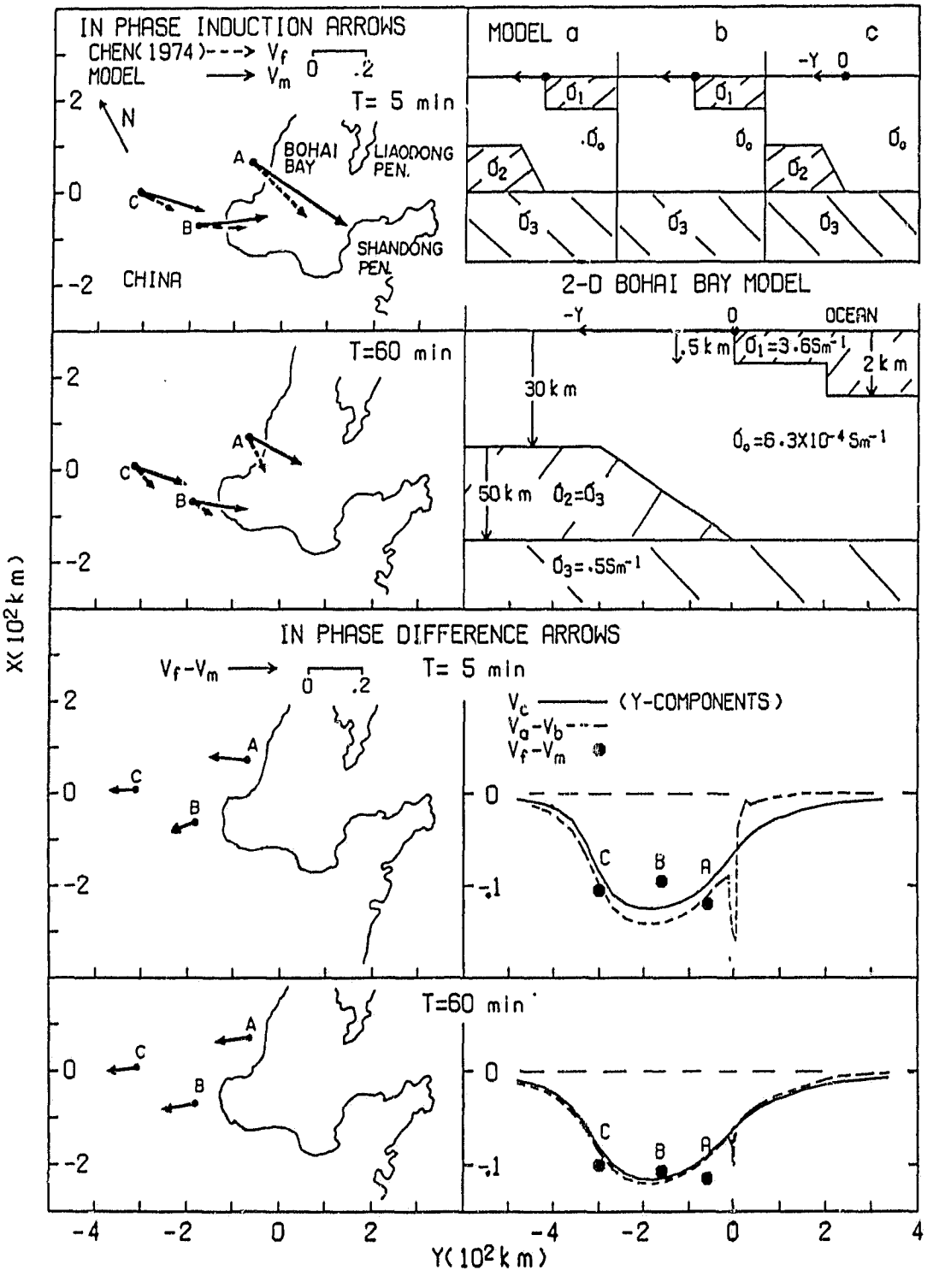

Figure 6.1: Analogue model V_m and field site (Chen, 1974) V_f and difference (V_f-V_m) induction arrows, and the 2-D model of an anomaly in the form of an upwelling in the conductive substratum for Bohai Bay region.

response to a distant common conductor, namely the ocean of the Yellow Sea. The induction arrow at A has rotated CCW by about 5°, while at B and C it has rotated CW by roughly 20° and 5° respectively, so that the three arrows now roughly point to a common distant location (the Yellow ocean) as expected. The field site arrows, however, have not behaved in as predictable a manner with increasing period. they have not rotated to point to the distant ocean, but rather have all rotated CW by relatively large angles (20°, 35°, 25°) to point in a more southerly direction. The field site arrows are shortened at each site, with the largest relative decrease at B, so that the arrow at B is now shorter than the arrow at C. The field site arrows appear to be responding to some conductive feature (not included in the analogue model) in addition to the distant ocean. It is seen that when the ocean effect, as typified by the model arrows, is removed from the field site arrows though subtraction, the resulting difference arrows ($V_f - V_m$) at both short and long periods point inland (-y direction in Fig. 6.1), indicating a conductive anomaly some distance inland. At short periods the shallow ocean of the nearby bay is important, while at long periods the distant Yellow Sea has a significant effect, and subtraction of the coast effects yields difference arrows that provide the same result for the short and long periods. The fact that the directions of the arrows are almost identical for the two periods, lends credence to this interpretation of an inland conductor.

Chen (1974) has interpreted the field observations at 60 min to be the response to an E-W striking conductor at 60 km depth. In this interpretation, while sites A and C would be north of the conductor, the arrows would show the combined responses to the distant ocean and the conductor at depth. The arrow at

B would be attenuated due to the underlying conductor, but the arrow direction could still be effected by the distant ocean. The direction at B supports this view. At 5 min, the effects of the deep conductor would be small relative to the effects of the nearby Bohai Bay, but the 10^{o} rotation of the field site arrows relative to the model arrows would be consistent with some response to the E-W striking conductor. The further southward rotation at 60 min are also consist with this conclusion.

Included also in Fig. 6.1 are 2D models (a, b, and c), and numerical results (V_c) for model c (a postulated inland anomalous conductor), difference arrow results (V_a-V_b) for models a and b, and the y-component of the field-model difference arrows (V_f-V_m). The conductive substratum in the 2D Bohai Bay model, taken to be at a depth of 80 km and of conductivity of 0.5 Sm^{-1}, is based on the results of magnetic surveys in the Bohai Bay region reported by Liu and Liu (1983) and Liu et al. (1983). From the numerical results (lower right in Fig. 6.1), it is concluded that the electromagnetic coupling of the anomalous conductor and ocean is sufficiently small to permit simple subtraction of the coast effect. The field-model difference arrows (V_a-V_b) agree more closely with the the model c results (V_c) at 60 min than 5 min, in keeping with the decreased response range with increasing period as observed in the 2D numerical results discussed earlier in chapter 5.

Figures 6.2 and 6.3 show in-phase and quadrature induction arrows and difference arrows (Kao, 1990) for the Bohai Bay region for 5, 10, and 40 min. These difference arrows also support the interpretation of a conductive anomaly inland, with the strike of the conductor roughly in the north-south direction as indicated

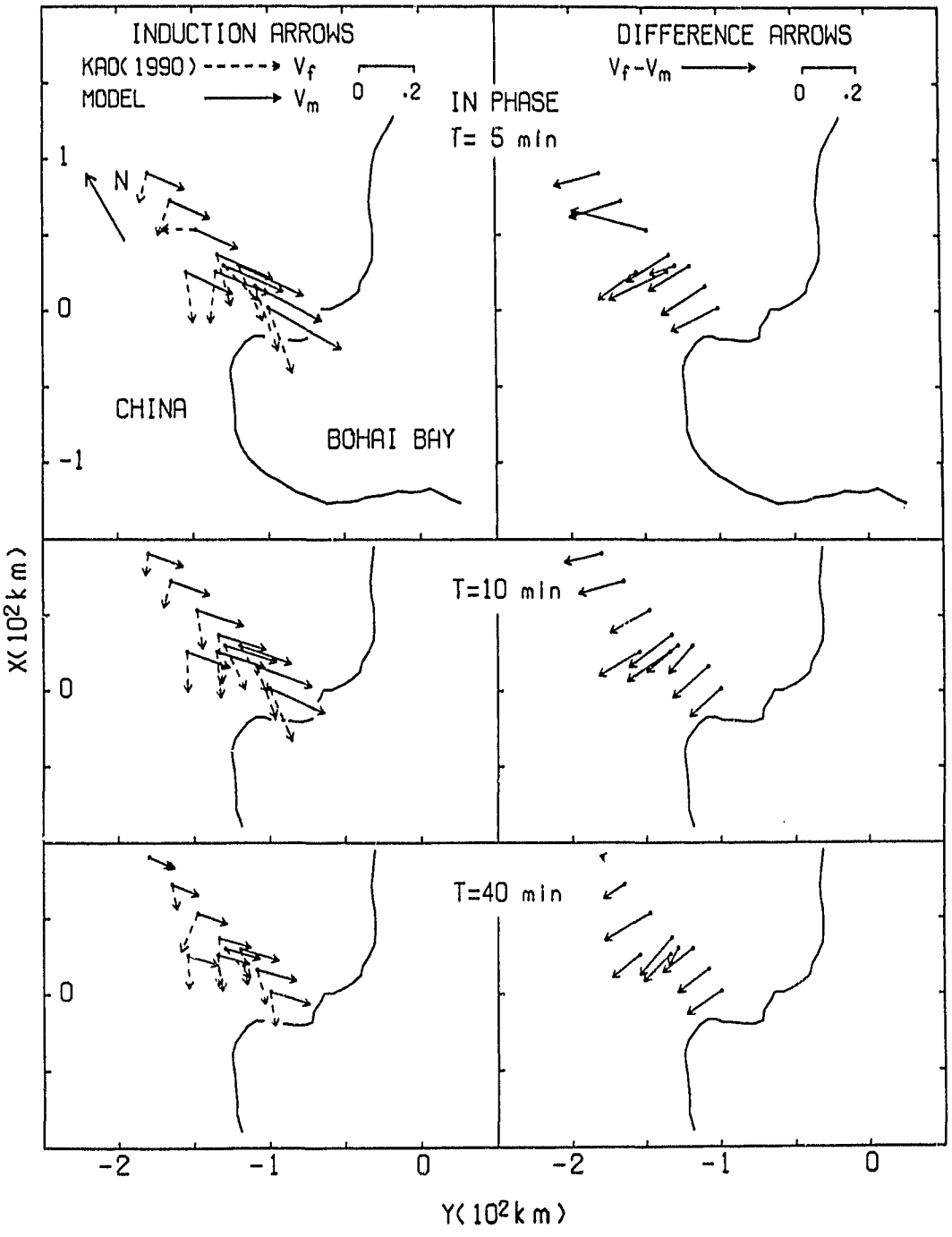

Figure 6.2: Analogue model V_m and field site (Kao, 1990) V_f in-phase induction arrows and difference arrows (V_f-V_m) for the Bohai Bay region of China.

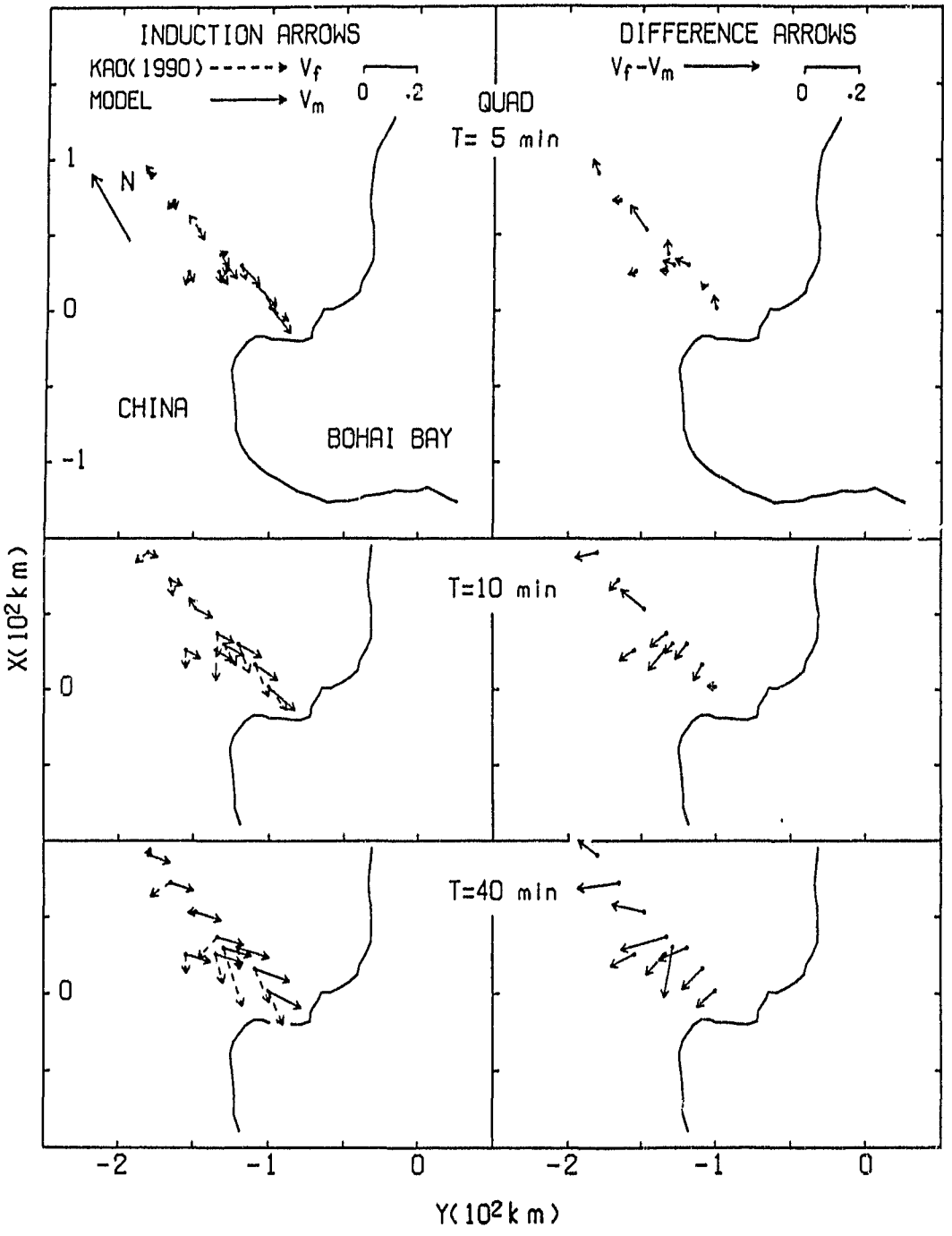

Figure 6.3: Analogue model V_m and field site (Kao, 1990) V_f quadrature induction arrows and difference arrows (V_f-V_m) for the Bohai Bay region.

by the Fig. 6.1 results. According to Liu and Liu (1983), the Bohai Bay region is located roughly on a Cenozoic rift system that has a mainly NNE striking geological trend, which is parallel to the Asian continental coastline (roughly the direction taken for E-polarization of the source field in the 2D Bohai Bay model in Fig. 6.1).

Figure 6.4 shows the model in-phase induction arrows and the field site arrows from the work carried out by the Institute of Geophysics, State Seismological Bureau of China (IGSSB) in the Bohai Bay region for 5 and 60 min at 27 field sites. The difference arrows ($V_f - V_m$), obtained by subtracting the model arrows from the field site arrows, are also shown. It is seen that the difference arrows in the southern and western areas of Bohai Bay consistently point in a westerly direction which supports the results of the previous discussion. As the period increases from 5 min to 60 min, the difference arrows in the western area of Bohai Bay all point roughly westward, but with slightly enhanced magnitudes. This behaviour of the in-phase difference arrows with increasing period in this area again suggests a N-S striking conductor. The fact that the difference arrows are not strongly dependent on period, indicates that the anomalous conductor must be at considerable depth. At the Shandong Peninsula sites, the difference arrows all point westward, while at the Liaodong Peninsula the difference arrows all point in the NW direction. The consistent direction of the difference arrows at the Shangdong Peninsula may be indicative of the effect of an upwelling of a highly conductive layer underneath Bohai Bay, and those at the Liaodong Peninsula indicative of an anomalous conductor to the north-west of Bohai Bay. These difference arrows also support the interpretation of a conductive anomaly inland, with the strike of

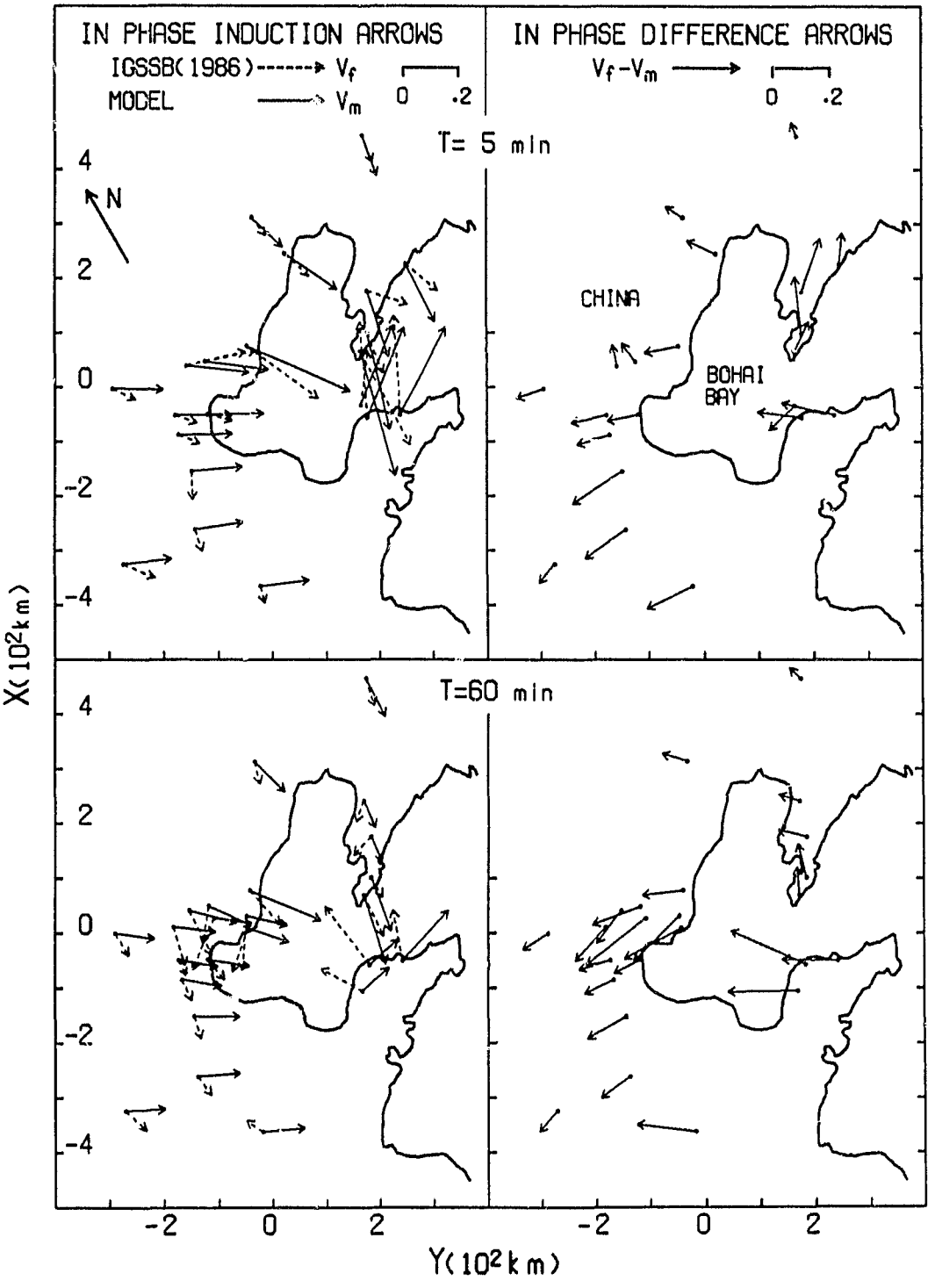

Figure 6.4: Analogue model V_m and field site (IGSSB, 1990) V_f in-phase induction arrows and difference arrows (V_f-V_m) for the Bohai Bay region of China.

the conductor roughly in the north-south direction as indicated by the Fig. 6.1 results.

The results of Figs. 6.1, 6.2, 6.3, and 6.4 for the Bohai Bay region provide examples of what appears to be the successful removal of the ocean coast effect from field site measurements over an anomalous conductor in the form of an upwelling in the conductive asthenosphere in a continental coastal region. Clearly, the conductor-ocean separation distance is sufficiently large for both the shallow and the deep ocean (as can be seen from the empirical response ranges of Figs. 5.5) so as to have negligible electromagnetic coupling at both short and long periods.

6.3 Apparent Resistivities in the Bohai Bay Region

In the Bohai Bay region, particularly west of Bohai bay, extensive magnetotelluric (MT) measurements have been carried by Liu et al. (1983). The field apparent resistivities and the analogue model apparent resistivities at sites HL and XS (Fig. 6.5) are shown in Fig. 6.6. The field measurements cover periods from 10 sec to 2000 sec (30 min), while the model results cover a range from 180 sec to 1800 sec (3-30 min). Figures 6.6 shows the components of the apparent resistivities parallel to the coast at sites HL, XS. It is seen that the model apparent resistivities are approximately an order of magnitude greater than the field site values at both sites. This is expected, since the analogue model only includes a conductive layer of .5 Sm^{-1} at a simulated depth of 80 km, and does not include the inland anomalous conductor discussed in the previous section. The sites HL and XS are at a distance of approximately 200 km from the Bohai Bay coast, and

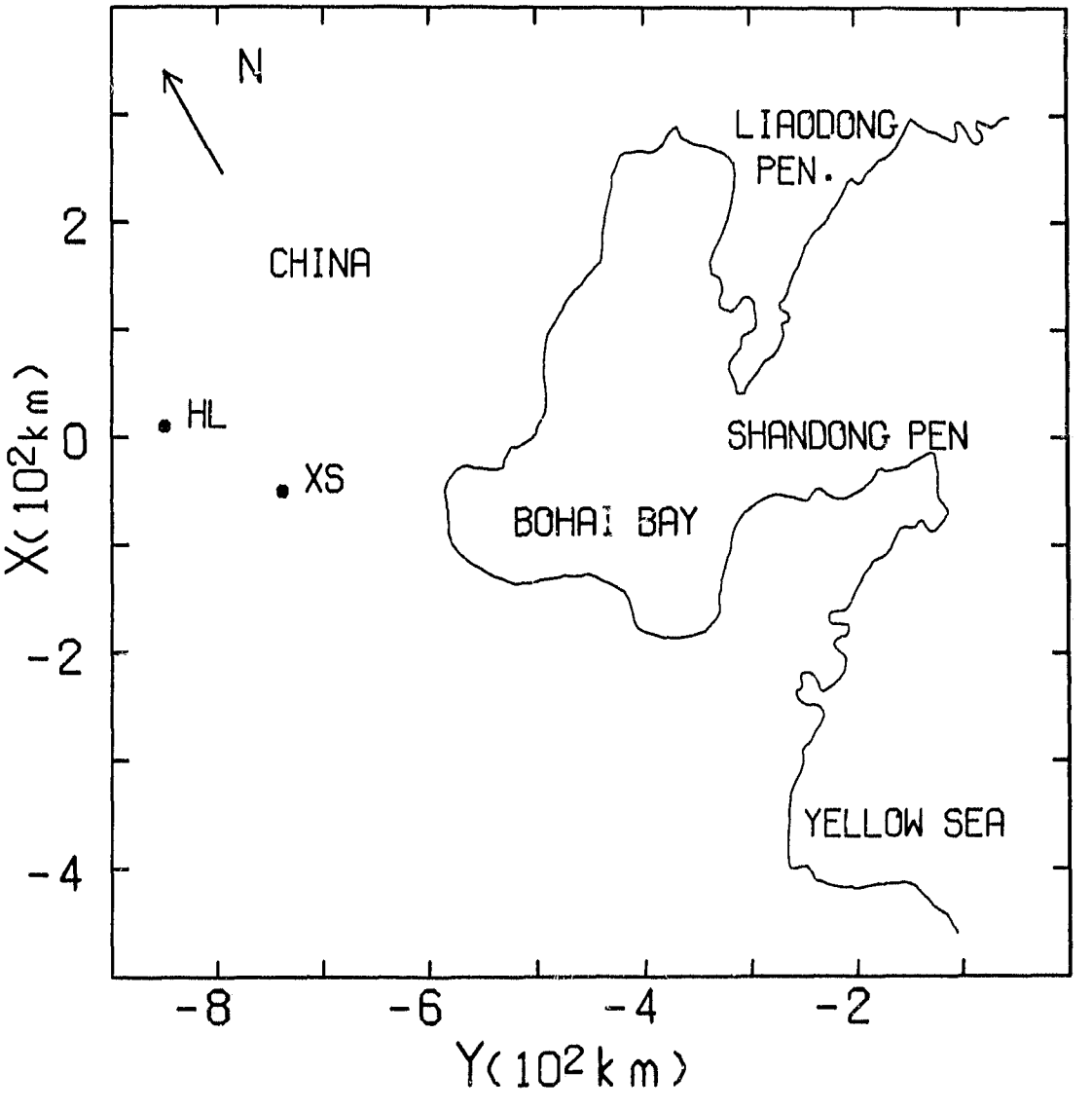

Figure 6.5: A simplified map of the Bohai Bay region showing the locations of two MT field sites, XS and HL.

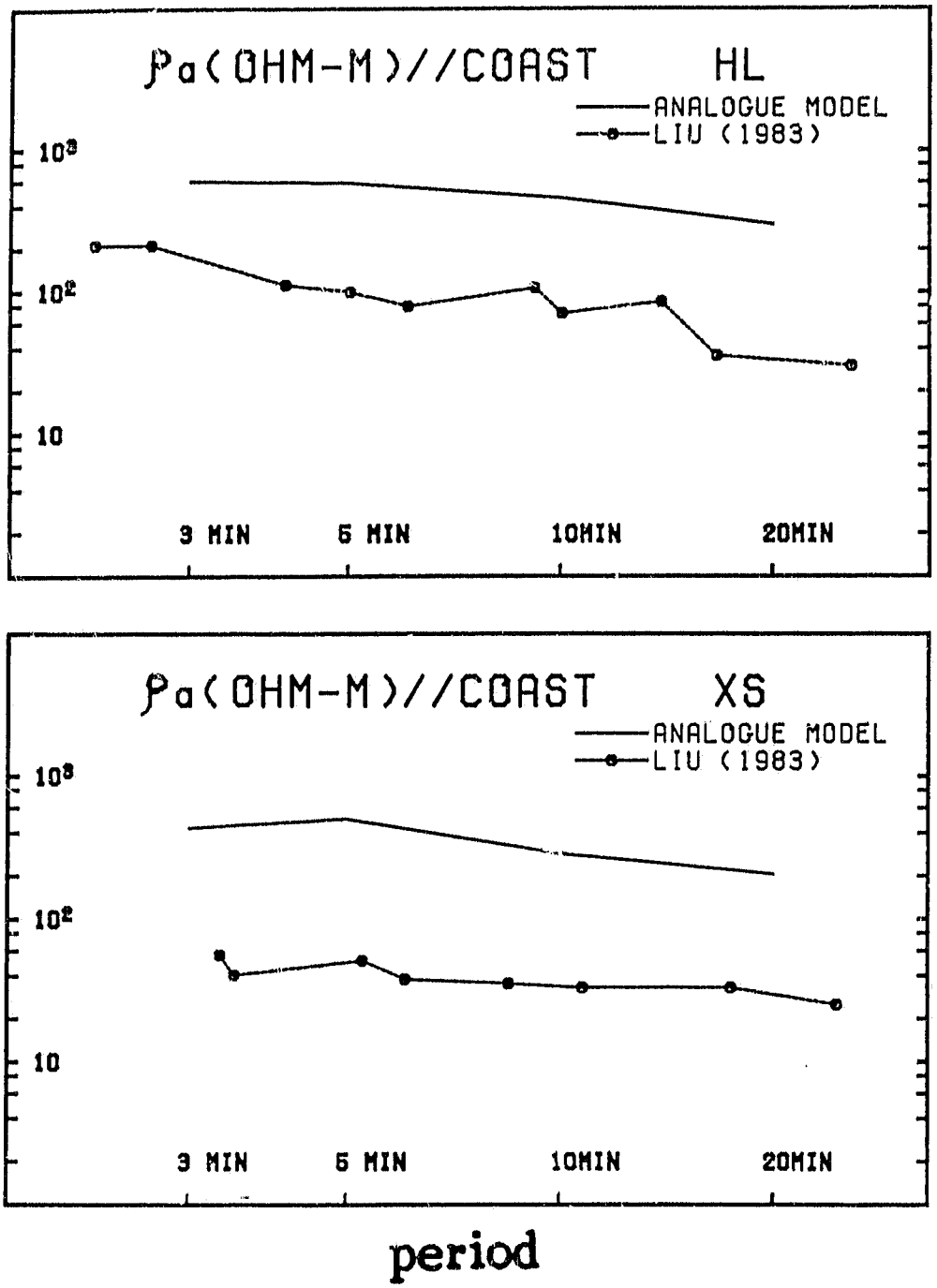

Figure 6.6: Analogue model and field site apparent resistivities at sites XS and HL.

directly over the anomalous conductor suggested in the 2D model of Fig. 6.1. A simulation of such a conductor in the analogue model, would considerably reduce the model apparent resistivities, particularly at the long periods. In conclusion, the comparison of the analogue model MT and field site MT results do support the premise of a conductive anomaly with a N-S strike to the west of Bohai Bay.

6.4 The Chapter Summary

With the coast effect, as typified by the model arrows, removed from the Bohai Bay field site arrows (Chen, 1974; IGSSB, 1986 and Kao, 1990) through subtraction, the resulting difference arrows indicate a N-S striking conductor to the west of Bohai Bay. Two dimensional numerical calculations support the premise of a conductor, in the form of an upwelling in the conductive substratum (with conductivity 0.5 Sm^{-1} at 80 km depth), situated at about 150 km from the Bohai Bay coastline to account for the field site observations. A comparison of the analogue model and field site MT results at two sites west of Bohai Bay shows that the model apparent resistivities are about an order of magnitude greater than the field site apparent resistivities. This result supports the premise of a conductive anomaly, in addition to the conductive substratum at 80 km depth.

Chapter VII

ANALOGUE MODEL AND FIELD SITE RESULTS FOR THE JAPAN REGION

7.1 Introduction

Field MT and GDS measurements have been extensively carried out in Japan in the past few decades, and various geomagnetic variation anomalies have been discovered. A large portion of the anomalies can be attributed to the ocean effects, namely island and peninsula effects (Honkura, 1971; 1974), however, there is evidence that conductivity anomalies do exist in the upper mantle beneath the Japan Islands, and that some of these anomalies also account for the anomalous distributions of heat flow and seismic wave velocity (e.g. Rikitake, 1969; Honkura,1974; Utada et al., 1986; Ogawa et al.,1986). Extensive 2D numerical models were investigated in these studies in order to delineate the regional coast effects, and thus to permit interpretation of EM field measurements in terms of anomalous conductivity structure. The effects of 3D conductivity features are certainly expected to be important for some areas of Japan, such as the irregular coastlines, straits, and peninsulas. In addition to these small-scale 3D features, the arc-shape of the Japan islands would significantly enhance induced current density in the Pacific Ocean and reduce current density in the local Japan Sea due to the cape and bay effects respectively (Chapter 4). Thus, the Pacific Ocean effect is expected to be important over the entire Japan Island region, particularly at longer periods. Such effects obviously can not be adequately modelled by a 2D model.

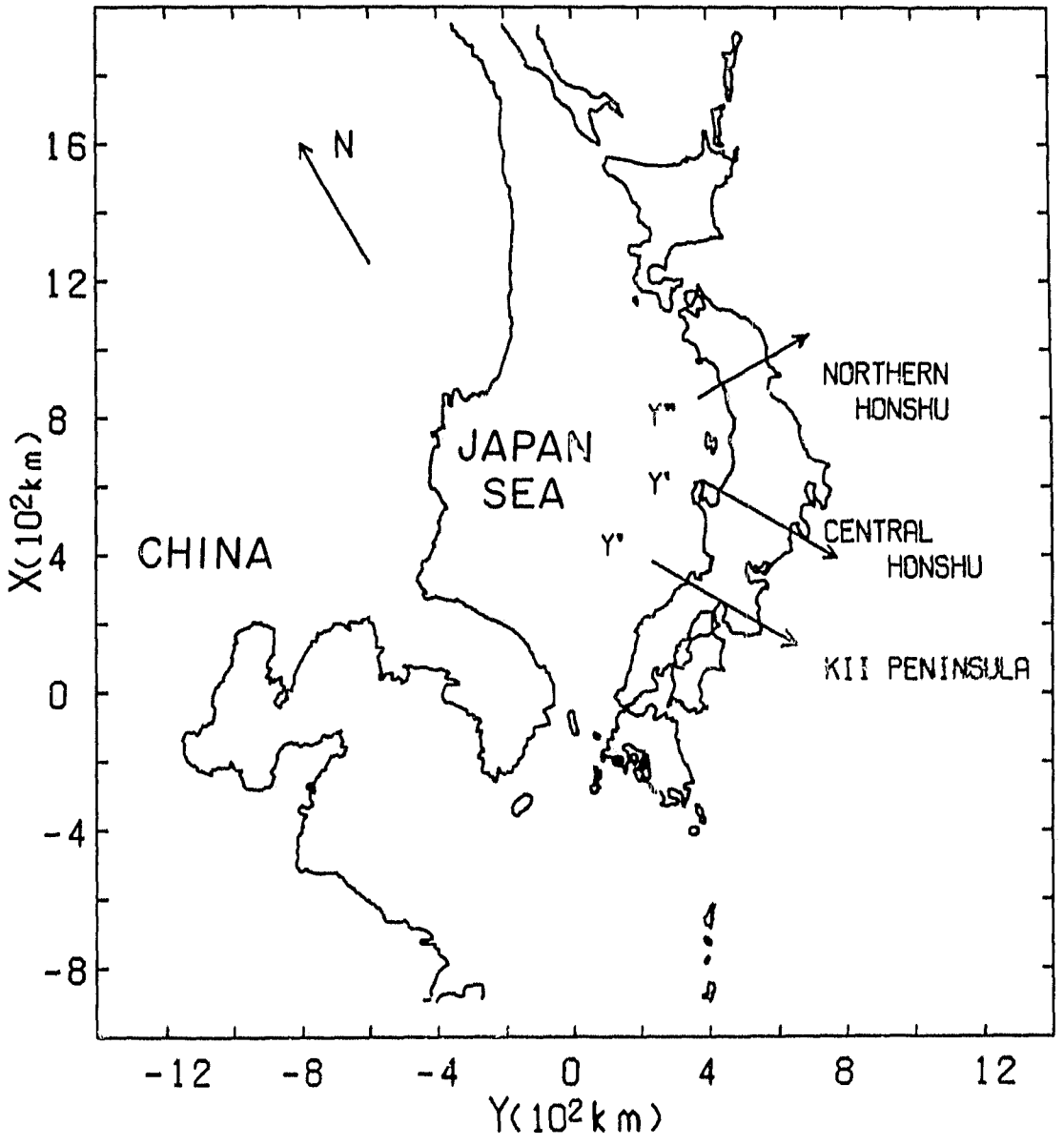

Figure 7.1: Simplified map of the China-Korea-Japan region showing 2-D profiles in the Kii Peninsula, Central Honshu and northern Honshu regions.

In the present chapter, the 3D analogue model measurements of the Japan region (discussed in detail in Chapter 4) will be compared with field site measurements available in the Japan Island regions. As well, difference induction arrows, obtained by subtracting the 3D laboratory analogue model coast effect responses from field site responses, are employed as an aid in the interpretation of the induction arrow responses. Figure 7.1 shows a map of the Japan-Korea-China coastal region with several profiles where field site measurements are available. These include the Kii Peninsula and centra Honshu regions (Sasai, 1969; Miyakoshi, 1979; Honkura, 1974; Yukitake, 1984 and Utada et al., 1986), and the northern Honshu and Hokkaido regions (Tanaka, 1972; RGCRSJ, 1983; Ogawa, 1986; Nishida and Kuboki, 1972). Two parallel profiles (y'-direction) traversing the Kii Peninsula and central Honshu regions form an angle of -30° relative to the y-direction, while a third profile (y"-direction) traversing the northern Honshu region forms an angle of $+30^{\circ}$ relative to the y-direction as shown in Fig. 7.1.

7.2 Induction arrows in the Japan region

7.2.1 The central Japan region

Since Rikitake and Yokoyama (1953) pointed out the anomalous behavior of the vertical component of geomagnetic variation at short periods in the Central Japan region, various field and numerical studies have been conducted to investigate the subsurface conductivity structure in the region. Sasai (1969) carried out a 10 site field study at the Kii Peninsula in the southwest coast (Pacific Ocean) of Central Japan. It was found that the magnitudes of the induction arrows at some sites were unexpectedly large (larger than unity), which, according to Honkura

(1974), can not be explained by the peninsula effect alone. Based on the field data of Sasai (1969), Honkura (1974) postulated a conductive anomalous structure subducting under the Pacific Ocean. Similarly, in the southwestern region of Central Japan, field measurements have focused on the investigation of an anomalous conductivity structure beneath the Japan Sea (Sumtomo, 1972; Miyakoshi 1976, 1979). In an attempt to interpret the behavicur of the field induction arrows in the region, Miyakoshi (1976, 1979) proposed a conducting layer at a depth of 30 km (or so), beneath the Japan Sea and extending further to the south. For the same purpose, the Research Group for Crustal Resistivity Structure, Japan (RGCRSJ, 1983) carried out a magnetometer array study at 16 sites in the Central Honshu region (Yukitake, 1984). In addition to these land based studies, geomagnetic field measurements on the sea floor off the southwestern coast of Central Japan have been carried out by Segawa et al., (1982). More recently, field measurements together with sea floor measurements, were carried out by Utada et al. (1986). In that study, geomagnetic transfer functions were obtained at 21 sites on land and 7 sites on the sea floor for periods between 15 and 120 min. A 2D conductivity model was proposed in the interpretation of the 3-component geomagnetic field data.

7.2.2 The Kii Peninsula region

The analogue model in-phase induction arrows, together with the field site induction arrows for the Kii Peninsula region (Sasai, 1969), are shown in the upper left of Fig. 7.2. The results generally show very good agreement between model and field site arrow directions, with all arrows directed towards the ocean, as would be expected for a typical coast effect. Further, the peninsula (or cape)

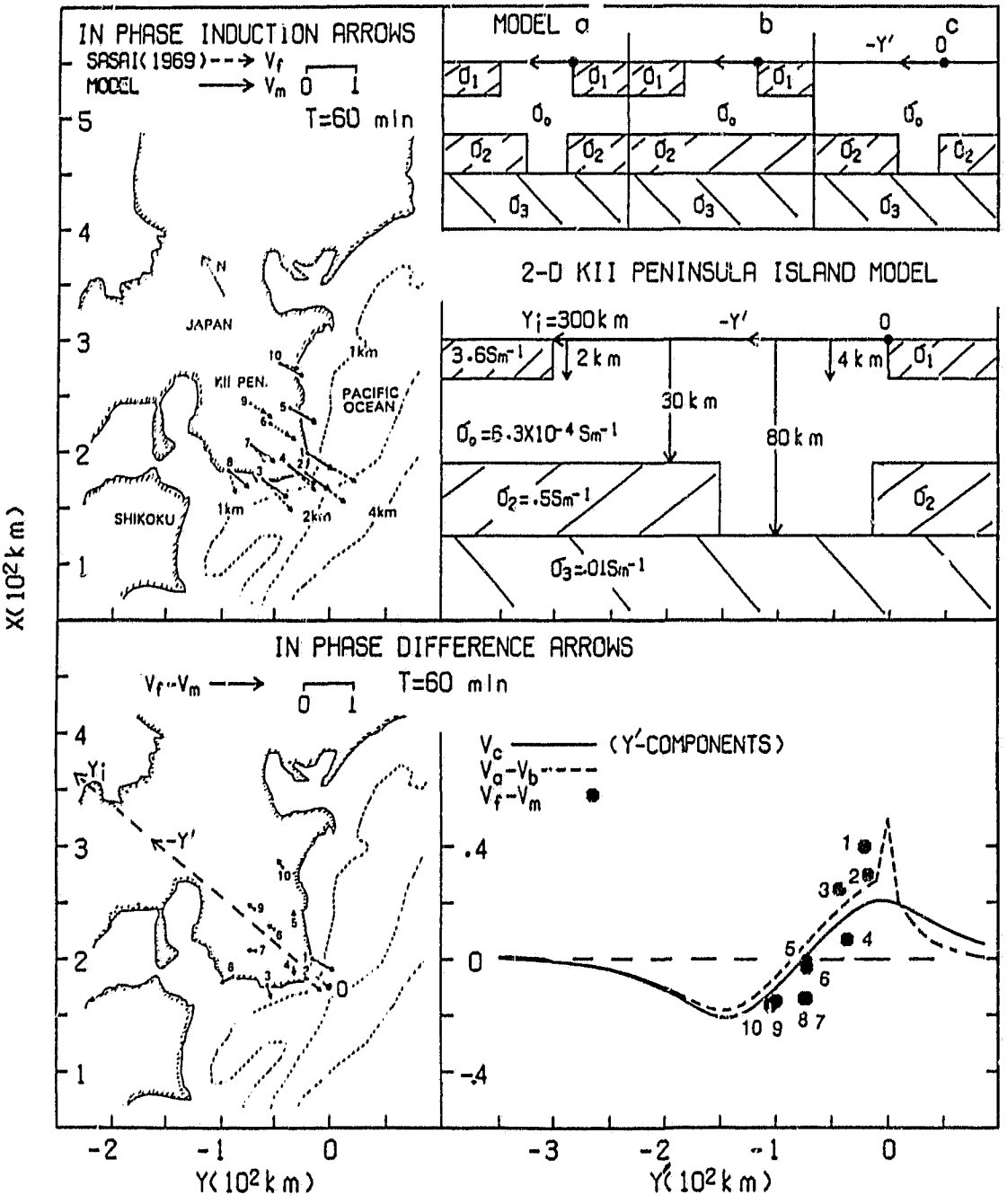

Figure 7.2: Analogue model V_m and field site (Sasai, 1969) V_f and difference (V_f-V_m) induction arrows, and the 2-D model for the Kii Peninsula region.

effect should, as observed, lead to enhanced magnitudes. However, there are considerable differences in the analogue model and field site arrow magnitudes, with the field site arrow magnitudes at the tip of the peninsula (e.g. sites 1 and 2) being 30-50% larger than the model arrows, and at the inland sites being roughly 20-30% smaller. Since the analogue model simulates only the effects of the surrounding oceans over a conductive horizontal substratum at depth (80 km), the differences between the field site arrows and the model arrows should be indicative of other lateral conductivity anomalies not included in the analogue model. For example, for the 2D model of Utada et al. (1986), a coastal 2D conductor at moderate depth (roughly perpendicular to the observed arrow direction) would have the effect of enhancing the coastal arrows to lengths greater than expected for a peninsula effect alone, while a second parallel subsurface conductor in the central region of the island (to yield a response oppositely directed to that due to the coast effect) should lead to shorter arrows than expected for a peninsula effect at field sites somewhat inland.

The difference arrows (V_f-V_m) are shown in the lower left of Fig. 7.2. It is seen that the seaward directed difference arrows at sites 1 and 2 support a model of a nearby anomalous 2D conductor beneath the coastal (or near off-shore) region, and the landward directed difference arrows at the inland sites 6, 7, 9, and 10 support the response to be expected for a nearby anomalous conductor beneath the central region of the island. The very small responses at sites 4 and 5, intermediate between the coastal and inland sites, would indicate roughly equal responses of an inland conductor to the left and a coastal conductor to the right. The arrow directions at sites 3 and 8, generally not parallel to the others at the coast-

al or inland sites, could be accounted for by an arc-like (rather than 2D) coastal conductor.

Included also in Fig. 7.2 are 2D models (a, b, c) and numerical result (V_c) for model c, a model that might represent a 2D approximation of the two conductive anomalies in the Kii Peninsula region. The y'-direction of the profile is roughly perpendicular to the geological trend of the region and forms an angle of -50° relative to the y-direction. In the numerical models, the conductivities of the host, the conductors and the conductive substratum are taken to be 6.25×10^{-4} Sm^{-1}, 5×10^{-1} Sm^{-1} and 10^{-2} Sm^{-1} respectiveiy. The 80 km depth of the substratum and the 30 km depth of the upwelling conductors, one beneath the Japan Sea and one beneath the Pacific Ocean, are based on the 2D model of Honkura (1975). The Japan Sea to the west and the Pacific Ocean to the east are taken to be uniform depth oceans, with depths of 2 km and 4 km respectively. In the model, the ocean extends 1000 km beyond the east coast and 800 km beyond the west coast of Japan, distances that are sufficiently great that these boundaries should not affect the coastal responses understudy. The y'-components of the in-phase numerical induction arrows (V_c) for model c (upper right of Fig. 7.2) that does not include the ocean, the numerical difference arrows ($V_a - V_b$), obtained by subtracting the induction arrows of model b (V_b) from the induction arrows of model a (V_a), and the field-model difference arrows ($V_f - V_m$) are also shown in the lower right of Fig. 7.2. The numerical difference arrows ($V_a - V_b$) generally show good agreement with the numerical induction arrows (V_c) over the entire range except right at the coast of the Pacific Ocean and over the oceans. The field - model difference induction arrows ($V_f - V_m$) at this 60 min period generally show reason-

able agreement with the model c numerical results, supporting the interpretation of both onshore and offshore upwelling conductive anomalies at depth, anomalies that would generally support the Pacific plate subduction beneath Japan.

Figure 7.3 and 7.4 respectively show in-phase and quadrature field (V_f) induction arrows and the field - model difference arrows (V_f-V_m) for two sites (Utada et al., 1986) in the same Kii Peninsula region as described in Fig. 7.2. The in-phase difference arrow results for 30 min and 60 min clearly support the interpretation of both an off-shore and an inland conductive anomaly at depth as described for Fig. 7.2. The in-phase difference arrows at the coastal site for both 15 and 120 min also support the interpretation of a conductor beneath the peninsula coastline region, but at the inland site the difference arrows at the short and long periods, do not provide as definite an indication of an inland conductor. At the shortest period, any near surface geological features not included in the model, would be expected to be important in the response, while at 120 min the model and field site arrows, being essentially identical at the inland site, could be interpreted as due to approximately equal and opposite responses of the coastal and inland conductors at this particular period, resulting in the field induction arrows showing the ocean response only. The quadrature difference arrows in Fig. 7.4 also support the interpretation of the two conductive anomalies, although at the inland site the difference arrows are very small.

Figure 7.5 shows the in-phase model induction arrows V_m, the field site induction arrows V_f and the difference arrows (V_f-V_m) at the Kii Peninsula region (Sasai, 1969; Utada et al., 1986), the southwest region of the central Japan (Miyakoshi, 1979) and the central Honshu region (Honkura, 1974). The induction arrows

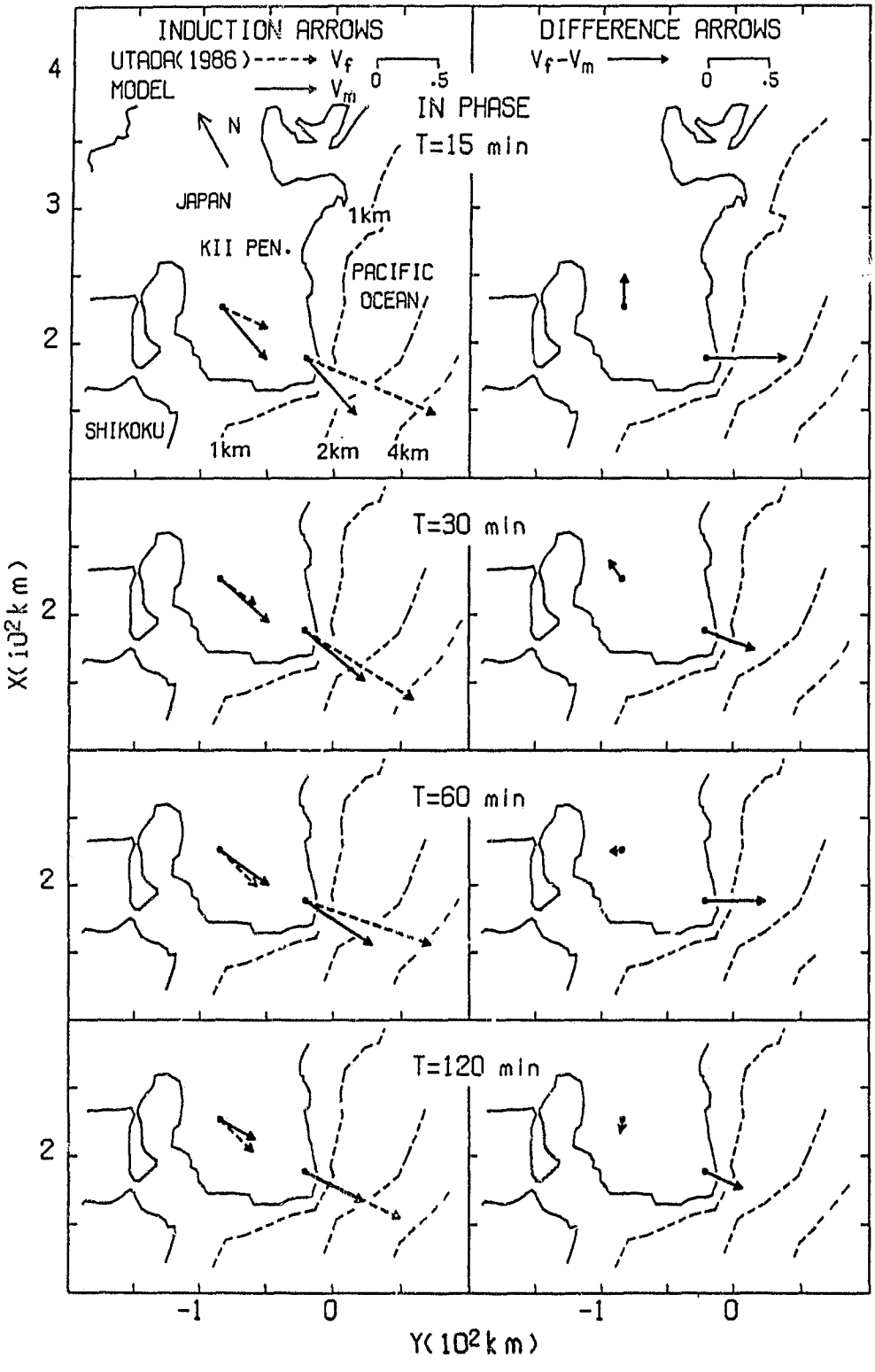

Figure 7.3: Analogue model V_m and field site (Utada et al.,1986) V_f and difference (V_f-V_m) in-phase induction arrows for the Kii Peninsula region.

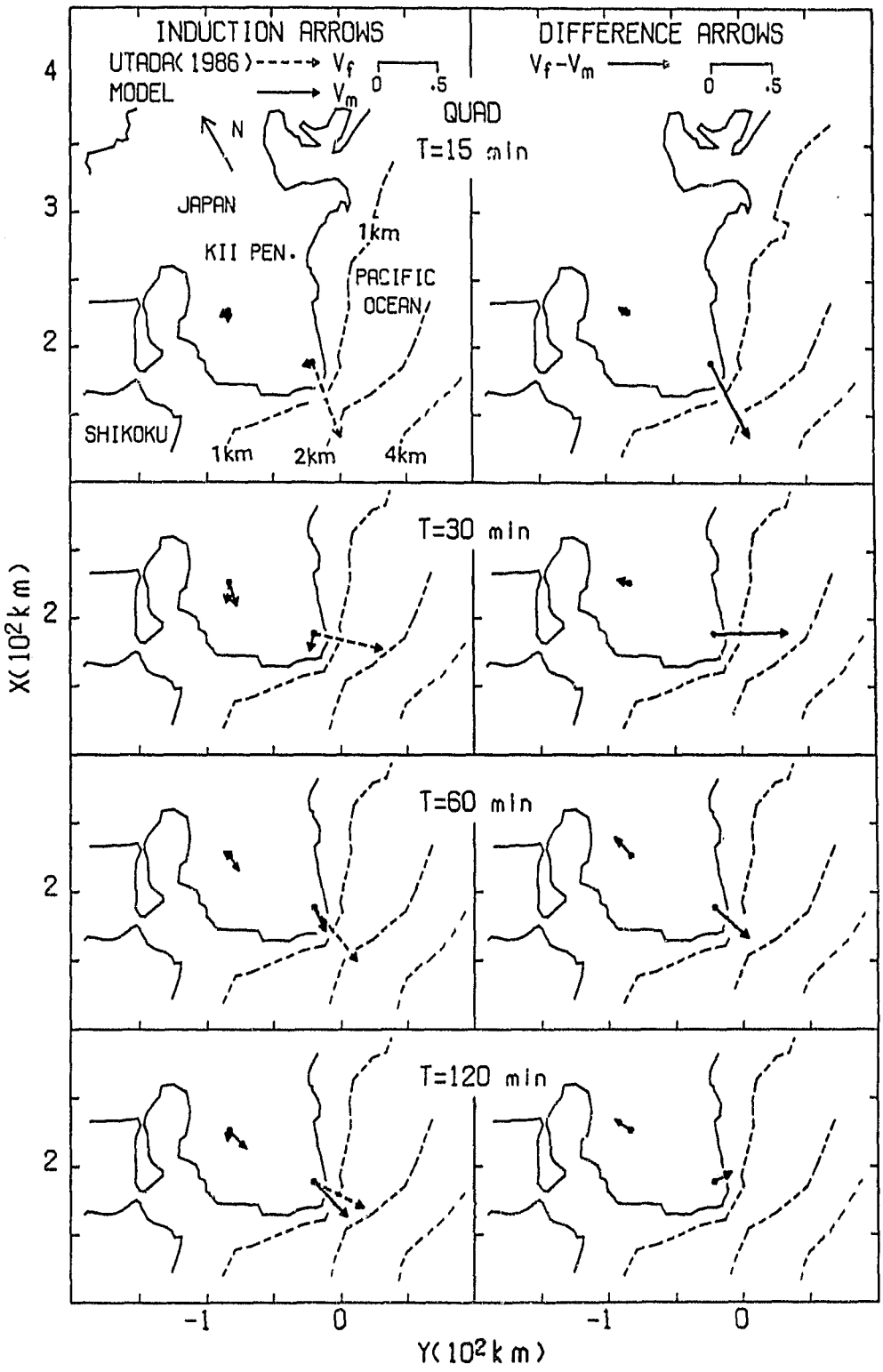

Figure 7.4: Analogue model V_m and field site (Utada et al.,1986) V_f and difference (V_f-V_m) quadrature induction arrows for the Kii Peninsula region.

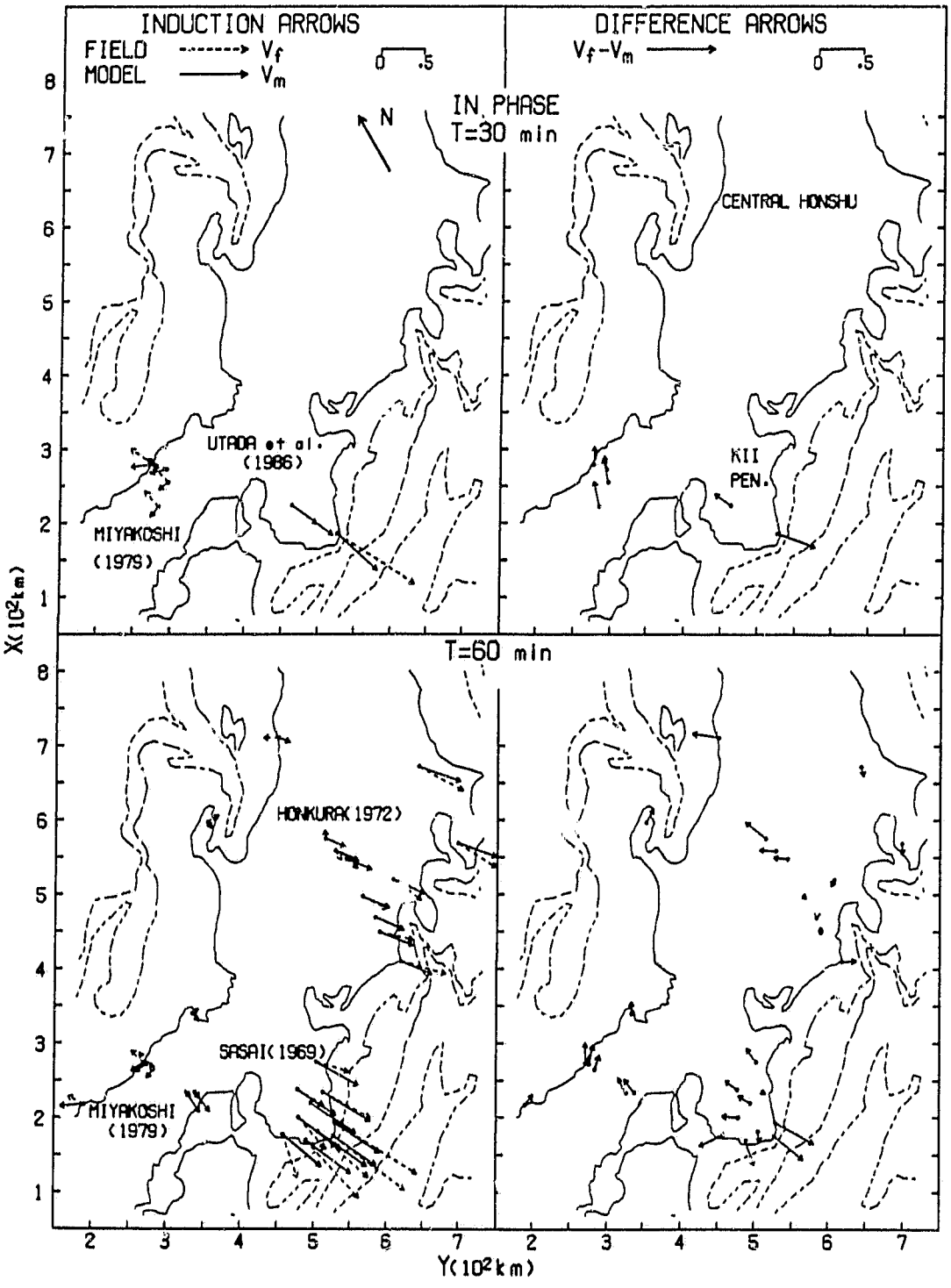

Figure 7.5: Analogue model V_m and field site V_f and difference (V_f-V_m) in-phase induction arrows for the Central Japan region.

of 60 min at the Kii Peninsula, though already shown in Fig. 7.2, are included to show the general trends of the induction arrow responses for the full width of the island. A conductivity structure in which one conductor beneath the Pacific Ocean and a second under the central island was proposed in Fig. 7.2 for the Kii Peninsula region. If the 2D model (Fig. 7.2) supported by the difference arrow results (obtained by substrating the analogue model induction arrows from the field induction arrows of Sasai, 1969), is realistic, it should also be supported by other independent field measurements in the region. For the sites of Miyakoshi (1979) near the western coast, substantial differences between the model and field site arrows are observed, with the model arrows rotated from south to southwest as the coastline is approached, indicating the effect of current channelling through the the Japan-Korea strait. Further, the field site arrows generally pointing towards the Japan Sea, are enhanced in magnitude.

In Fig. 7.5, it is seen that, for locations on the west coast (Miyakoshi, 1979), the difference arrows ($V_m - V_f$) at the 2 sites near the central region of the island are roughly parallel to those of Sasai (1969) at inland sites, and have approximately equal magnitudes, suggesting that the vertical interface of the conductor could be located somewhere between these sites, while the somewhat northward directed difference arrows at the Japan Sea coast indicate that the conductor may extend to the Japan Sea. the difference arrows at 30 min, in general, are consistent with those at 60 min, except that the magnitudes of the arrows at 30 min at the west coast are slightly enhanced relative to those at 60 min.

At the field sites of Honkura (1974) in the central Honshu region (about 100 km northeast of the Kii peninsula), it is seen that the field site arrows agree very

well with the model arrows at the easterly coast, but the field site arrow are much smaller the than model arrows at the central island region, which is similar to that observed at the Kii Peninsula (Sasai,1969) in Fig. 7.2, where the interpretation was that of two conductive anomalies, one beneath the Pacific Ocean and one beneath the central region of the island.

Generally, the difference arrows in Figs. 7.2, 7.3 7.4 and 7.5 for the Kii Peninsula region appear to be valid responses of the conductive anomalies, with the ocean-conductive anomaly separation distances being sufficiently large (as supported by an interpolation of the results of Figs. 5.8 and 5.9) for minimal electromagnetic coupling with the ocean. It is noted that σ_2 in the Kii Peninsula numerical model (Fig. 7.2) is a factor of 5 greater than was the case for the idealized models of Figs. 5.8 and 5.9, and calculations carried out (not shown) for a factor of 5 increased conductivity for the conductive substratum in the idealized models, indicated a resulting sharp decrease in response range with increasing conductivity.

In comparing the present 2D model (shown in Fig. 7.2) with models proposed by others in earlier work as shown in Table 7.1, it is noted that the existence of a conductor ($0.5 Sm^{-1}$) at a depth of 30 km beneath the Pacific Ocean agrees with the models of Honkura (1975) and Utada et al. (1986). It was pointed out by Filloux (1980) that, a layer with conductivity of 0.1 - 0.5 Sm^{-1} at a depth of 30 km is commonly observed beneath a moving oceanic plate. It is believed that this depth corresponds to the top of the asthenosphere (Filloux, 1980; Oldenburg, 1981). The highly conductive structure beneath the Japan Sea in the present model, agrees with the results of Honkura (1975), except that the conductor in the present model

the models of Honkura (1975) and Utada et al. (1986). It was pointed out by Filloux (1980) that, a layer with conductivity of 0.1 - 0.5 Sm^{-1} at a depth of 30 km is commonly observed beneath a moving oceanic plate. It is believed that this depth corresponds to the top of the asthenosphere (Filloux, 1980; Oldenburg, 1981). The highly conductive structure beneath the Japan Sea in the present model, agrees with the results of Honkura (1975), except that the conductor in the present model extends further inland. The conductive anomaly, according to Honkura (1975), could be attributed to the observed high heat flow, implying a high temperature state and possibly the existence of partial melting at depth beneath the Japan Sea. It is noted that the two conductors (σ_2 = .5 Sm^{-1}), one beneath the Japan Sea and the other beneath the Pacific Ocean, together with the highly conductive substratum (σ=0.01 Sm^{-1}) at 80 km depth (shown in Fig. 7.2), form a depression in the conductive substratum, a structure which agrees in principle with the Rikitake (1969) model, although the shape of the depression and the conductivity of the substratum differ from those in Rikitake's model, where the conductivity of the substratum was taken to be infinite.

Table 7.1. 2-D Conductivity Model For The Kii Peninsula And Central Honshu

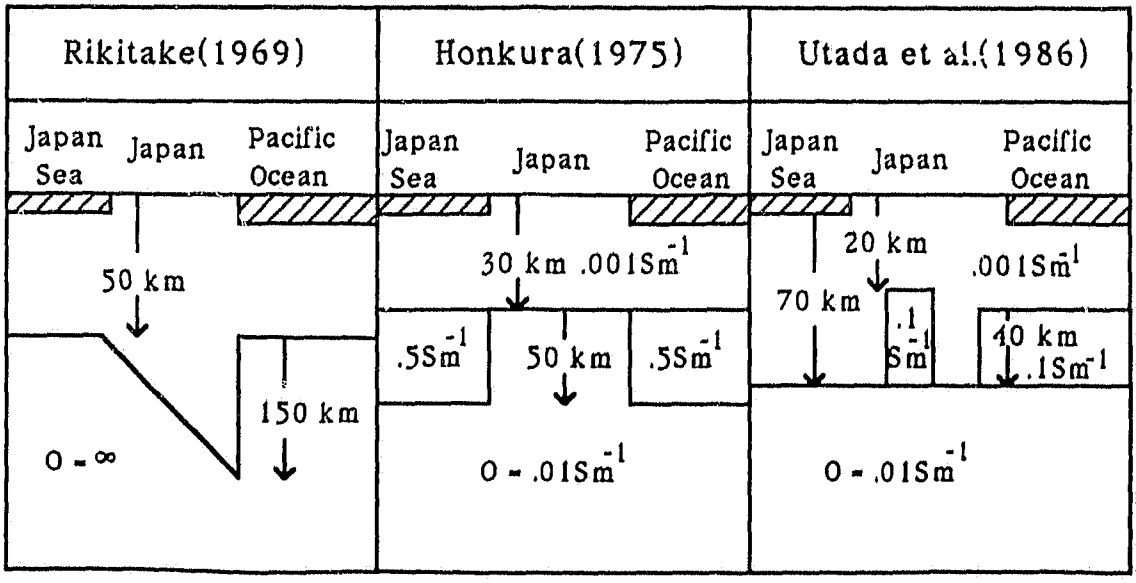

7.2.3 The Central Honshu Region

Figures 7.6 and 7.7 respectively show the in-phase and quadrature model and field site (Utada et al. 1986) induction arrows and the difference arrows at the central Honshu region about 100 km north east of the Kii Peninsula for a period range of 15 to 120 min. In the Utada et al. (1986) study, sea floor measurements were included at seven off-shore sites. However, the sea floor results are not included here, since the sea floor measurements are not simulated in the present analogue model measurements. In Fig. 7.6, all the in-phase field site arrows for the period range 15 -120 min point to the southeast, roughly normal to the general trend of the Pacific Ocean coastline, with large amplitudes. The analogue model and field site in-phase induction arrows show good agreement in direction, with less than 10^{o} difference for all but a few sites, indicating that the Pacific Ocean has an important effect on the field measurements. However, the field site amplitudes are generally larger than the model arrow amplitudes, supporting the premise of a conductor at depth beneath the Pacific Ocean (which is not simulated in the analogue model) that enhances the field induction arrows beyond that expected due to the Pacific Ocean coast effect alone. It is interesting to note that the field site induction arrows at stations further inland are generally smaller than the model arrows. A similar situation was observed at the Kii Peninsula (Figs. 7.2-7.5), which was interpreted as being due to the response of a conductor at depth in the central island region competing with the response of a conductor beneath the Pacific Ocean, stated otherwise, due to the effects of a depression in the conductive substratum as shown in the numerical model of Fig. 7.2. Since the field sites of Utada et al. (1986) are only about 100 km from the field sites of the

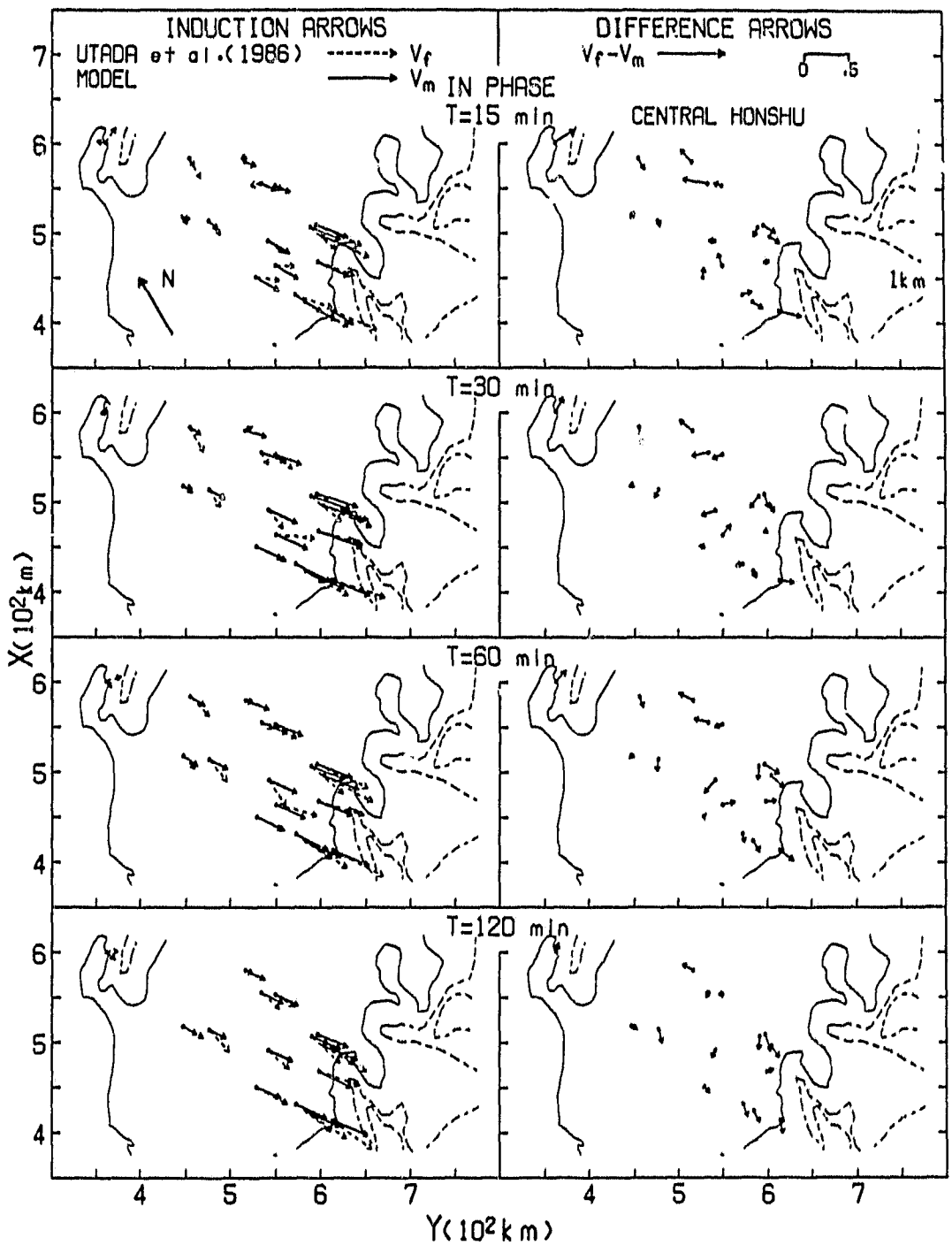

Figure 7.6: Analogue model V_m and field site (Utada et al.,1986) V_f and difference (V_f-V_m) in-phase induction arrows for the central Honshu region.

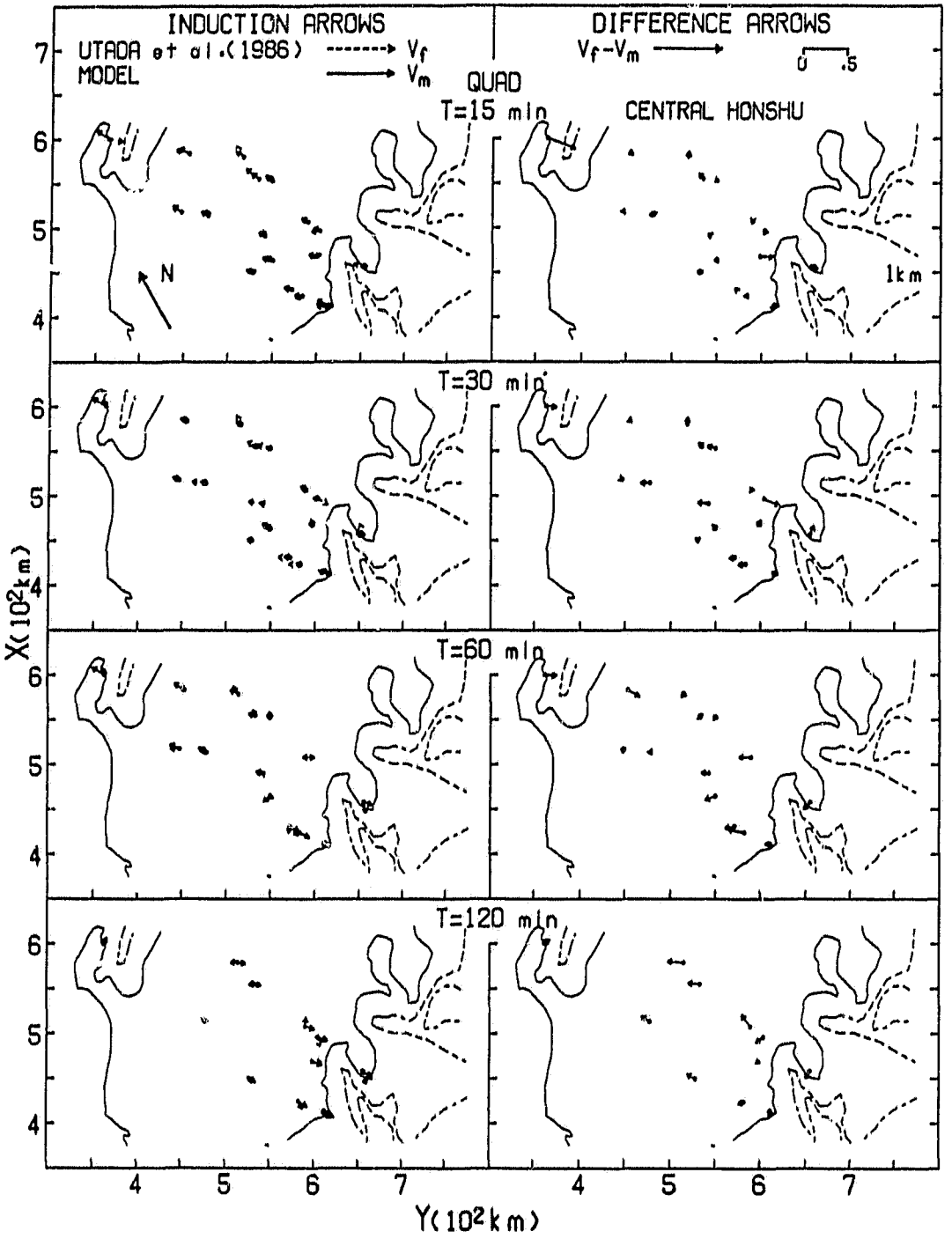

Figure 7.7: Analogue model V_m and field site (Utada et al.,1986) V_f and difference (V_f-V_m) quadrature induction arrows for the central Honshu region.

Kii Peninsula, it is reasonable to assume that the two anomalous conductive structures at depth in the Kii Peninsula area extend northeast along the general trend of the Japan island to the central Honshu region. Although most of the in-phase field arrows at the field sites in the central island and near the Japan Sea, are pointing towards the Pacific Ocean, indicating a predominating Pacific Ocean coast effect over the Japan Islands (as shown by the model arrows), there are significant discrepancies in direction and magnitude between the analogue model arrows and field site arrows, particularly in the central island region. It should be pointed out that these central island field sites are near Quaternary Volcanics (Utada, et al., 1986) and the discrepancies between the model and field site arrows could be accounted for by high conductivity due to higher temperatures.

For the quadrature components of the induction arrows, it is interesting to note that except at a few sites, both model and field site arrows at 15 min all point towards the Japan Sea rather than towards the Pacific Ocean. This is expected, since the quadrature induction arrows tend to point away from, rather than towards, the major current concentrations at sufficiently short periods as has been pointed out for 2D models by Agrawal and Dosso (1990). As the period increases, it is seen that the model quadrature arrows rotate anti-clockwise from pointing towards the Japan Sea to pointing towards the Pacific Ocean. The field site quadrature arrows in general show fairly good agreement with the model arrows.

Also included in Figs. 7.6 and 7.7 are the in-phase and quadrature difference arrows for periods of 15, 30, 60 and 120 min. In Fig.7.6 at a period of 15 min, it is

seen that southward directed difference arrows near the Pacific coast support the response of a model of an anomalous conductor beneath the Pacific Ocean, and the northward directed difference arrows at inland sites support the response to be excepted for an anomalous conductor beneath the central island region. For longer periods, the difference arrows are fairly consistent with those at 15 min, although with some discrepancies. The quadrature arrows in Fig. 7.7 generally are small in comparison with the in-phase arrows in Fig. 7.6. With increasing period, the quadrature difference arrows are enhanced in magnitude, and tend to point towards the conductor at the central island region.

Figure 7.8 shows in-phase induction and difference arrows for additional 15 sites (Yukitake, 1984) in the same area of the central Japan as described in Figs. 7.6 and 7.7. The difference arrows at locations near the southerly Pacific Ocean coast for the period range 15 - 120 min clearly support the interpretation of a conductor beneath the Pacific Ocean coastal region. The inland difference arrows, pointing in roughly the opposite direction, indicate the effect of an inland conductive anomaly at depth. In general, results for the Yukitake (1984) sites in Fig. 7.8 are consistent with those Utada et al. (1986) as shown in Figs. 7.6 and 7.7.

The 2D model proposed for the central Honshu region is shown in Fig. 7.9. Similar to the case for the Kii Peninsula, the 2D profile (the y'-direction as shown in Fig.7.1) is roughly perpendicular to the geological trend of the region and forms an angle of roughly -50^{o} relative to the y-direction. In Fig. 7.9 the dots represent these y'-components of the difference arrows for the field sites of Utada et al.(1986), denoted as UT(86), the triangles represent those of Yukitake (1984), denoted as YU(84), and the crosses represent those of Honkrua (1974), denoted as

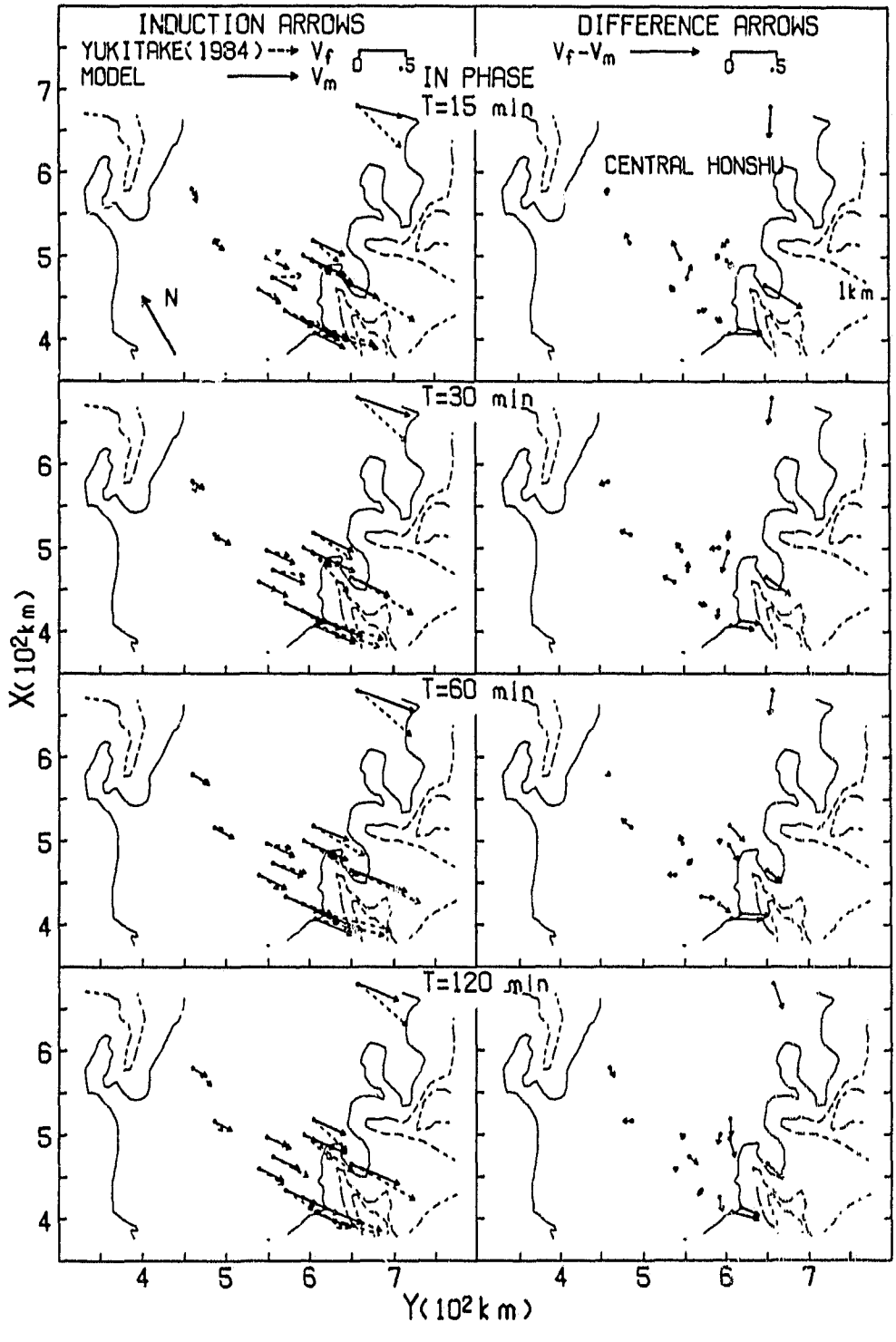

Figure 7.8: Analogue model V_m and field site (Yukitake,1984) V_f and difference (V_f-V_m) in-phase induction arrows for the central Honshu region.

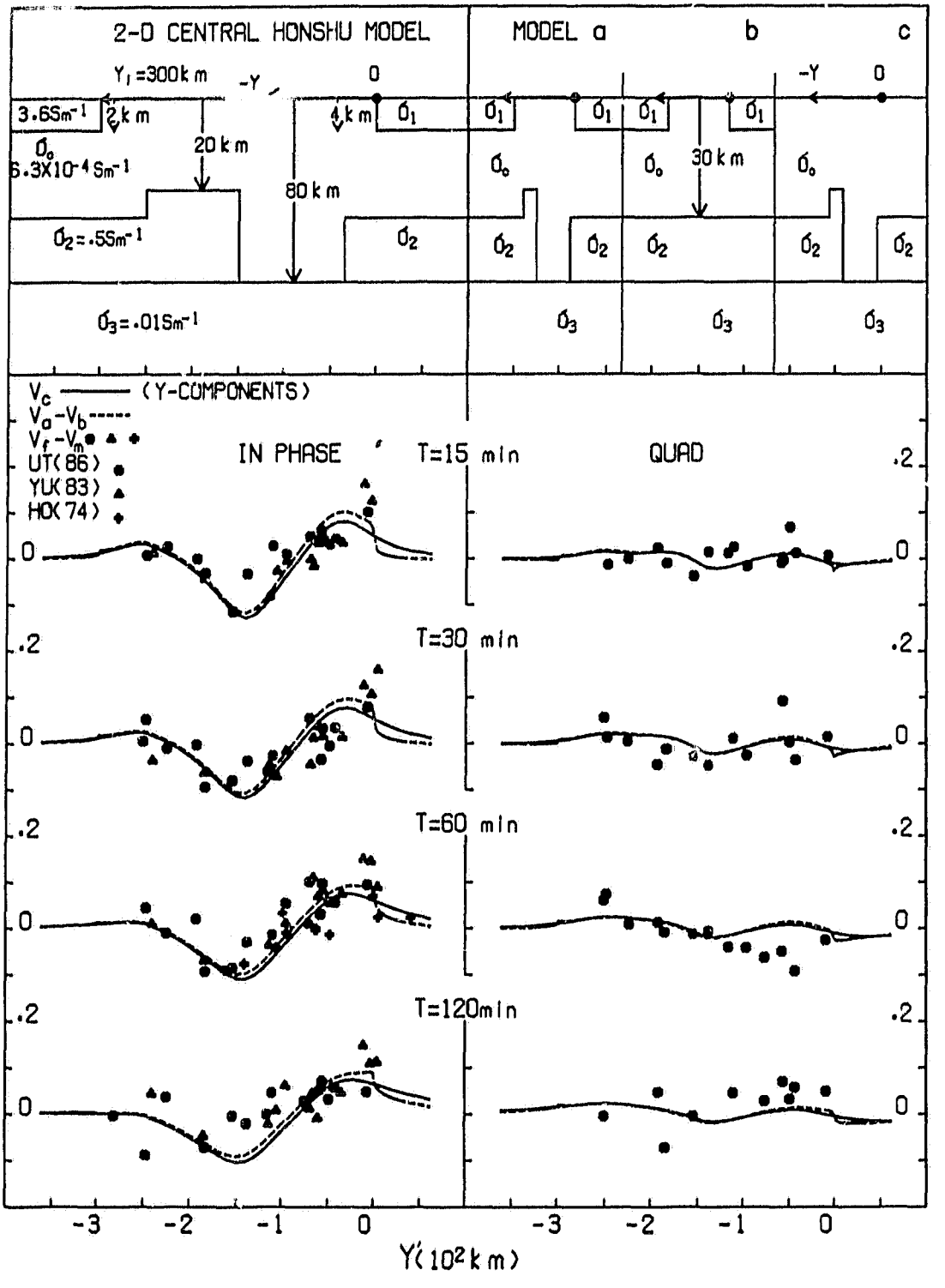

Figure 7.9: The y'-components of 2-D numerical model induction arrows and field-analogue model difference arrows for the central Honshu region.

HO(74). It is seen that the numerical difference arrows (V_a - V_b) generally show good agreement with the numerical induction arrows of model c (V_c) over the entire range over the island, except near the the Pacific Ocean, and over the oceans for all four periods.

In comparing the field site difference arrows with the numerical difference arrows, it is found that they are generally in good agreement, particularly for the in-phase component. Taking the difference arrow responses at 60 min as an example, it is seen that these field difference arrows reach a positive maximum near the Pacific Ocean coast and a negative maximum at approximately the middle of the island, suggesting that the subducting conductor beneath the Japan Sea is extending to the middle of island (about 150 km inland), while the anomalous conductor beneath the Pacific Ocean is subducting a few tens of kilometers inland. For the quadrature component, both the field and the numerical difference arrows are very small, agreeing well with the model c results.

The y'-component of the difference arrows for the central Honshu region behave quite similarly to those for the Kii Peninsula except that the central Honshu induction arrows have smaller magnitudes. This could indicate a smaller separation distance between the two conductors at the central Honshu region, compared with that at the Kii Peninsula, resulting in greater mutual coupling between the two conductors, and thus resulting in reduced vertical magnetic fields. In order to account for the negative responses near the Japan Sea coast (about 50 km from the coastline), an additional conductive anomaly (with conductivity of 0.5 Sm^{-1}) at depth of 20 km as shown in Fig. 7.9 was included in the model. Reasonable agreement between the numerical model V_c and the field difference arrows is

seen over the entire period range. It is noted that Quaternary Volcanics (Utada et al., 1986) exist in this region. This fact, and the present results for the central Honshu region, support the view that the southern edge of the subducting conductor beneath the Japan Sea is coincident with the volcanic front in this region, and suggests there exists a relationship between the volcanic activity and the conductive anomalies.

In summary, there are three significant features in the 2D conductivity model of the central Honshu region. The first is the existence of a highly conductive structure beneath the Pacific Ocean (at as shallow a depth as 30 km) that could be caused by partial melting at the near surface of the asthenospere (Honkura, 1975). The second feature is the existence of an upwelling of the conductive material beneath the Japan Sea, and extending somewhat inland Japan. The observed heat flow is known to be high in the Japan Sea region, implying a high temperature state, and possibly the existence of partial melting (Honkura, 1975). The third feature is that the anomalous conductor at a depth of 20 km beneath the westerly coast of Japan (Fig. 7.9), is coincident with the distribution of the Quaternary Volcanics in the region.

7.3 Northern Honshu, Tsugaru strait, and Hokkaido Region

The northern Honshu of Japan is known as the region with a typical island arc structure. A large amount of geophysical data, such as seismic wave velocity, gravity, heat flow, seismicity and electrical resistivity (Yoshii, 1975), have been accumulated for this region. The geological structure here is comparatively simple, showing almost a 2D character perpendicular to the direction of the island arc

axis (the north-south direction) for much of the Northern Honshu region, except near Tsugaru Strait, where the channelling effects of the strait (connecting the Pacific Ocean and Japan Sea) is strong, particularly at short periods (see Chapter 4).

The resistivity structure of the region has been investigated by a number of scientists, including Kato et al. (1971), Honkura (1974), Yukutake et al. (1983), RGCRSJ (1983), and Ogawa et al. (1986). Kato et al. (1971) employed a 2D model of an anomalous perfect conductor to explain the amplitude ratios of the vertical to the horizontal component of magnetic field observed at 15 sites. In the 2D model, the conductor was taken to be at a depth of 200 km beneath the east coast (Japan Sea), raised to about 35 km west of the volcanic front, (about 80 km west from the Pacific coast). Honkura (1974), employing a 2D model, concluded that for the period range of 10 to 120 minutes, the effect of the ocean is predominant, and thus the field measurements observed along the east-west profile in the northern Honshu region could be explained by the ocean effect alone. However, according to the more recent study of Ogawa et al. (1986), the field responses observed in the region between the volcanic front and the Japan Sea coast are difficult to explain in terms of the coast effect alone. Ogawa et al. (1986) proposed a 2D conductivity model that included conductive layers (with conductivity of $0.01 Sm^{-1}$) situated beneath the Pacific Ocean and the Japan Sea at depths of 80 and 30 km respectively. In addition, a conductor (with conductivity $0.2\ Sm^{-1}$) at a depth of 30 km in the lower crust extended from the Japan Sea to the volcanic front.

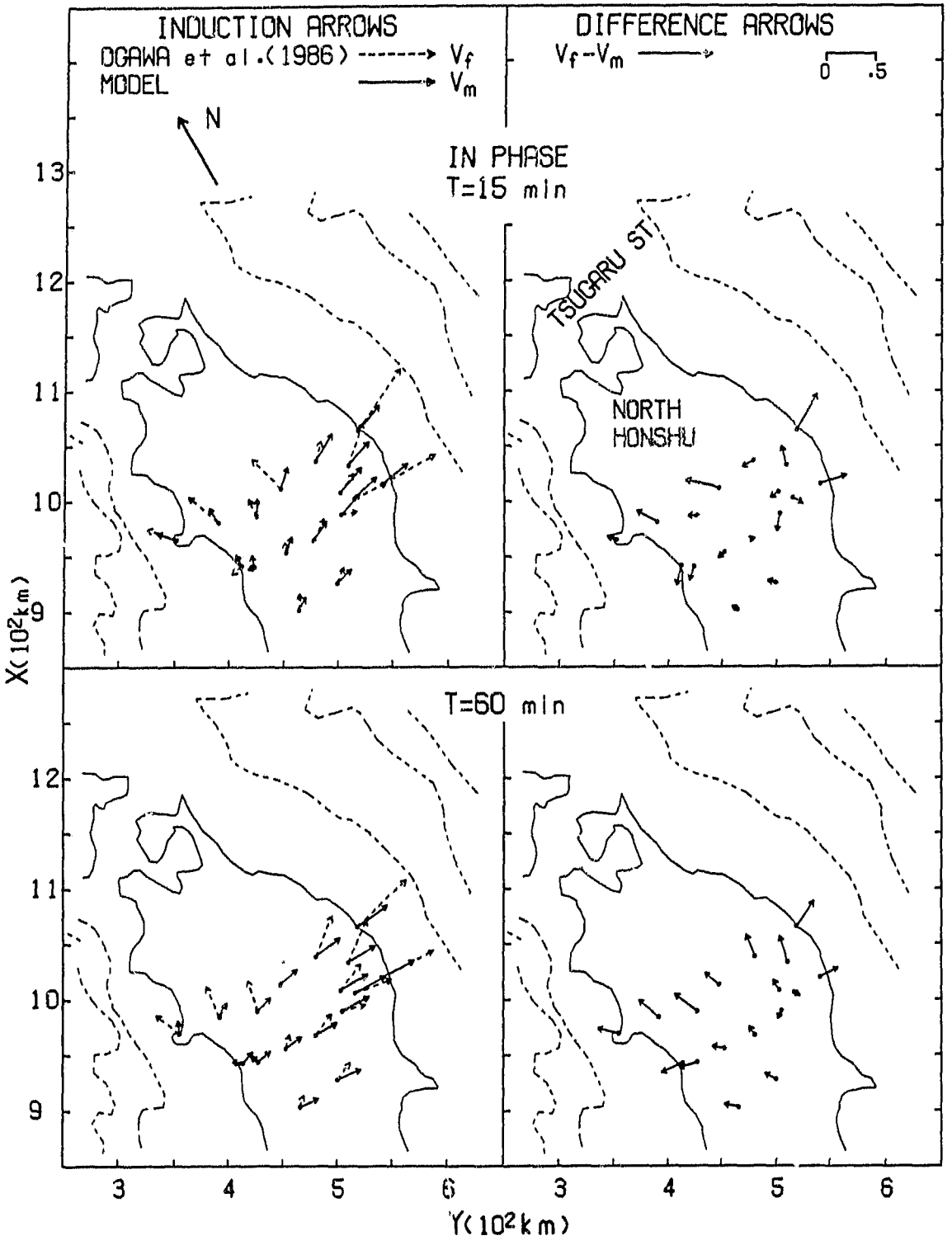

Figure 7.10: Analogue model V_m and field site (Ogawa et al.,1986) V_f and difference (V_f-V_m) in-phase induction arrows for the northern Honshu region.

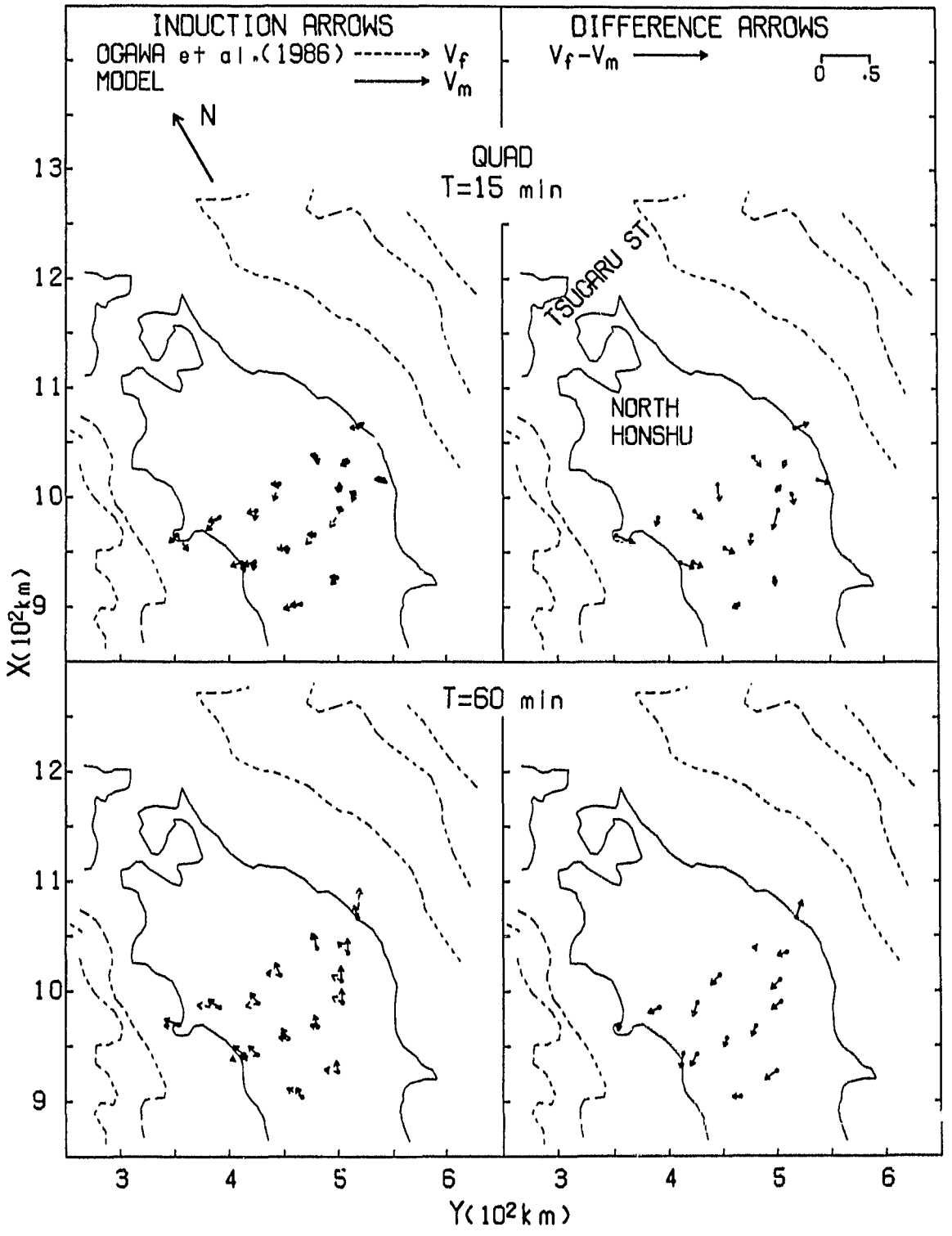

Figure 7.11: Analogue model V_m and field site (Ogawa et al.,1986) V_f and difference (V_f-V_m) quadrature induction arrows for the northern Honshu region.

Figures 7.10 and 7.11 show the field site induction arrows (V_f) of Ogawa et al. (1986), the analogue model induction arrows (V_m) and the difference arrows (V_f-V_m) over the northern Honshu region of Japan at 15 and 60 min for the in-phase and quadrature induction arrows respectively. For the field sites near the Pacific Ocean, the coast effect is clearly observed, with the in-phase field induction arrows behaving very similar to the analogue model arrows, pointing normal to the coastline, however, with much enhanced magnitudes at both 15 and 60 min. In the central part of the island, the in-phase field induction arrows at 15 min period point northward to Tsugaru strait while the model arrows point eastward. The difference between the model and field site arrows becomes more pronounced at the longer 60 min period. For much of the inland region, it is seen that the field site arrows have much larger north components than the analogue model arrows, indicating the effect of current concentration in the east-west direction in the strait to the north. The Japan Sea coast effect is seen to be relatively small for both field and model induction arrows, even near the Japan Sea coast. This is expected since the Japan Sea is a back-arc sea with a bay shaped coastline, thus resulting in reduced current density.

The quadrature arrows show quite a different behaviour from that of the in-phase arrows, with magnitudes much smaller than the in-phase arrows. At the short period of 15 min, it is seen that the field quadrature arrows point westward, to the Japan Sea, while the in-phase arrows here point eastward. This is consistent with the observed behaviour of the quadrature arrows in central Japan. As the period increases to 60 min, both the field and model quadrature arrows have rotated anti-clockwise about 60° to 80°, with the field quadrature arrows now pointing westward and the model quadrature arrows pointing northwards.

In examining the difference arrows in Figs. 7.10 and 7.11, it is seen that in-phase arrows at 60 min point northwards and increase in magnitude further north along the island arc axis, indicating the effect of current concentration in the east-west direction in the northern strait region. If the ocean effect has been removed from the field responses, the difference arrows should indicate the effect of any additional conductivity structure, rather than the channelling effect of Tsugaru strait. According to Nishida (1982), there exists a high heat flow region to the north, thus the northward components of the difference arrows could be attributed to the high conductivity structure beneath Tsugaru strait and the surrounding ocean. For locations near both the Pacific Ocean and Japan Sea, the in-phase difference arrows point perpendicular to the coastlines, indicating the effect of the conductors, one beneath the Pacific Ocean and one beneath the Japan Sea. Similar features are also indicated at 15 min, however the discrepancies between the in-phase model and arrows are increasing with decreasing period, since near-surface conductors may contribute the field responses at short periods. The behaviour of the quadrature difference arrows is consistent with that of the in-phase arrows. At 15 min, the quadrature arrows point southward, opposite direction relative to the in-phase arrows, then rotate to point towards the conductor beneath the Japan Sea.

Figure 7.12 shows the in-phase components of the field site induction arrows (V_f) of RGCRS (1983), the analogue model induction arrows (V_m), and the difference arrows (V_f-V_m) over the northern Honshu region of Japan at 30 and 60 min. The behaviour of the field site arrows are fairly consistent with those of Ogawa et al. (1986). It is seen that the east-west components of the difference arrows

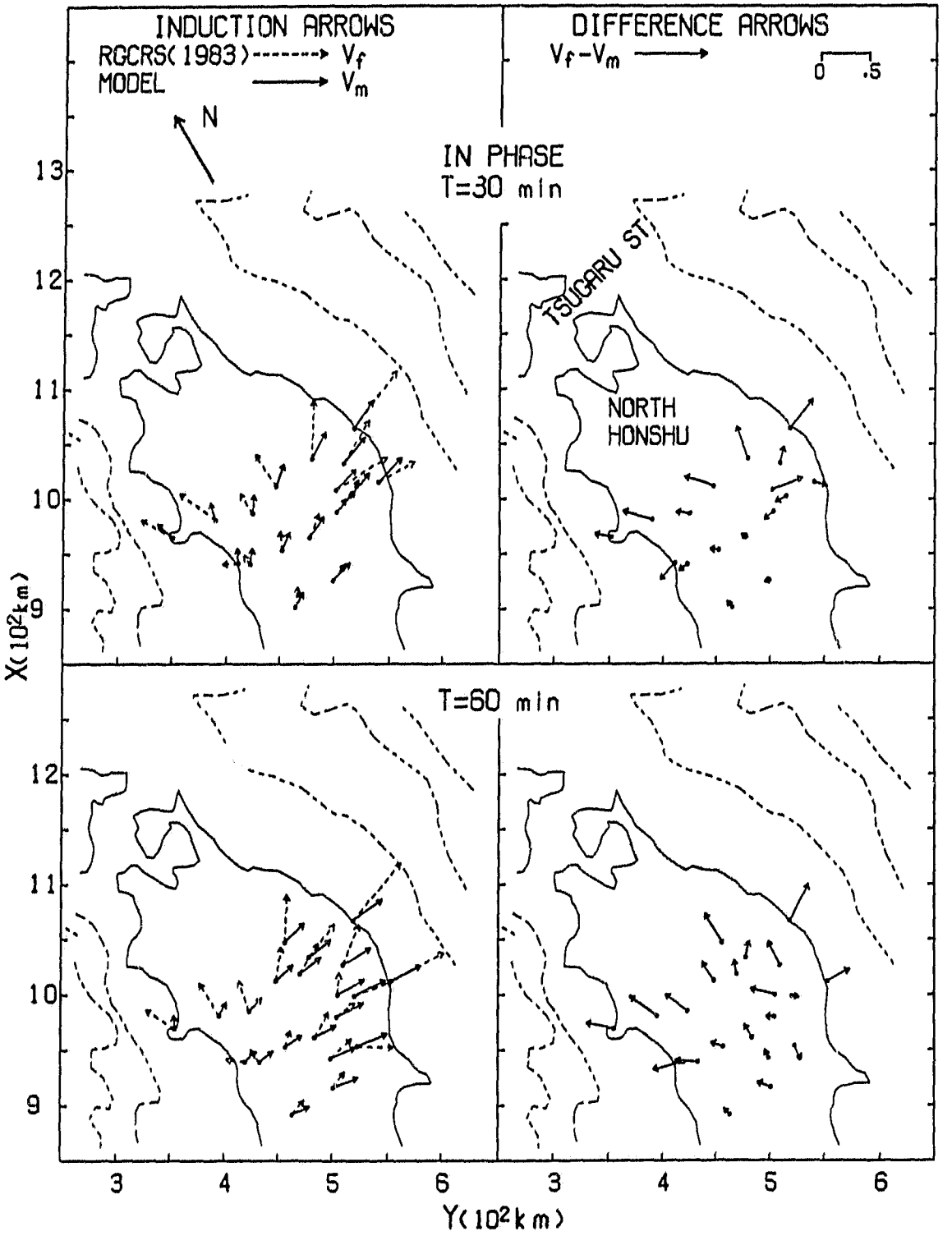

Figure 7.12: Analogue model V_m and field site (RGCRS,1986) V_f and difference (V_f-V_m) in-phase induction arrows for the northern Honshu region.

clearly indicate the effect of two parallel conductors, one beneath the Pacific Ocean and the other beneath the Japan Sea, while the significantly large N-S components of the difference arrows indicate the effect of a conductor beneath Tsugaru strait. It is noted that although the coastlines and the baythmetrey of the region would suggest a 2D model as being a good approximation, the difference arrows indicate a 3D conductivity distribution, one that might include an anomalous conductor at depth in Tsugaru strait region, in addition to the parallel conductors beneath the coasts of the island. Previous studies (e.g. Ogawa et al., 1986) neglected the northward components of the induction arrows, but the difference arrow results suggest that both the northward and eastward components should be considered in any interpretation of the field measurements.

Figure 7.13 shows the model (V_m) and field (V_f) induction arrows and the difference arrows (V_f-V_m) in the northern Honshu, Tsuguaru strait and Hokkaido regions for 60 min. The field site measurements include those of Tanaka (1972) and Honkura (1974) at the northern Honshu region, those of Yamashita (1976) in the vicinity of Tsguaru strait, and those of Nishida and Kuboki (1972) at Hokkaido. One of the predominate features of the difference arrows is that the arrows in the northern Honshu and Tsugaru strait region have significantly large north components. In addition, the magnitudes of the difference arrows increase as the strait is approached, reaching a maximum at the two sites north of Tsugaru strait, then decrease further northward.

To explain the behaviour of the difference arrows in the northern Honshu region, a 2D profile along the EW direction (denoted as the y"-direction as shown in Fig. 7.1) is studied. The upper part of Fig. 7.14 shows the proposed 2D model of

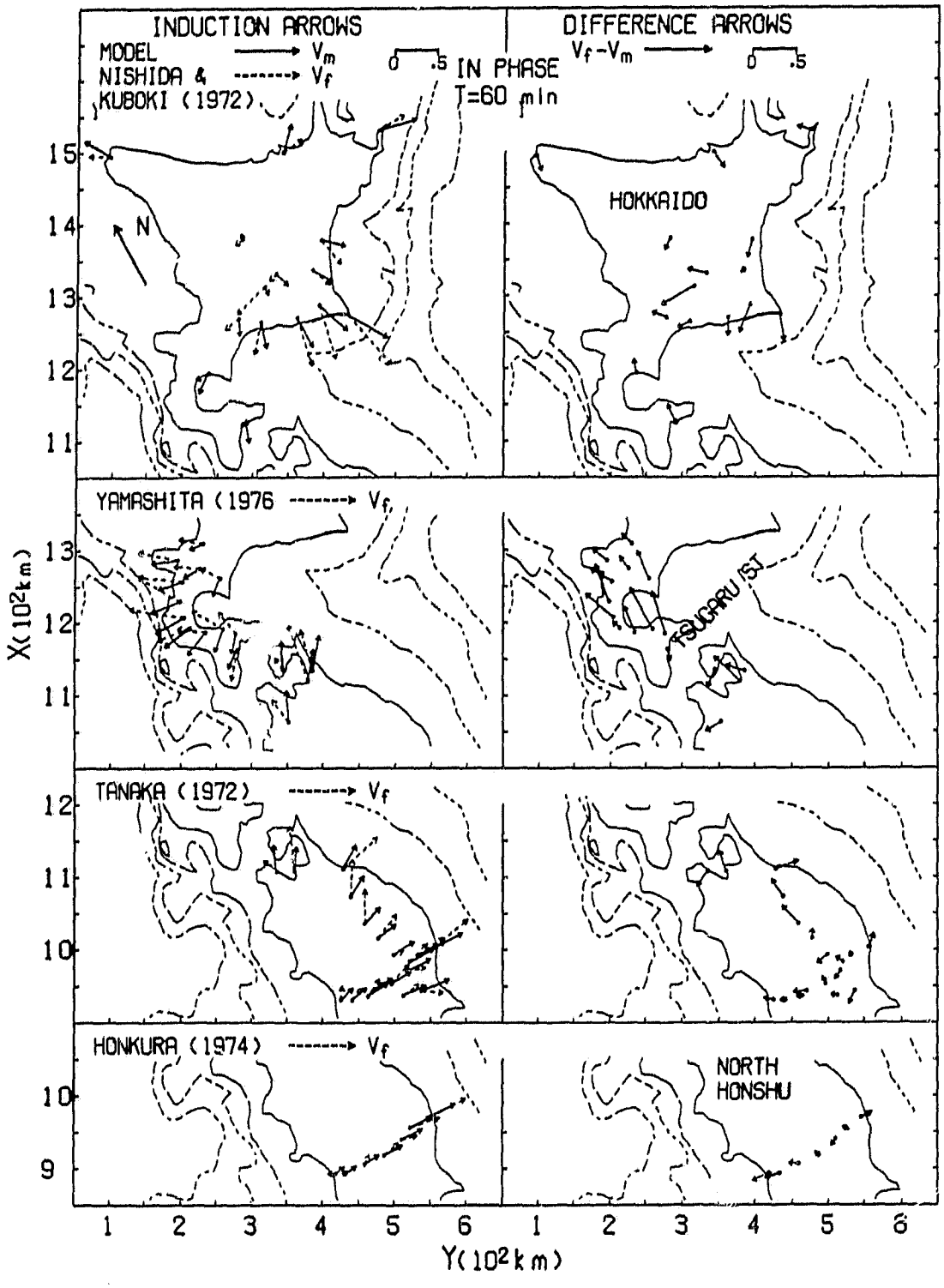

Figure 7.13: Analogue model V_m and field site V_f and difference (V_f-V_m) in-phase induction arrows for the northern Honshu, Tsugaru strait and Hokkaido regions.

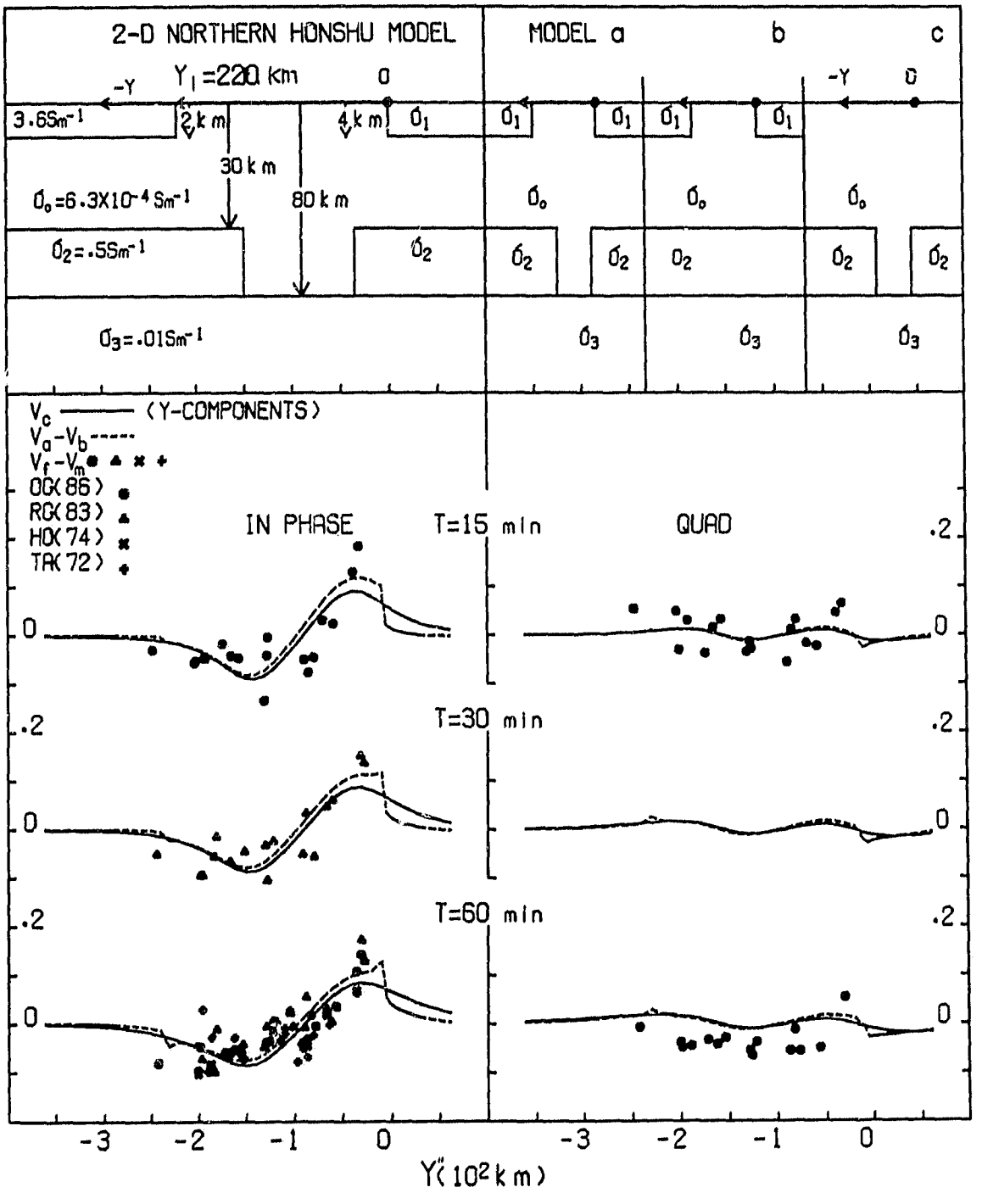

Figure 7.14: The y"-components of 2-D numerical model induction arrows and field-analogue model difference arrows for the northern Honshu region.

the profile in which anomalous conductors with conductivity of $0.5Sm^{-1}$ are situated beneath the Pacific Ocean and the Japan Sea, similar to the model for the Kii Peninsula (Fig. 7.2). The ocean depths are taken to be 2 and 4 km for the Japan Sea and Pacific Ocean respectively, and the island width is about 220 km. It is known that in the northern Honshu region, terrestrial heat flow measurements show that the heat flow value across the volcanic front is about 100% higher than that at the Pacific Ocean, and 50% higher than that at the Japan Sea. The lower part of Fig. 7.14 shows the numerical induction arrows (V_c), the numerical difference arrows (V_a-V_b), and the projected difference arrows (V_f-V_m) along the y"-direction for the periods of 15, 30, and 60 min. In Fig. 7.14 the dots represent the difference arrows for the field sites of Ogawa et al. (1986), denoted as OG(86), the triangles represent those of RGCRS (1983), denoted as RG(83), the crosses represent those of Honkrua (1974), denoted as HO(74), and the plus signs represent those of Tanaka (1972), denoted as TA(72).

7.4 Summary of the conductive substructure of Japan

Based on the vertical and horizontal magnetic field measurements, Rikitake (1969) proposed a 3D conductivity model for the Japan islands, a model in which a highly conductive substratum at 50 km depth subsides to a depth of 200 km beneath an area extending from the northeast to the southwest along the Pacific coast of Honshu, and rises to a depth of 50 km toward the Japan Sea. further, the depression in the conductive substratum rises to depths shallower than 50 km beneath the Tsguaru strait to the north. According to Uyeda and Rikitake (1970), their model is consistent with enhanced heat flow and low seismic wave velocity

at these coastal regions. The difference arrows, obtained by subtracting the analogue model induction arrows from the field site induction arrows at the Kii Peninsula, the central Honshu region, and the northern Honshu region support the model of two conductive anomalies, one beneath the Pacific Ocean and the other beneath the Japan Sea. These two conductors, together with the highly conductive substratum at 80 km depth, form a depression in the conductive substratum, which agrees in principle with the Rikitake (1969) model.

Figures 7.15-7.18 provide general views of the difference arrow distribution for 15, 30, 60 and 120 min respectively. The field measurements available for the Japan islands include those of Ogawa et al. (1986), Utada et al. (1986), Yukitake (1984), RGCRS (1983), Miyakoshi(1979), Yamashita (1976), Honkura(1974), Tanaka (1972), Nishida and Kuboki (1972) and Sasai (1969). For the regions of the Kii Peninsula, the central Honshu and the northern Honshu, it is seen that the in-phase difference arrows near the Pacific Ocean coast all tend to point toward the ocean with the maximum responses right at the coastline, indicating that the anomalous conductor beneath the Pacific Ocean is a large-scale tectonic structure which may extend from the Kii Peninsula region all the way to the northern Honshu region along the general trend of the Japan island arc. Further landward, the in-phase difference arrows are reduced in magnitude and rotated in direction to point towards the Japan Sea. The westward directed in-phase difference arrows have maximum lengths in the central region of central Honshu, and at the Japan Sea coastal region of the northern Honshu. This suggests that the anomalous conductor beneath the Japan Sea extends about 150 km inland at the Central Japan region and a few tens of kilometers inland at the northern Honshu region. The sig-

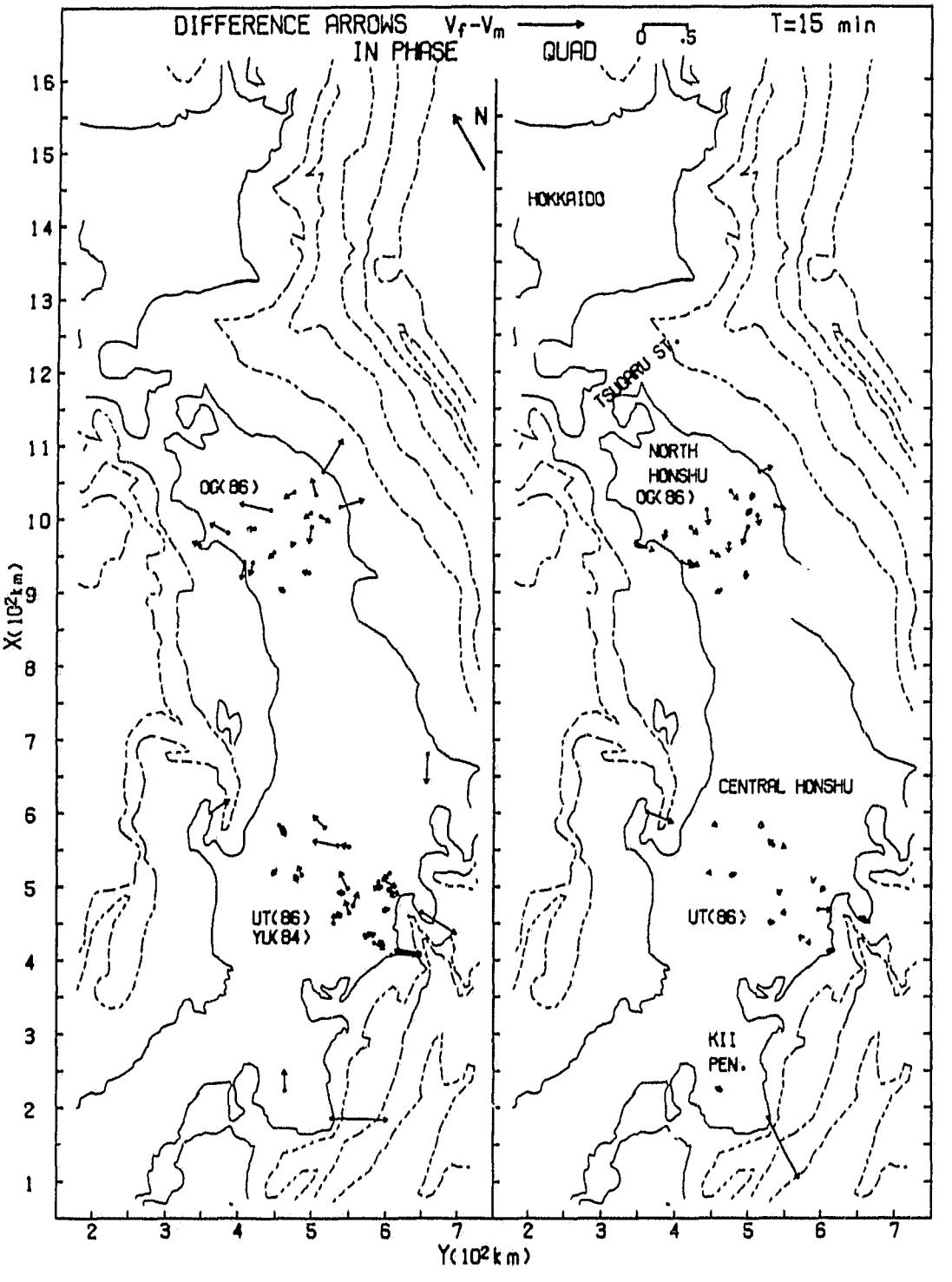

Figure 7.15: The in-phase and quadrature field - analogue model difference arrows ($V_f - V_m$) for the Japan Islands for 15 min.

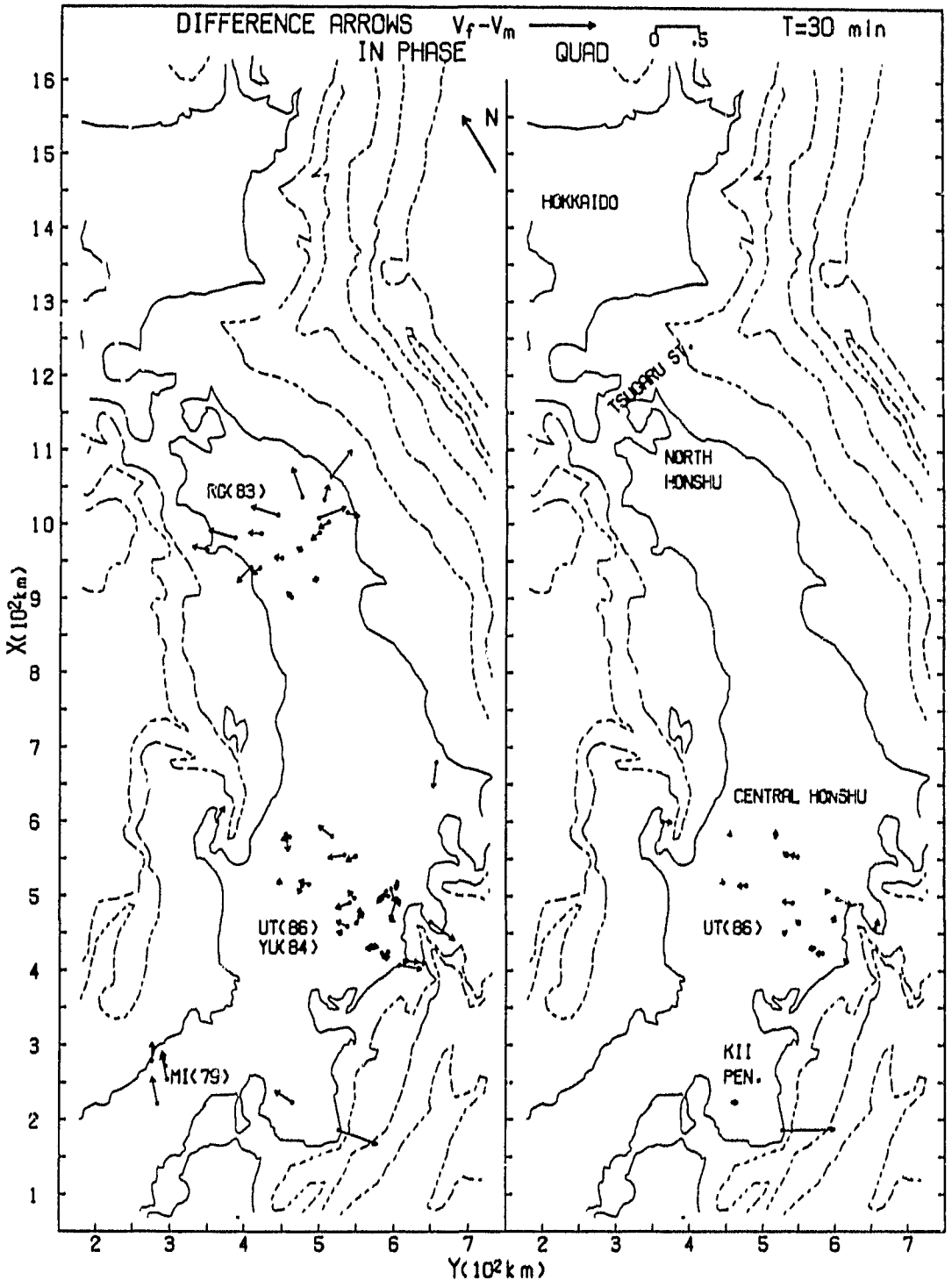

Figure 7.16: The in-phase and quadrature field - analogue model difference arrows ($V_f - V_m$) for the Japan Islands for 30 min.

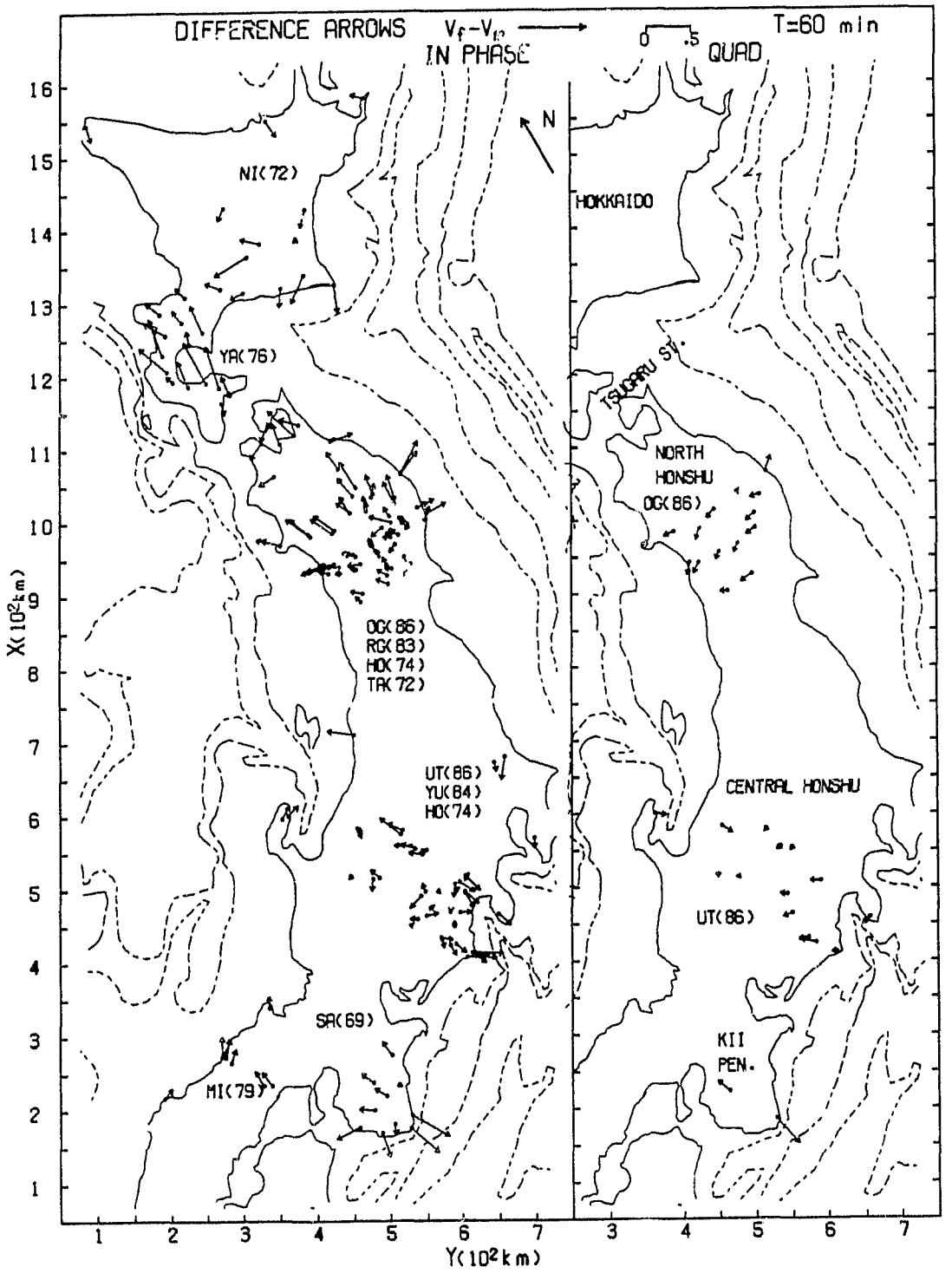

Figure 7.17: The in-phase and quadrature field - analogue model difference arrows (V_f - V_m) for the Japan Islands for 60 min.

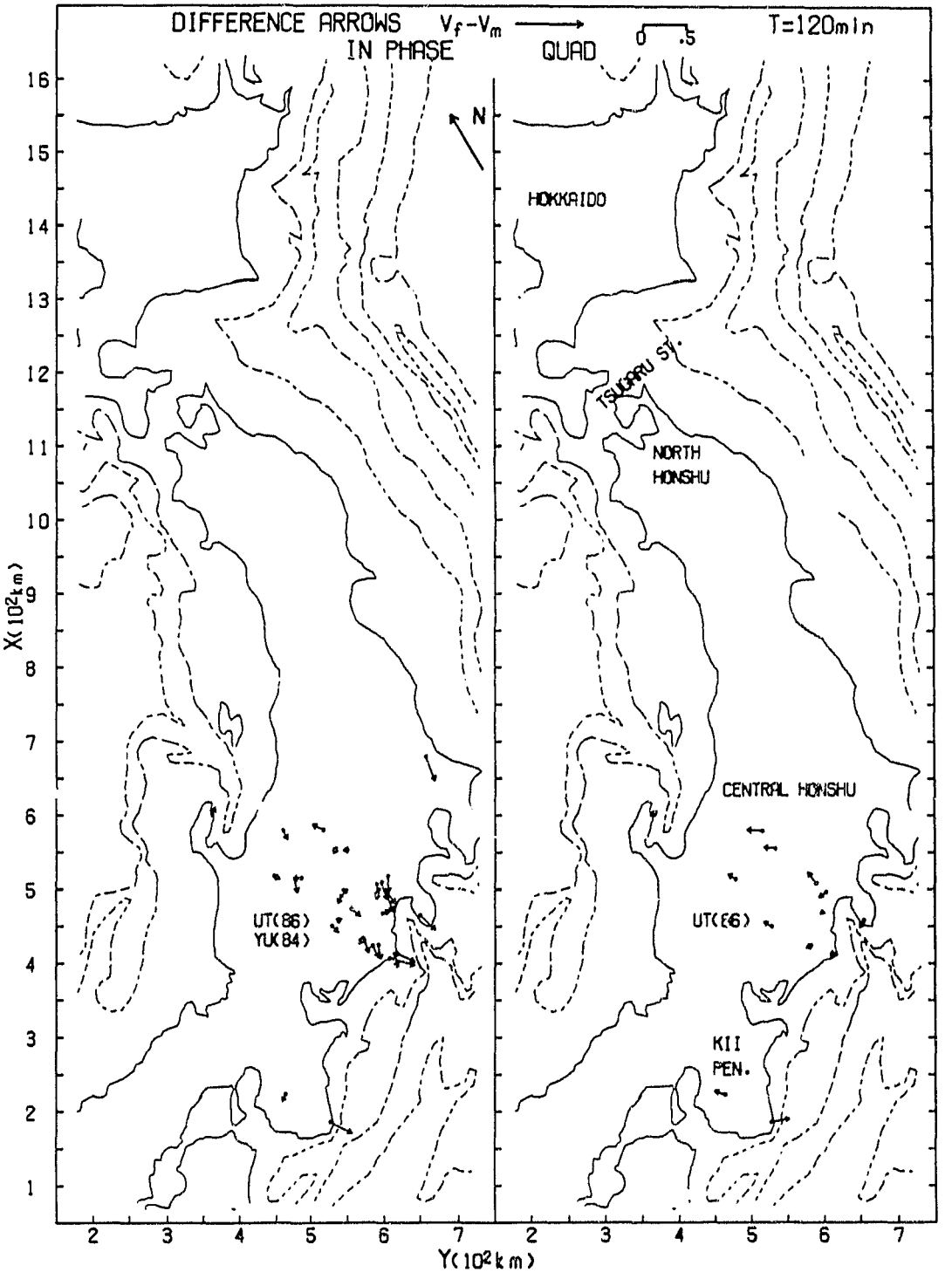

Figure 7.18: The in-phase and quadrature field - analogue model difference arrows ($V_f - V_m$) for the Japan Islands for 120 min.

nificantly large north components of the in-phase difference arrows observed at the northern Honshu region for all periods, could be explained by an E-W striking conductive anomaly beneath Tsugaru strait to the north. The quadrature difference arrows, although much smaller in magnitude than the in-phase arrows, are seen to be consistent with the behaviour of the in-phase components.

In summary, the magnetic field responses of the conductive anomalies in the Japan Island region, as delineated by the difference arrows in Figs. 7.15-7.19, suggest an arc-shaped conductive substructure in which the conductors, one beneath the Pacific Ocean and one beneath the Japan Sea, roughly follow the general trend of the island arc, and eventually are connected by an E-W striking conductor beneath Tsugaru strait to the north. It is noted that such a substructure can also be viewed as a depression in a conductive layer (conductivity 0.5 Sm^{-1}) overlaying a conductive substratum (conductivity 0.01 Sm^{-1}), which agrees in principle with the Riktitake (1969) 3D model, and with the 2D profile of the substructure in Central Japan (Fig. 7.2) proposed by Honkura (1974).

7.5 The Chapter Summary

Difference arrows were employed in an attempt to remove the ocean effect from field site measurements available in the Kii Peninsula region, the central Honshu region and the regions of northern Honshu, Hokkaido and Tsugaru strait. Calculations for 2D numerical models for the Kii Peninsula region, the central Honshu region and northern Honshu region support the premise of two conductive anomalies (with conductivity 0.5Sm^{-1}), one beneath the Pacific Ocean and the other beneath the Japan Sea at a depth of 30 km. Further, the difference arrows

over the entire Japan region suggest that the two conductors roughly follow the general trend of the island arc, and eventually may be connected by an E-W striking conductor beneath Tsugaru strait to the north.

Chapter VIII

SUMMARY AND CONCLUSIONS

The primary thrust of this thesis is the study of the coast effects in the continental Bohai Bay coastal region of China and the island coastal region of Japan. These 3D laboratory analogue model measurements are used to remove these coast effect responses from the observed field responses.

8.1 Analogue Model Results For The Bohai Bay Region

Electromagnetic induction in the continental Bohai Bay coastal region of China is studied using a scaled laboratory analogue model. The model includes a simulation of the known ocean bathymetry of Bohai Bay, the Yellow and the East China Seas, and the deeper Japan Sea. Major geographic features are the three peninsulas (Sandong, Liaodong and Korea) and two straits (the Bohai and the Korea-Japan straits).

Detailed measurements of the electric and magnetic field components for E- and B-polarizations were carried out along 15 traverses over the Bohai Bay model for simulated source periods of 3, 5, 10, 20, 60 min. The model results for E-polarization of the source field indicate that a large amount of the current induced in the deep ocean is channelled through the Korea-Japan strait. The current deflected by the Korean, Shandong and Liadong peninsulas leads to large B_z responses, particularly at short periods. The anomalous fields observed at the

Bohai Bay coast and the west coast of the Korean peninsula are generally small, due to minimal induction in the shallow Bohai Bay.

For B-polarization of the source field, the shapes of the coastlines provide a much more abrupt obstacle to the induced current than was the case for E-polarization. The responses at the eastern coast of Korea show the effects of some current channelling through the Korea-Japan strait, but much less than is observed for E-polarization. Current induced in the East China sea is in part funnelled into the Yellow Sea and eventually into Bohai Bay where it diffuses into the continent. The peninsulas (Korea, Shandong, and Liaodong) provide obstacles to the current funnelling and lead to local current concentrations at the tips of the peninsulas. The induction arrows for the Bohai Bay region show that the induction in the shallow local Bohai bay is important primarily at short periods. Large induction arrows occur at the tips of the Korean, Liadong and Sandong peninsulas due to the cape effect.

8.2 Analogue Model Results Of The Japan Island Region

The laboratory analogue model fields of the Japan-Korea-China region are studied in an attempt to delineate the coast effects for the complex Japan islands region. Included in the model simulation are the Asian continent, the Japan Sea, the Japan Islands, and the deep Pacific Ocean.

For E-polarization of the source field, induced current in the oceans flows roughly parallel to the west and east coastlines of Japan. Off the east coast, current is concentrated due to the cape effect, as it is deflected to flow around the convex shaped coastline, while off the concave shaped west coastline, current

density is reduced due to the bay effect. This current density distribution generally leads to greater B_z coast effects on the eastern than on the western coastal regions of Japan. The greatly enhanced current concentrations resulting from channelling through the straits leads to the large B_z responses observed in the Korea-Japan strait and Tsugaru and La Perouse straits. As the period increases, the in-phase components over the Korea-Japan strait first increase, reach a maximum at roughly 60 min, then gradually fall off at longer periods. The quadrature components, however, first decrease with increasing period, approach a minimum at about 60 min, then following a reversal of sign, increase to a maximum at 180 min.

For B-polarization, The enhanced current concentration resulting from the channelling effect in Tsugaru strait leads to the large negative B_z responses observed in the northern Honshu region over a range of periods. The responses clearly indicate that Tsugaru strait, although shallow, plays an important role for the fields over Honshu region of Japan. In general, the field responses for B-polarization, are much smaller than those for E-polarization, however, the B_z responses in particular are more complex for B- than for E-polarization. For E-polarization the character and the gradient of the B_z responses change little from traverse to traverse, while for B-polarization both change radically, including sign changes in the field gradients from traverse to traverse.

The in-phase induction arrows in the coastal region have substantial lengths and point seaward at the locations where the current concentrations, due to current deflection occur, for example at the tip of the Korean peninsula, the convex shaped east coastline of Japan, and the Korea-Japan strait. In contrast, the quad-

rature arrows at the short periods tend to point away from the deep ocean everywhere, and are of much smaller magnitude. As the period increases, the quadrature arrows over the coastlines generally rotate to point seaward and roughly parallel to the direction of the in-phase arrows. The magnitudes of the in-phase induction arrows along the east coast of Japan are much larger than those along the west coast of Japan for all periods.

8.3 Difference Arrows and Removal Of The Coast Effect

If the coast effect responses, as delineated by the laboratory analogue model results for the continental Bohai Bay region and the Japan island region, can be successfully removed by subtracting them from the field site responses, the resulting responses (or the difference arrows) should be characteristic of any local subsurface anomalous conductor not simulated in the analogue model. The level of validity of such a subtraction will depend on the mutual inductive coupling between the conductors (i.e. ocean, anomalous conductor and the underlying conductive substratum). If the anomalous conductor-ocean separation were sufficiently large so that mutual coupling were negligible, then the difference arrows should yield the approximate response of the anomalous conductor alone. In the present work, a measure of the required separation distance for negligible coupling was taken to be the range for which the ocean coast effect $|B_z/B_{yn}|$ at the anomalous conductor location is reduced to a value of 0.2. This separation distance is defined as the response range Y_R. Calculations for 2D numerical models of EM induction in continental and island coastal region for an anomalous conductor in the form of an upwelling or a depression in the conductive substratum,

show that if the ocean-conductor separation distance is at least as great as the coast effect response range Y_R, then the coast effect can be removed by vector subtraction to yield a response, approximately that of the anomalous conductor alone. The coast effect response ranges, as empirical criteria for permitting subtraction of the coast effect from field measurements, are numerically studied for both continental and island coastal sites.

For the ocean-continent 2D model with an infinite depth resistive host, the response range for each ocean depth model increases smoothly with increasing period. However, for a more realistic geophysical model that includes a conductive substratum at finite depth, the response range decreases with increasing period. Thus, it is concluded that an underlying conductive substratum greatly reduces the separation distance required for minimal electromagnetic coupling between an ocean and an onshore anomalous conductor. The response range at all periods decreases as the ocean depth decreases. Empirical curves are presented for the continent-ocean model showing how the response range depends on ocean depth, conductive substratum, and period.

The coast effect field response for the ocean- island model is found to decrease more rapidly with distance than was observed for the ocean-continent model, and the field response as a function of distance from the coast changes little with period, quite different from that observed for the ocean - continent model. It is found that the response range Y_R decreases rather uniformly with decreasing island width for all ocean depths studied, and decreases with decreasing ocean depth for the entire period range. For a deep ocean (d_1 = 2, 4 km) model, the response range depends only weakly on period, while for a shallow ocean

(d_1= .5, 1 km), Y_R decreases significantly with increasing period. The conductive substratum greatly reduces the response range as compared with the response range in the absence of the conductive substratum. Generally Y_R decreases with decreasing conductive substratum depth. Empirical curves are presented showing how the response range depends on the ocean depth, the conductive substratum depth, the island width and the period.

As "rules of thumb" for a typical conductive substratum depth d_3 = 100 km, the continental coast effect response range is roughly of the order of the substratum depth d_3 for the 1 km ocean depth case, and (3/2)d_3 for the 4 km ocean depth case, for all periods. The island coast effect response range is of the order of, or smaller than, (1/4)d_3 for the narrow island case ($Y_i \simeq 100$ km), and of the order of (3/4)d_3 for wide island case ($Y_i \simeq 300$ km). Further, Y_R is less than (1/4)Y_i for all island widths studied ($Y_i < 500$ km). For a given depth ocean, the response range for a narrow island is less than 1/4 the response range for a continent, and for a wide island is less than 1/2 that for a continent.

8.4 Applications To Field Measurements in China And Japan

8.4.1 The Bohai Bay region

For the continental Bohai Bay coastal region, difference arrows ($V_f - V_m$) are obtained by subtracting model induction arrows from field site induction arrows (Chen, 1974; IGSSB, 1986 and Kao, 1990). It is noted that the difference arrows at both short (5 min) and long (60 min) periods point inland (westward), suggesting a conductive anomaly some distance inland. The fact that the difference arrows are not strongly dependent on period, indicates that the anomalous conductor must be at considerable depth.

Two dimensional numerical calculations support the premise of a conductor, in the form of an upwelling in the conductive substratum (with conductivity 0.5 Sm^{-1} at 80 km depth), situated at about 150 km from the Bohai Bay coastline to account for the field site observations.

A comparison of the analogue model and field site MT results at two sites west of Bohai Bay shows that the model apparent resistivities are about an order of magnitude greater than the field site apparent resistivities. This result also supports the premise of a conductive anomaly, in addition to the conductive substratum at 80 km depth.

8.4.2 The Kii Peninsula Region

For the Kii Peninsula region, the difference arrows (V_f-V_m), obtained by subtracting model induction arrows from the field site induction arrows (Sasai, 1969; Miyakoshi, 1979; and Utada et a'., 1986) support a model of an anomalous 2D conductor beneath the Pacific Ocean coastal (or near off-shore) region and an anomalous 2D conductor at a depth of 30 km beneath the central region of the island.

8.4.3 The Central Honshu Region

The difference arrows, obtained by subtracting analogue model coastal regions from field site responses (Honkura, 1974; Yukitake, 1984 and Utada et al. 1986) for coastal sites in the central Honshu region Ocean coast for the period range 15 - 120 min, point towards the Pacific Ocean and thus clearly support the interpretation of a conductor beneath the Pacific Ocean coastal region. The inland difference arrows, pointing inland in roughly the opposite direction, indicate the effect of an inland conductive anomaly at depth. The 2D numerical calculations for the

central Honshu region suggests that in addition to the two parallel anomalous conductors, one beneath the Pacific Ocean and the other beneath Japan Sea at a depth of 30 km, there is an anomalous conductor at a depth of 20 km beneath the westerly coast of Japan, which is coincident with the distribution of the Quaternary Volcanics in the region.

8.4.4 Northern Honshu, Tsugaru strait, and Hokkaido Region

In this northerly region, the difference arrows ($V_f - V_m$), obtained by subtracting analogue model coast effect responses from field site responses (Tanaka, 1972; RGCRSJ, 1983; Ogawa et al., 1986; and Nishida and Kuboki (1972), indicate the effect of two parallel conductors, one beneath the Pacific Ocean and the other beneath the Japan Sea, similar to the cases of the Kii Peninsula and the central Honshu region, while the significantly large N-S components of the difference arrows could be accounted for by an anomalous conductor beneath Tsugaru strait. Although the coastlines and the baythmetrey of the region would suggest a 2D model as being a good approximation, the difference arrows indicate a 3D conductivity distribution, one that might include an anomalous conductor at depth in Tsugaru strait region, in addition to the parallel conductors beneath the coasts of the island.

In summary, the magnetic field responses of the conductive anomalies in the Japan Island region, as supported by the difference arrow interpretation, suggest arc-shaped substructures in which one conductor beneath the Pacific Ocean and the other conductor beneath the Japan Sea, roughly follow the general trend of the island arc, and eventually are connected by an E-W striking conductor beneath Tsugaru strait to the north.

Generally, the results for the continental coastal Bohai Bay region and the island region of Japan treated in this work provide examples of what appear to be successful removal of the ocean coast effects from field site measurements over an anomalous conductor in the form of an upwelling or depression in the conductive substratum in the continental and island coastal regions.

8.5 Suggestions For Further Work

In the present work, it is seen that for the period range of 5 - 120 min, the response range Y_R, generally increases with decreasing period. However, for much shorter periods at which the ocean depth is more than a skin depth, the response range Y_R should decrease with decreasing period, since the ocean can then be treated as being infinitely deep. A maximum in the response range Y_R thus is expected to appear at some period. This period at which a maximum in the response range occurs should be related to the characteristic period (Agarwal and Dosso, 1990), since the period (at which maximum Y_R occurs) and the characteristic period both depend on the depths of the ocean and the conductive substratum. A more detailed study of the response range for shorter periods (a few second to 5 min) should be carried out to investigate this further.

The study of the removal of the coast effect in sea floor measurements would also be an interesting topic in further work. For the case of an anomalous conductor (or conductive sediment) beneath the ocean floor, the mutual inductive coupling between the ocean and the conductor will depend not only on the coast effect response range, but also on the depth of the conductor. The behavior of the response range for points on the sea floor, thus, is expected to be much more complex than that for the continent and the island cases for land based measurements.

It would also be of interest to study aspects of the coast effect in magnetotelluric measurements in coastal regions. This could take the form of determining the ranges at which the coast would have minimal effects for the E- and B- polarization cases.

REFERENCES

Agarwal, A.K. and Dosso, A.K., 1990. On the behaviour of the induction arrows over a buried conductive plate - a numerical model study. Phys. Earth Planet. Inter., **60**, 265-277.

Agarwal, A.K. and Weaver, J.T., 1989. Regional electromagnetic induction around the Indian Peninsula and Sri Lanka: a three-dimensional numerical model study using the thin sheet approximation. Phys. Earth Planet. Inter., **54**, 320-331.

Bahr, K. 1990. An all-purpose MT interetation algorithm. The 10th workshop on electromagnetic induction in the earth. Ensenada, Mexico.

Bailey, R.C. and Edwards, R.N., 1976. The effect of source field polarization on geomagnetic variation anomalies in the British Isles. Geophys. J.R. Astro. Soc., **45**, 97-104.

Berdichevsky, M.N. and Zhdanov, M.S., 1984. Advanced theory of deep geomagnetic sounding. 408 pp., Elsever, Amsterdam.

Best, M. E., Duncan P., Jacobs J., and Scheen W. L., 1985 Numerical modelling of the electromagnetic response of three-dimensional conductors in a layered earth. Geophysics. **50**, 665-676.

Brewitt-Taylor, C.R. and Weaver, J.T., 1976. On the finite difference solution of two-dimensional induction problems. Geophys. J. R. Astro. Soc., **47**, 375-396.

Cagniard, L., 1953. Basic theory of the magneto-telluric method of geophysical prospecting. Geophys., 8, 605-635.

Chan, G.H., Dosso, H.W. and Law, L.K., 1981a. An analogue model study of electromagnetic induction for cape and bay coastlines. Phys. Earth Planet. Inter., 25, 167-176.

Chan, E., Dosso, H.W. and Nienaber, W., 1981b. An analogue model study of electromagnetic induction in the Queen Charlotte Island region. J. Geomagn. Geoelectr., 33, 587-605.

Chan, E., Dosso, H.W., Law, L.K., Auld, D.R. and Nienaber, W., 1983. Electromagnetic induction in the Queen Charlotte Island region : analogue model and field station results. J. Geomagn. Geoelectr., 35, 501-516.

Charters, R.A., Dosso, H.W., Best, M.E. and Nienaber, W., 1989. Induction coupling for a conductive dike in a resistive Earth. Phys. Earth Planet. Inter., 54, 140-148.

Chen, Po-Fang, 1974. Conductivity Anomaly on the West coast of Po Hai. Acta Geophys. Sin., 17 (3): 169-172.

Chen, P. F. and Fung, P. C. W., 1985. On the finite difference method of three-dimensional electromagnetic induction problem. Acta Geophysica Sinica. vol. 28, No. 3.

Chen, P. F. and Fung, P. C. W., 1988. Frequency Response of the transfer functions of the current channeling between two oceans. J. Geomag. Geoelectr. 40, 335-355.

Chen, J., Dosso, H.W. and Nienaber, W., 1989. Laboratory Electromagnetic Model Results for the EMSLAB Region. J. Geophys. Res., 84, 14167-14172.

Chen, J., Dosso, H.W. and Ingham, M. 1990. Electromagnetic Induction in New Zealand: Analogue model and field results. Phys. Earth Planet. Inter. 62, 257-270.

Dawson, T.W. and Weaver, J.T., 1979. Three-dimensional induction in a non-uniform thin sheet at the surface of a uniformly conducting earth. Geophys. J. R. astr. Soc., 59, 445-462.

Dawson, T.W. Weaver, J.T., and Raval, U., 1982. B-polarization induction in two thin sheets at the surface of conductive halfspace. Geophys. J. R. astr. Soc., 69, 209-234.

Dawson, T.W., 1983. E-polarization induction in two thin sheets. Geophys. J. R. astr. Soc., 73, 83-107.

Dey, A and Morisson, H.F., 1979. Resistivity modelling for arbitrarity two dimensional structure. Geophys, Prosp. 27. 106-136.

Dosso, H.W., 1966a. A plane wave analogue model for studying electromagnetic variations. Can. J. Phys., 44, 67-80.

Dosso, H.W., 1966b. Analogue model measurements for electromagnetic variations near vertical faults and dikes. Can. J. Earth Sci., 3, 287-303.

Dosso, H.W., 1966c. A plane-wave analogue model for studying electromagnetic variations. Can. J. Phys., 44, 67-80.

Dosso, H.W., 1966d. The electric and magnetic fields at the surface of a flat conducting earth in the near field of an oscillating line current. Can. J. Phys., 44, 1923-1931.

Dosso, H.W. and Jacobs, J.A., 1968. Analogue model measurements of electromagnetic variations in the near field of an oscillating line current. Can. J. Earth Sci., 5, 23-29.

Dosso, H.W., 1969. Analogue model study of electromagnetic variations over an anisotropic conductor. J. Geomag. Geoelectr., 21, 647-653.

Dosso, H.W., 1973. A review of analogue model studies of the coast effect. Phys. Earth Planet. Inter., 7, 294-302.

Dosso, H.W., Nienaber, W. and Hutton, V.R.S., 1980a. An analogue model study of electromagnetic induction in the British Isles region. Phys. Earth Planet. Inter., 22, 68-85.

Dosso, H.W., Nienaber, W., Wright, J.A., Greenhouse, J.P. and Bailey, R.C., 1980b. An analogue model study of electromagnetic induction in the eastern coastal region of North America. Phys. Earth Planet. Inter., 23, 13-30.

Dosso, H.W., Nienaber, W. and Parkinson, W.D., 1985. An Analogue Model study of Electromagnetic induction in the Tasmania region. Phys. Earth Planet. Inter., 39, 118-133.

Dosso, H.W. and Nienaber, W., 1986. A laboratory electromagnetic model study of the Juan de Fuca plate region. Phys. Earth Planet. Inter., 43, 34-46.

Dosso, H.W., Chan, G.H. and Nienaber, W., 1986. An analogue model study of EM induction for an island near bay and cape coastlines. Phys. Earth Planet. Inter., 42, 178-183. Dosso, H.W., Nienaber, W. and Chen, J., 1989. Laboratory electromagnetic modelling of the subducting Juan de Fuca plate. Phys. Earth Planet. Inter., 53, 221-227.

Dosso, H.W., Chen, J. and Nienaber, W., 1990. Comparison of analogue model and field station EM responses on Southern Vancouver Island. Phys. Earth Planet. Inter., 60, 18-24.

D'Erceville, I. and Kunetz, G., 1962. The effect of a fault on the earth's electromagnetic field. Geophysics, 27, 651-665.

Edwards, R.N., Law, L.K. and White, A., 1971. Geomagnetic variations in the British Isles. Phios. Trans. R. Soc. London, Ser. A., 270, 289-323.

Eggers, D.E., 1982. An eigenstate formulation of the magnetotelluric impedance tensor. Geophysics, 47, 1204-1214.

Filloux, J.H., 1979. Magnetotelluric and related electromagnetic investigations in geophysics. Rev. Geophys., 17, 282-294.

Filloux, J. H., 1980. Magnetotelluric sounding over the north-east Pacific may reveal spatial dependence of depth and conductance of the asthenosphere. Earth Planet. Sci. Lett., 46, 244-252.

Frischknecht, F.C., 1971. Electromagnetic scale modelling. in Electromagnetic Probing in Geophysics, edited by Wait, J.R., The Golem Press, Boulder, Colorado.

Geyer, R. G., 1972. The effect of dipping contact on the behavior of the electromagnetic field. Geophysics. 37, 337-350.

Gregori, G.P. and Lanzerotti, L.J., 1980. Geomagnetic Depth Sounding by Induction Arrow Representation: A Review. Rev. Geophys. Space Phys., 18, 203-209.

Gregori, G.P. and Lanzerotti, L.J. and Meloni, A., 1982. Reply. Rev. Geophys. Space Phys., 20, 523-528.

Groom, R. 1988. The effects of inhomgeneities on magnetellurics. Uni. Of Toronto. Thesis.

Gupta, P.K. Bennett, L.A., and Raiche, A.P., 1987. Hybrid calculations of the three dimensional electromagnetic response of buried conductors. Geophysics, 51, 1450-1461.

Gupta, P.K., Raiche, A.P.,and Sugeng, F., 1989. Three-dimensional time-domain electromagnetic modeling using a compact finite-element frequency-stepping method. Geophysical J., 96, 457-468.

Heard, G.J., Dosso, H.W., Nienaber, W. and Lokken, J.E., 1985. Laboratory analogue modelling of the Schumann resonance source field. Phys. Earth Planet. Inter., 39, 178-181.

Hebert, D., Dosso, H.W. and Nienaber, W., Wright, J.A., 1983a. Analogue model study of electromagnetic induction in the Newfoundland region. Phys. Earth Planet. Inter., 32, 65-84.

Hebert, D., 1982. An analogue model study of electromagnetic induction in the Newfoundland region. (M.Sc.thesis) Phys. Dept. Univ. Victoria.

Herbert, D., Wright, J.A., Dosso, H.W. and Nienaber, W., 1983b. Comparison of analogue model and field station results for the Newfoundland region. J. Geomagn. Geoelectr., 35, 673-682.

Hohmann, G.W., 1975. Three-dimensional induced polarization and electromagnetic Modeling. Geophysics, 40, 309-324.

Hohmann, G.W., 1983. Three-dimensional EM modeling. Geophysical Surveys, 6, 27-53.

Honkura, Y. 1971. Geomagnetic variation anomaly on Miyake-Jima Island. J. Geomag. Geoelectr., 23, 307-333.

Honkura, Y. 1974. Electrical conductivity anomalies beneath the Japan and Philippine Seas. J. Geomag. Geoelectr., 26, 147-171.

Honkura, Y. 1975. Partial melting and electrical conductivity anomalies beneath Japan and Philippine Seas. Phys. Earth Planet. Inter., 10, 128-134.

Honkura, Y. 1978. Electrical conductivity anomalies in the earth. Geophysical Survey, 3, 225-253.

Honkura, Y. 1983. Peninsula effects in central Japan and their relation to the electrical conductivity structure, J. Geomag. Geoelectr., 35, 39-56

Hu, W.B., Nienaber, W. and Dosso, H.W., 1983. Laboratory model magnetic field for the Hainan Island region. J. Geomagn. Geoelectr., 35, 683-692.

Hu, W.B., Dosso, H.W. and Nienaber, W., 1984. Analogue model magnetic field responses of an ocean channel, and island and a seamount in the Hainan Island region. J. Geophys., 55, 222-227.

Hu, W.B., Dosso, H.W. and Nienaber, W., 1986. Model magnetic field responses of an ocean channel, an island, and a seamount for two polarizations. Annales Geophysicae, 4, 165-172.

Hu, W.B., Nienaber, W. and Dosso, H.W., 1989. Vertical magnetic field response of a seamount. Phys. Earth Planet. Inter., 54, 135-139.

Hubbert, M.K., 1937. Theory of scale models as applied to the study of geologic structures. Bull. Geol. Soc. Am., 48, 1459-1520.

IGSSB 1986. A private communication with Prof. G. H. Fang, Institute of Geophysics, the state Seismological Bureau of China, Beijing.

Jones, A.G., 1981. Comment on "Geomagnetic depth sounding by induction arrow representation : A review" by G.P. Gregori and L. J. Lanzerotti. Rev. Geophys. Space Phys., 19, 687-688.

Jones, F.W. and Pascoe, L.J., 1971. A general computer program to determine the perturbation of alternating electric currents in a two-dimensional model. Geophys. J.R. Astro. Soc., 23, 3-30.

Jones, F.W. and Pascoe, L.J., 1972. The perturbation of alternating geomagnetic fields by three-dimensional conductivity inhomogeneities. Geophys. J. R. Astr. Soc., 27, 479-485.

Kao, D., 1990. Magnetotelluric study in the Tongshan earthquake area of Eastern China. 10th Workshop on Electromagnetic induction in the earth. Ensenada, Mexico.

Kato, Y., Daguchi, M., Seto, M., and Aruga, T. 1971. Sci. Rep. Tohoku Univ., Ser. 5, 21, 19.

LaTorraca, G.A., Madden, T.R., Korringa, J., 1986. An analysis of the magnetotelluric impedance tensor for three- dimensional conductivity structures. Geophysics, 51, 1819-1829.

Lee, K.H., Pridmore, D.F. and Morisson, H.P., 1981. A hybrid 3D EM modelling scheme. Geophysics, 46, 796-805.

Lee, K.H., Morisson, H.P., 1985. A numerical solution for the electromagnetic scattering by a two-dimensional inhomogeneity. Geophysics, 50, 1163-1165.

Lee, K.H., Liu, G. and Morrison, H.F., 1989. A new approach to modelling the electromagnetic response of conductive media. Geophysics. 54. Vol. 9. 1180-1192.

Lilley, F.E.M. and Arora, B.R., 1982. The sign convention for quadrature Parkinson arrows in geomagnetic induction studies. Rev. Geophys. Space Phys., 20, 513-518.

Lines, L.R. and Jones, F.W., 1973. The perturbation of alternating Geomagnetic fields by 3D island structures. Geophys. J.R. Astron. Soc., 32, 133-154.

Liu, G. and Liu, C. 1983. Structures of crust and upper mantle and their relation to cenozoic tectonism in northern part of North China. Scientia Sinica, Series B, 26, No.5, 551-560.

Liu, G.,Gu Q., Shi, S Sun, J. ShiZ. and Liu, J., 1983. The electrical structure of the crust and upper mantle and its relationship with seismicity in the Beijing-Tianjin-Tangshan region and adiacent area. Acta Geophysica Sinica 26, 149-157.

Liu, G., Shi, S. and Wang B., 1984. Conductive layer in the crust in North China and its relation to crustal tectonism, Vol. XXVII No. 10. Scientia Sinia (Series B). 1093-1104.

Liu, G., 1985. Genozic rift system of North China Plain and deep internal processes. Research on recent crust movement (1) Continental rift and deep internal processes. Institute of Geology, State Seismological Bureau. (Seismological Press, Beiging). pp 17-25.

Liu, G., 1987. MT studies on the Upper Mantle Conductivity in China. PAGEOPH. Vol, 125, No.2. 466-482.

Ma, X., Liu, G. and Su, J. 1984. The structure and dynamics of the continental lithosphere in north-northeast China. Annales Geophysicae, 2, 6, 611-620.

McKirdy, D.M. and Weaver J.T., 1983. A numerical study of the channeling of induced current between two oceans. J. Geomag. Geoelctr. 35, 623-642.

McKirdy, D.M. and Weaver J.T., 1984. Induction in a thin sheet of variable conductance at the surface of a stratified earth-I. Two dimensional theory. Geophys. J. R. astro. Soc. 78, 93-103.

McKirdy, D.M., Weaver J.T., and Dawson, 1985. Induction in a thin sheet of variable conductance at the surface of a stratified earth-II. Three dimensional theory. Geophys. J. R. astro. Soc. 78, 93-103.

Meng, Z., Dosso, H.W. and Nienaber, W., 1990. An analogue model study of EM induction in the North China-Korea coastal region. Phys. Earth Planet. inter., 60, 25-39.

Meng, Z. and Dosso, H.W., 1990. An analogue model study of EM Induction in the Japan- Korea-China region. Phys. Earth Planet. Inter., 62, 246-256.

Miles, T. and Dosso, H.W., 1979. A laboratory analogue model study of oceanwave induced magnetic field for cases of non-uniform depths and sea-land interfaces. Phys. Earth Planet. Inter., 19, 12-20.

Miles, T., and Dosso, H.W., 1980. An analogue model study of oceanwave induced magnetic field variations near a coastline. J. Geomag. Geoelectr., 32, 151-154.

Miyakoshi, J., 1976. Electrical conductivity structure beneath the Japan Island Arc by geomagnetic induction study. Tech. Rep. Geol. Survey. Japan. ?1-40.

Miyakoshi, J. 1979. Electrical conductivity structure beneath the Japan island arc by geomagnetic induction study. J. Phys. Earth, 27, S153-S161.

Morisson, H.F., Clarke, A.J., Hansen, W.D. and Becker, A., 1982. A versatile EM scale modelling system (SEG 1981 annual meeting abstracts). Geophysics, 47, 435.

Nienaber, W., Dosso, H.W., Law, L.K., Jones, F.W. and Ramaswamy, V., 1976. An analogue model study of electromagnetic induction for island-continent ocean channels. Phys. Earth Planet. Inter., 13, 169-183.

Nienaber, W., Dosso, H.W., Law, L.K., Jones, F.W. and Ramaswamy, V., 1977. Studies of electromagnetic induction for island-continent ocean channels with applications to Vancouver Island. Acta. Geodaet., Geophys. et Montanist. Acad. Sci. Hung., 12, 187-190.

Nienaber, W., Dosso, H.W., Law, L.K., Jones, F.W. and Ramaswamy, V., 1979a. An analogue model study of electromagnetic induction in the Vancouver Island region. J. Geomagn. Geoelectr., 31, 115-132.

Nienaber, W., Dosso, H.W., Law, L.K.. Jones, F.W. and Ramaswamy, V., 1979b. Electromagnetic induction in the Vancouver Island region - field station and analogue model results. J. Geomagn. Geoelectr., 31, 599-613.

Nienaber, W., Dosso, H.W. and Hutton, V.R.S., 1981. Electromagnetic induction in the British Isles region - analogue model and field station results. Phys. Earth Planet. Inter., 27, 122-132.

Nienaber, W., Hibbs, R.D., Dosso, H.W. and Law, L.K., 1982. An estimate of the conductivity structure for the Vancouver Island region from geomagnetic results. Phys. Earth Planet. Inter., 27, 300-205.

Nienaber, W., Hebert D. and Dosso, H.W., 1983. Induction Arrows for a Buried Conducting Plate Phys. Earth Planet. Inter., 32, 306-311.

Nienaber, W., Dosso, H.W., Law, L.K., Jones, F.W. and Ramaswamy, V., 1989a. An analogue model study of electromagnetic induction in the Vancouver Island region. J. Geomagn. Gelelectr., 31, 115-132.

Nishida, Y. and Kuboki, T., 1972. personal communication with Rikitake T. and Honkura Y. The field site measurement results were shown in the paper: Rikitake T. and Honkura Y., 1973. Recent Japanese studies on conductivity anomalies. Phys. Earth Planet. Inter., 7, 203-212.

Nishida, Y. 1982. Conductivity structure in and around Hokkaido, Japan as revealed by the period dependence of the CA transfer functions. J. Geomag. Geoelectr., 28, 375-394.

Nishida, Y. 1976. Conductivity anomalies in the southern half of Hokkaido, Japan. J. Geomag. Geoelectr., 28, 375-394.

Ogawa, Y., Yukutake, T., and Utada, H. 1986. Two-dimensional modeling of resistivity structure beneath the Tohoku district, northern Honshu of Japan, by a finite element method. J. Geomag. Gecelectr., 38, 45-79

Ogawa, Y. 1987. Two-dimensional resistivity modeling based on regional magnetotelluric survey in the northern Tohoku District, northeastern Japan. J. Geomag. Geoelectr., 39, 349-366.

Ogawa, Y. 1988. Preliminary interpretation on detailed magnetovariational profiling in the northern Tohoku District. J. Geomag. Geoelectr., 40, 349-366.

Ogunade, S.O., Ramaswamy, V. and Dosso, H.W., 1974. Electromagnetic responses of a conducting sphere buried in a conducting earth. J. Geomagn. Geoelectr., 26, 417-427.

Ogunade, S.O. and Dosso, H.W., 1977. Subsurface electromagnetic response of a conducting sphere embedded in the lower layer of a two-layer earth. Acta. Geodaet., Geophys. et Montanist. Acad. Sci. Hung., 12, 311-314.

Ogunade, S.O. and Dosso, H.W., 1980. The inductive response of a horizontal conductive cylinder buried in a uniform earth for a uniform inducing field. Geophysical Prospecting, 28, 601-609.

Ogunade, S.O. and Dosso, H.W., 1981. The response of a horizontal conductive cylinder embedded in a uniform earth for a uniform and line current source. Pure and Applied Geophys., 119, 51-58.

Oldenburg, D. W., 1981. Conductivity structure of oceanic upper mantle beneath the Pacific plate. Geophys. J. R. Astron. Soc., 65, 359-394.

Parkinson, W.D., 1959. Direction of rapid geomagnetic fluctuation. Geophys. J.R. Astr. Soc., 2, 1-14.

Parkinson, W.D., 1962. The influence of continents and oceans on geomagnetic variations. Geophys. J.R. Astron. Soc., 6, 441-449.

Parkinson, W.D., Hermanto, R., Sayers, J., Bidoff, N.L., Dosso, H.W. and Nienaber, W., 1988. the Tamar conductivity anomaly. Phys. Earth Planet. Inter., 52, 8-22.

Price, A.T., 1964. A note on the interpretation of magnetic variations and magnetotelluric data. J. GEomag. Geoelec., 15, 241-248.

Pridmore, D.F., Hohmann, G.W., Ward, S.H. and Sill, W.R., 1981. An investigation of finite element modeling for electrical and electromagnetic data in three dimensions. Geophysics, 46, 1009-1024.

Qi, G., Zhan, Z., Hou, Z., Fang, G., Wang, Z. and Bai, C. 1981. A study of relations between the magnetic anomalies of the Bohai Bay region for short period variations, the conductivity distribution of the upper mantle, and the Tangsan earthquake (Title translated from Chinese). Scientia Sinica, 7, 869-879.

Ramaswamy, V., Dosso, H.W. and Weaver, J.T., 1972. Horizontal magnetic dipole embedded in a two-layer conducting medium. Can. J. Phys., 50, 607-616.

Ramaswamy, V. and Dosso, H.W., 1973. Locating a horizontal magnetic dipole buried in a 2-layer earth. Electronics Letters. Vol. 9 No. 4.

Ramaswamy, V. and Dosso, H.W., Effect of a conducting overburden on the fields of a buried dipole source. Can. J. Phys., 53, 598-609.

Ramaswamy, V., Nienaber, W., Dosso, H.W., Jones, F.W. and Law, L.K., 1975. Numerical and analogue model results for electromagnetic induction for an island situated near a coastline. Phys. Earth Planet. Inter., 11, 81-90.

Ramaswamy, V. and Dosso, H.W., 1977. The response of a conducting cylinder to the inducing fields of various sources. J. Geomag. Geoelec., 29, 181-189.

Ramaswamy, V. and Dosso, H.W., 1978. Analogue model measurements for a horizontal magnetic dipole embedded within a conducting medium. Phys. Earth Planet. Inter., 17, 295-299.

Ramaswamy, V., Jones, F.W., Dosso, H.W. and Nienaber, W., 1980. A comparison of numerical, analogue model, and field-station vertical magnetic-fields for the Vancouver Island region. Phys. Earth Planet. Inter., 22, 60-67.

Ranganayaki, R.P. and Madden, T.R., 1980. Generalized thin sheet analysis in magnetotellurics: An extension of Price's analysis. Geophys. J. Roy. Astron. Soc. 60, 445-447.

Rankin, D., 1962. The magneto telluric effect on a dike. Geophysics, 27, 666-676.

Research Group for Crustal Resistivity Structure, Japan. 1983. Preliminary report on a study of resistivity structure beneath the northern Honshu of Japan. J. Geomag. Geoelectr., 35, 589-608.

Research Group for Explosion Seismology, 1977. Regionality of upper mantle around Northeastern Japan as derived from explosion seismic observations and its seismological implications. Tectonophysics, 7, 117-130.

Rikitake,T. and Yokoyama, I. 1953. Anomalous relations between H and Z components of transient geomagnetic variations. J. Geomag. Geoelectr., 5, 59-65

Rikitake, T. 1959. Anomaly of geomagnetic variation in Japan. Geophys. J. R.astr. Soc., 2, 276-287.

Rikitake, T. 1966. Electromagnetism and the Earth's Interior. 308 pp. Elsevier, Amsterdam.

Rikitake, T. 1969. The undulation of an electrical conductive layer beneath the island of Japan. Techtonophys., 7, 257-264.

Rikitake, T., and Honkura, Y. 1973. Recent Japanese study on conductivity anomalies. Phys. Earth Planet. Inter., 7, 203-212.

Rikitake, T., and Honkura, Y. 1986. Solid earth geomagnetism. 384. pp. Terra Sci. Pub. Com.

Sasai, Y. 1969. Observations of geomagnetic variation in Kii peninsula. Proc. Conductivity Anomaly Symp., 2 Earthq. Res. Inst. Univ. Tokyo, p 43-55

Schmucker, U., 1964. Anomalies of geomagnetic variations in the southwestern United States. J. Geomag. Geoelectr., 15, 193-221.

Scheen, W.L., 1978 EMMMMA, a computer program for three-dimensional modelling of airborne electromagnetic survey. Proc. workshop on modelling of Electric and magnetic methods, LBL-7053, 53.

Schmucker, U., 1970. Anomalies of geomagnetic variations in the southwestern United States. Bull. Scripps Inst. Oceanography, University of California. 13, 1-165.

Swift, C.M., Jr., 1967. A magnetotelluric investigation of an electrical conductivity anomaly in the southwestern United States. Ph.D Thesis, Mass. Inst. of Tech.

Sinclair, G., 1948. Theory of models of electromagnetic systems. Proc. I.R.E. 36, 1364-1370.

Song, Z., 1985. P Wave velocity structure of the upper mantle in Chinese continent and its marginal area. Acta Geophysica Sinica, 28, 342-356.

Strangway, D. W., 1966. Electromagnetic scale modelling. in Methods and Techniques in geophysics, ed. by S.K. Runcorn, Interscience, New York, 1-31.

Tanaka, M., 1972. personal communication with Rikitake T. and Honkura Y. The field site measurement results were shown in the paper: Rikitake T. and Honkura Y., 1973. Recent Japanese studies on conductivity anomalies. Phys. Earth Planet. Inter., 7, 203-212.

Teng, G., Sun, K., Xuong, S. and Yao, H. 1985. Explosion seismological study for velocity distribution and structure of the crust and and upper mantle from Mamshan to Qidong of the southern parts of China. Acta Geophysica Sinica, 28, No. 2, 155-169.

Thomson, D.J., Ramaswamy, V. and Dosso, H.W., 1972. Model measurements of electromagnetic variations near a coastline for localized source fields. J. Geomagn. Geoelectr., 24, 317-336.

Tikonov, A. V., 1950. Determination of the electrical characteristics of the deep strata of the Earth's crust. Dokl. Akak. Nauk., U.S.S.R. 75 pp. 295-297

Ting, S.C. and Hohmann, G.W., 1981. Integral equation modeling of three-dimensional magnetotelluric response. Geophysics, 46, 182-197.

Utada, H., Hamano, Y., and Yukutake, T., 1986. A two-dimensional conductivity model across central Japan. J. Geomag. Geoelectr., 38, 447-473.

Uyeda, S. and Rikitake, T., 1970. Electrical conductivity anomaly and terrestrial heat flow. J. Geomag. Geoelectr., 22, 75-90.

Vasseur, G. and Weidelt, P., 1977. Bimodal electromagnetic induction in Non-Uniform thin sheets with an application to the Northern Pyrenean induction anomaly. Geophys. J. R. Astro. Soc., 51, 669-690.

Vozoff, K., 1972 The magnetotelluric method in the exploration of sedimentary basins. Geophysics, 37, 98-141.

Wait, J.R, 1982 **Geo-electro magnetism.**, pp197-201. Academic Press, New York.

Wannamaker, P.E., Hohmann, G.W., and SanFilipo, W.A., 1984. Electromagnetic modeling of three-dimensional bodies in layered earth using integral equations. Geophysics, 49, 60-74.

Wannamaker, P.E., Stodt, J.A., and Rijo, L., 1987. A stable finite element solution for two-dimensional magnetotelluric modeling. Geophys. J. R. astr. Soc., 88, 277-296.

Ward, S.H., 1967. Electromagnetic theory for geophysical applications. in Mining Geophysics: Vol. 2, Theory, SEG, Tulsa, pp. 10-196.

Weaver, J.T., 1963. The electromagnetic field within a discontinuous conductor with reference to geomagnetic micropulsations near a coast line. Canad. J. Phys. 41, 484-495.

Weaver, J.T., 1982. Regional induction in Scotland: an example of three-dimensional numerical modelling using the thin sheet approximation. Phys., Earth and Planet. Inter., 28, 161-180.

Weaver, J.T., Le Quang, B.V., and Fischer, G., 1985. A comparison of analytical and results for a two-dimensional control model in electromagnetic induction. Geophys. J. R. astr. soc., 82, 263-278.

Weaver, J.T., 1987. The mathematic solution of the geomagnetic coast effect. Conference on Applied Maths. In Honour of Prof. A.A.Ashore Cairo, .3-6.

Weaver, J.T. and Agarwal, A.K., 1991. Is addition of Induction Vectors meaningful? Phys. Earth Planet. Inter., **65**, 267-275.

Weidelt, P., 1977. Numerical study of a conductivity channelling effect. Acta Geodaet., Geophys. Montanist. Acad. Sci. Hung. **12**, 195-205.

Wiese, H., 1962. Geomagnetische Tiefentellurik. I. Die elektrische Leitahigkeit der Erdkruste und des oberen Erdmantels. Geofis. Pura Appl., **51**, 59-78.

Wolf, D., 1982. Comment on 'Geomanetic depth sounding by induction arrow representation: a review' by G.P Gregori and L.J. Lanzerotti. Rev. Geophys. Space Phys., **20**, 519-521.

Wolf, D., 1983. Inductive Coupling Between idealized conductors and its significance for the geomagnetic coast effect. J. Geophysics, **52**, 22-33.

Yamashita, H., 1976. personal communcation with Rikitake T. The field site menasurement results were shown in the book: **Solid Earth Geomagnetism** (p307) written by Rikitake, T. and Honkura, Y. (1986).

Yee, E. and Paulson, K.V., 1987. The Canonical decomposition and its relationship to other forms of magnetictelluric impedance tensor analysis. J. Geophys. **61**, 173-189

Yoshii, T., 1975. Regionality of group velocities of Rayleigh waves in the pacific and thickening of the plate. Earth Planet. Sci. Lett., **25**, 305-312.

Yukutake, T., Filloux, J.H., Segawa, J., Hamano, Y., and Utada, H. 1983. Preliminary Report on a magnetotelluric array study in the northwest Pacific. J. Geomag. Geoelectr., **35**, 575-587.

Yukutake, T., 1984. Electromagnetic observations in Tokai Koushin'etsu District, in Proc. Conductivity Anomaly Symp. Earthq. Res. Inst., Univ. Tokyo, p35-44.

Yukutake, T. 1985. A review of studies on the electrical resistivity structure of the crust in Japan. Earthq. Predict. Res.,

APPENDIX A

THREE-DIMENSIONAL VIEWS OF B_X AND E_Y FOR E-POLARIZATION

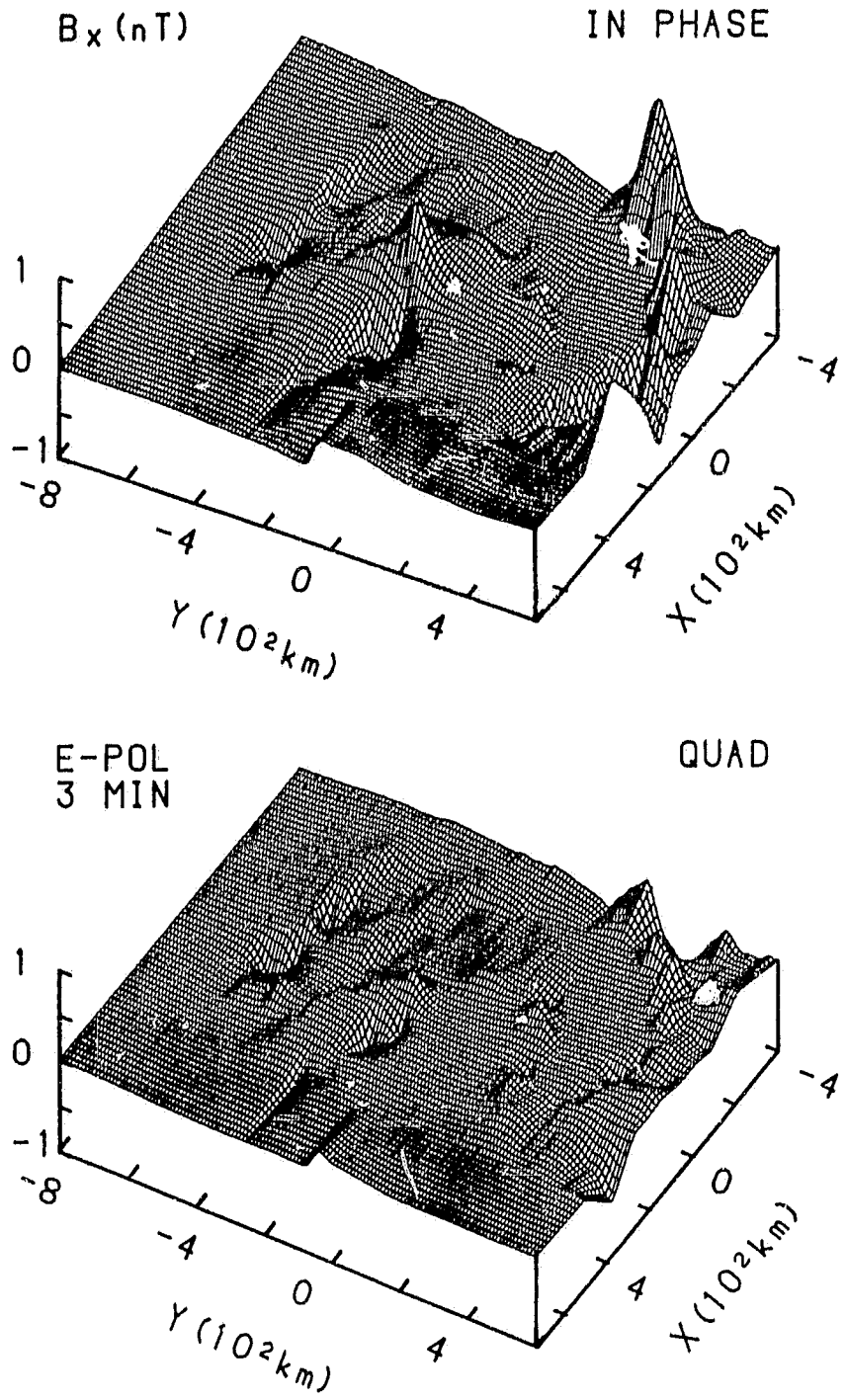

Figure A.1: Three-dimensional views of in-phase and quadrature B_x for the Bohai Bay model for E-polarization at 3 min.

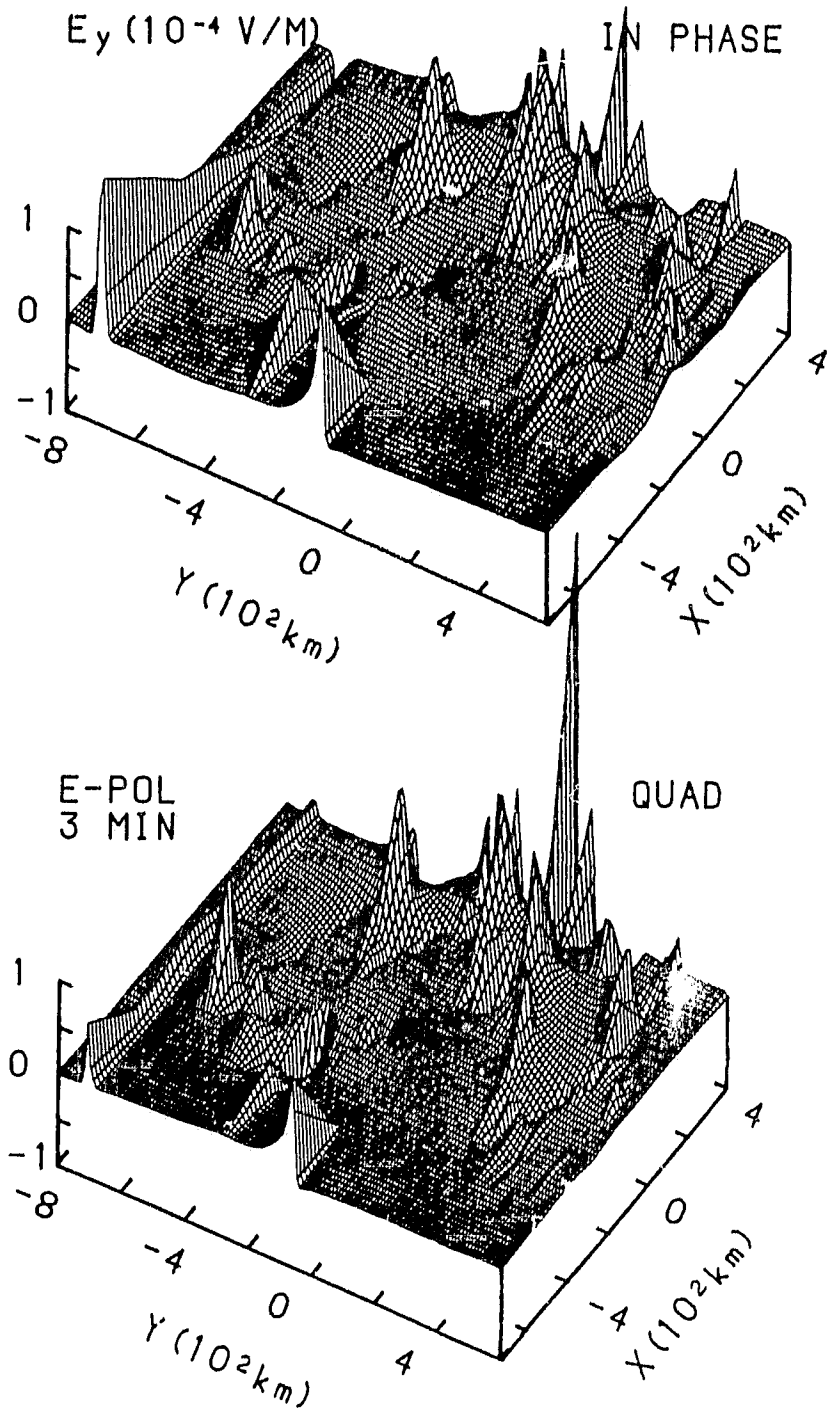

Figure A.2: Three-dimensional views of in-phase and quadrature E_y for the Bohai Bay model for E-polarization for 3 min.

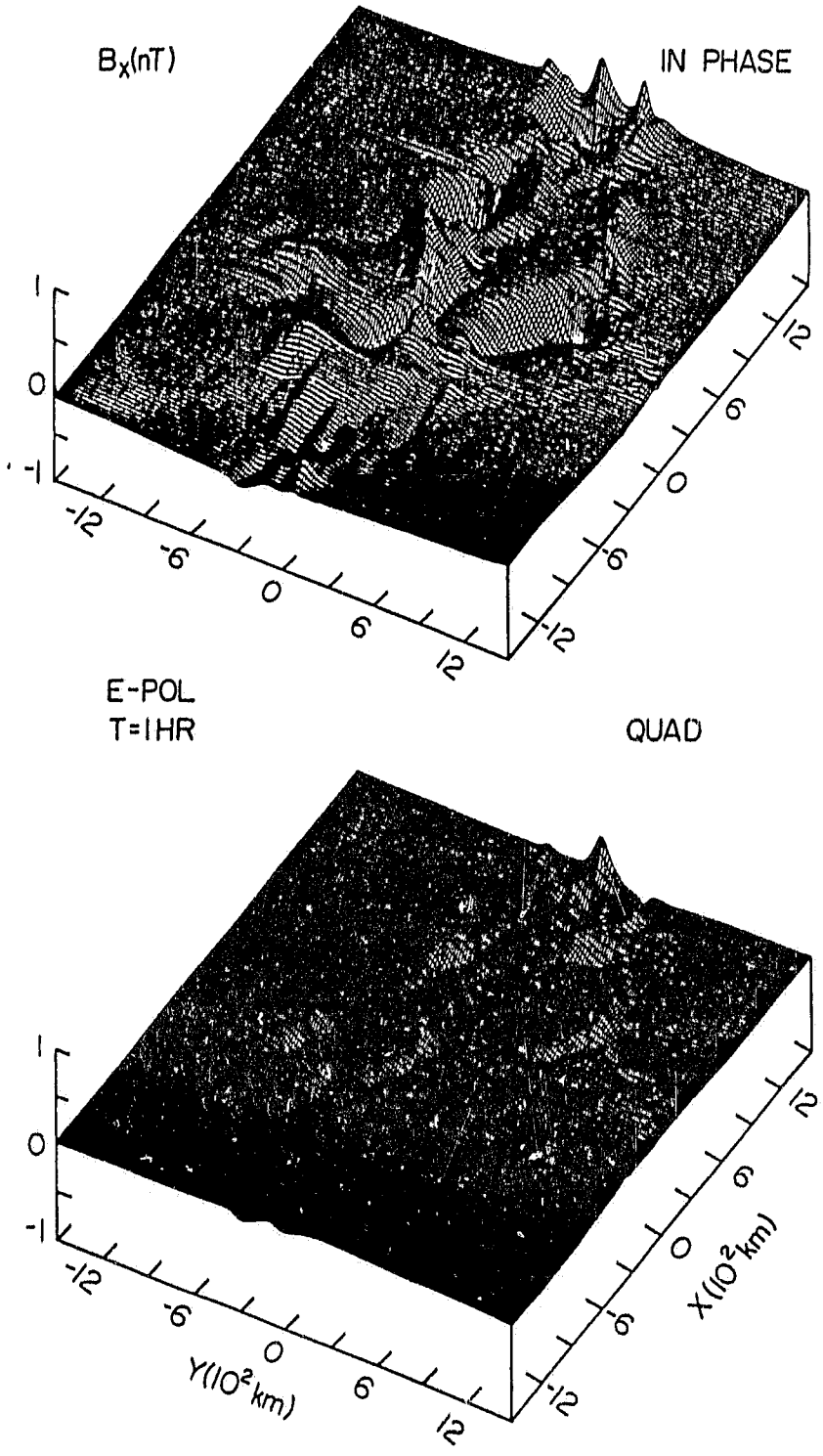

Figure A.3: Three-dimensional views of in-phase and quadrature B_x for the Japan model for E-polarization at 3 min.

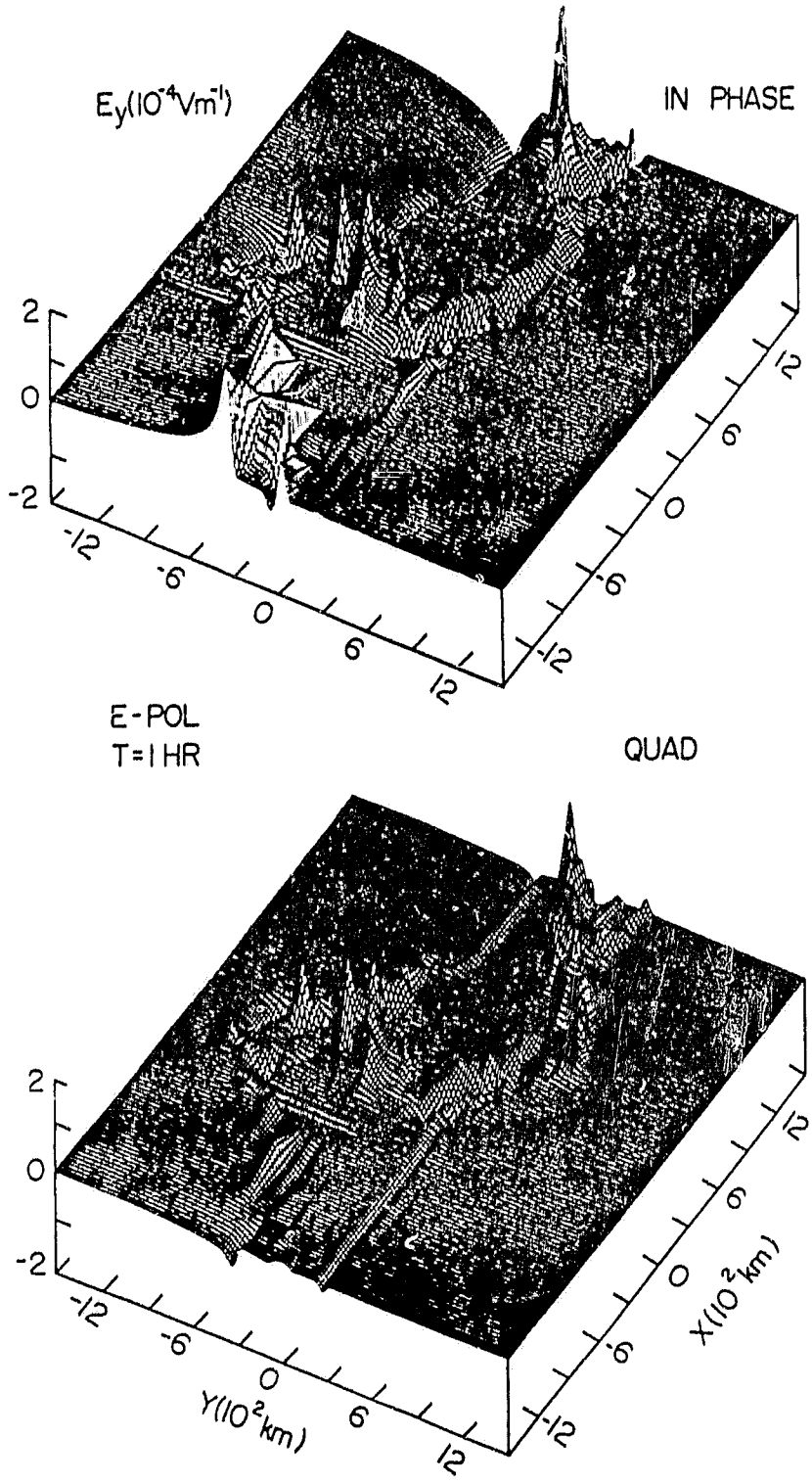

Figure A.4: Three-dimensional views of in-phase and quadrature E_y for the Japan model for E-polarization for 3 min.

APPENDIX B

THREE-DIMENSIONAL VIEWS OF B_Y AND E_X FOR B-POLARIZATION

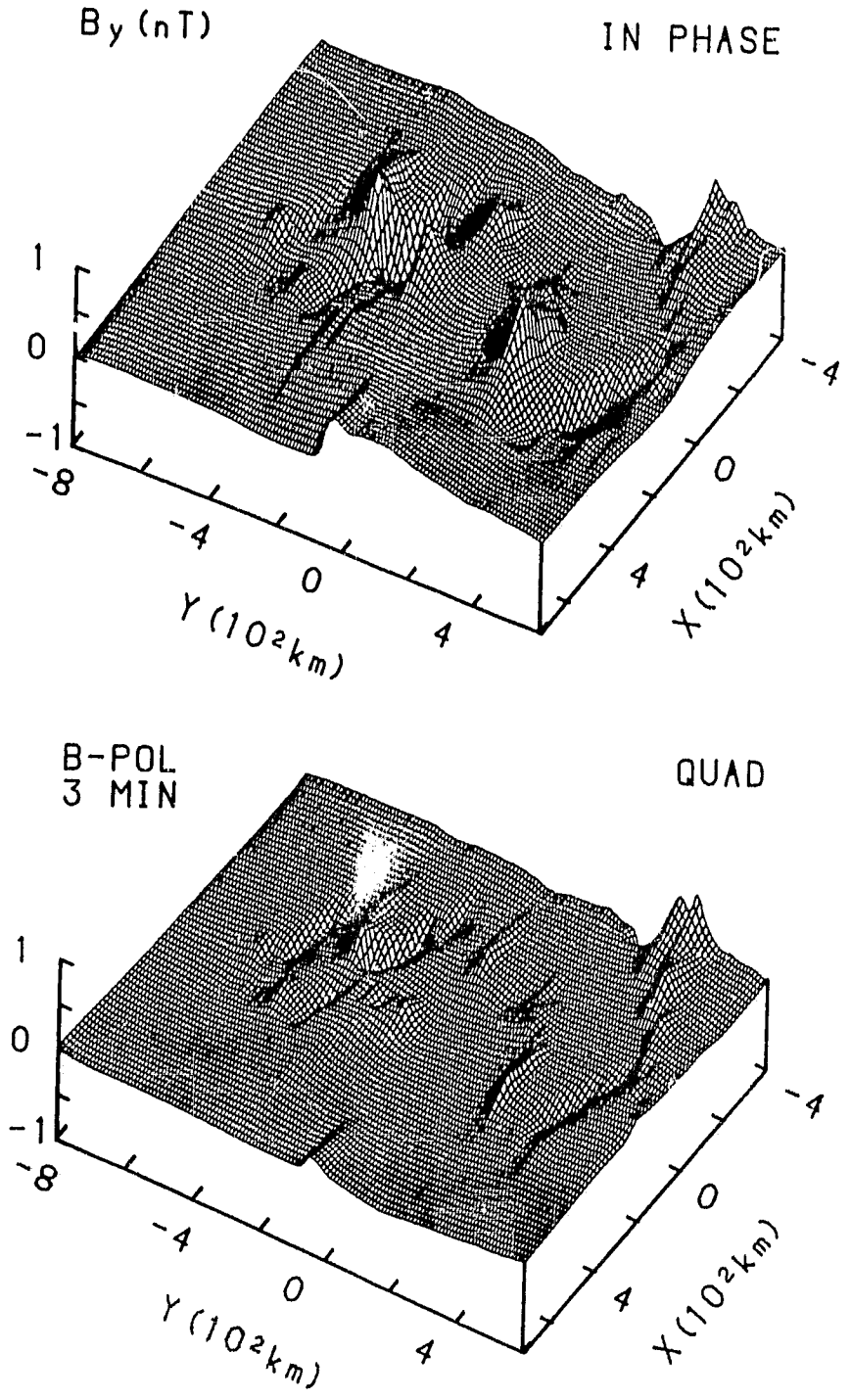

Figure B.1: Three-dimensional views of in-phase and quadrature B_y for the Bohai Bay model for B-polarization for 3 min.

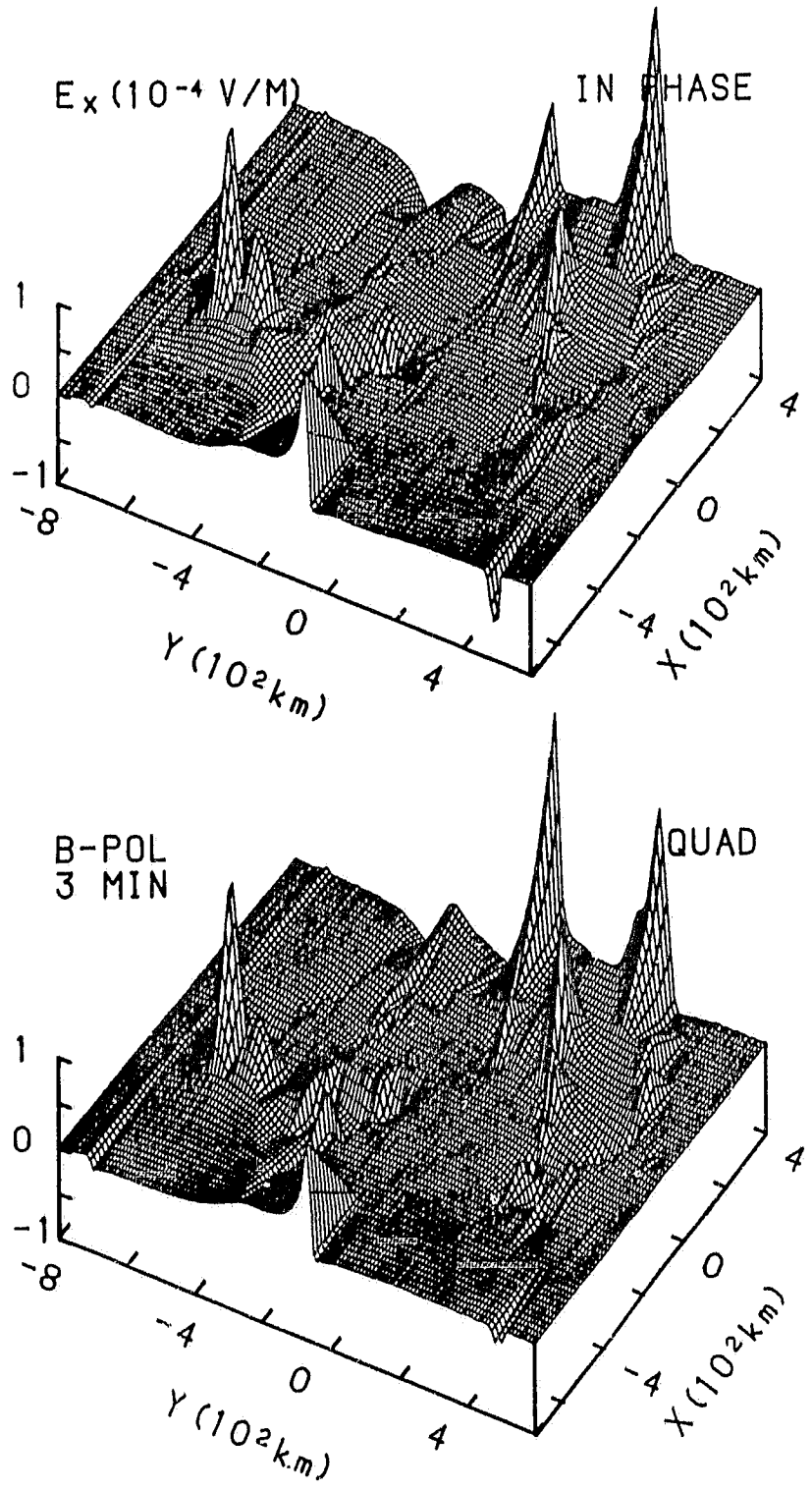

Figure B.2: Three-dimensional views of in-phase and quadrature E_x for the Bohai Bay model for B-polarization for 3 min.

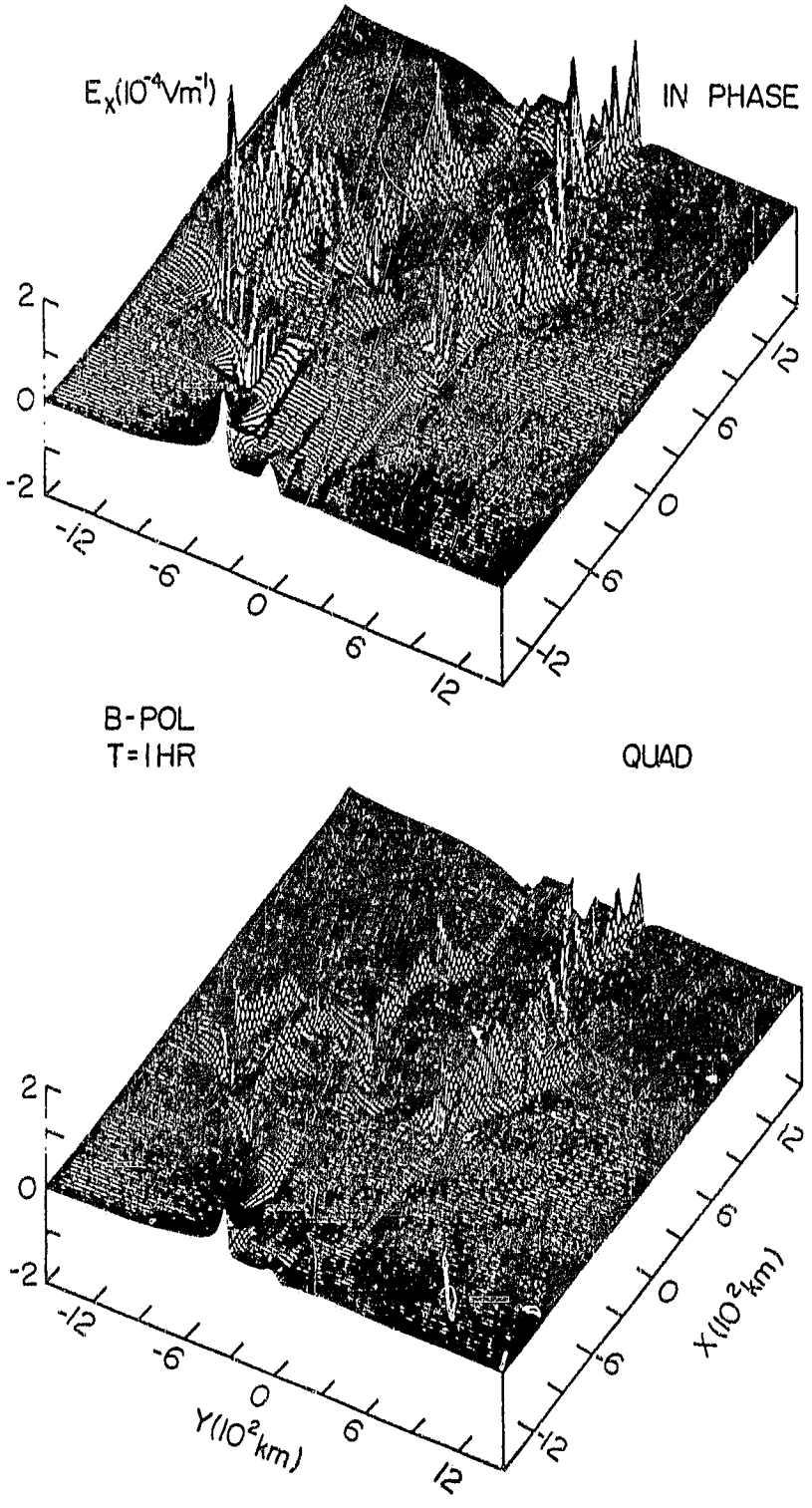

Figure B.3: Three-dimensional views of in-phase and quadrature B_y for the Japan model for B-polarization for 3 min.

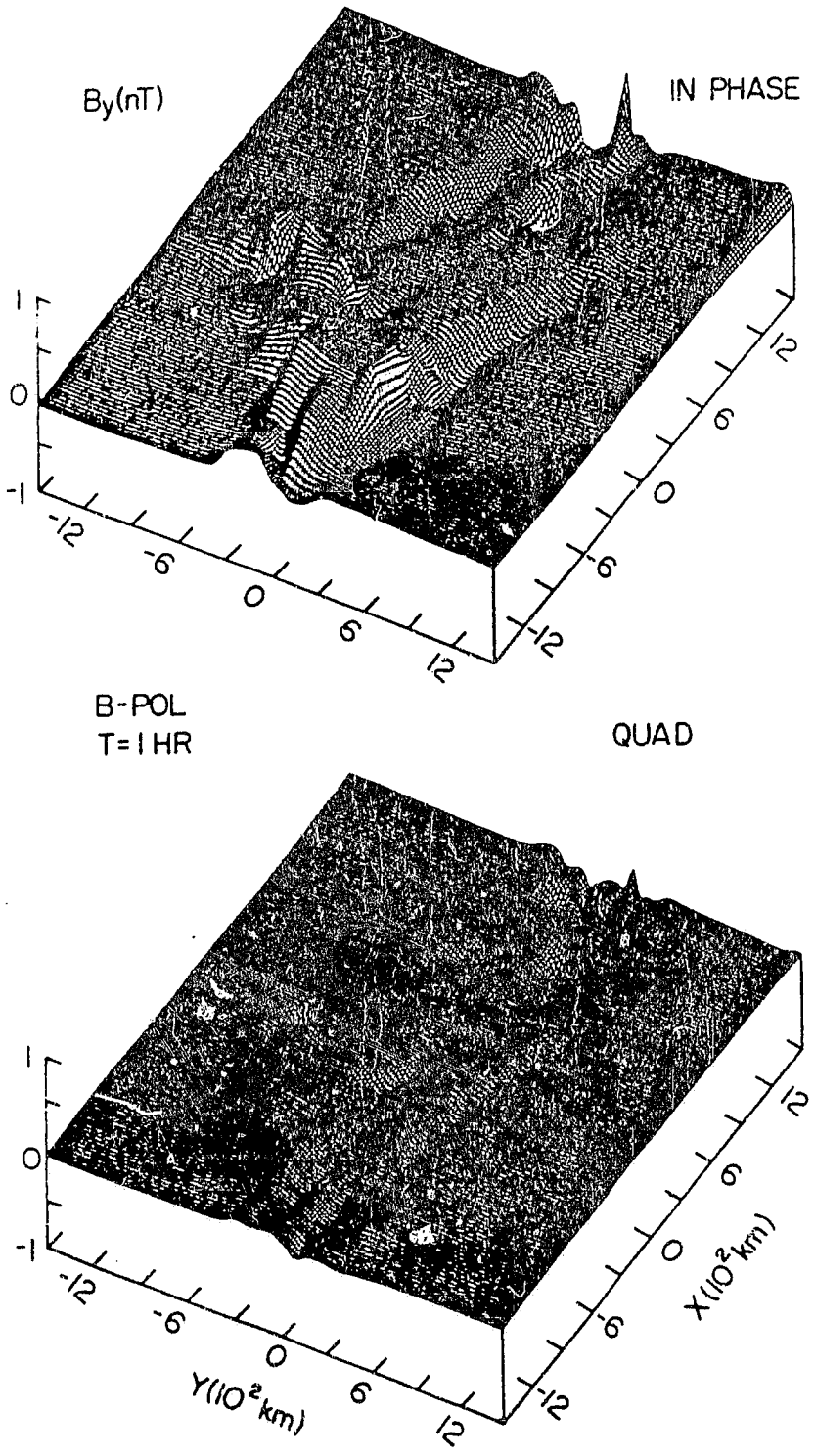

Figure B.4: Three-dimensional views of in-phase and quadrature E_x for the Japan model for B-polarization for 3 min.